Topics In The Asymptotic Analysis of Linear and NonLinear Eigenvalue Problems.

by

Alan Euan Lindsay

A THESIS SUBMITTED IN PARTIAL FULFILLMENT OF
THE REQUIREMENTS FOR THE DEGREE OF

DOCTOR OF PHILOSOPHY

in

The Faculty of Graduate Studies

(Mathematics)

THE UNIVERSITY OF BRITISH COLUMBIA

(Vancouver)

May 2010

Abstract

In Applied Mathematics, linear and nonlinear eigenvalue problems arise frequently when characterizing the equilibria of various physical systems. In this thesis, two specific problems are studied, the first of which has its roots in micro engineering and concerns Micro-Electro Mechanical Systems (MEMS).

A MEMS device consists of an elastic beam deflecting in the presence of an electric field. Modelling such devices leads to nonlinear eigenvalue problems of second and fourth order whose solution properties are investigated by a variety of asymptotic and numerical techniques.

The second problem studied in this thesis considers the optimal strategy for distributing a fixed quantity of resources in a bounded two dimensional domain so as to minimize the probability of extinction of some species evolving in the domain. Mathematically, this involves the study of an indefinite weight eigenvalue problem on an arbitrary two dimensional domain with homogeneous Neumann boundary conditions, and the optimization of the principal eigenvalue of this problem. Under the assumption that resources are placed on small patches whose area relative to that of the entire domain is small, the underlying eigenvalue problem is solved explicitly using the method of matched asymptotic expansions and several important qualitative results are established.

Table of Contents

List of Tables

List of Figures

Acknowledgements

I would like to thank very much my supervisor Michael Ward whose expert guidance and passion for Mathematics has been inspirational. I would also like to thank Professors Neil Balmforth, Dan Coombs and Brian Wetton who have been greatly supportive throughout my studies.

For making my time at UBC so enjoyable, there are many people whose deserve acknowledgement, but special thanks is certainly due to Sasha, Ryan, Sionnach, Steve, Kelp, Jason, Hana and Omer and all the Vaughn-Jones/Metcalf family.

For always being there for me, thank you Mum, Dad and Fraser.

I would also like to acknowledge the financial support of a NSERC postgraduate fellowship throughout my studies and the support of all the Mathematics office staff.

Chapter 1

Introduction

The method of matched asymptotic expansions has become a staple technique in the toolbox of applied mathematicians over the last 50 years. Its original and perhaps still most significant contribution, was the deduction of the boundary layer equations whereby, under an assumption of high Reynolds number, the well-known Navier-Stokes equations are decoupled into two simpler problems. One problem concerns a region of inviscid flow where the effects of viscosity are neglected and another region, governed by the boundary equations, where the no slip condition can be applied. In essence, the method approximated the solution of one intractable problem by two much simpler ones along with precise bounds on the error induced by this decoupling process.

Subsequently, matched asymptotic methods, or more generally singular perturbation methods, have evolved into a vast array of techniques which can be employed to systematically reduce difficult problems arising in the natural sciences and engineering into a sequence of tractable ones. These reductions make use of a small (or large) parameter arising in the problem to make assertions about the relative importance of its components. This parameter typically appears naturally when considering physical problems, however, it may also be introduced to facilitate the analysis of a problem in a particular regime. Both of these scenarios are realized in this work.

This thesis is concerned with an application of contemporary asymptotic and numerical methods to two particular problems in Applied Mathematics. The first problem has its origin in the field of Engineering and arises from modeling a class of devices called Micro-Electro Mechanical Systems (MEMS). The second problem has its roots in Ecology and addresses the question of deploying a fixed quantity of resource in a bounded two dimensional domain so as to ensure the survival of some species evolving in the domain for the largest range of physical parameters. Mathematically, this involves the study of a indefinite weight eigenvalue problem on an arbitrary two dimensional domain with homogeneous Neumann boundary conditions, and requires the optimization of the principal eigenvalue of this problem.

The following sections introduce in detail the problems to be considered, provide the reader with an account of previous work undertaken and outline the aims of the thesis.

1.1 Micro-Electro Mechanical Systems

In 1959, Nobel Laureate and Physicist Richard P. Feynman gave a lecture titled *There's Plenty of Room at the Bottom* and initiated a new field of human endeavour. In his seminal lecture, he posed the question *Why cannot we write the entire 24 volumes of the Encyclopedia Britannica on the head of a pin?* He argued that to accomplish this, one would need to shrink the text by a factor of $25,000$ which equates, roughly, to writing with a pen whose point has an area corresponding to $1,000$ atoms - an achievable task. Feynman used this example to demonstrate that a huge quantity of information can be stored on small scales.

Feynman went on to outline two additional avenues for exploration; the miniaturization of circuits and of motors. The natural progression of the former has led to the microchip; an invention which has subsequently revolutionized almost every aspect of science and technology. The natural progression of the latter has led to the development of Micro-Electro Mechanical Systems (MEMS) which are now on the verge of providing a similar revolution.

A MEMS device is a combination of mechanical components and integrated circuits constructed on a miniature scale. Current manufacturing techniques have made it possible to construct fully functioning motors visible only with the aid of a microscope; accelerometers with length less than one millimeter; needles so tiny they administer injections without stimulating nerve cells and many more devices, all with numerous applications. However, these advances have not been matched by our understanding and ability to control physical processes on such small scales.

Indeed, when shrunk by many orders of magnitude, a device whose mechanical processes may be well understood on a macro scale must be reexamined as different physical processes become dominant at small scales. For example, MEMS devices typically have a large surface area to volume ratio which favors electrostatic forces over magnetic forces as a means of actuation. The need to understand physical processes on such small scales has given mathematical modeling a central role in the design of MEMS devices.

Simple capacitance devices consisting of a rigid inelastic conducting ground plate opposite a thin deformable elastic plate, held fixed along its boundary, are a key component of MEMS (c.f. Fig. 1.1). The upper part of this device consists of a thin deformable elastic plate that is held clamped along its boundary, and which lies above a fixed ground plate. When a voltage V is applied to the upper plate, the upper plate can exhibit a significant deflection towards the lower ground plate.

Beyond some critical voltage V^* called the *pull-in* voltage, the deflecting plate can *touchdown* on the ground plate, an event which can compromise the operation of some devices and is essential for the operation of others, *e.g.* switches and valves.

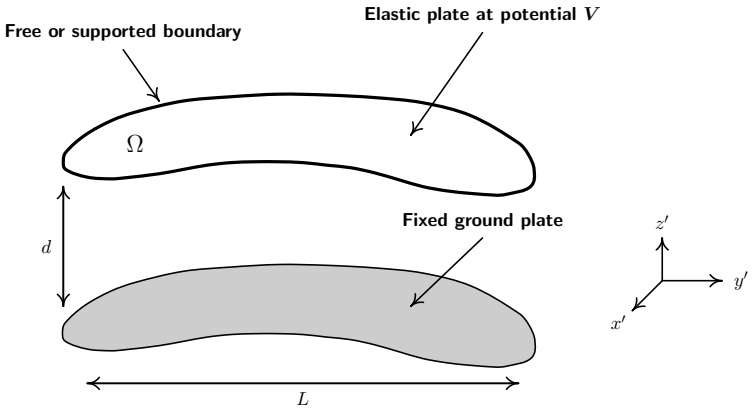

Figure 1.1: Schematic plot of the MEMS capacitor with a deformable elastic upper surface that deflects towards the fixed lower surface under an applied voltage.

From a point of view of MEMS design, a larger value of V^* would be detrimental to devices which require touchdown to occur in their operation as this would necessitate a higher input voltage. On the other hand, transducer type devices which operate by measuring one quantity through its effect on the deflection of the upper plate, may require a larger operating voltage range to prevent touchdown. In every case accurate determination of the maximum voltage V^* is essential to effective MEMS design and is a central goal in mathematical modeling of the device's operation.

The first batch fabricated Micro Electro-Mechanical System (MEMS) device was the resonant gate transistor (RGT) created in 1964 at Westinghouse [4]. The device, manufactured on a length scale of $0.1mm$, was essentially a tuning fork which provided a resonant output to an electrical input of a predetermined frequency. One of the key components of the RGT was the capacitor like device displayed in Fig. 1.1. The authors developed a simple model of the device based on the assumption that the deflection of the upper surface was a function of time only. By incorporating the mechanical properties of the device into a mass-spring system, the ordinary differential equation (ODE)

$$\alpha^2 \frac{d^2u}{dt^2} + \frac{du}{dt} + u = \frac{\lambda}{(1-u)^2}. \tag{1.1.1}$$

was proposed for the dimensionless deflection $u(t)$ of the upper plate. The dimensionless parameter α is known as the quality factor in engineering parlance while the non-negative parameter λ, proportional to V^2, represents the relative importance of electrostatic and mechanical forces in the system. The steps leading to (1.1.1) and discussion of its predictions are presented in § 2.1. To investigate the pull-in instability, as predicted by (1.1.1), time derivatives are set to zero to determine that equilibrium

deflections of the device satisfy the relationship $u(1-u)^2 = \lambda$. The solutions of this expression are conveniently displayed in the bifurcation diagram of Fig. 1.2.

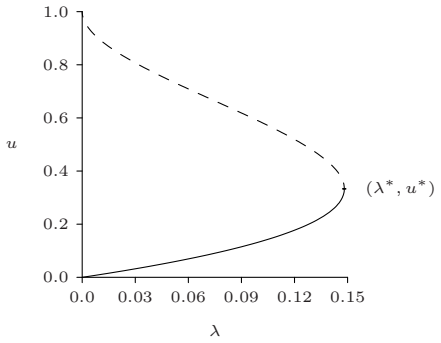

Figure 1.2: Bifurcation diagram of steady state solutions to equation (1.1.1). A saddle-node or fold bifurcation is observed at the point $(\lambda^*, u^*) = (4/27, 1/3)$ with a stable (solid) and an unstable (dashed) solution branch emanating from the bifurcation point.

The bifurcation diagram of Fig. 1.2 indicates that for $\lambda < \lambda^* = 4/27$ one stable and one unstable equilibria are attained, while for $\lambda > \lambda^*$, no equilibrium deflections are possible. The critical value, λ^*, represents the non-dimensional pull-in voltage of the device and knowledge of its value is key to predicting the behaviour of the device. Despite the simple nature of this model, *i.e.* no elastic effects and no boundary conditions at the edges of the device, it does capture the pull-in instability and provides a compact expression for the pull-in voltage.

In an effort to better capture the geometry and the material properties of the deflecting surface, Pelesko coupled the theories of linear elasticity and electrostatics [33] (see also [59] and the references therein) to show that the dimensionless equilibrium deflection $u(x)$ of the upper plate satisfies the partial differential equation (PDE)

$$\Delta u = \frac{\lambda}{(1+u)^2}\,, \qquad x \in \Omega\,; \qquad u = 0 \quad x \in \partial\Omega\,. \tag{1.1.2}$$

The non-negative quantity λ, which is directly proportional to the square of the voltage V applied to the upper plate, represents a ratio of electrostatic and elastic forces in the system and acts as a natural bifurcation parameter. A solution of (1.1.2) can be interpreted physically as a balance between an elastic restoring force and an attracting coulomb force. The model (1.1.2) was derived in [33] from a narrow-gap asymptotic analysis. The steps involved in the derivation of (1.1.2) are detailed in § 2.2.

This simple nonlinear eigenvalue problem has been studied using formal asymptotic analysis in [34] and [17] for the unit slab $\Omega = (0,1)$ and the unit disk $\Omega = \{(x,y)|x^2 + y^2 \leq 1\}$. For the unit disk, one of the key qualitative features for (1.1.2) is that the

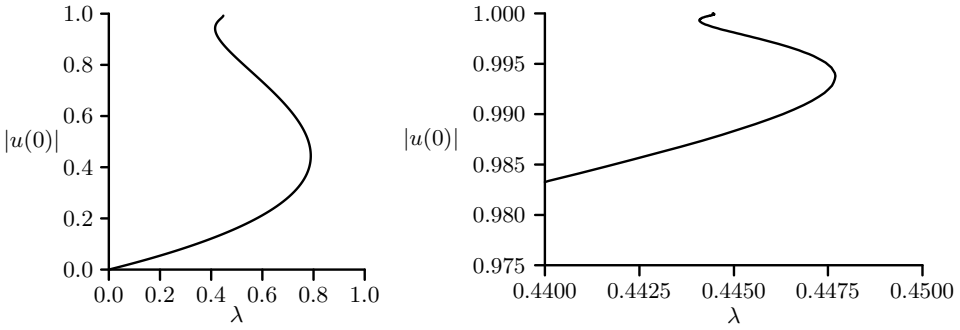

(a) $\Omega = \{|x| \leq 1\}$. (b) $\Omega = \{|x| \leq 1\}$ (Zoomed).

Figure 1.3: Panel (a) shows steady state solutions for the unit disc $\Omega = \{|x| \leq 1\}$ and is seen to exhibit multiple fold points as $|u(0)|$ approaches 1 from below. The critical value is determined to be $\lambda^* = 0.789$. Panel (b) is an enlargement of the upper portion of panel (a) and shows the curve undergoing additional folds as $|u(0)|$ nears 1.

bifurcation diagram $|u(0)|$ versus λ for radially symmetric solutions of (1.1.2) has an infinite number of fold points with $\lambda \to 4/9$ as $|u(0)| \to 1$ (cf. [34], Fig. 1.3).

Analytical bounds for the pull-in voltage instability threshold, representing the fold point location λ_c at the end of the minimal[1] solution branch for (1.1.2), have been derived (cf. [34], [13], [17]). A generalization of (1.1.2) that has received considerable interest from a mathematical viewpoint a problem with a variable permittivity profile $|x|^\alpha$ in an N-dimensional domain Ω, namely

$$\Delta u = \frac{\lambda |x|^\alpha}{(1+u)^2}\,, \quad x \in \Omega\,; \qquad u = 0 \qquad x \in \partial\Omega\,. \tag{1.1.3}$$

There are now many rigorous results for (1.1.2) and (1.1.3) in the unit ball in spatial dimension N and in more general domains Ω. In particular, upper and lower bounds for λ_c have been derived for (1.1.2) and for (1.1.3) for the range of parameters α and N where solution multiplicity occurs (cf. [13]). In [20] it has been proved that there are an infinite number of fold points for (1.1.2) in a certain class of symmetric domains. Many other rigorous results for solution multiplicity for (1.1.3) under various ranges of α and N have been obtained in [13], [9], and [19].

In this work, three distinct perturbations to (1.1.2) and their effect on the pull-in voltage and the infinite fold point structure are investigated. These are;

[1] A solution whose L^2 norm is smaller than any other solution. Similarly a maximal solution has a larger L^2 norm than any other solution.

- The beam problem:

$$-\delta\Delta^2 u + \Delta u = \frac{\lambda}{(1+u)^2}\,, \quad x \in \Omega\,; \qquad u = \partial_n u = 0 \quad x \in \partial\Omega. \tag{1.1.4}$$

  In this case the deflecting surface exhibits rigidity and δ represents the relative importance of tension and rigidity.

- The fringing field problem:

$$\Delta u = \frac{\lambda(1+\delta|\nabla u|^2)}{(1+u)^2}\,, \quad x \in \Omega\,; \qquad u = 0 \quad x \in \partial\Omega. \tag{1.1.5}$$

  Here, $\delta \equiv d^2/L^2$ is the square of the aspect ratio and the term $\delta|\nabla u|^2$ accounts for the fact that the electric field between the plates is not quite uniform.

- The annulus problem:

$$\Delta u = \frac{\lambda}{(1+u)^2}\,, \quad \delta < |x| < 1; \qquad u(\delta) = u(1) = 0. \tag{1.1.6}$$

  The value of $\delta > 0$ represents the radius of a small circular sub-domain removed from the unit disc.

Although the quantity δ has a different physical interpretation in each of the three above cases, it is used generally to represent a small perturbation from the unperturbed membrane problem (1.1.2).

The bihamonic term $-\delta\Delta^2 u$ of (1.1.4) arises by considering the deflecting surface to be a plate supporting bending stresses. By contrast with (1.1.2) and (1.1.3), only a few rigorous results are available for (1.1.4) and similar fourth-order variants. Under Navier boundary conditions $u = \Delta u = 0$ on $\partial\Omega$, the existence of a maximal solution for (1.1.4) was proved in [26] and its uniqueness established in [22]. Under Navier boundary conditions and in the three-dimensional unit ball it, was proved in [21] that $-\Delta^2 u = \lambda/(1+u)^2$ has infinitely many fold points for the bifurcation branch corresponding to radially symmetric solutions. In [8], the regularity of the minimal solution branch together with bounds for the pull-in voltage for the corresponding clamped problem $-\Delta^2 u = \lambda/(1+u)^2$ with $u = \partial_n u = 0$ on $|x| = 1$ in the N-dimensional unit ball are established for $N \leq 8$. Some related rigorous results are given in [5].

The fringing fields problem (1.1.5) was developed in [38] from careful consideration of the edge effects in the electric field of a drum shaped device with disk-shaped membrane end sections. It was shown in [38] that such edge effects induce a global perturbation of the basic nonlinear eigenvalue problem, replacing λ with $\lambda(1+\delta|\nabla u|^2)$ where $\delta = (d/L)^2$

is the aspect ratio of a MEMS device with gap width between the upper and lower surfaces d and whose surfaces have length scale L as shown in Fig. 1.1.

For the unit disk, equation (1.1.5) was studied numerically in § 5 of [38], where it was shown that the effect of the fringing-field is to reduce the pull-in voltage. In addition, numerical investigation of (1.1.5) indicated that the effect of the fringing-field is to destroy the infinite fold point structure of the basic membrane problem (1.1.2) in the unit disk, leaving a finite number of fold points on the upper branch of solutions followed by a branch of solutions with limiting behaviour $\lambda \to 0$ as $|u(0)| \to 1$.

The third modification of the membrane problem (1.1.2) in the unit disk is to pin the rim of a concentric inner disk in the undeflected state (cf. [35], [10]). The perturbed problem for $0 < \delta \ll 1$ in the concentric circular domain $\delta < |x| < 1$ is formulated as in (1.1.6). This change in the domain topology due to the insertion of a small inner disk has a two-fold effect on the solution. First, it increases significantly the pull-in voltage. Second, it allows for the existence of non-radially symmetric solutions that bifurcate off the radially symmetric solution branch (cf. [35], [10]).

For $\delta \ll 1$, the problems (1.1.4), (1.1.5), and (1.1.6), can all be viewed as perturbations of the basic and well-studied membrane problem (1.1.2). Of principal interest is the effect of these perturbations on the pull-in stability and on the infinite fold point structure of the unperturbed problem (1.1.2). The work undertaken to investigate these points is now described.

Chapter 2, describes the steps required to derive MEMS equations (1.1.1)-(1.1.6). In §3.1, the numerical methods employed to solve the relevant equations are outlined and preliminary findings discussed. Generally, it is observed that each of the aforementioned perturbations has a pronounced effect on the fold point location and that they also act to destroy the infinite fold points structure, leaving a solution branch with a finite number of turns. For the unit slab and unit disk, a simple upper bound for the fold point location λ_c at the end of the minimal solution branch for (1.1.4) is derived and calculated numerically. The remainder of Chapter 3 concentrates on the effect of the perturbations on fold point location.

A rather precise determination of the pull-in voltage threshold is required for the actual design of a MEMS capacitor since, typically, the operating range of the device is chosen rather close to the pull-in instability threshold (cf. [33], [38]). Therefore, in mathematical terms, the primary goal of the analysis is to calculate asymptotic expansions for the fold point location λ_c at the end of the lower, or minimal, solution branch for (1.1.4), (1.1.5), and (1.1.6), in the limit $\delta \to 0$.

In §3.3, asymptotic expansions for the fold point location of the biharmonic problem (1.1.4), denoted by λ_c, at the end of the minimal solution branch are derived in the limiting parameter ranges $\delta \ll 1$ and $\delta \gg 1$ for an arbitrary domain Ω with smooth

boundary. To treat the $\delta \ll 1$ limit of (1.1.4), singular perturbation techniques are used to resolve the boundary layer near the boundary $\partial\Omega$ of Ω, which arises from the term $\delta\Delta^2 u$ in (1.1.4). This analysis yields effective boundary conditions for the corresponding outer solution, which is defined away from an $\mathcal{O}(\delta^{1/2})$ neighbourhood of $\partial\Omega$. Then, appropriate solvability conditions are imposed to determine analytical formulae for the coefficients in the asymptotic expansion of λ_c for $\delta \ll 1$. These coefficients are evaluated numerically for the unit slab and the unit disk. By contrast, the analysis of (1.1.4) for the limiting case $\delta \gg 1$ consists of a regular perturbation expansion of the solution to the pure biharmonic nonlinear eigenvalue problem $-\Delta^2 u = \tilde{\lambda}/(1+u)^2$, with $\tilde{\lambda} \equiv \lambda/\delta$. In this way, it is shown for the unit disk and the unit slab that

$$\begin{aligned} \lambda_c &\sim 70.095\delta + 1.729 + \cdots, \quad \delta \gg 1; \\ \lambda_c &\sim 1.400 + 5.600\,\delta^{1/2} + 25.451\,\delta + \cdots, \quad \delta \ll 1; \end{aligned} \qquad \text{(Unit Slab)}, \tag{1.1.7a}$$

$$\begin{aligned} \lambda_c &\sim 15.412\delta + 1.001 + \cdots, \quad \delta \gg 1; \\ \lambda_c &\sim 0.789 + 1.578\,\delta^{1/2} + 6.261\,\delta + \cdots, \quad \delta \ll 1; \end{aligned} \qquad \text{(Unit Disk)}. \tag{1.1.7b}$$

Good agreement between (1.1.7) and full numerical results for λ_c computed from (1.1.4) is established. In particular, it is observed that the asymptotic result for λ_c in (1.1.7) derived for the $\delta \gg 1$ limit can give a reliable estimate of λ_c even for $\delta \approx 0.03$. The asymptotic results in (1.1.7) for $\delta \ll 1$ accurately predict λ_c for $0 < \delta < 0.03$ (see Fig. 3.5(b) and Fig. 3.6(b)). Therefore, for the unit slab and the unit disk, it is apparent that (1.1.7) gives a rather accurate estimate of λ_c for (1.1.4) for essentially the entire range $0 < \delta < \infty$, and hence (1.1.7) can give a good prediction of the pull-in voltage for (1.1.4).

In §3.5.1 an analysis of the fold point location λ_c of (1.1.5) shows that the effect of a fringing-field is to reduce the pull-in voltage by an amount of $\mathcal{O}(\delta)$ for $\delta \ll 1$. For the unit disk, it is calculated through a solvability condition that $\lambda_c \sim 0.789 - 0.160\delta$ for $\delta \ll 1$. This asymptotic result is shown to compare very favorably with full numerical results computed from (1.1.5).

In §3.5.2, a singular perturbation analysis of the fold point location λ_c for the annulus problem (1.1.6) in the limit $\delta \to 0$ shows that $\lambda_c \sim 0.789 + \mathcal{O}(-1/\log\delta)$. The coefficient of this logarithmic term, which is evaluated numerically, is shown to be positive. Therefore, the effect of the inner disk of radius δ is to perturb the pull-in voltage for the membrane problem (1.1.2) rather significantly even when $\delta \ll 1$. Some related nonlinear eigenvalue problems with small holes were treated in [41] and [40].

Following on, Chapter 4 addresses the effects of the perturbations made in (1.1.4)-(1.1.6) to the upper branch of solutions of the unperturbed problem (1.1.2). It is

observed by numerical calculation that in each case a positive value of δ acts to destroy the infinite fold point structure of the problem leaving behind a branch of solutions that undergoes a finite number of turning points before taking on limiting behaviour $\lambda \to 0$ as $||u||_\infty \to 1^-$. In the fringing fields case it was shown in [23] that for λ sufficiently small, (1.1.5) admits at least two solutions. This is in contrast to (1.1.2) which admits one unique solution, the minimal solution, for λ sufficiently small. In general, few rigorous results pertaining to the maximal solution branch of the fourth order problem (1.1.4) and the annulus problem (1.1.6) are available.

A primary goal in the analysis of Chapter 4 is to develop a formal asymptotic analysis, based on the method of matched asymptotic expansions, to provide an *explicit* analytical characterization of the asymptotic behaviour of the maximal solution branch to (1.1.4) in the limit $\varepsilon = 1 - ||u||_\infty \to 0^+$, for which $\lambda \to 0$. This problem is studied for the unit slab, the unit disk and a certain class of general geometries $\Omega \subset \mathbb{R}^2$. For these domains, explicit asymptotic expansions for λ as $\varepsilon \to 0$ are derived for any $\delta > 0$, and the results are shown to compare very favorably with full numerical results. In the case of the unit disc, the solution u to (1.1.4) in the limit $\varepsilon \to 0$ has a strong concentration near the origin owing to the nearly singular behaviour of the nonlinearity in (1.1.4). For more general two dimensional geometries, additional work is required to determine the location and multiplicity of concentration points. The singular perturbation analysis required to resolve these regions of concentration solution relies heavily on the systematic use of logarithmic switchback terms. Such terms are notorious in the asymptotic analysis of PDE models arising in the study of low Reynolds number flows (cf. [27], [28], [36], [37]).

The outline of this chapter is as follows. In § 4.1 a formal asymptotic approach is employed to obtain the asymptotic behaviour of the bifurcation curve to (1.1.3) in the unit ball in the limit $\varepsilon \equiv 1 - ||u||_\infty \to 0^+$. In § 4.2 an explicit characterization of the maximal solution branch for the fringing-field problem (1.1.5) and for the biharmonic problem (1.1.4) in the limit $\varepsilon \equiv 1 - ||u||_\infty \to 0^+$ is developed for the unit slab. In § 4.3, similar results are given for (1.1.4) in the unit disk. In § 4.3.2 the limiting asymptotic behaviour of the maximal solution branches of (1.1.6) are constructed. In § 4.4, the problem of constructing the maximal solution branch of (1.1.4) for general $\Omega \subset \mathbb{R}^2$ is discussed. A necessary condition for a solution to concentrate at some $x_0 \in \Omega$ is proposed and the corresponding maximal branch is constructed in the limit as $\varepsilon \to 0^+$

1.2 Persistence on Patchy Domains - An Eigenvalue Optimization Problem

In the field of Ecology, a natural line of inquiry is that regarding the effect of habitat fragmentation on any occupying species. Fragmentation may occur naturally when weather changes (*i.e.* droughts, floods) facilitate the emergence of discontinuities in an organism's preferred habitat. Although more frequently it is due to human activities such as agriculture, development and conservation to name a few.

Mathematical models provide a natural framework to address such problems through reaction-diffusion theory. The diffusive logistic model, which describes the evolution of a population with density $u(x,t)$ diffusing with constant diffusivity $D > 0$ throughout some habitat represented by a bounded domain $\Omega \subset \mathbb{R}^2$, is formulated as

$$u_t = D\Delta u + u\left[m(x) - u\right], \quad x \in \Omega\,; \qquad \partial_n u = 0\,, \quad x \in \partial\Omega\,; \tag{1.2.1a}$$

$$u(x,0) = u_0(x) \geq 0\,, \qquad x \in \Omega\,. \tag{1.2.1b}$$

The no-flux boundary condition in (1.2.1a) specifies that no individuals cross the boundary of the habitat Ω. The initial population density $u_0(x)$ is non-negative and not identically zero. The function $m(x)$ represents the growth rate for the species, with $m(x) > 0$ in favourable parts of the habitat, and $m(x) < 0$ in unfavourable parts of the habitat. The integral $\int_\Omega m\,dx$ measures the total resources available in the spatially heterogeneous environment. With respect to applications in ecology, this model was first formulated in [69].

To determine the stability of the extinction equilibrium solution $u = 0$, set $u = \phi(x)e^{-\sigma t}$ in (1.2.1), where $\phi(x) \ll 1$, to obtain that ϕ satisfies

$$\Delta\phi + \lambda m(x)\phi = -\sigma\phi\,, \quad x \in \Omega; \qquad \partial_n\phi = 0\,, \quad x \in \partial\Omega \tag{1.2.2}$$

where $\lambda = 1/D > 0$. The threshold for species persistence is determined by the stability border of the extinct solution $u = 0$. At this bifurcation point, the eigenvalue of the linearized problem about the zero solution must pass through zero. Therefore, by setting $\sigma = 0$ in (1.2.2) the problem reduces to the determination of a scalar λ and a function ϕ that satisfies the indefinite weight eigenvalue problem

$$\Delta\phi + \lambda m(x)\phi = 0\,, \quad x \in \Omega\,; \qquad \partial_n\phi = 0\,, \quad x \in \partial\Omega\,; \quad \int_\Omega \phi^2\,dx = 1\,. \tag{1.2.3}$$

It is said that $\lambda_1 > 0$ is a positive principal eigenvalue of (1.2.3) if the corresponding eigenfunction ϕ_1 of (1.2.3) is positive in Ω. It is well-known (cf. [43], [55], [68]) that

(1.2.3) has a unique positive principal eigenvalue λ_1 if and only if $\int_\Omega m\,dx < 0$ and the set $\Omega^+ = \{x \in \Omega\ ;\ m(x) > 0\}$ has positive measure. Such an eigenvalue is the smallest positive eigenvalue of (1.2.3).

The positive principal eigenvalue λ_1 is interpreted as the persistence threshold for the species. It is well-known that if $\lambda < \lambda_1$, then $u(x,t) \to 0$ uniformly in $\bar{\Omega}$ for all non-negative and non-trivial initial data, so that the population tends to extinction. Alternatively, if $\lambda > \lambda_1$, then $u(x,t) \to u^*(x)$ uniformly in $\bar{\Omega}$ as $t \to \infty$, where u^* is the unique positive steady-state solution of (1.2.1). For this range of λ the species will persist. Many mathematical results for (1.2.1) under different boundary conditions are given in the pioneering works of [45], [46], and [47]. Related results for multi-species interactions and other mathematical problems in ecology are given in [48] (see also the survey article of [60]).

An interesting problem in mathematical ecology is to determine, among all functions $m(x)$ for which a persistence threshold exists, which $m(x)$ yields the smallest λ_1 for a fixed amount of total resources $\int_\Omega m\,dx$. In other words, we seek to determine the optimum arrangement of favourable habitats in Ω in order to allow the species to persist for the largest possible diffusivity D. This optimization problem was originally posed and studied in [45] and [47]. For (1.2.1) under Neumann boundary conditions in a two-dimensional domain Ω it was proved in [59] that the optimum $m(x)$ is piecewise continuous and of bang-bang type. An earlier result showing the existence of a similar bang-bang optimal control for $m(x)$ for the Dirichlet problem was given in [45]. For (1.2.1) posed in a one-dimensional interval $0 < x < 1$ it was proved in [59] that the optimal $m(x)$ consists of a single favourable habitat attached to one of the two endpoints of the interval. Related results were given in [47] under Dirichlet, Neumann, or Robin type boundary conditions.

The minimization of λ_1 in cylindrical domains of type $(0,1) \times \Omega \subset \mathbb{R}^n$ for $\Omega \in \mathbb{R}^{n-1}$ was studied in [56]. It was shown that if $|\int_\Omega m(x)\,dx|$ is below some threshold value, the optimum λ_1 occurs when the favourable habitat is concentrated near one of the corners of the domain. Otherwise, the optimum λ_1 occurs when the favourable habitat is attached to either of the two ends of the domain with the shortest edge. For spatially periodic environments, the effect of fragmentation of the favourable resources was studied in [42] using Steiner symmetrization, and some results were obtained for Dirichlet boundary conditions. Related applications of symmetrization ideas are given in [58]. A treatise on the modeling of biological invasions in periodic spatial environments is given [67]. In [64] stochastic methods were used to determine the persistence threshold for the diffusive logistic model for an infinitely periodic heterogeneous media. This study, which eliminated the effect of boundary conditions, showed that habitat fragmentation decreases the persistence of the species. For (1.2.1) in a bounded two-dimensional do-

main with Neumann boundary conditions, the existence of an optimal configuration for $m(x)$ was proved in [63]. Moreover, numerical methods were used to show that the optimal favourable spatial habitats are either ball-shaped or strip-shaped, depending on the amount of available resources.

Although these previous studies give considerable insight into the effect of spatial fragmentation of habitat resources on the persistence threshold in specific situations, such as cylindrical domains or periodic environments, the problem of the optimum choice for $m(x)$ in arbitrary two-dimensional domains with no periodicity assumption is largely an open problem.

In Chapter 5, the persistence threshold λ_1 is calculated asymptotically, and then optimized, for a particular class of piecewise constant growth rate function $m = m_\varepsilon(x)$ in an arbitrary two-dimensional domain. It is assumed that $m_\varepsilon(x)$ is localized to n small circular patches of radii $\mathcal{O}(\varepsilon)$, each of which is centered either inside Ω or on $\partial\Omega$. The boundary $\partial\Omega$ is assumed to be piecewise differentiable, but corners with nonzero angle are permitted on the domain boundary. The set of the centers of the interior patches is defined to be $\Omega^I \equiv \{x_1, \ldots, x_n\} \cap \Omega$ while $\Omega^B \equiv \{x_1, \ldots, x_n\} \cap \partial\Omega$ is the set of the centers of the boundary patches. The patches are assumed to be well-separated in the sense that $|x_i - x_j| \gg \mathcal{O}(\varepsilon)$ for $i \neq j$ and that the interior patches are not too close to the boundary, i.e. $\mathrm{dist}(x_j, \partial\Omega) \gg \mathcal{O}(\varepsilon)$ whenever $x_j \in \Omega^I$. To accommodate a boundary patch, an angle $\pi\alpha_j$, representing the angular fraction of a circular patch that is contained within Ω, is associated with each x_j for $j = 1, \ldots, n$. More specifically, $\alpha_j = 2$ whenever $x_j = \Omega^I$, $\alpha_j = 1$ when $x_j \in \Omega^B$ and x_j is a point where $\partial\Omega$ is smooth, and $\alpha_j = 1/2$ when $x_j \in \partial\Omega$ is at a $\pi/2$ corner of $\partial\Omega$, etc. The growth rate function $m = m_\varepsilon(x)$ in (1.2.3) is taken to have the specific form

$$m = m_\varepsilon(x) \equiv \begin{cases} m_j/\varepsilon^2\,, & x \in \Omega_{\varepsilon_j}\,, \quad j = 1, \ldots, n\,, \\ \\ -m_b\,, & x \in \Omega \backslash \bigcup_{j=1}^n \Omega_{\varepsilon_j}\,. \end{cases} \tag{1.2.4}$$

Here $\Omega_{\varepsilon_j} \equiv \{x \,|\, |x - x_j| \leq \varepsilon\rho_j \cap \Omega\}$, so that each patch Ω_{ε_j} is the portion of a circular disk of radius $\varepsilon\rho_j$ that is strictly inside Ω. The constant m_j is the local growth rate of the j^{th} patch, with $m_j > 0$ for a favourable habitat and $m_j < 0$ for a non-favourable habitat. The constant $m_b > 0$ is the background bulk decay rate for the unfavourable habitat. In terms of this growth rate function, the condition of [43], [55], and [68] for the existence of a persistence threshold is that one of the m_j for $j = 1, \ldots, n$ must be positive, and that the asymptotically valid inequality

$$\int_\Omega m_\varepsilon \, dx = -m_b|\Omega| + \frac{\pi}{2}\sum_{j=1}^n \alpha_j m_j \rho_j^2 + \mathcal{O}(\varepsilon^2) < 0\,. \tag{1.2.5}$$

holds for the total resources. Here $|\Omega|$ denotes the area of Ω. We assume that the parameters are chosen so that (1.2.5) is satisfied. A schematic plot of a domain with circular patches is shown in Fig. 1.4

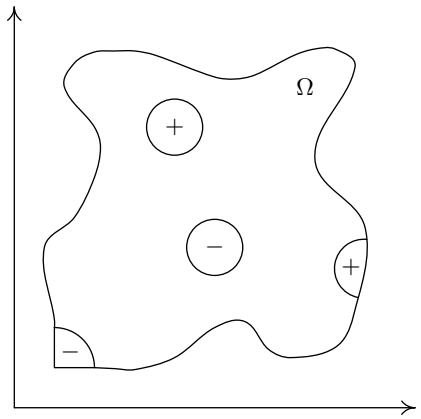

Figure 1.4: Schematic plot of a two-dimensional domain with localized strongly favourable (+) or unfavourable (−) habitats or patches, as described by (1.2.4). The patches inside the domain are small circular disks. On the domain boundary, the patches are the portions of circular disks that lie within the domain.

This specific form for $m_\varepsilon(x)$ is motivated by Theorem 1.1 of [59] which states that the optimal growth rate function must be of bang-bang type, and the result of [63] which shows that a sufficiently small optimum favourable habitat must be a circular disk.

In § 5.1 the method of matched asymptotic expansions is used to derive a two-term asymptotic expansion for the persistence threshold λ_1 for the case of either a single favourable interior or boundary habitat. The asymptotic analysis is extended in § 5.2 to calculate asymptotically λ_1 for (1.2.3) with growth rate function (1.2.4), which allows for multiple interior or boundary habitats. The analysis, which is summarized at the end of §5.2, shows that λ_1 has the two-term asymptotic expansion

$$\lambda_1 = \mu_0\nu + \nu^2\mu_1(x_1,\ldots,x_n) + \mathcal{O}(\nu^3)\,, \qquad \nu(\varepsilon) = -1/\log\varepsilon\,. \tag{1.2.6}$$

Here the leading-order coefficient μ_0 is the unique positive root of $\mathcal{B}(\mu_0) = 0$ on $0 < \mu_0 < 2/(m_J\rho_J^2)$, where

$$\mathcal{B}(\mu_0) \equiv -m_b|\Omega| + \pi\sum_{j=1}^{n}\frac{\alpha_j m_j\rho_j^2}{2 - m_j\rho_j^2\mu_0}\,, \qquad m_J\rho_J^2 \equiv \max_{m_j>0}\{m_j\rho_j^2\,|\,j=1,\ldots,n\}\,. \tag{1.2.7}$$

The coefficient μ_1, which depends explicitly on the spatial configuration $\{x_1,\ldots,x_n\}$

of patches, is determined in terms of a matrix involving the Neumann Green's function and the surface Neumann Green's function for Ω.

In § 5.3 the effects of resource fragmentation on the coefficients μ_0 and μ_1 of the asymptotic expansion of the persistence threshold are analyzed. For a prescribed amount of resources, for which $\int_\Omega m_\varepsilon \, dx$ in (1.2.5) is fixed, the patch configuration that minimizes μ_0, or in certain degenerate situations, minimizes the coefficient μ_1 in (1.2.6), is determined.

In §5.3.2 an analysis of the leading-order coefficient μ_0 in (1.2.6) is presented. This coefficient provides a surprisingly large amount of information on the relationship between habitat fragmentation and the persistence threshold. There are several key qualitative principles that are established. First, the fragmentation of a favourable interior habitat into two smaller favourable interior habitats is shown to be deleterious to species persistence, whereas the migration of an interior favourable habitat to the boundary of the domain is always advantageous. The optimal boundary location to concentrate a favourable resource is at a corner of the domain boundary with the smallest opening angle. Second, the fragmentation of a favourable interior habitat into a smaller favourable interior habitat together with a favourable boundary habitat is advantageous to species persistence when the boundary habitat is sufficiently strong. Further general principles, based on the optimization of μ_0, are summarized in Qualitative Results I–III of § 5.3.2. In addition, an illustration of these principles for certain patch distributions in the unit disk is given.

In § 5.3.3 it is also demonstrated that in certain degenerate situations, the problem of determining the optimal location for a favourable resource requires the examination of the coefficient μ_1 of the second term in the asymptotic expansion of λ. In particular, such a problem occurs in optimizing λ with respect to the boundary location of a single favourable boundary patch in a domain with a smooth boundary. In this case, it is shown that λ is minimized when the boundary patch is centered at a point $x_0 \in \partial\Omega$ at which the regular part of the surface Neumann Green's function attains its global maximum value on the boundary. The relationship between the global maximum of the boundary curvature and the regular part of the surface Neumann Green's function for smooth perturbations of the unit disk is investigated. In § 5.3.3 the optimization of λ for the case where an additional favourable resource is to be located inside a domain with a pre-existing and fixed patch distribution is considered. In this case, the optimization of λ typically requires the examination of the coefficient μ_1 of the second-order term in the asymptotic expansion of λ. The theory is illustrated for two specific examples involving the unit disk and the unit square, for which the required Green's functions are known analytically.

Related problems involving the asymptotic calculation and optimization of the fun-

damental eigenvalue of the Laplacian have been studied in perforated two-dimensional domains (cf. [51], [57], [61], [41], and [71]), in two-dimensional domains with perforated boundaries (cf. [44], [52], [53], [62]), and under the effect of strongly localized potentials (cf. [54]).

Chapter 2

Mathematical Modeling of Micro-Electro Mechanical Systems

In this section, models of the MEMS capacitor device introduced in §1.1 will be presented. In §2.1 the original analysis from [4] is presented. In § 2.2 a more contemporary model, introduced by Pelesko [33], will be detailed along with some preliminary results.

2.1 Lumped Mass Spring Model

In their initial work on MEMS, Nathanson *et al.* [4] concluded that allowing the deflection of the beam to be a function of space would complicate the resulting analysis unnecessarily and obscure the simplicity of the device. For this reason, they assumed that beam deflection was a function of time only and formulated a model in which the deflecting plate was represented by a mass on a spring whose spring constant, k, would approximately characterize the mechanical properties of the beam. The imagined configuration is represented schematically in Figure 2.1.

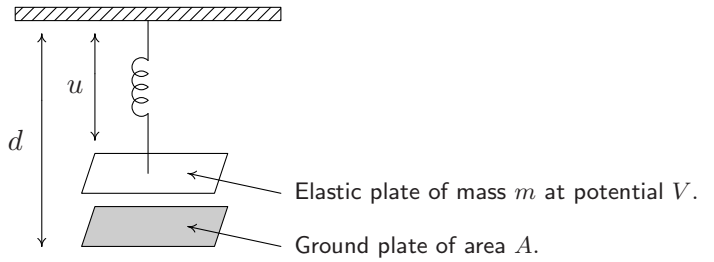

Figure 2.1: Schematic diagram of lumped mass spring model of MEMS deflection. The upper plate is assumed to be of mass m, surface area A and at potential V.

To determine a differential equation satisfied by $u(t)$, Newton's Second Law of motion is applied to all forces acting on the plate. There are three forces to be considered; the restoring force of the Hookean spring, $F_s = -k(u - l)$ where l is the rest length of

the spring, some damping effect assumed to be proportional to the velocity of the plate, that is $F_d = -au_t$ and an electrostatic force F_e between the two plates.

To calculate F_e, note that the potential ϕ between the two plates satisfies

$$\Delta\phi = 0, \quad 0 < z' < d - u; \qquad \begin{aligned} \phi(d-u) &= V \\ \phi(0) &= 0 \end{aligned} \tag{2.1.1}$$

which generates an electric field $\boldsymbol{E} = -\nabla\phi$ with resulting total energy

$$U = \frac{\epsilon_0}{2}\int_S |\boldsymbol{E}|^2$$

where S is the volume of the capacitor and ϵ_0 is the permittivity of free space. By operating in the small aspect ratio regime $d/L \ll 1$, equation (2.1.1) is well approximated by $\phi_{z'z'} = 0$ and is therefore easily solved to give the linear potential

$$\phi = \frac{Vz'}{d-u}$$

between the plates. The electric field $\boldsymbol{E} = -\phi_{z'}$ is then constant - the standard approximation for a parallel plate capacitor based on a small aspect ratio. The expression for the total energy is now reduced to

$$U = \frac{\epsilon_0}{2}\int_S \frac{V^2}{(d-u)^2} = \frac{\epsilon_0 A V^2}{2(d-u)}$$

and differentiation with respect to $(d-u)$ reveals that the electrostatic force is given by

$$F_e = \frac{\epsilon_0}{2}\frac{AV^2}{(d-u)^2}.$$

Combining all the forces in Newton's Equation of motion, the ODE

$$m\frac{d^2u}{dt^2} + a\frac{du}{dt} + k(u-l) = \frac{\epsilon_0}{2}\frac{AV^2}{(d-u)^2}. \tag{2.1.2}$$

is obtained for the displacement $u(t)$ of the upper plate. This equation is now reduced in complexity by introducing non-dimensional variables. The time scale of the system is chosen to reflect that viscosity is the dominant resistive force in the system. In other words, the primary restorative force acting against the electrostatic force is damping. This motivates the introduction of variables

$$t' = \frac{k}{a}t, \qquad u' = \frac{u-l}{d-l} \tag{2.1.3}$$

which reduces (2.1.2) to

$$\alpha^2 \frac{d^2u}{dt^2} + \frac{du}{dt} + u = \frac{\lambda}{(1-u)^2}. \tag{2.1.4}$$

after dropping the primes where

$$\alpha = \frac{\sqrt{mk}}{a}, \qquad \lambda = \frac{1}{2}\frac{\epsilon_0 A V^2}{k(d-l)^3}. \tag{2.1.5}$$

The parameter α is known in engineering parlance as the quality factor or Q for the system. The quality factor compares the rate at which a system oscillates to the rate at which it dissipates energy. In a viscosity dominated system, a small value of Q is to expected corresponding to a system in which oscillatory behavior is quickly damped out. The parameter λ, proportional to V^2, is a ratio of electrostatic forces to spring forces and acts as a natural bifurcation parameter for the system.

By setting time derivatives to zero in equation (2.1.2), the equilibrium spacing of the plates is shown to satisfy $\lambda = u(1-u)^2$ where physical constraints fix $0 \leq u < 1$. The steady state defections are readily determined from this relationship and conveniently displayed in the bifurcation diagram, Fig. 2.2.

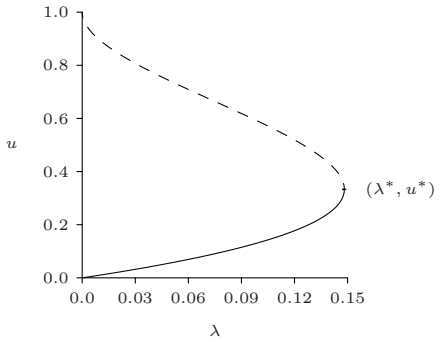

Figure 2.2: Bifurcation diagram of steady state solutions to equation (2.1.2). A saddle-node or fold bifurcation is observed at the point $(\lambda^*, u^*) = (4/27, 1/3)$ with a stable (solid) and an unstable (dashed) solution branch emanating from the bifurcation point.

From the bifurcation diagram, it is observed that for a certain range of λ, there exists one stable and one unstable branch (linear stability is easily determined). It is also observed that when λ is increased beyond some critical value λ^*, a steady state deflection is no longer achieved and therefore the top plate will touchdown on the ground plate. The location of this saddle-node or fold bifurcation is determined by the condition $du/d\lambda = 0$ and found to be $\lambda^* = 4/27$ with a corresponding $u^* = 1/3$. In

terms of dimensional quantities, this bifurcation point is given by

$$u^* = \frac{1}{3}(d-l), \qquad V^* = \sqrt{\frac{8}{27}\frac{k(d-l)^3}{\epsilon_0 A}}.$$

The assumption that the deflection of the plate is a function of time alone allows a tractable analysis of the steady state problem, although, it cannot take into account the geometry or the elastic properties of the deflecting plate. Despite these shortcomings, the model is still useful as it predicts qualitative properties of the device including touchdown for voltages above the critical V^*; a quantity for which a compact expression is provided.

2.2 A Model From Linear Elasticity

To better accommodate the geometry and elastic nature of the deflecting plate, Pelesko [33] developed a model which coupled equations of linear elasticity with those of electrostatics. In addition, a spatially varying dielectric permittivity profile $\epsilon_1(x,y)$ in the deflecting plate is accounted for, which in turn requires that a potential ϕ_1 be determined in the gap and another potential ϕ_2 determined inside the plate. In dimensional form, the model requires that the deflection $u(x,y,t)$ of a plate occupying a region $\Omega \subset \mathbb{R}^2$ with smooth boundary $\partial\Omega$, satisfies

$$\rho h \frac{\partial^2 u}{\partial t^2} + a\frac{\partial u}{\partial t} + D\,\Delta_\perp^2 u - T\,\Delta_\perp u = -\frac{\epsilon_1}{2}|\nabla\phi_2|^2, \qquad z = u(x,y,t) - h/2 \tag{2.2.1}$$

$$\Delta\phi_1 = 0, \qquad 0 < z < u(x,y,t) - h/2 \tag{2.2.2}$$

$$\nabla\cdot(\epsilon_1\nabla\phi_2) = 0 \qquad |z - u(x,y,t)| < h/2, \tag{2.2.3}$$

The potential at the ground plate is zero and a voltage V is applied on the top of the upper plate so that

$$\phi_1(0) = 0, \tag{2.2.4}$$

$$\phi_2(u + h/2) = V. \tag{2.2.5}$$

The specification of the potential is completed by demanding continuous differentiability at the boundary of the gap and upper plate. Therefore

$$\phi_1 = \phi_2, \qquad \epsilon_1\nabla\phi_2\cdot\hat{\boldsymbol{n}} = \epsilon_0\nabla\phi_1\cdot\hat{\boldsymbol{n}} \qquad z = u(x,y,t) - h/2 \tag{2.2.6}$$

where $\hat{\boldsymbol{n}}$ is the normal vector to the surface $z = u(x, y, t) - h/2$. In equation (2.2.1), D is the flexural rigidity, ρ and h are the density and thickness of the deflecting plate respectively while T represents the tension on the plate. The value of a reflects the strength of damping in the system while ϵ_0 is the permittivity of free space. The subscript $\perp$ indicates differentiation restricted to the xy plane. Specifically, we have

$$\Delta \equiv \frac{\partial^2}{\partial x^2} + \frac{\partial^2}{\partial y^2} + \frac{\partial^2}{\partial z^2}, \qquad \Delta_\perp \equiv \frac{\partial^2}{\partial x^2} + \frac{\partial^2}{\partial y^2}, \qquad \nabla \equiv \left(\frac{\partial}{\partial x}, \frac{\partial}{\partial y}, \frac{\partial}{\partial z} \right).$$

There are several options for the conditions satisfied by $u(x, y, t)$ on the boundary $\partial\Omega$, though a common requirement is that the plate is clamped which requires

$$u = d, \quad \partial_n u = 0, \qquad (x, y) \in \partial\Omega \tag{2.2.7}$$

where $\partial_n u$ is the outward facing normal derivative with respect to $\partial\Omega$.

The problem may be decoupled by taking advantage of the small aspect ratio $\sigma \equiv d/L$. Focusing on the equations for the potential for now, non-dimensionalize with

$$x' = \frac{x}{L} \quad y' = \frac{y}{L} \quad z' = \frac{z}{d}, \quad u' = \frac{u}{d}, \quad \phi_1' = \frac{\phi_1}{V}, \quad \phi_2' = \frac{\phi_2}{V}, \tag{2.2.8}$$

gives after dropping primes,

$$\frac{\partial^2 \phi_1}{\partial z^2} + \sigma^2 \left(\frac{\partial^2 \phi_1}{\partial x^2} + \frac{\partial^2 \phi_1}{\partial y^2} \right) = 0, \qquad 0 < z < u - \frac{h}{2d} \tag{2.2.9}$$

$$\epsilon_1 \frac{\partial^2 \phi_2}{\partial z^2} + \sigma^2 \left(\frac{\partial}{\partial x} \left(\epsilon_1 \frac{\partial \phi_2}{\partial x} \right) + \frac{\partial}{\partial y} \left(\epsilon_1 \frac{\partial \phi_2}{\partial y} \right) \right) = 0, \qquad |z - u| < \frac{h}{2d} \tag{2.2.10}$$

with continuous differentiability enforced by

$$\phi_1 = \phi_2, \qquad \epsilon_1 \frac{\partial \phi_2}{\partial z} - \epsilon_0 \frac{\partial \phi_1}{\partial z} = \sigma^2 \left(\epsilon_1 \left(\frac{\partial u}{\partial x} \frac{\partial \phi_2}{\partial x} + \frac{\partial u}{\partial y} \frac{\partial \phi_2}{\partial y} \right) - \epsilon_0 \left(\frac{\partial u}{\partial x} \frac{\partial \phi_1}{\partial x} + \frac{\partial u}{\partial y} \frac{\partial \phi_1}{\partial y} \right) \right) \tag{2.2.11}$$

when $z = u - h/2d$. Solving this system to leading order (*i.e.* $\sigma \ll 1$) reveals that the potential is well approximated by a linear function of z in each region. Applying the relevant boundary and continuity conditions this potential is found to be

$$\phi = \begin{cases} \dfrac{\epsilon_1 z}{\epsilon_1 (u - h/2d) + \epsilon_0 (h/d)} & 0 < z < u - h/2d \\ 1 + \dfrac{\epsilon_0 (z - (u + h/2d))}{\epsilon_1 (u - h/2d) + \epsilon_0 h/d} & u - h/2d < z < u + h/2d \end{cases} \tag{2.2.12}$$

With this explicit representation of ϕ, the right hand side of equation (2.2.1) satisfies

$|\nabla\phi_2| = (\partial_z\phi_2)^2 + \mathcal{O}(\sigma^2)$ on $z = u - h/2d$ where

$$\partial_z\phi_2 = \frac{\epsilon_0}{\epsilon_1(u - h/2d) + \epsilon_0 h/d}$$

By applying the thin plate limit, $h/d \to 0$, this expression simplifies to

$$\partial_z\phi_2 = \frac{\epsilon_0}{\epsilon_1 u}$$

Finally, a time scale dominated by viscous effects, $t = k/a$, is chosen and so (2.2.1) can be written in non dimensional form as

$$\alpha^2\frac{\partial^2 u}{\partial t^2} + \frac{\partial u}{\partial t} + \delta\Delta_\perp^2 u - \Delta_\perp u = -\frac{\lambda f(x,y)}{u^2} \tag{2.2.13}$$

with boundary conditions

$$u = 1, \quad \partial_n u = 0, \qquad (x,y) \in \partial\Omega \tag{2.2.14}$$

The dimensionless quantities α, δ, λ and $f(x,y)$ are defined as follows:

$$\alpha = \frac{\sqrt{T\rho h}}{aL}, \quad \delta = \frac{D}{TL^2}, \quad \lambda = \frac{\epsilon_0 L^2 V^2}{2d^3 T}, \quad f(x,y) = \frac{\epsilon_0}{\epsilon_1(x,y)} \tag{2.2.15}$$

where α is the quality factor for the system, δ measures the relative importance of tension and rigidity, λ is a ratio of electrostatic and elastic forces in the system while $f(x,y)$ is the permittivity of the plate relative to that of free space. The parameter λ is proportional to the square of the applied voltage, V^2, and because the operation of a MEMS device may necessitate V varying over some range, λ is a natural bifurcation parameter for the system. In addition, it should be noted that $\lambda \geq 0$ for all physical situations.

For the convenience of homogeneous boundary conditions, the transformation $u \mapsto 1+u$ is made and the $\perp$ notation is dropped as all differentiation is now restricted to the xy plane. The three dimensional problem has now been reduced to a two dimensional problem where $z = u(x,y)$ and

$$\alpha^2\frac{\partial^2 u}{\partial t^2} + \frac{\partial u}{\partial t} + \delta\Delta^2 u - \Delta u = -\frac{\lambda f(x,y)}{(1+u)^2} \quad (x,y) \in \Omega; \qquad u = \partial_n u = 0 \quad (x,y) \in \partial\Omega \tag{2.2.16}$$

The focus of our attention is further restricted to the case of small quality factor for which the $\alpha^2 u_{tt}$ term in (2.2.16) is considered negligible. This approximation, called the viscous damping limit, assumes that inertial effects are negligible compared to those of damping. By providing some initial data $u_0(x,y)$ at time $t = 0$ the deflection $z =$

$u(x,y,t)$ of the upper plate occupying a region $\Omega \subset \mathbb{R}^2$ with smooth boundary $\partial\Omega$ satisfies

$$\frac{\partial u}{\partial t} = -\delta\Delta^2 u + \Delta u - \frac{\lambda f(x,y)}{(1+u)^2}, \quad (x,y) \in \Omega; \qquad \begin{array}{c} u = \partial_n u = 0, \quad (x,y) \in \partial\Omega \\ u(x,y,0) = u_0(x,y), \quad (x,y) \in \Omega \end{array} \tag{2.2.17}$$

Equation (2.2.17) represents a model for electrostatically actuated MEMS devices in its most general form. In subsequent studies of this equation, further simplifications have been employed to reduce the complexity and permit more ready analysis. In the original work of Pelesko ([33]), the approximations $\delta = 0$ and $f(x,y) = 1$ were adopted, thus approximating the deflecting plate as a membrane with a homogeneous dielectric profile. Omitting the boundary condition $\partial_n u = 0$ on $\partial\Omega$, the reduced equation is

$$\frac{\partial u}{\partial t} = \Delta u - \frac{\lambda}{(1+u)^2}, \quad (x,y) \in \Omega; \quad u = 0, \quad (x,y) \in \partial\Omega; \quad u(x,y,0) = u_0(x,y). \tag{2.2.18}$$

Steady state and dynamical solutions to equation (2.2.18) have received significant attention recently and have been shown to exhibit a rich collection of mathematical phenomena [33],[13],[9]. In §3.1, some preliminary results on the steady state equation

$$\Delta u = \frac{\lambda}{(1+u)^2}, \quad (x,y) \in \Omega; \quad u = 0, \quad (x,y) \in \partial\Omega \tag{2.2.19}$$

are presented.

Another interesting variation of the basic membrane equation (2.2.18) is the so-called *fringing fields* problem, introduced in [38]. In this problem, the radially symmetric deflection of a membrane with homogeneous dielectric permittivity profile ($f(x,y) = 1$) is considered in a drum shaped device $(r,z) \in [0,L] \times [0,d]$. The formulation of this problem requires careful determination of the electric potential in the gap up to and including the $\mathcal{O}(\sigma^2)$ term. The equation for the potential in the gap, in dimensionless variables, is

$$\frac{\partial^2\phi}{\partial z^2} + \sigma^2\left(\frac{\partial^2\phi}{\partial r^2} + \frac{1}{r}\frac{\partial\phi}{\partial r}\right) = 0, \quad (r,z) \in [0,1] \times [0,1]; \qquad \begin{array}{c} \phi(1,z) = 0 \\ \phi(r,1) = 1, \ \phi(r,0) = 0 \end{array} \tag{2.2.20}$$

To satisfy the condition at $r = 1$, a local analysis in the vicinity of the boundary is required. After a little work, the following uniformly valid asymptotically approximation

of ϕ is obtained

$$\phi(r,z) = \frac{z}{u(r)} + \frac{2}{\pi}\sum_{n=1}^{\infty}\frac{(-1)^n}{n}e^{-n\pi(\frac{1-r}{\sigma})}\sin(n\pi z) \tag{2.2.21}$$

as so

$$|\nabla\phi^2|_{z=u} = \left(\frac{\partial\phi}{\partial z}\right)^2\Big|_{z=u} + \sigma^2\left(\frac{\partial\phi}{\partial r}\right)^2\Big|_{z=u} = \frac{1+\sigma^2\,u'^2}{u^2} + \cdots$$

This leads to the following model for the equilibrium deflection of a membrane MEMS device

$$\Delta u = \frac{\lambda(1+\sigma^2|\nabla u|^2)}{(1+u)^2}, \quad (x,y)\in\Omega \qquad u = 0 \quad (x,y)\in\partial\Omega$$

where, as usual, $\sigma = d^2/L^2$.

Chapter 3

Fold Point Asymptotics

This chapter breaks down as follows. In § 3.1 the methods employed to obtain numerical solutions to the various nonlinear eigenvalue problems describing MEMS, are outlined. Some of the key qualitative features of the numerical solutions are discussed. In particular, it is observed that in each of the perturbed equations; the beam (1.1.4), fringing fields (1.1.5) and the annulus (1.1.6), the location of the primary fold point, located at the end of the minimal branch, exhibits significant deviation from the unperturbed problem.

In § 3.2, an asymptotic expansion for the location of the perturbed fold point is formulated for (1.1.4) and the case $\Omega = (-1, 1)$. In the limit $\delta \to 0$, a boundary layer of width $\delta^{1/2}$ is required to enforce the derivative boundary condition which in turn provides boundary conditions to problems in the $r = \mathcal{O}(1)$ region. In § 3.3, the analysis is extended to develop an asymptotic formulation of the principal fold point for (1.1.4) on an arbitrary 2D domain. In § 3.4 the limit $\delta \to \infty$ is considered for (1.1.4) and an expansion of the fold point is developed. This case is somewhat simpler that the $\delta \to 0$ limit as only a regular expansion is required. When Ω reduces to the unit disc or unit slab, asymptotic results are verified with full numerics and interestingly, by combining the results for $\delta \to 0$ and $\delta \to \infty$, the asymptotic predictions of the fold point are observed to be accurate for the entire range $0 < \delta < \infty$.

In § 3.5, similar asymptotic expansions for the principal fold point are established for the fringing field (1.1.5) and the annulus problem (1.1.6). In the annulus case, it is observed that in the limit $\delta \to 0$, the fold point is deflected by a quantity $\mathcal{O}(\log^{-1} \delta)$, indicating that a change in domain topology has a significant effect on the onset of the pull-in instability.

3.1 Numerical Solution Nonlinear Eigenvalue Problems

In this section, an outline of the numerical methods used to compute the bifurcation diagrams associated with the nonlinear eigenvalue problems (1.1.4), (1.1.2), (1.1.5), and (1.1.6), is provided. The results of these computations provide motivation for the asymptotic analysis in §3.2-3.5 and are useful for validating our asymptotic results.

For the membrane problem (1.1.2), the use of scale invariance as a computational

technique to compute bifurcation diagrams was explored in [34]. By introducing the new variables t and w by

$$u(r) = -1 + \alpha w(y)\,, \qquad y = \eta r\,,$$

it was shown in [34] that the bifurcation diagram for (1.1.2) can be parameterized as

$$|u(0)| = 1 - \frac{1}{w(\eta)}, \qquad \lambda = \frac{\eta^2}{w^3(\eta)}, \qquad \eta > 0\,, \tag{3.1.1}$$

where $w(\eta)$ is the solution of the initial value problem

$$w'' + \frac{1}{y}w' = \frac{1}{w^2}\,, \qquad 0 < y < \eta\,; \qquad w(0) = 1\,, \quad w'(0) = 0\,. \tag{3.1.2}$$

By solving (3.1.2) numerically, the bifurcation diagram, as shown in Fig. 3.1, is obtained. For this problem, it was shown in [34] that there are an infinite number of fold points that have the limiting behaviour $|u(0)| \to 1^-$ as $\lambda \to 4/9$. A similar scale invariance method can also be used for computing solutions to the generalized membrane problem (1.1.3).

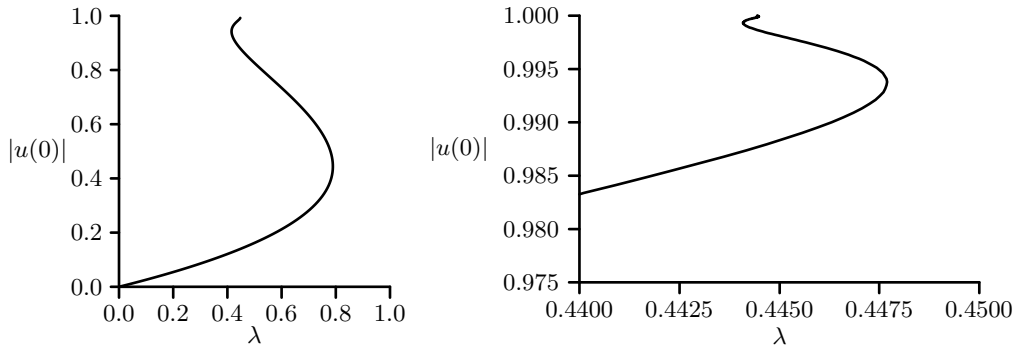

(a) Unit Disk: Membrane Problem (b) Unit Disk (Zoomed): Membrane Problem

Figure 3.1: Numerical solutions for $|u(0)|$ versus λ computed from (1.1.2) for the unit disk $\Omega = \{|x| \le 1\}$ in two-dimensions. The magnified figure on the right shows the beginning of the infinite set of fold points.

Next, the scale invariance method is extended to compute solutions to the fourth-order problem (1.1.4) for the two-dimensional unit disk. By introducing new variables v and y by

$$u = -1 + \alpha v(y)\,, \qquad y = Tr\,,$$

equation (1.1.4) becomes

$$-\delta\alpha T^4\Delta_y^2 v + \alpha T^2\Delta_y v = \frac{\lambda}{\alpha^2 v^2}\,.$$

The conditions $u'(0) = u'''(0) = 0$ imply that $v'(0) = v'''(0) = 0$. The free parameter $v(0)$ is chosen as $v(0) = 1$ so that $u(0) = -1 + \alpha$. Enforcing the boundary condition $u(1) = 0$ requires that $\alpha = 1/v(T)$, while $u'(1) = 0$ is satisfied if $v'(T) = 0$. Finally, by letting $\lambda = \alpha^3 T^4$, a parametric form of the bifurcation diagram is given by

$$|u(0)| = 1 - \frac{1}{v(T)}\,, \qquad \lambda = \frac{T^4}{v^3(T)}\,,$$

where $v(y)$ is the solution of

$$\begin{gathered} -\delta\Delta_y^2 v + \frac{1}{T^2}\Delta_y v = \frac{1}{v^2}\,, \quad 0 < y < T\,; \\ v(0) = 1\,,\ \ v'(0) = 0\,,\ \ v'''(0) = 0\,,\ \ v'(T) = 0\,. \end{gathered} \tag{3.1.3}$$

There are two options for solving (3.1.3). The first option, representing a shooting approach, consists of solving (3.1.3) as an initial value problem and choosing the value of $v''(0)$ so that $v'(T) = 0$. The second option is to solve (3.1.3) directly as a boundary value problem. For this approach it is convenient to rescale the interval to $[0, 1]$ by making the transformation $y \to Ty$, resulting in

$$\begin{gathered} -\delta\Delta_y^2 v + \Delta_y v = \frac{T^4}{v^2}\,, \quad 0 \le y \le 1\,; \\ v(0) = 1\,,\ \ v'(0) = 0\,,\ \ v'''(0) = 0\,,\ \ v'(1) = 0\,. \end{gathered} \tag{3.1.4}$$

In these variables, the bifurcation diagram for (1.1.4) is then parameterized in terms of T by

$$|u(0)| = 1 - \frac{1}{v(1)}\,, \qquad \lambda = \frac{T^4}{v^3(1)}\,, \tag{3.1.5}$$

where $v(y)$ is the solution to (3.1.4). A similar approach is used to compute the bifurcation diagram of (1.1.4) in a slab.

It is remarked that the solution of the membrane problem (1.1.2) using the scale invariance method requires that the initial value problem (3.1.2) be solved exactly once. In contrast, for the fourth-order problem (1.1.4) the solution of either (3.1.3) or (3.1.4) must be computed for each point on the bifurcation branch. However, notice that in contrast to solving (1.1.4) directly using a two-parameter shooting method, the scale invariance method leading to (3.1.3) involves only a one-parameter shooting.

In Fig. 3.2 the numerically computed bifurcation diagram of $|u(0)|$ versus λ is plot-

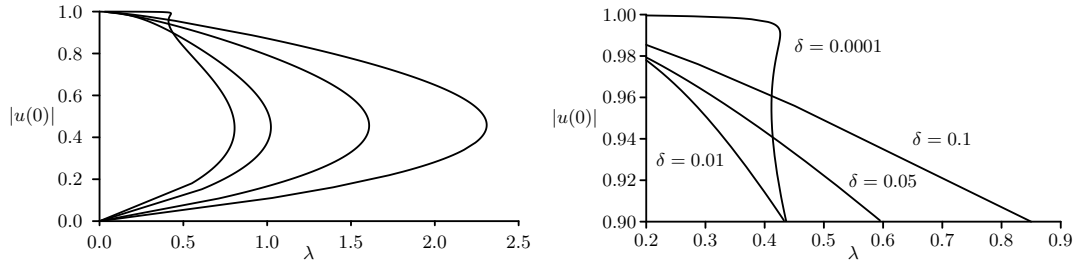

(a) Unit Disk (b) Unit Disk (Zoomed)

Figure 3.2: Numerical solutions of (1.1.4) for the unit disk $\Omega = \{|x| \leq 1\}$ for several values of δ. From left to right the solution branches correspond to $\delta = 0.0001,\ 0.01,\ 0.05,\ 0.1$. The figure on the right is a magnification of a portion of the left figure.

ted for $\Omega = \{|x| \leq 1\}$ and for various small positive values of δ. These numerical results indicate that the presence of the biharmonic term in (1.1.4) with small nonzero coefficient δ destroys the infinite fold point behaviour associated with the membrane problem (1.1.2) shown previously in Fig. 3.1. Furthermore, numerical results suggest the existence of some critical value $\delta_c \ll 1$, such that for $\delta > \delta_c$ equation (1.1.4) exhibits either zero, one, or two, solutions, with the resulting bifurcation diagram having only one fold point at the end of the minimal solution branch. In §3.3 an asymptotic expansion of the fold point at the end of the minimal solution branch for (1.1.4) in powers of $\delta^{1/2}$ for $\delta \ll 1$ is developed. In §3.2 the corresponding problem in the unit slab is considered. In §3.4 an asymptotic expansion of the fold point for (1.1.4) when $\delta \gg 1$ for both the unit disk and the unit slab is constructed.

To numerically compute the bifurcation diagram associated with the fringing-field problem (1.1.5) in the unit disk the numerically observed fact that the solution can be uniquely characterized by the value of $u(0)$ is exploited. By assigning a range of values to $u(0)$ in the interval $(-1, 0)$, (1.1.5) is solved as an initial value problem and the value of λ is uniquely determined by the zero of $g(\lambda) = u(1; \lambda)$. A Newton iteration scheme is implemented on $g(\lambda)$ with initial guess $u(0) = \lambda = 0$. This method was found to be effective provided the stepsize in $u(0)$ is sufficiently small.

In order to numerically treat the annulus problem (1.1.6) it is advantageous to rescale the domain to $[0, 1]$ with the change of variables $\rho = (r - \delta)/(1 - \delta)$. Then (1.1.6) transforms to

$$\frac{d^2u}{d\rho^2} + \frac{(1-\delta)}{\delta + (1-\delta)\rho}\frac{du}{d\rho} = \frac{\lambda(1-\delta)^2}{(1+u)^2}\,, \quad 0 < \rho < 1\,; \qquad u(0) = u(1) = 0\,. \tag{3.1.6}$$

In a way similar to the numerical approach for the fringing-fields problem (1.1.5), solutions to (3.1.6) are computed at predetermined values of $u'(0) < 0$ so that (3.1.6)

becomes an initial value problem. The value of λ is then fixed by the unique zero of $g(\lambda) = u(1;\lambda)$, which is computed using Newton's method.

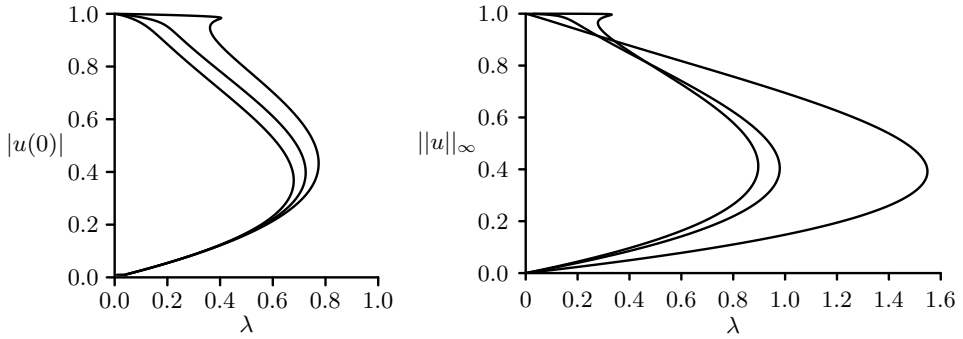

(a) Unit Disk: Fringing Field (b) Annulus

Figure 3.3: Left figure: Numerical solutions for $|u(0)|$ versus λ computed from the fringing-field problem (1.1.5) for the unit disk $\Omega = \{|x| \leq 1\}$ with, from left to right, $\delta = 1, 0.5,\ 0.1$. Right figure: Numerical solutions for $||u||_\infty$ versus λ computed from (1.1.6) in the annulus $\delta < r < 1$ with, from left to right, $\delta = 0.00001,\ 0.001,\ 0.1$.

The numerically computed bifurcation diagrams for the fringing-fields problem (1.1.5) and the annulus problem (1.1.6) are plotted in Fig. 3.3(a) and Fig. 3.3(b), respectively, for various values of δ. It is again observed that, for δ small, that the effect of the perturbation is to destroy the infinite fold point behaviour associated with the membrane problem (1.1.2). In §3.5 asymptotic results for the location of the fold point at the end of the minimal solution branch are given for (1.1.5) and (1.1.6) when $\delta \ll 1$.

A straightforward approach to compute solutions to (1.1.4), (1.1.5), and (1.1.6), is to solve the underlying ODE boundary value problems by using a standard boundary value solver such as COLSYS [1]. This approach works well provided that the bifurcation diagram can be parameterized in terms of the coordinate on the vertical axis of the bifurcation diagram, such as $u(0)$. Then, the BVP solver can be formulated to solve for $u(x)$ and λ.

Next, a more general approach to the numerical solution of the bifurcation branch of (1.1.4) is described, which also applies to a multi-dimensional domain Ω. For the unit square $\Omega = [0,1] \times [0,1]$, (1.1.4) is not amenable to the scale invariance technique and a more general approach based on pseudo-arclength continuation (cf. [24]) is required. This method takes a direct approach to compute solutions of the general problem

$$f : \mathbb{R}^n \times \mathbb{R} \to \mathbb{R}^n, \qquad f(u,\lambda) = 0\,. \tag{3.1.7}$$

Starting with an initial solution (u_0, λ_0), the method seeks to determine a sequence of

points (u_j, λ_j) which satisfy (3.1.7) to within some specified tolerance.

The following is a brief outline of this method based on [24]. In order to compute solutions around fold points at which the system has a singular jacobian and the bifurcation curve has a vertical tangent, the method introduces a parameterization of the curve $n(u(s), \lambda(s), ds) = 0$ in terms of an arclength parameter s and seeks new points on the solution branch at predetermined values of the steplength ds. To choose $n(u(s), \lambda(s), ds) = 0$, consider some accepted point (u_j, λ_j) and its tangent vector to the curve at that point $(\dot{u}_j, \dot{\lambda}_j)$, where an overdot represents differentiation with respect to arclength s. Now, define

$$n(u(s), \lambda(s), ds) = \dot{u}_j^T \cdot (u - u_j) + \dot{\lambda}_j(\lambda - \lambda_j) - ds\,, \tag{3.1.8}$$

as the hyperplane whose normal vector is $(\dot{u}_j, \dot{\lambda}_j)$ and whose perpendicular distance from (u_j, λ_j) is ds. The intersection of this hyperplane with the bifurcation curve will be non-zero provided the curvature of the branch and ds are not too large. With this specification of n, the pseudo-arclength continuation method seeks a solution to the augmented system

$$f(u(s), \lambda(s)) = 0\,, \qquad n(u(s), \lambda(s), s) = 0\,, \tag{3.1.9}$$

which is non-singular at simple fold points (cf. [24]). Applying Newton's method with initial guess (u_j, λ_j) to the solution of (3.1.9) results in the following iteration scheme:

$$\begin{pmatrix} f_u(u^{(k)}, \lambda^{(k)}) & f_\lambda(u^{(k)}, \lambda^{(k)}) \\ \dot{u}_j^T & \dot{\lambda}_j \end{pmatrix} \begin{pmatrix} \Delta u \\ \Delta\lambda \end{pmatrix} = - \begin{pmatrix} f(u^{(k)}, \lambda^{(k)}) \\ n(u^{(k)}, \lambda^{(k)}) \end{pmatrix}$$
$$u^{(k+1)} = u^{(k)} + \Delta u \tag{3.1.10}$$
$$\lambda^{(k+1)} = \lambda^{(k)} + \Delta\lambda \quad .$$

By differentiating (3.1.7) with respect to λ and solving the resulting linear system $f_u u_\lambda + f_\lambda = 0$, the tangent vector $(\dot{u}, \dot{\lambda})$ is specified as

$$\dot{u} = a u_\lambda, \quad \dot{\lambda} = a, \qquad a = \frac{\pm 1}{\sqrt{1 + ||u_\lambda||_2^2}}.$$

The sign of a is chosen to preserve the direction in which the branch is traversed.

To compute solutions of (1.1.4) by the pseudo-arclength method in the unit square $\Omega = [0,1] \times [0,1]$, the partial derivatives are approximated by central finite difference quotients, which results in a large system of nonlinear equations. In Fig. 3.4(b) the numerically computed bifurcation diagram for (1.1.4) in the unit square is plotted for

several values of δ. The computations were done with a uniform mesh-spacing of $h = 1/100$ in the x and y directions. The bifurcation diagram is similar to that of the unit disk shown in Fig. 3.2(a). In Fig. 3.4(a) the corresponding numerical bifurcation diagram for (1.1.4) in the one-dimensional unit slab is plotted.

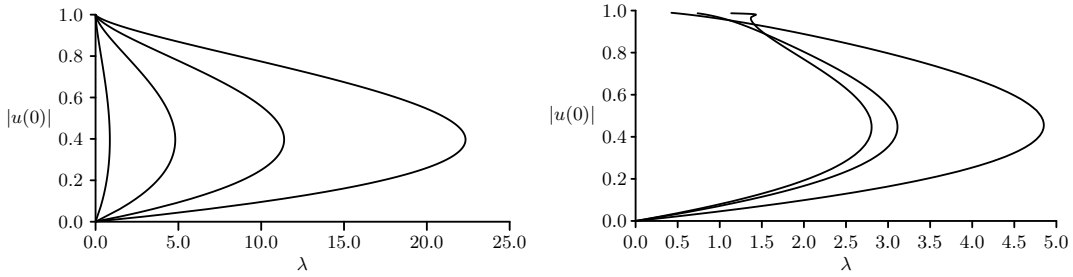

(a) Unit Slab (b) Unit Square

Figure 3.4: Numerical solutions of (1.1.4) for the slab $0 < x < 1$ (left figure) and the unit square for several values of δ. From left to right the solution branches correspond to $\delta = 0.1$, 1.0, 2.5, 5.0 (left figure) and $\delta = 0.0001$, 0.001, 0.01 (right figure).

A quantitative asymptotic theory describing the destruction of the infinite fold points for (1.1.2) when (1.1.2) is perturbed for $0 < \delta \ll 1$ to either the biharmonic problem (1.1.4), the fringing-field problem (1.1.5), or the annulus problems (1.1.6), is given in Ch. 4. This is done by constructing the limiting form of the bifurcation diagram when $||u||_\infty = 1 - \varepsilon$, where $\varepsilon \to 0^+$. Asymptotic results for the limiting behaviour $\lambda \to 0$ and $\varepsilon \to 0$ of the maximal solution branch are also presented for these perturbed problems.

3.1.1 Simple Upper Bounds For λ_c

In the case where Ω represents either the unit slab or the unit disk, a simple upper bound for the fold point location at the end of the minimal solution branch, λ_c, is obtained for (1.1.4). The existence of this bound demonstrates that λ_c is finite and provides a rather good estimate of its value. The bound is established in terms of the principal eigenvalue of the differential operator appearing on the left hand side of (1.1.4). Therefore the associated eigenvalue problem requires the determination of a function ϕ and a scalar μ such that

$$-\delta\Delta^2\phi + \Delta\phi = -\mu\phi\,, \quad x \in \Omega\,; \qquad \phi = \partial_n\phi = 0\,, \quad x \in \partial\Omega\,. \tag{3.1.11}$$

When Ω is either the unit slab or the unit disk the positivity of the first eigenfunction ϕ_0 is verified numerically from the explicit formulae for ϕ_0 given below in (3.1.16) and (3.1.17). Owing to the lack of a maximum principle, the positivity of the first

eigenfunction for (3.1.11) is not guaranteed for more general domains. In particular, for domains such as squares or rectangles or annuli, the principle eigenfunction of the limiting problem $\delta \to \infty$ in (3.1.11) is known to change sign (cf. [6], [7]). For a survey of such results see [39]. Therefore, the following discussion is limited to either the unit slab or the unit disk.

To derive an upper bound for λ_c, the approach in [34] needs to be modified only slightly. We assume that u exists and use Green's second identity on u and the principal eigenfunction ϕ_0 and eigenvalue μ_0 of (3.1.11) to obtain

$$0 = \delta \int_\Omega \left(-\phi_0 \Delta^2 u + u \Delta^2 \phi_0\right)\, dx = \int_\Omega \phi_0 \left(\frac{\lambda}{(1+u)^2} + \mu_0 u\right)\, dx - \int_\Omega \left(\phi_0 \Delta u - u \Delta \phi_0\right)\, dx\,. \tag{3.1.12}$$

The second integral on the right-hand side of (3.1.12) vanishes identically, and so a necessary condition for a solution to (1.1.4) is that

$$\int_\Omega \phi_0 \left(\frac{\lambda}{(1+u)^2} + \mu_0 u\right)\, dx = 0\,. \tag{3.1.13}$$

Since $\phi_0 > 0$, then there is no solution to (3.1.13) when

$$\frac{\lambda}{(1+u)^2} + \mu_0 u > 0, \quad \forall u > -1\,. \tag{3.1.14}$$

By considering the point at which the inequality (3.1.14) ceases to hold, it is clear that there is no solution to (1.1.4) when $\lambda > 4\mu_0/27$ and therefore

$$\lambda_c \le \bar{\lambda} \equiv \frac{4\mu_0}{27}\,, \tag{3.1.15}$$

where μ_0 is the first eigenvalue of (3.1.11).

For the unit slab $0 < x < 1$, a simple calculation shows that the eigenfunctions of (3.1.11) are given up to a scalar multiple by

$$\phi = \cosh(\xi_1 x) - \cos(\xi_2 x) - \left(\frac{\xi_2 \sinh(\xi_1 x) - \xi_1 \sin(\xi_2 x)}{\xi_2 \sinh \xi_1 - \xi_1 \sin \xi_2}\right)\left(\cosh \xi_1 - \cos \xi_2\right)\,. \tag{3.1.16a}$$

Here $\xi_1 > 0$ and $\xi_2 > 0$ are defined in terms of μ by

$$\xi_1 = \sqrt{\frac{1+\sqrt{1+4\mu\delta}}{2\delta}}\,, \quad \xi_2 = \sqrt{\frac{-1+\sqrt{1+4\mu\delta}}{2\delta}}\,, \tag{3.1.16b}$$

where the eigenvalues μ are the roots of the transcendental equation

$$2\xi_1 + \left(\frac{\xi_1^2 - \xi_2^2}{\xi_2}\right)\sin \xi_2 \sinh \xi_1 - 2\xi_1 \cosh \xi_1 \cos \xi_2 = 0\,. \tag{3.1.16c}$$

	Slab		Unit Disc	
δ	$\bar{\lambda}$	λ_c	$\bar{\lambda}$	λ_c
0.25	20.3576	19.249	4.886	4.395
0.5	38.900	36.774	8.754	7.871
1.0	75.979	71.823	16.486	14.826
2.0	150.137	141.918	31.948	28.704

Table 3.1: Upper bounds, $\bar{\lambda}$, for the fold point location given in (3.1.15) compared with the numerically computed fold point location λ_c of (1.1.4).

Similarly, for the unit disk $0 < r < 1$, the eigenfunctions are given up up to a scalar multiple by

$$\phi = J_0(\xi_2 r) - \frac{J_0(\xi_2)}{I_0(\xi_1)} I_0(\xi_1 r)\,, \tag{3.1.17a}$$

where J_0 and I_0 are the Bessel and modified Bessel functions of the first kind of order zero, respectively. The eigenvalues μ are the roots of the transcendental equation

$$\xi_1 I_1(\xi_1) + \xi_2 \frac{I_0(\xi_1)}{J_0(\xi_2)} J_1(\xi_2) = 0\,, \tag{3.1.17b}$$

where $J_1(\rho) = -J_0'(\rho)$ and $I_1(\rho) = I_0'(\rho)$.

The first root of (3.1.16c) and (3.1.17b) corresponding to the principle eigenvalue, μ_0, of (3.1.11) is readily computed using Newton's method as a function of $\delta > 0$. Then, the corresponding principal eigenfunction ϕ_0 from either (3.1.16a) or (3.1.17a) can be readily verified numerically to have one sign on Ω. Then, in terms of μ_0, (3.1.15) gives an explicit upper bound for λ_c. These bounds for λ_c together with the full numerical results for λ_c are compared in Table 3.1. From this table it is observed that the upper bound provides is actually relatively close to the true location for the fold point.

3.2 Biharmonic Nonlinear Eigenvalue Problem: Slab Geometry

In this section an asymptotic expansion for the fold point at the end of the minimal solution branch for (1.1.4) is developed in a slab domain. This fold point determines the onset of the pull-in instability, and hence its determination is important in the actual design of a MEMS device.

In a slab domain (1.1.4) becomes

$$-\delta u'''' + u'' = \frac{\lambda}{(1+u)^2}\,, \quad 0 < x < 1\,; \qquad u(0) = u(1) = u'(0) = u'(1) = 0\,. \quad (3.2.1)$$

In the limit $\delta \ll 1$, (3.2.1) is a singular perturbation problem for which the solution u has boundary layers near both endpoints $x = 0$ and $x = 1$. The width of these boundary layers is found below to be $\mathcal{O}(\delta^{1/2})$, which motivates an asymptotic expansion for the fold point location in powers of $\mathcal{O}(\delta^{1/2})$. Therefore, in the outer region defined away from $\mathcal{O}(\delta^{1/2})$ neighborhoods of both endpoints, u and λ are expanded as

$$u = u_0 + \delta^{1/2}u_1 + \delta u_2 + \cdots\,, \qquad \lambda = \lambda_0 + \delta^{1/2}\lambda_1 + \delta\lambda_2 + \cdots\,. \quad (3.2.2)$$

Upon substituting (3.2.2) into (3.2.1), and collecting powers of $\delta^{1/2}$, the following sequence of problems is obtained

$$u_0'' = \frac{\lambda_0}{(1+u_0)^2}\,, \qquad 0 < x < 1\,, \quad (3.2.3a)$$

$$\mathcal{L}u_1 = \frac{\lambda_1}{(1+u_0)^2}\,, \qquad 0 < x < 1\,, \quad (3.2.3b)$$

$$\mathcal{L}u_2 = \frac{\lambda_2}{(1+u_0)^2} - \frac{2\lambda_1 u_1}{(1+u_0)^3} + \frac{3\lambda_0 u_1^2}{(1+u_0)^4} + u_0''''\,, \qquad 0 < x < 1\,. \quad (3.2.3c)$$

Here $\mathcal{L}$ is the linear operator defined by

$$\mathcal{L}\phi \equiv \phi'' + \frac{2\lambda_0}{(1+u_0)^3}\phi\,. \quad (3.2.4)$$

Next, appropriate boundary conditions for u_0, u_1 and u_2 as $x \to 0$ and $x \to 1$ are determined. These conditions are obtained by matching the outer solution to boundary layer solutions defined in the vicinity of $x = 0$ and $x = 1$.

In the boundary layer region near $x = 1$, the following inner variables y and $v(y)$ are introduced together with the inner expansion for v;

$$y = \delta^{-1/2}(x-1)\,, \qquad u = \delta^{1/2}v\,, \qquad v = v_0 + \delta^{1/2}v_1 + \delta v_2 + \cdots\,. \quad (3.2.5)$$

Upon substitution of (3.2.5) and (3.2.2) for λ into (3.2.1), powers of $\delta^{1/2}$ are collected to obtain on $-\infty < y < 0$ that

$$-v_0'''' + v_0'' = 0\,, \qquad v_0(0) = v_0'(0) = 0\,, \quad (3.2.6a)$$

$$-v_1'''' + v_1'' = \lambda_0\,, \qquad v_1(0) = v_1'(0) = 0\,, \quad (3.2.6b)$$

$$-v_2'''' + v_2'' = \lambda_1 - 2\lambda_0 v_0\,, \qquad v_2(0) = v_2'(0) = 0\,. \quad (3.2.6c)$$

The solution to (3.2.6) with no exponential growth as $y \to -\infty$ is given in terms of unknown constants c_0, c_1, and c_2, by

$$v_0 = c_0\left(-1 - y + e^y\right), \tag{3.2.7a}$$

$$v_1 = c_1\left(-1 - y + e^y\right) + \lambda_0 y^2/2\,, \tag{3.2.7b}$$

$$v_2 = c_2\left(-1 - y + e^y\right) + \lambda_1 y^2/2 + c_0\lambda_0 y\left(-1 + y + e^y + y^2/3\right). \tag{3.2.7c}$$

The matching condition to the outer solution is obtained by letting $y \to -\infty$ and substituting v_0, v_1, and v_2 into (3.2.5) for u, and then writing the resulting expression in terms of outer variables. In this way, the following matching condition as $x \to 1$ is established:

$$\begin{aligned} u \;&\sim -c_0(x-1) + \mathcal{O}((x-1)^2) + \delta^{1/2}\left[-c_0 - c_1(x-1) + \mathcal{O}((x-1)^2)\right] \\ &+\delta\left[-c_1 - (c_0\lambda_0 + c_2)(x-1) + \mathcal{O}((x-1)^2)\right] + \cdots . \end{aligned} \tag{3.2.8}$$

This matching condition not only gives appropriate boundary conditions to the outer problems for u_0, u_1, and u_2, defined in (3.2.3), but it also determines the unknown constants c_0, c_1, and c_2 in the inner solutions (3.2.7) in a recursive way. In particular, the $\mathcal{O}(\delta^0)$ term in (3.2.8) yields that $u_0 = 0$ at $x = 1$ and that c_0 is then given by $c_0 = -u_0'(1)$. The remaining $\mathcal{O}(\delta^0)$ terms in (3.2.8) then match identically as seen by using the solution u_0 to (3.2.3a). In a similar way, boundary conditions for u_1 and u_2 and formulae for the constants c_1 and c_2 are established. A similar analysis can be performed for the boundary layer region at the other endpoint $x = 0$. This analysis is identical to that near $x = 1$ since u_0, u_1 and u_2 are symmetric about the mid-line $x = 1/2$.

In this way, the following boundary conditions for (3.2.3) are obtained:

$$u_0(0) = u_0(1) = 0\,, \qquad u_1(0) = u_1(1) = u_0'(1)\,, \qquad u_2(0) = u_2(1) = u_1'(1)\,. \tag{3.2.9}$$

The constants c_0, c_1, and c_2, in (3.2.7) that are associated with the boundary layer solution near $x = 1$ are given by

$$c_0 = -u_0'(1)\,, \qquad c_1 = -u_1'(1)\,, \qquad c_2 = -u_2'(1) + \lambda_0 u_0'(1)\,, \tag{3.2.10}$$

which then determines the boundary layer solution in (3.2.7) explicitly.

Therefore, (3.2.3) for u_0, u_1, and u_2, must be solved subject to the boundary conditions as given in (3.2.9). With the introduction of $\alpha = u_0(1/2)$, a parameterization of the minimal solution branch for u_0 and λ_0 is established and the dependence $u_j = u_j(x, \alpha)$ for $j = 0, 1, 2$ follows. It is readily verified that the solution to (3.2.3b) is given by (see

Lemma 3.2 below)

$$u_1 = \frac{\lambda_1}{3\lambda_0}\,(1+u_0)\,, \tag{3.2.11}$$

where λ_1 is found by satisfying $u_1(1) = u_0'(1)$. Therefore, for $\delta \ll 1$, the following explicit two-term expansions for both the outer solution and for the global bifurcation curve $\lambda(\alpha)$ is developed:

$$\begin{aligned} u &\sim u_0(x;\alpha) + \delta^{1/2} u_0'(1,\alpha)\,[1+u_0(x,\alpha)] + \mathcal{O}(\delta)\,, \\ \lambda &\sim \lambda_0(\alpha) + 3\lambda_0(\alpha) u_0'(1,\alpha)\delta^{1/2} + \mathcal{O}(\delta)\,. \end{aligned} \tag{3.2.12}$$

It is noted that this "global" perturbation result for λ is not uniformly valid in the limit $\alpha \to -1$ corresponding to $\lambda_0 \to 0$. In this limit, the term $(1+u_0)^{-2}$ is nearly singular at $x = 1/2$, and a different asymptotic analysis is required (see § 5 of [30] and Chapter (4) of this work).

A higher-order local analysis of the bifurcation diagram near the fold point on the minimal solution branch is now constructed. This minimal solution branch for u_0 is well-known to have a fold point at $\alpha = \alpha_0 \approx -0.389$ at which $\lambda_c \equiv \lambda_0(\alpha_0) \approx 1.400$. This point determines the pull-in voltage for the unperturbed problem. To determine the location of the fold point for the perturbed problem, expand $\alpha(\delta) = \alpha_0 + \delta^{1/2}\alpha_1 + \delta\alpha_2$, where α_j is determined by the condition that $d\lambda/d\alpha = 0$ is independent of δ. Defining $\lambda_c(\delta) = \lambda(\alpha(\delta),\delta)$, the expansion of the fold point for (3.2.1) when $\delta \ll 1$ is determined to be

$$\lambda_c = \lambda_{0c} + \delta^{1/2}\lambda_1(\alpha_0) + \delta\left[\lambda_2(\alpha_0) - \frac{\lambda_{1\alpha}^2(\alpha_0)}{2\lambda_{0\alpha\alpha}(\alpha_0)}\right] + \mathcal{O}(\delta^{3/2})\,. \tag{3.2.13}$$

Here the subscript indicates derivatives in α.

Therefore, to determine a three-term expansion for the fold point as in (3.2.13), the quantities λ_1, λ_2, $\lambda_{1\alpha}$ and $\lambda_{0\alpha\alpha}$ must be calculated at the unperturbed fold point location α_0 from the solution to (3.2.3) with boundary conditions (3.2.9). To do so, the problems for u_0 and u_1 in (3.2.3) are first differentiated with respect to α to obtain on $0 < x < 1$ that

$$\mathcal{L}u_{0\alpha} = \frac{\lambda_{0\alpha}}{(1+u_0)^2}\,, \tag{3.2.14a}$$

$$\mathcal{L}u_{0\alpha\alpha} = \frac{\lambda_{0\alpha\alpha}}{(1+u_0)^2} - \frac{4\lambda_{0\alpha}u_{0\alpha}}{(1+u_0)^3} + \frac{6\lambda_0 u_{0\alpha}^2}{(1+u_0)^4}\,, \tag{3.2.14b}$$

$$\mathcal{L}u_{1\alpha} = \frac{\lambda_{1\alpha}}{(1+u_0)^2} - \frac{2\lambda_1 u_{0\alpha}}{(1+u_0)^3} - \frac{2\lambda_{0\alpha}u_1}{(1+u_0)^3} + \frac{6\lambda_0 u_1 u_{0\alpha}}{(1+u_0)^4}\,. \tag{3.2.14c}$$

Here $\mathcal{L}$ is the linear operator defined in (3.2.4). At the unperturbed fold location

$\alpha = \alpha_0$, where $\lambda_{0\alpha} = 0$, the function $u_{0\alpha}$ is a nontrivial solution satisfying $\mathcal{L}u_{0\alpha} = 0$. Therefore, $\lambda_1(\alpha_0)$, $\lambda_2(\alpha_0)$, $\lambda_{0\alpha\alpha}(\alpha_0)$, and $\lambda_{1\alpha}(\alpha_0)$, can be calculated by applying a Fredholm solvability condition to each of (3.2.3b), (3.2.3c), (3.2.14b), and (3.2.14c), respectively. Upon applying Lagrange's identity to (3.2.14a) and (3.2.3b) at $\alpha = \alpha_0$, the following equality is established:

$$\int_0^1 u_{0\alpha}\mathcal{L}u_1\,dx = \int_0^1 u_1\mathcal{L}u_{0\alpha}\,dx = -u_1(1)u'_{0\alpha}(1) + u_1(0)u'_{0\alpha}(0)\,.$$

Therefore, since $u_1(1) = u_1(0) = u'_0(1)$ from (3.2.9), and $u'_{0\alpha}(1) = -u'_{0\alpha}(0)$, it follows at $\alpha = \alpha_0$ that

$$\lambda_1 I = -2u'_0(1)u'_{0\alpha}(1)\,, \qquad I \equiv \int_0^1 \frac{u_{0\alpha}}{(1+u_0)^2}\,dx\,. \tag{3.2.15}$$

The integral I can be evaluated more readily using the following lemma:
Lemma 3.1: *At $\alpha = \alpha_0$, the following identity holds:*

$$I \equiv \int_0^1 \frac{u_{0\alpha}}{(1+u_0)^2}\,dx = -\frac{2}{3\lambda_0}u'_{0\alpha}(1)\,. \tag{3.2.16}$$

To prove this lemma, (3.2.14a) is first multiplied by $(1+u_0)$ and then integrated over $0 < x < 1$. Setting $\alpha = \alpha_0$, integrating by parts twice, and then using $u''_0 = \lambda_0/(1+u_0)^2$, results in the following sequence of equalities:

$$\begin{aligned} I &= -\frac{1}{2\lambda_0}\int_0^1 (1+u_0)\,u''_{0\alpha}\,\mathrm{d}x = -\frac{1}{2\lambda_0}\left[2u'_{0\alpha}(1) + \int_0^1 u_{0\alpha}u''_0\,\mathrm{d}x\right] \\ &= -\frac{u'_{0\alpha}(1)}{\lambda_0} - \frac{1}{2}\int_0^1 \frac{u_{0\alpha}}{(1+u_0)^2}\,\mathrm{d}x\,. \end{aligned}$$

This last expression gives $I = -u'_{0\alpha}(1)/\lambda_0 - I/2$ which is rearranged to yield (3.2.16), and completes the proof of Lemma 3.1.

Next, (3.2.16) is substituted into (3.2.15) and evaluated at $\alpha = \alpha_0$ to reveal that

$$\lambda_1 = 3\lambda_0 u'_0(1)\,. \tag{3.2.17}$$

This result is consistent with the global perturbation result (3.2.12) when it is evaluated at $\alpha = \alpha_0$.

The values of $\lambda_{0\alpha\alpha}$, $\lambda_{1\alpha}$, and $\lambda_{0\alpha\alpha}$, at $\alpha = \alpha_0$ can be evaluated by imposing similar solvability conditions with respect to $u_{0\alpha}$. From (3.2.14a) and (3.2.14b), and by using

(3.2.16) for I, it is readily shown at $\alpha = \alpha_0$ that

$$\lambda_{0\alpha\alpha} = \frac{9\lambda_0^2}{u'_{0\alpha}(1)} \int_0^1 \frac{u_{0\alpha}^3}{(1+u_0)^4}\, dx\,. \tag{3.2.18}$$

Next, from (3.2.14a) and (3.2.14c), we calculate at $\alpha = \alpha_0$ that

$$\int_0^1 u_{0\alpha} \mathcal{L} u_{1\alpha}\, dx = -u_{1\alpha} u'_{0\alpha}\Big|_0^1 = -2u_{1\alpha}(1) u'_{0\alpha}(1)\,.$$

Upon using (3.2.14c) for $\mathcal{L}u_{1\alpha}$ and $u_{1\alpha}(1) = u'_{0\alpha}(1)$ from (3.2.9), the expression above becomes

$$\lambda_{1\alpha} I = -\int_0^1 u_{0\alpha} \left(\frac{6\lambda_0 u_1 u_{0\alpha}}{(1+u_0)^4} - \frac{2\lambda_1 u_{0\alpha}}{(1+u_0)^3} \right) dx - 2\left[u'_{0\alpha}(1)\right]^2\,. \tag{3.2.19}$$

In a similar way, λ_2 is evaluated at $\alpha = \alpha_0$ by application of Lagrange's identity to (3.2.14a) and (3.2.3c) to obtain

$$\lambda_2 I = -\int_0^1 u_{0\alpha} \left[\frac{3\lambda_0 u_1^2}{(1+u_0)^4} - \frac{2\lambda_1 u_1}{(1+u_0)^3} + u_0'''' \right] dx - 2u'_{0\alpha}(1) u'_1(1)\,. \tag{3.2.20}$$

The formulae above for $\lambda_{1\alpha}$ and λ_2 at $\alpha = \alpha_0$, which are needed in (3.2.13), can be simplified considerably by using the following simple result:

Lemma 3.2: *At $\alpha = \alpha_0$, the solution u_1 to (3.2.3b) with $u_1(1) = u_1(0) = u_0'(1)$ is given, for any constant D, by*

$$u_1 = \frac{\lambda_1}{3\lambda_0}(1+u_0) + D u_{0\alpha}\,. \tag{3.2.21}$$

Moreover, the correction term of order $\mathcal{O}(\delta)$ in the expansion (3.2.13) of the fold point is independent of D.

The proof is by a direct calculation. Clearly u_1 solves (3.2.3b) at $\alpha = \alpha_0$ since

$$\begin{aligned} \mathcal{L}u_1 &= \frac{\lambda_1}{3\lambda_0}\mathcal{L}(1+u_0) = \frac{\lambda_1}{3\lambda_0}\left[u_0'' + \frac{2\lambda_0}{(1+u_0)^2}\right] = \frac{\lambda_1}{3\lambda_0}\left[\frac{\lambda_0}{(1+u_0)^2} + \frac{2\lambda_0}{(1+u_0)^2}\right] \\ &= \frac{\lambda_1}{(1+u_0)^2}\,. \end{aligned}$$

In addition, since $u_0(1) = 0$, then $u_1(1) = \lambda_1/3\lambda_0 = u_0'(1)$ from (3.2.17), as required by (3.2.9). Finally, a tedious but direct computation using (3.2.18), (3.2.19), and (3.2.20), shows that $\lambda_2 - \lambda_{1\alpha}^2/[2\lambda_{0\alpha\alpha}]$ at $\alpha = \alpha_0$ is independent of the constant D in (3.2.21). Therefore, the fold point correction is independent of the normalization of u_1. The details of this latter calculation are left to the reader.

Therefore, $D = 0$ is taken to get $u_1 = \lambda_1(1+u_0)/(3\lambda_0)$. Upon substitution of u_1 into (3.2.19), it is observed that the integral term on the right-hand side of (3.2.19) vanishes identically. Then, using (3.2.16) for I, the following compact formula is obtained at $\alpha = \alpha_0$:

$$\lambda_{1\alpha} = 3\lambda_0 u'_{0\alpha}(1)\,. \tag{3.2.22}$$

Reassuringly, this agrees with differentiation of (3.2.12) by α followed by evaluation at α_0. Similarly, in (3.2.20) for λ_2, one sets $u_1 = \lambda_1(1+u_0)/(3\lambda_0)$ and $u_2(1) = u'_1(1) = \lambda_1 u'_0(1)/(3\lambda_0)$, to obtain

$$\lambda_2 I = -\frac{2\lambda_1}{3\lambda_0}u'_0(1)u'_{0\alpha}(1) + \frac{\lambda_1^2}{3\lambda_0}I - \int_0^1 u_{0\alpha}u_0''''\,dx\,. \tag{3.2.23}$$

Expression (3.2.23) can be reduced further by integrating twice by parts as follows:

$$\begin{aligned}\int_0^1 u_{0\alpha}u_0''''\,dx &= -\int_0^1 u'_{0\alpha}u_0'''\,dx = -u'_{0\alpha}u_0''\Big|_0^1 + \int_0^1 u''_{0\alpha}u_0''\,dx\\ &= -2u'_{0\alpha}(1)\lambda_0 + \int_0^1\left(-\frac{2\lambda_0 u_{0\alpha}}{(1+u_0)^3}\right)\left(\frac{\lambda_0}{(1+u_0)^2}\right)dx\\ &= -2\lambda_0 u'_{0\alpha}(1) - 2\lambda_0^2\int_0^1\frac{u_{0\alpha}}{(1+u_0)^5}\,dx\,.\end{aligned}$$

Combining this last expression with (3.2.23) together with the formula for I in (3.2.16) and $\lambda_1 = 3\lambda_0 u'_0(1)$, it follows at $\alpha = \alpha_0$ that

$$\lambda_2 = 6\lambda_0\left[u'_0(1)\right]^2 - 3\lambda_0^2 - \frac{3\lambda_0^3}{u'_{0\alpha}(1)}\int_0^1\frac{u_{0\alpha}}{(1+u_0)^5}\,dx\,. \tag{3.2.24}$$

The results of the preceding calculations are summarized in the following statement:
Principal Result 3.3: *Let α_0, $\lambda_{0c} \equiv \lambda_0(\alpha_0)$ be the location of the fold point at the end of the minimal solution branch for (3.2.3a) with boundary conditions $u_0(0) = u_0(1) = 0$. Then, for the singularly perturbed problem (3.2.1), a three-term expansion for the perturbed fold point location is*

$$\lambda_c = \lambda_{0c} + 3\lambda_0\delta^{1/2}u'_0(1) + \delta\hat{\lambda}_2 + \cdots\,, \qquad \hat{\lambda}_2 \equiv \lambda_2(\alpha_0) - \frac{\lambda_{1\alpha}^2(\alpha_0)}{2\lambda_{0\alpha\alpha}(\alpha_0)}\,. \tag{3.2.25a}$$

Here $\hat{\lambda}_2$ is defined in terms of u_0 and $u_{0\alpha}$ by

$$\hat{\lambda}_2 = 6\lambda_0\left[u'_0(1)\right]^2 - 3\lambda_0^2 - \frac{3\lambda_0^3}{u'_{0\alpha}(1)}\int_0^1\frac{u_{0\alpha}}{(1+u_0)^5}\,dx - \frac{[u'_{0\alpha}(1)]^3}{2}\left(\int_0^1\frac{u_{0\alpha}^3}{(1+u_0)^4}\,dx\right)^{-1}. \tag{3.2.25b}$$

For the unit slab, the minimal solution branch for the unperturbed problem (3.2.3a) can be obtain implicitly in terms of the parameter $\alpha \equiv u_0(1/2)$. Multiply (3.2.3a) by u_0' and integrate once to obtain

$$u_0' = \sqrt{\frac{2\lambda_0}{1+\alpha}}\left(\frac{u-\alpha}{u+1}\right)^{1/2}. \tag{3.2.26}$$

A further integration using $u_0(1/2) = \alpha$ and $u_0(1) = 0$, determines $\lambda_0(\alpha)$ as

$$\begin{aligned} \lambda_0(\alpha) &= 2(1+\alpha)\left[2\int_{\sqrt{1+\alpha}}^{1} \frac{s^2\,ds}{\sqrt{s^2-(1+\alpha)}}\right]^2 \\ &= 2(1+\alpha)\left[\sqrt{-\alpha} + (1+\alpha)\log\left(\frac{1+\sqrt{-\alpha}}{\sqrt{1+\alpha}}\right)\right]^2. \end{aligned} \tag{3.2.27}$$

Upon setting $\lambda_{0\alpha} = 0$, the fold point $\alpha_0 \approx -0.389$ and $\lambda_{0c} \approx 1.400$ is determined. By using this solution the various terms needed in (3.2.25) are easily calculated. In this way, (3.2.25) leads to the following explicit three-term expansion valid for $\delta \ll 1$:

$$\lambda_c = 1.400 + 5.600\,\delta^{1/2} + 25.451\,\delta + \cdots. \tag{3.2.28}$$

In Fig. 3.5(b) a comparison of the two-term and three-term asymptotic results for λ_c versus δ from (3.2.28) is provided alongside the corresponding full numerical result computed from (1.1.4). The three-term approximation in (3.2.28) is seen to provide a reasonably accurate determination of λ_c. For $\delta = 0.01$, in Fig. 3.5(a) the two-term approximation (3.2.12) is compared with the global bifurcation curve with the full numerical result computed from (1.1.4) and from the membrane MEMS problem (1.1.2), corresponding to $\delta = 0$. It is clear that the fold point location depends rather sensitively on δ, even when $\delta \ll 1$, owing to the $\mathcal{O}(\delta^{1/2})$ limiting behaviour.

3.3 Biharmonic Nonlinear Eigenvalue Problem: Multidimensional Domain

The results of § 3.2 are now extended to the case of a bounded two-dimensional domain Ω with smooth boundary $\partial\Omega$. Equation (1.1.4) is considered in the limit $\delta \to 0$, and it is assumed that the fold point location at the end of the minimal solution branch $u_0(x,\alpha)$, $\lambda_0(\alpha)$ for the unperturbed problem

$$\Delta u_0 = \frac{\lambda_0}{(1+u_0)^2}, \qquad x \in \Omega; \qquad u_0 = 0, \quad x \in \partial\Omega, \tag{3.3.1}$$

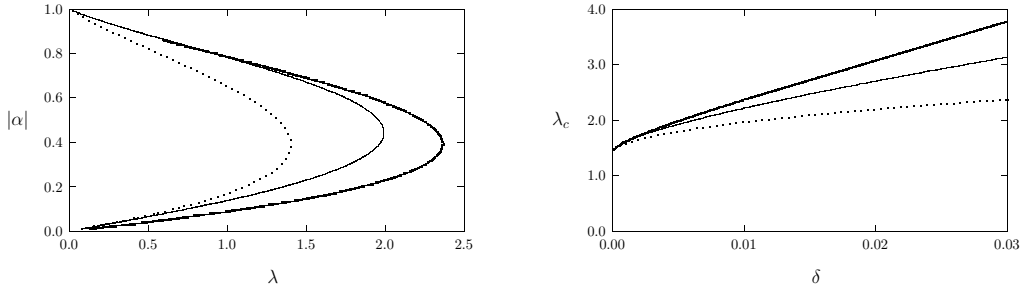

(a) $|\alpha|$ vs. λ (Unit Slab)

(b) λ_c vs. δ (Unit Slab)

Figure 3.5: Left figure: Plot of numerically computed global bifurcation diagram $|\alpha| = |u(1/2)|$ versus λ for (1.1.4) with $\delta = 0.01$ (heavy solid curve) compared to the two-term asymptotic result (3.2.12) (solid curve) and the unperturbed $\delta = 0$ membrane MEMS result from (1.1.2) (dashed curve). Right figure: Comparison of numerically computed fold point λ_c versus δ (heavy solid curve) with the two-term (dashed curve) and the three-term (solid curve) asymptotic result from (3.2.28).

has been determined. This fold point location is labeled as $\lambda_{0c} = \lambda_0(\alpha_0)$ for some $\alpha = \alpha_0$. For an arbitrary domain Ω, α can be chosen to be the L_2 norm of u_0. For the unit disk, where $u_0(r)$ is radially symmetric, it is more convenient to define α by $\alpha = u_0(0)$.

For the perturbed problem (1.1.4), λ and the outer solution for u are expanded in powers of $\delta^{1/2}$ as in (3.2.2), to obtain

$$\mathcal{L}u_1 \equiv \Delta u_1 + \frac{2\lambda_0}{(1+u_0)^3}u_1 = \frac{\lambda_1}{(1+u_0)^2}\,, \qquad x \in \Omega\,, \tag{3.3.2a}$$

$$\mathcal{L}u_2 = \frac{\lambda_2}{(1+u_0)^2} - \frac{2\lambda_1 u_1}{(1+u_0)^3} + \frac{3\lambda_0 u_1^2}{(1+u_0)^4} + \Delta^2 u_0\,, \qquad x \in \Omega\,. \tag{3.3.2b}$$

The expansion of the perturbed fold point location is again as given in (3.2.13).

To derive boundary conditions for u_1 and u_2, a boundary layer solution near $\partial\Omega$ with width $\mathcal{O}(\delta^{1/2})$ is constructed. It is advantageous to implement an orthogonal coordinate system η, s, where $\eta > 0$ measures the perpendicular distance from $x \in \Omega$ to $\partial\Omega$, whereas on $\partial\Omega$ the coordinate s denotes arclength. In terms of (η, s), (1.1.4) transforms to

$$\begin{aligned} &-\delta\left(\partial_{\eta\eta} - \frac{\kappa}{1-\kappa\eta}\partial_\eta + \frac{1}{1-\kappa\eta}\partial_s\left(\frac{1}{1-\kappa\eta}\partial_s\right)\right)^2 u \\ &+\left(\partial_{\eta\eta}u - \frac{\kappa}{1-\kappa\eta}\partial_\eta u + \frac{1}{1-\kappa\eta}\partial_s\left(\frac{1}{1-\kappa\eta}\partial_s u\right)\right) = \frac{\lambda}{(1+u)^2}\,. \end{aligned} \tag{3.3.3}$$

Here $\kappa = \kappa(s)$ is the curvature of $\partial\Omega$, with $\kappa = 1$ for the unit disk. The inner variables and the inner expansion, defined in an $\mathcal{O}(\delta^{1/2})$ neighborhood of $\partial\Omega$, are then introduced as

$$\hat{\eta} = \eta/\delta^{1/2}\,, \qquad u = \delta^{1/2} v\,, \qquad v = v_0 + \delta^{1/2} v_1 + \delta v_2 + \cdots\,. \tag{3.3.4}$$

After substituting (3.3.4) into (3.3.3) and collecting powers of δ, some lengthy but straightforward algebra produces the following sequence of problems on $-\infty < \hat{\eta} < 0$:

$$-v_{0\hat{\eta}\hat{\eta}\hat{\eta}\hat{\eta}} + v_{0\hat{\eta}\hat{\eta}} = 0\,, \qquad v_0 = v_{0\hat{\eta}} = 0\,, \quad \text{on} \quad \hat{\eta} = 0\,; \tag{3.3.5a}$$

$$-v_{1\hat{\eta}\hat{\eta}\hat{\eta}\hat{\eta}} + v_{1\hat{\eta}\hat{\eta}} = -2\kappa v_{0\hat{\eta}\hat{\eta}\hat{\eta}} + \kappa v_{0\hat{\eta}} + \lambda_0\,, \qquad v_1 = v_{1\hat{\eta}} = 0\,, \quad \text{on} \quad \hat{\eta} = 0\,, \tag{3.3.5b}$$

$$\begin{aligned} -v_{2\hat{\eta}\hat{\eta}\hat{\eta}\hat{\eta}} + v_{2\hat{\eta}\hat{\eta}} &= -2\kappa v_{1\hat{\eta}\hat{\eta}\hat{\eta}} + \kappa v_{1\hat{\eta}} - 2\kappa^2 \hat{\eta} v_{0\hat{\eta}\hat{\eta}\hat{\eta}} - \kappa^2 v_{0\hat{\eta}\hat{\eta}} + \kappa^2 \hat{\eta} v_{0\hat{\eta}} \\ &\quad + 2v_{0\hat{\eta}\hat{\eta}ss} - v_{0ss} + \lambda_1 - 2\lambda_0 v_0\,, \qquad v_2 = v_{2\hat{\eta}} = 0\,, \quad \text{on} \quad \hat{\eta} = 0\,. \end{aligned} \tag{3.3.5c}$$

The asymptotic behaviour of the solution to (3.3.5) with no exponential growth as $\eta \to -\infty$ is given in terms of unknown functions $c_0(s)$, $c_1(s)$, and $c_2(s)$ by

$$v_0 \sim -c_0 + c_0\hat{\eta}\,, \qquad v_1 \sim -c_1 + \left(c_1 - \frac{c_0\kappa}{2}\right)\hat{\eta}\,,$$

with $v_2 \sim -c_2 + \mathcal{O}(\eta)$ as $\eta \to 0$. Therefore, with $u = \delta^{1/2} v$, and by rewriting v in terms of the outer variable $\eta = \hat{\eta}\delta^{1/2}$, the following matching condition, analogous to (3.2.8), is obtained for the outer solution:

$$u \sim c_0\eta + \delta^{1/2}\left[-c_0 + \eta\left(c_1 - \frac{c_0\kappa}{2}\right)\right] + \delta\left[-c_1 + \mathcal{O}(\eta)\right] + \cdots\,. \tag{3.3.6}$$

Noting that the outer normal derivative $\partial_n u$ on $\partial\Omega$ is simply $\partial_n u = -\partial_\eta u$, (3.3.6) then implies the following boundary conditions for the outer solutions u_1 and u_2 in (3.3.2):

$$u_0 = 0\,, \qquad u_1 = \partial_n u_0\,, \qquad u_2 = \partial_n u_1 + \frac{\kappa}{2}\partial_n u_0\,, \quad x \in \partial\Omega\,. \tag{3.3.7}$$

The functions $c_0(s)$ and $c_1(s)$, which determine the leading two boundary layers solutions explicitly, are given by

$$c_0 = -\partial_n u_0\,, \qquad c_1 = -\partial_n u_1 - \frac{\kappa}{2}\partial_n u_0\,, \qquad x \in \partial\Omega\,,$$

with a more complicated expression, which we omit, for $c_2(s)$. Notice that the boundary condition for u_2 on $\partial\Omega$ depends on the curvature κ of $\partial\Omega$.

The remainder of the analysis to calculate the terms in the expansion of the fold point is similar to that in §3. At $\alpha = \alpha_0$, $\mathcal{L}u_{0\alpha} = 0$, and so each of the problems in (3.3.2) must satisfy a solvability condition. By applying Green's identity to $u_{0\alpha}$ and u_1,

together with the boundary condition $u_1 = \partial_n u_0$ on $\partial\Omega$, it follows at $\alpha = \alpha_0$ that

$$\lambda_1 I = -\int_{\partial\Omega} (\partial_n u_0)\,(\partial_n u_{0\alpha})\; dx\,, \qquad I \equiv \int_\Omega \frac{u_{0\alpha}}{(1+u_0)^2} dx\,. \tag{3.3.8}$$

The integral I can be written more conveniently by using the following lemma:
Lemma 3.4: *At $\alpha = \alpha_0$, the following identity holds:*

$$I \equiv \int_\Omega \frac{u_{0\alpha}}{(1+u_0)^2}\, dx = -\frac{1}{3\lambda_0}\int_{\partial\Omega} \partial_n u_{0\alpha}\, dx. \tag{3.3.9}$$

To prove this result, the equation for $u_{0\alpha}$ together with Green's second identity and the divergence theorem is used to calculate

$$\begin{aligned} I &= -\frac{1}{2\lambda_0}\int_\Omega (1+u_0)\,\Delta u_{0\alpha}\, dx = -\frac{1}{2\lambda_0}\left[\int_{\partial\Omega} \partial_n u_{0\alpha}\, dx + \int_\Omega u_{0\alpha}\Delta u_0\, dx\right] \\ &= -\frac{1}{2\lambda_0}\int_{\partial\Omega} \partial_n u_{0\alpha}\, dx - \frac{I}{2}\,. \end{aligned}$$

Solving for I then gives the result.

Upon substituting (3.3.9) into (3.3.8), λ_1 can be expressed at $\alpha = \alpha_0$ as

$$\lambda_1 = 3\lambda_0 \left(\frac{\int_{\partial\Omega} (\partial_n u_0)\,(\partial_n u_{0\alpha})\; dx}{\int_{\partial\Omega} \partial_n u_{0\alpha}\, dx}\right). \tag{3.3.10}$$

From (3.2.13) this then specifies the correction of order $\mathcal{O}(\delta^{1/2})$ to the fold point location.

To determine the $\mathcal{O}(\delta)$ term in the expansion (3.2.13) of the fold point, the terms $\lambda_{0\alpha\alpha}$, $\lambda_{1\alpha}$, and λ_2 at $\alpha = \alpha_0$ must be calculated. This is done through solvability conditions with $u_{0\alpha}$ in a similar way as in § 3.2. This procedure leads to the following identities at $\alpha = \alpha_0$:

$$\lambda_{0\alpha\alpha} = \frac{18\lambda_0^2}{\left(\int_{\partial\Omega} \partial_n u_{0\alpha}\, dx\right)} \int_\Omega \frac{u_{0\alpha}^3}{(1+u_0)^4}\, dx\,, \tag{3.3.11a}$$

$$\lambda_{1\alpha} I = -\int_\Omega u_{0\alpha}\left(\frac{6\lambda_0 u_1 u_{0\alpha}}{(1+u_0)^4} - \frac{2\lambda_1 u_{0\alpha}}{(1+u_0)^3}\right) dx - \int_{\partial\Omega} [\partial_n u_{0\alpha}]^2\; dx\,, \tag{3.3.11b}$$

$$\lambda_2 I = -\int_\Omega u_{0\alpha}\left[\frac{3\lambda_0 u_1^2}{(1+u_0)^4} - \frac{2\lambda_1 u_1}{(1+u_0)^3} + \Delta^2 u_0\right] dx - \int_{\partial\Omega}\left[\partial_n u_1 + \frac{\kappa}{2}\partial_n u_0\right]\partial_n u_{0\alpha}\, dx\,. \tag{3.3.11c}$$

In contrast to the one-dimensional case of § 3.2, u_1 cannot be obtained as explicitly as in Lemma 3.2. In place of Lemma 3.2, it is readily shown that u_1 admits the following

decomposition at $\alpha = \alpha_0$:

$$u_1 = \frac{\lambda_1}{3\lambda_0}(1+u_0) + u_{1a} + Du_{0\alpha}\,. \tag{3.3.12}$$

Here D is any scalar constant, and u_{1a} at $\alpha = \alpha_0$ is the unique solution to

$$\mathcal{L}u_{1a} = 0\,, \quad x \in \Omega\,; \qquad u_{1a} = \partial_n u_0 - \frac{\lambda_1}{3\lambda_0}\,, \quad x \in \partial\Omega\,; \qquad \int_\Omega u_{1a}u_{0\alpha}\,dx = 0\,. \tag{3.3.13}$$

By substituting (3.3.12) into (3.3.11), a straightforward calculation shows that the quantity $\lambda_2 - \lambda_{1\alpha}^2/[2\lambda_{0\alpha\alpha}]$ is independent of D. Hence, set $D = 0$ in (3.3.12) for simplicity. By substituting (3.3.12) for u_1 into (3.3.11b), and then using (3.3.9) for I, $\lambda_{1\alpha}$ at $\alpha = \alpha_0$ can be written as

$$\lambda_{1\alpha} = \frac{18\lambda_0^2}{\left(\int_{\partial\Omega}\partial_n u_{0\alpha}\,dx\right)}\int_\Omega \frac{u_{1a}u_{0\alpha}^3}{(1+u_0)^4}\,dx + 3\lambda_0\left(\frac{\int_{\partial\Omega}\left[\partial_n u_{0\alpha}\right]^2\,dx}{\int_{\partial\Omega}\partial_n u_{0\alpha}\,dx}\right). \tag{3.3.14}$$

Similarly, equation (3.3.12) for u_1 and (3.3.9) for I are substituted into (3.3.11c). In addition, in the resulting expression, the following identity which is readily derived by integration by parts, is used:

$$\int_\Omega u_{0\alpha}\Delta^2 u_0\,dx = -2\lambda_0^2\int_\Omega \frac{u_{0\alpha}}{(1+u_0)^5}\,dx - \lambda_0\int_{\partial\Omega}\partial_n u_{0\alpha}\,dx\,. \tag{3.3.15}$$

In this way, expression (3.3.11c) for λ_2 at $\alpha = \alpha_0$ simplifies to

$$\begin{aligned}\lambda_2 = \frac{2\lambda_1^2}{3\lambda_0} - 3\lambda_0^2 + \frac{3\lambda_0}{\left(\int_{\partial\Omega}\partial_n u_{0\alpha}\,dx\right)}\int_{\partial\Omega}\left[\partial_n u_{1a} + \frac{\kappa}{2}\partial_n u_0\right]\partial_n u_{0\alpha}\,dx \\ - \frac{6\lambda_0^3}{\left(\int_{\partial\Omega}\partial_n u_{0\alpha}\,dx\right)}\int_\Omega \frac{u_{0\alpha}}{(1+u_0)^5}\,dx + \frac{9\lambda_0^2}{\left(\int_{\partial\Omega}\partial_n u_{0\alpha}\,dx\right)}\int_\Omega \frac{u_{1a}^2 u_{0\alpha}}{(1+u_0)^4}\,dx\,.\end{aligned} \tag{3.3.16}$$

The results of the preceding calculations are summarized as follows:

Principal Result 3.5: *Let $\lambda_c \equiv \lambda_0(\alpha_0)$ be the fold point location at the end of the minimal solution branch for the unperturbed problem (3.3.1) in a bounded two-dimensional domain Ω, with smooth boundary $\partial\Omega$. Then, for (1.1.4) with $\delta \ll 1$, a three-term expansion for the perturbed fold point location is*

$$\lambda_c = \lambda_{0c} + 3\lambda_0\delta^{1/2}\left(\frac{\int_{\partial\Omega}\left(\partial_n u_0\right)\left(\partial_n u_{0\alpha}\right)\,dx}{\int_{\partial\Omega}\partial_n u_{0\alpha}\,dx}\right) + \delta\hat{\lambda}_2 + \cdots\,, \quad \hat{\lambda}_2 \equiv \lambda_2(\alpha_0) - \frac{\lambda_{1\alpha}^2(\alpha_0)}{2\lambda_{0\alpha\alpha}(\alpha_0)}\,. \tag{3.3.17}$$

Here $\lambda_{0\alpha\alpha}(\alpha_0)$, $\lambda_{1\alpha}(\alpha_0)$, and $\lambda_2(\alpha_0)$ are as given in (3.3.11a), (3.3.14), and (3.3.16), respectively.

The form of the $\delta^{\infty/\in}$ correction term in (3.3.17) of Principal Result 3.5 may give

some insight into the relationship between the curvature of the domain boundary and the principal fold point λ_c of (1.1.4). Specifically, a boundary with large curvature generates a larger perimeter $|\partial\Omega|$ and as $\partial_n u_0$ is positive on $\partial\Omega$, one expects that the value of the integral term is larger for domains with large curvatures.

For the special case of the unit disk where $\Omega := \{x \,|\, |x| \le 1\}$, then $u_0 = u_0(r)$ and $u_{0\alpha} = u_{0\alpha}(r)$ are radially symmetric, and $\kappa = 1$. Therefore, for this special geometry, $u_{1a} \equiv 0$ from (3.3.13), and consequently the various terms in (3.3.17) can be simplified considerably. In analogy with Principal Result 3.3, the following asymptotic expansion is obtained for the fold point location of (1.1.4) in the limit $\delta \to 0$ for the unit disk:

Corollary 3.6: *For the special case of the unit disk, let $\alpha_0 = u_0(0)$ and $\lambda_{0c} \equiv \lambda_0(\alpha_0)$ be the location of the fold point at the end of the minimal radially symmetric solution branch for the unperturbed problem (3.3.1). Then, for (1.1.4) with $\delta \ll 1$, a three-term expansion for the perturbed fold point location is*

$$\lambda_c = \lambda_{0c} + 3\lambda_0\delta^{1/2}u_0'(1) + \delta\hat{\lambda}_2 + \cdots, \qquad \hat{\lambda}_2 \equiv \lambda_2(\alpha_0) - \frac{\lambda_{1\alpha}^2(\alpha_0)}{2\lambda_{0\alpha\alpha}(\alpha_0)}\,. \tag{3.3.18a}$$

Here $\hat{\lambda}_2$ is defined in terms of u_0 and $u_{0\alpha}$ by

$$\begin{aligned}\hat{\lambda}_2 &= \frac{3}{2}\lambda_0 u_0'(1) + 6\lambda_0\left[u_0'(1)\right]^2 - 3\lambda_0^2 \\ &- \frac{6\lambda_0^3}{u_{0\alpha}'(1)}\int_0^1 \frac{r u_{0\alpha}}{(1+u_0)^5}\,dr - \frac{[u_{0\alpha}'(1)]^3}{2}\left(\int_0^1 \frac{r u_{0\alpha}^3}{(1+u_0)^4}\,dr\right)^{-1}.\end{aligned} \tag{3.3.18b}$$

The first term in $\hat{\lambda}_2$ above arises from the constant curvature of $\partial\Omega$.

For the unit disk, numerical values for the coefficients in the expansion (3.3.18) are obtained by first using COLSYS [1] to solve for u_0 and $u_{0\alpha}$. In this way, the explicit three-term expansion for the unit disk is

$$\lambda_c = 0.789 + 1.578\,\delta^{1/2} + 6.261\,\delta + \cdots. \tag{3.3.19}$$

In addition, for the unit disk it follows as in (3.2.12) that the global bifurcation diagram is given for $\delta \ll 1$ by

$$\lambda \sim \lambda_0(\alpha) + 3\lambda_0(\alpha)u_0'(1,\alpha)\delta^{1/2} + \mathcal{O}(\delta)\,. \tag{3.3.20}$$

For the unit disk, Fig. 3.6(b) provides a comparison of the two-term and three-term asymptotic results for λ_c versus δ from (3.3.19) along with the corresponding full numerical result computed from (1.1.4). Since the coefficients in (3.3.19) are smaller than those in (3.2.28), the three-term approximation for the unit disk is seen to provide a more accurate determination of λ_c than the result for the slab shown in Fig. 3.5(b).

For $\delta = 0.01$, Fig. 3.6(a) provides a comparison of the two-term approximation (3.3.20) to the global bifurcation curve with the full numerical result computed from (1.1.4) and also the membrane MEMS problem (1.1.2), corresponding to $\delta = 0$. From this figure it is seen that (3.3.20) compares favorably with the full numerical result provided that α is not too close to -1. Recall that $\lambda \to 4/9$ as $\alpha \to -1$ for (1.1.2), whereas from the numerical results in §2, $\lambda \to 0$ as $\alpha \to -1$ for (1.1.4) when $\delta > 0$. The singular limit $\alpha \to -1$ is examined in Chapter 4.

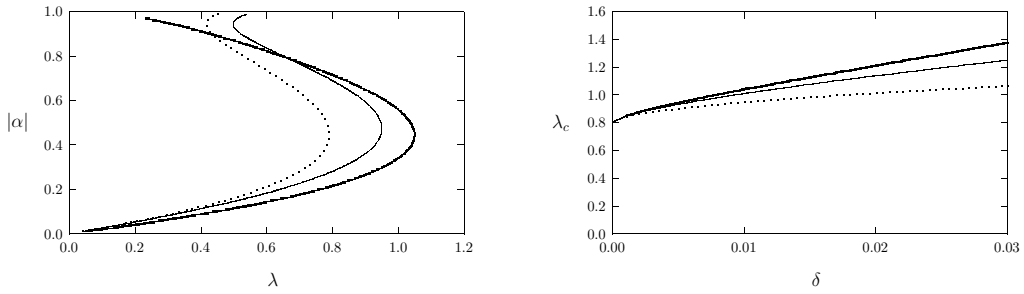

(a) $|\alpha|$ vs. λ (Unit Disk)

(b) λ_c vs. δ (Unit Disk)

Figure 3.6: Left figure: Plot of numerically computed global bifurcation diagram $|\alpha| = |u(0)|$ versus λ for (1.1.4) with $\delta = 0.01$ (heavy solid curve) compared to the two-term asymptotic result (3.3.20) (solid curve) and the unperturbed $\delta = 0$ membrane MEMS result from (1.1.2) (dashed curve). Right figure: Comparison of numerically computed fold point λ_c versus δ (heavy solid curve) with the two-term (dashed curve) and the three-term (solid curve) asymptotic result from (3.3.19).

3.4 Perturbing from the Pure Biharmonic Eigenvalue Problem

Next, equation (1.1.4) is considered in the limit $\delta \gg 1$. To study this limiting case, (1.1.4) is rewritten as

$$-\Delta^2 u + \frac{1}{\delta}\Delta u = \frac{\tilde{\lambda}}{(1+u)^2}\,, \quad x \in \Omega\,; \qquad u = \partial_n u = 0\,, \quad x \in \partial\Omega\,, \tag{3.4.1}$$

where $\tilde{\lambda} \equiv \lambda/\delta$. For $\delta \gg 1$, the solution u and the nonlinear eigenvalue parameter $\tilde{\lambda}$ are expanded as

$$u = u_0 + \frac{1}{\delta}u_1 + \cdots\,, \qquad \tilde{\lambda} = \tilde{\lambda}_0 + \frac{1}{\delta}\tilde{\lambda}_1 + \cdots\,. \tag{3.4.2}$$

Inserting this expansion in (3.4.1) and collecting terms, requires that u_0 satisfies

$$-\Delta^2 u_0 = \frac{\tilde{\lambda}_0}{(1+u_0)^2}\,, \quad x\in\Omega\,; \qquad u_0 = \partial_n u_0 = 0\,, \quad x\in\partial\Omega\,, \tag{3.4.3a}$$

and that u_1 satisfies

$$\mathcal{L}_b u_1 \equiv \Delta^2 u_1 - \frac{2\tilde{\lambda}_0}{(1+u_0)^3}u_1 = \Delta u_0 - \frac{\tilde{\lambda}_1}{(1+u_0)^2}, \quad x\in\Omega; \qquad u_1 = \partial_n u_1 = 0\,, \quad x\in\partial\Omega. \tag{3.4.3b}$$

The minimal solution branch for the unperturbed problem (3.4.3a) is parameterized as $\tilde{\lambda}_0(\alpha)$, $u_0(x,\alpha)$. It is assumed that there is a simple fold point at the end of this branch with location $\alpha=\alpha_0$, where $\tilde{\lambda}_{0c}=\tilde{\lambda}_0(\alpha_0)$. Since $\mathcal{L}_b u_{0\alpha}=0$ at $\alpha=\alpha_0$, the solvability condition for (3.4.3b) determines $\tilde{\lambda}_1$ at $\alpha=\alpha_0$ as

$$I_b\tilde{\lambda}_1 = \int_\Omega u_{0\alpha}\Delta u_0\,dx\,, \qquad I_b = \int_\Omega \frac{u_{0\alpha}}{(1+u_0)^2}\,dx\,. \tag{3.4.4}$$

By using the equation and boundary conditions for $u_{0\alpha}$ and u_0, we can calculate I_b using Green's identity as

$$\begin{aligned} I_b &= \frac{1}{2\lambda_0}\int_\Omega (u_0+1)\,\Delta^2 u_{0\alpha}\,dx = \frac{1}{2\lambda_0}\left[\int_{\partial\Omega}\partial_n\left(\Delta u_{0\alpha}\right)\,dx + \int_\Omega u_{0\alpha}\Delta^2 u_0\,dx\right] \\ &= \frac{1}{2\lambda_0}\int_{\partial\Omega}\partial_n\left(\Delta u_{0\alpha}\right)\,dx - \frac{I_b}{2}\,. \end{aligned} \tag{3.4.5}$$

This yields that

$$I_b = \frac{1}{3\lambda_0}\int_{\partial\Omega}\partial_n\left(\Delta u_{0\alpha}\right)\,dx\,. \tag{3.4.6}$$

Principal Result 3.7: *Let $\tilde{\lambda}_0(\alpha)$ and $u_0(x,\alpha)$ be the minimal solution branch for the pure biharmonic problem (3.4.3a), and assume that there is a simple fold point at $\alpha=\alpha_0$ where $\tilde{\lambda}_{0c}=\tilde{\lambda}_0(\alpha_0)$. Then, for $\delta\gg 1$, the expansion of the fold point for (1.1.4) is given by*

$$\lambda_c \sim \delta\left[\tilde{\lambda}_{0c} + \delta^{-1}\tilde{\lambda}_1(\alpha_0) + \mathcal{O}(\delta^{-2})\right]\,, \qquad \tilde{\lambda}_1(\alpha_0) \equiv 3\lambda_0\left(\frac{\int_\Omega u_{0\alpha}\Delta u_0\,dx}{\int_{\partial\Omega}\partial_n\left(\Delta u_{0\alpha}\right)\,dx}\right)\,. \tag{3.4.7a}$$

For the special case of the unit disk or a slab domain of unit length, then $\tilde{\lambda}_1(\alpha_0)$ reduces to

$$\begin{aligned} \tilde{\lambda}_1(\alpha_0) &= \frac{3\lambda_0}{\partial_r\left(\Delta u_{0\alpha}\right)\Big|_{r=1}}\int_0^1 u_{0\alpha}\left(r u_{0r}\right)_r\,dr\,, \quad \text{(Unit Disk)}\,; \\ \tilde{\lambda}_1(\alpha_0) &= \frac{3\lambda_0}{2u'''_{0\alpha}(1)}\int_0^1 u_{0\alpha}u_0''\,dx \quad \text{(Unit Slab)}\,. \end{aligned} \tag{3.4.7b}$$

For the slab and the unit disk, the numerical values of the coefficients in the expansion (3.4.7) are calculated by using COLSYS [1] to solve for u_0 and $u_{0\alpha}$ at the fold point of the minimal branch for the pure Biharmomic problem (3.4.3a). In this way, the following is obtained for $\delta \gg 1$:

$$\begin{aligned} \lambda_c &\sim \delta\left[70.095 + \frac{1}{\delta}1.729 + \cdots\right] \quad \text{(Unit Slab)}\,; \\ \lambda_c &\sim \delta\left[15.412 + \frac{1}{\delta}1.001 + \cdots\right] \quad \text{(Unit Disk)}\,. \end{aligned} \tag{3.4.8}$$

Although (3.4.8) was derived in the limit $\delta \gg 1$, in Fig. 3.7 it is shown, rather remarkably, that (3.4.8) is also in rather close agreement with the full numerical result for λ_c, computed from (1.1.4), even when $\delta < 1$. Therefore, for the unit disk and the unit slab, the limiting approximations for λ_c when $\delta \ll 1$ from (3.2.28) and (3.3.19), together with the $\delta \gg 1$ result (3.4.8), can be used to rather accurately predict the fold point λ_c for (1.1.4) for a wide range of $\delta > 0$.

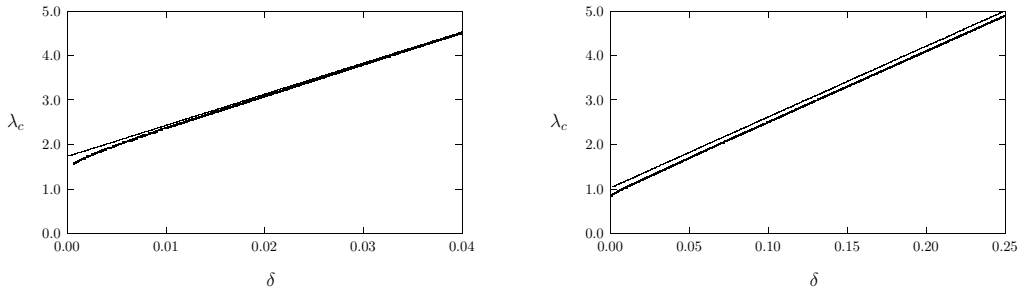

(a) λ_c vs. δ (Unit Slab)

(b) λ_c vs. δ (Unit Disk)

Figure 3.7: Comparison of full numerical result for λ_c versus δ (heavy solid curves) computed from (1.1.4) with the two-term asymptotic results (3.4.8) (solid curves) for the unit slab (left figure) and the unit disk (right figure).

3.5 The Fringing-Field And Annulus Problems

3.5.1 Fringing-Field Problem

Next, the fringing-field problem (1.1.5) is considered in the limit $\delta \to 0$ in a two-dimensional domain Ω with smooth boundary $\partial\Omega$. Let α_0, $\lambda_{0c} = \lambda_0(\alpha_0)$ be the location of the fold point for the unperturbed problem (3.3.1). To determine the leading order correction to the fold point location for (1.1.5) when $\delta \ll 1$, the solution to (1.1.5) is

expanded along the minimal solution branch as

$$u = u_0 + \delta u_1 + \cdots , \qquad \lambda = \lambda_0 + \delta\lambda_1 + \cdots . \tag{3.5.1}$$

The problem for u_1 is obtained by substituting (3.5.1) into (1.1.5), which yields

$$\mathcal{L}u_1 \equiv \Delta u_1 + \frac{2\lambda_0}{(1+u_0)^3}u_1 = \frac{\lambda_1}{(1+u_0)^2} + \lambda_0\frac{|\nabla u_0|^2}{(1+u_0)^2}\,, \quad x \in \Omega\,; \qquad u_1 = 0 \quad x \in \partial\Omega\,. \tag{3.5.2}$$

Since $\mathcal{L}u_{0\alpha} = 0$ at $\alpha = \alpha_0$, the solvability condition for (3.5.2) at $\alpha = \alpha_0$ determines λ_1 at $\alpha = \alpha_0$ as

$$\lambda_1(\alpha_0) = -\frac{\lambda_0}{I}\int_\Omega \frac{|\nabla u_0|^2 u_{0\alpha}}{(1+u_0)^2}\,dx\,, \qquad I \equiv \int_\Omega \frac{u_{0\alpha}}{(1+u_0)^2}\,dx\,, \tag{3.5.3}$$

where I is given in Lemma 4.1. For the special case of the unit disk and the unit slab the result is summarized as follows:

Principal Result 3.8: *Consider the fringing-field problem (1.1.5) with $\delta \ll 1$, and let λ_{0c} be the fold point location for the unperturbed problem (3.3.1). Then, for $\delta \ll 1$, the fold point for the fringing-field problem (1.1.5) for the unit disk and a slab domain of unit length satisfies*

$$\begin{aligned} \lambda_c &\sim \lambda_{0c} + \frac{3\lambda_0^2\delta}{u'_{0\alpha}(1)}\int_0^1 \frac{r u_{0r}^2 u_{0\alpha}}{(1+u_0)^2}\,dr\,, \quad \text{(Unit Disk)}\,; \\ \lambda_c &\sim \lambda_{0c} + \frac{3\lambda_0^2\delta}{2u'_{0\alpha}(1)}\int_0^1 \frac{(u_0')^2 u_{0\alpha}}{(1+u_0)^2}\,dx\,. \quad \text{(Unit Slab)}\,. \end{aligned} \tag{3.5.4}$$

For the special case of the unit slab, as well as the unit disk considered in [38], the coefficient in (3.5.4) can be evaluated from the numerical solution of (3.3.1) to obtain

$$\lambda_c \sim 0.789 - 0.160\delta\,, \quad \text{(Unit Disk)}\,; \qquad \lambda_c \sim 1.400 - 0.529\delta\,, \quad \text{(Unit Slab)}\,; \tag{3.5.5}$$

Since the coefficients of δ are negative, the fringing field reduces the pull-in voltage. In Fig. 3.8(a) a very favorable comparison is shown between (3.5.5) for λ_c in the unit disk and the full numerical result computed from (1.1.5). A similar comparison for the unit slab is shown in Fig. 3.8(b). Since the coefficients of δ in (3.5.5) are rather small, (3.5.5) provides a rather good prediction of λ_c even for only moderately small δ.

3.5.2 The Annulus Problem

Finally, the annulus problem (1.1.6) is considered in the limit $\delta \ll 1$ of a small inner radius. In this limit, (1.1.6) is singularly perturbed, and the construction of the solution

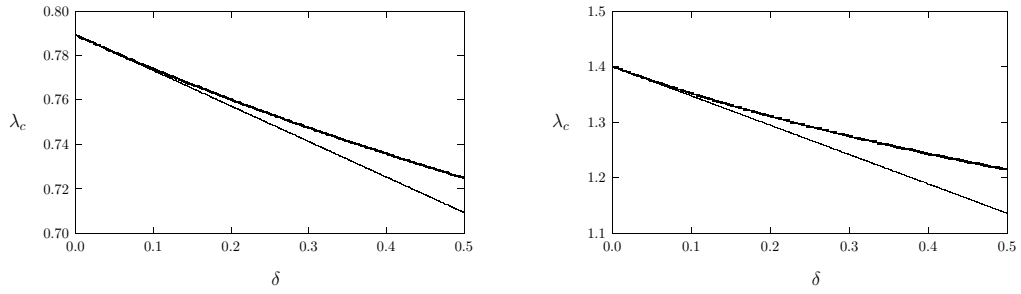

(a) λ_c vs. δ (Unit Disk)

(b) λ_c vs. δ (Unit Slab)

Figure 3.8: Left figure: Comparison of full numerical result for λ_c versus δ (heavy solid curve) for the fringing-field problem computed from (1.1.5) with the two-term asymptotic result (3.5.5) (solid curve) for the unit disk. Right figure: A similar comparison for the unit slab.

requires the matching of an outer solution defined for $r = \mathcal{O}(1)$ to an appropriate inner solution defined near $r = \delta \ll 1$. Related nonlinear eigenvalue problems for Bratu's equation have been considered previously in [40] and [41]. Therefore, only a rather brief outline of the singular perturbation analysis is given here.

Let $u_0(r,\alpha)$, $\lambda_0(\alpha)$ be the radially symmetric minimal solution branch for the unperturbed problem (3.3.1) on $0 \le r \le 1$. For the perturbed problem (1.1.6), λ and the outer solution u, valid for $r = \mathcal{O}(1)$, are expanded as

$$u = u_0 + \left(\frac{-1}{\log\delta}\right) u_1 + \cdots , \qquad \lambda = \lambda_0 + \left(\frac{-1}{\log\delta}\right)\lambda_1 + \cdots . \tag{3.5.6}$$

From (1.1.6) it follows that u_1 satisfies

$$\mathcal{L}u_1 \equiv \Delta u_1 + \frac{2\lambda_0}{(1+u_0)^3}u_1 = \frac{\lambda_1}{(1+u_0)^2}\,, \qquad 0 < r < 1\,; \qquad u_1 = 0\,, \quad \text{on} \quad r = 1\,. \tag{3.5.7}$$

The matching condition to the inner solution will then lead to a Coulomb singularity for u_1 as $r \to 0$, which then completes the specification of the problem for u_1.

In the inner region, defined for $r = \mathcal{O}(\delta)$, the inner variables $\rho = r/\delta$ and $u = v/(-\log\delta)$ are introduced. To leading order, it follows from (1.1.6) that $\Delta v = 0$ with $v(1) = 0$. Thus, $v = A\log\rho$ for some unknown constant A. In terms of outer variables this yields the matching condition

$$u \sim A + \left(\frac{-1}{\log\delta}\right) A\log r\,, \qquad r \to 0\,.$$

The matching of the inner and outer solutions then determines $A = u_0(0)$, and that u_1

has the singular behaviour

$$u_1 \sim u_0(0)\log r\,, \qquad \text{as} \quad r \to 0\,. \tag{3.5.8}$$

The problem (3.5.7) with singular behaviour (3.5.8) determines u_1 and λ_1. To determine $\lambda_1(\alpha_0)$ from a solvability condition, Green's identity is applied to $u_{0\alpha}$ and u_1 over a punctured disk $\varepsilon < r < 1$ in the limit $\varepsilon \to 0$. This yields that $\lambda_1 I = -2\pi u_0(0)u_{0\alpha}(0)$, where I is given in Lemma 4.1. The result is summarized as follows:

Principal Result 3.9: *Consider the annulus problem (1.1.5) with $\delta \ll 1$, and let λ_{0c} be the fold point location at the end of the minimal solution branch for the unperturbed problem (3.3.1). The, for $\delta \ll 1$, the fold point for (1.1.6) satisfies*

$$\lambda_c \sim \lambda_{0c} + \left(\frac{-1}{\log\delta}\right)\frac{3\lambda_0 u_0(0)u_{0\alpha}(0)}{u'_{0\alpha}(1)} + \mathcal{O}\left(\frac{-1}{\log\delta}\right)^2. \tag{3.5.9}$$

With the parameterization $u_0(0) = \alpha$ for the unperturbed solution, the terms in (3.5.9) are calculated from the numerical solution of the unperturbed problem (3.3.1). This yields the explicit two-term expansion

$$\lambda_c \sim 0.789 + 1.130\left(\frac{-1}{\log\delta}\right) + \mathcal{O}\left(\frac{-1}{\log\delta}\right)^2. \tag{3.5.10}$$

Owing to the logarithmic dependence on δ, the fold point location experiences a rather large perturbation even for δ rather small. This was observed in Fig. 3.3(b).

3.6 Conclusions

Asymptotic expansions for the fold point location at the end of the minimal solution branch for (1.1.4) were calculated in the limiting parameter range $\delta \ll 1$ and $\delta \gg 1$ for an arbitrary domain Ω with smooth boundary. In addition, two-term asymptotic approximations for the fold point location of the fringing-field (1.1.5) and annulus problems (1.1.6) were derived for small δ. The coefficients in these asymptotic expansions were evaluated numerically for both the unit slab and the unit disk. The results can be used to determine the shift in the pull-in voltage when the basic membrane problem (1.1.2) is perturbed to either (1.1.4), (1.1.5), or (1.1.6).

Accurate location of the principal fold is crucial in the design of MEMS devices as such devices tend to be operated very close to this threshold value, even although exceeding it may cause the device to fail. For this reason, these techniques and results may be useful to MEMS practitioners who require accurate determination of the pull-in voltage.

In the annulus problem (1.1.6), the change in topology induces a positive shift in the pull-in voltage of $\mathcal{O}(\log^{-1}\delta)$. This indicates that the device has a significantly higher range of operating voltages.

This Chapter forms the basis of the paper [29] titled *Asymptotics of some nonlinear eigenvalue problems for a MEMS capacitor: Part I: Fold point asymptotics* appearing in Methods and Applications of Analysis, Vol. 15, No. 3.

Chapter 4

Multiple Fold Points And Singular Asymptotics

The ubiquitous $\lambda/(1+u)^2$ nonlinearity which appears in all MEMS equations considered here naturally motivates the question of characterizing solutions as $u(x) \to -1$ for some point(s) $x \in \Omega$. Inspection of (1.1.2) in the eyeball norm suggests that regularity of the solution should be lost as the $u \to -1$ and the term $\lambda/(1+u)^2$ becomes singular. Note that since physical constraints demand the deflections remain continuous. As we shall see, the manner in which this regularity is lost can generate solutions with interesting qualitative features - the most engaging of which is the infinite fold points feature first identified in [34].

In this Chapter, singular solutions of MEMS equations (1.1.4)-(1.1.6) are analyzed in the limit $\varepsilon \to 0^+$ where $||u||_\infty = 1-\varepsilon$ via matched asymptotic methods. The techniques developed in this Chapter allow for the resolution of the $\lambda/(1+u)^2$ nonlinearity and the construction of singular solutions in the limit $\varepsilon \to 0^+$.

In § 4.1, the infinite fold point feature of the membrane problem (1.1.3) is analyzed in the limit $\varepsilon \to 0^+$ where $||u||_\infty = 1-\varepsilon$. The asymptotic analysis deployed allows for an *explicit* characterization of the singular solution branch, moreover, it provides an accurate asymptotic formula for the location of the fold points on the upper branch which are observed to be *exponentially* close to $u = -1$. The closely related Bratu problem is also investigated in § 4.1.3. Asymptotic predictions are observed to agree very well with numerical calculations.

In § 4.2, attention is restricted to the one dimensional domain $\Omega = (-1, 1)$ and solutions to (1.1.4)-(1.1.6) are developed in the limit $\varepsilon \to 0^+$ where $\varepsilon \equiv 1 + u(0)$. Asymptotic predictions are shown to agree well with numerical calculations.

In § 4.3, the radially symmetric maximal solution branch for (1.1.4) and a pure biharmonic cousin (4.3.1) are constructed on the unit disk in the limit $\varepsilon \to 0^+$ where $\varepsilon \equiv 1 + u(0)$. The analysis requires that the nonlinearity $\lambda/(1+u)^2$ be resolved in a local region in the vicinity of the origin. The extent of this region is determined to be $\mathcal{O}(\gamma)$, where γ satisfies the implicit relationship $-\gamma^2 \log \gamma = \varepsilon$.

In § 4.3.2, the radially symmetric maximal solution branch for (1.1.6) is constructed

in the annulus $\delta \leq |x| \leq 1$, where $x \in \mathbb{R}^2$. As the deflecting beam is pinned down at both of its end points, the location of maximum deflection occurs must be determined in the solution of the problem.

A characterization of the maximal solution branch of the fringing fields problem (1.1.5) in the limit as $||u||_\infty \to 1$ remains elusive.

Finally, in § 4.4, the maximal solution branch for the pure biharmonic MEMS problem (4.3.1) is constructed on an arbitrary 2D domain under the assumption the solution concentrates on a unique $x_0 \in \Omega$. This maximal solution is then characterized in terms of the Neumann Green's function (4.4.2) and conditions on the concentration point x_0 are established.

4.1 Asymptotics Of The Infinite Fold Points Structure

In this section, the bifurcation branch of radially symmetric solutions to the generalized membrane problem (1.1.3) is constructed in the limit $\varepsilon \to 0^+$ where $||u||_\infty = 1 - \varepsilon$.

4.1.1 Infinite Number Of Fold Points For $N = 1$

Considered first is the case of the slab domain $\Omega = (-1, 1)$ in the parameter range $\alpha > \alpha_c$, where $\alpha_c = -1/2 + (3/2)^{3/2}$ is the threshold above which an infinite fold point structure exists (cf. [34]). The symmetry condition $u_x(0) = 0$ is imposed so that attention may be restricted to the region $0 < x < 1$ and so the problem

$$u_{xx} = \frac{\lambda\, x^\alpha}{(1+u)^2}\,, \quad 0 < x < 1; \qquad u(1) = u_x(0) = 0\,, \tag{4.1.1}$$

is considered in the limit $u(0) + 1 = \varepsilon \to 0^+$. The nonlinear eigenvalue parameter λ and the outer solution for (4.1.1), defined away from $x = 0$, are expanded for $\varepsilon \to 0$ as

$$u = u_0 + \varepsilon^q u_1 + \cdots\,, \qquad \lambda = \lambda_0 + \varepsilon^q \lambda_1 + \cdots\,, \tag{4.1.2}$$

where $q > 0$ is to be found. In order to match to the inner solution below, the leading-order terms u_0, λ_0 are taken to be the singular solution of (4.1.1) for which $u_0(1) = 0$ and $u_0(0) = -1$. This solution is given by

$$u_0 = -1 + x^p\,, \qquad \lambda_0 = p(p-1)\,, \qquad p \equiv \frac{\alpha+2}{3}\,. \tag{4.1.3}$$

By substituting (4.1.2) into (4.1.1), and equating the $\mathcal{O}(\varepsilon^q)$ terms, the following equation for u_1 is determined after applying the explicit form of u_0 in (4.1.3);

$$\mathcal{L}u_1 \equiv u_{1xx} + \frac{2\lambda_0}{x^2}u_1 = \lambda_1 x^{p-2}\,, \quad 0 < x < 1\,; \qquad u_1(1) = 0\,. \tag{4.1.4}$$

By introducing an inner expansion, valid near $x = 0$, the appropriate singularity behaviour for u_1 as $x \to 0$ is determined. This behaviour will allow for the determination of λ_1 from a solvability condition.

In the inner region near $x = 0$, local variables y and $v(y)$ are introduced by the definition

$$y = x/\gamma\,, \qquad u = -1 + \varepsilon v(y)\,. \tag{4.1.5}$$

Substituting (4.1.5), together with (4.1.2) for λ, into (4.1.1) gives that

$$v'' = \frac{\gamma^{2+\alpha}}{\varepsilon^3}\frac{y^\alpha}{v^2}\left[\lambda_0 + \varepsilon^q\lambda_1 + \cdots\right]\,, \tag{4.1.6}$$

which suggests a boundary layer width of $\gamma = \varepsilon^{1/p}$, where p is defined in (4.1.3). Expanding (4.1.6) with

$$v = v_0 + \varepsilon^q v_1 + \cdots\,, \tag{4.1.7}$$

and equating terms at $\mathcal{O}(1)$ and $\mathcal{O}(\varepsilon^q)$, the following equations are obtained for v_0 and v_1;

$$v_0'' = \frac{\lambda_0 y^\alpha}{v_0^2}\,, \quad 0 < y < \infty\,; \qquad v_0(0) = 1\,, \quad v_0'(0) = 0\,, \tag{4.1.8a}$$

$$v_1'' + \frac{2\lambda_0 y^\alpha}{v_0^3}v_1 = \frac{\lambda_1 y^\alpha}{v_0^2}\,, \quad 0 < y < \infty\,; \qquad v_1(0) = v_1'(0) = 0\,. \tag{4.1.8b}$$

The leading-order matching condition is that $v_0 \sim y^p$ as $y \to \infty$. Linearizing about this far field behaviour by writing $v_0 = y^p + w$, where $w \ll y^p$ as $y \to \infty$, determines that w satisfies $w'' + 2\lambda_0 w/y^2 = 0$. This Euler type equation admits an explicit solution which determines that the far-field behaviour of the solution to (4.1.8a) is

$$v_0 \sim y^p + Ay^{1/2}\sin\left(\omega\log y + \phi\right)\,, \quad \text{as} \quad y \to \infty\,, \qquad \omega \equiv \frac{1}{2}\sqrt{8\lambda_0 - 1}\,, \tag{4.1.9}$$

where A and ϕ are constants depending on α, which must be computed from the numerical solution of (4.1.8a) with $v_0 \sim y^p$ as $y \to \infty$. Note that $8\lambda_0 - 1 > 0$ when $\alpha > \alpha_c \equiv -1/2 + (3/2)^{3/2}$. In contrast, the far-field behaviour for (4.1.8b) is determined by its particular solution. For $y \to \infty$ we use $v_0 \sim y^p$ in (4.1.8b), to obtain

that

$$v_1 \sim \frac{\lambda_1}{3\lambda_0} y^p\,, \quad \text{as} \quad y \to \infty\,. \tag{4.1.10}$$

Therefore, by combining (4.1.9) and (4.1.10), the far-field behaviour of the inner expansion $v \sim v_0 + \varepsilon^q v_1$ is determined. The matching condition is that this far-field behaviour as $y \to \infty$ must agree with the near-field behaviour as $x \to 0$ of the outer expansion in (4.1.2). By using $u = -1 + \varepsilon v$ and $x = \varepsilon^{1/p} y$, this matching condition yields

$$u \sim -1 + x^p + A\varepsilon^{1-1/(2p)} x^{1/2} \sin\left(\omega \log x - \frac{\omega}{p}\log\varepsilon + \phi\right) + \varepsilon^q \left(\frac{\lambda_1}{3\lambda_0}\right) x^p\,, \quad \text{as} \quad x \to 0\,. \tag{4.1.11}$$

Now, comparing (4.1.11) with the outer expansion for u in (4.1.2), it is clear that u_1 must solve (4.1.4), subject to the singular behaviour

$$u_1 \sim A x^{1/2} \sin\left(\omega \log x + \phi_\varepsilon\right) + \frac{\lambda_1}{3\lambda_0} x^p\,, \quad \text{as} \quad x \to 0\,, \tag{4.1.12}$$

where the exponent q and the phase ϕ_ε are defined to be $q = 1 - 1/(2p)$ and $\phi_\varepsilon \equiv -\omega p^{-1}\log\varepsilon + \phi$.

Next, we solve the problem (4.1.4) for u_1, with singular behaviour (4.1.12). Since the first term in the asymptotic behaviour in (4.1.12) is a solution to the homogeneous problem in (4.1.4), while the second term is the particular solution for (4.1.4), it is convenient to decompose u_1 as

$$u_1 = \frac{\lambda_1}{3\lambda_0} x^p + A x^{1/2} \sin\left(\omega \log x + \phi_\varepsilon\right) + U_{1a}\,, \tag{4.1.13}$$

to obtain that U_{1a} solves

$$\mathcal{L}U_{1a} = 0\,, \quad 0 < x < 1\,; \qquad U_{1a}(1) = -\frac{\lambda_1}{3\lambda_0} - A\sin\phi_\varepsilon\,; \qquad U_{1a} = o(x^{1/2})\,, \quad \text{as} \quad x \to 0\,. \tag{4.1.14}$$

To value of λ_1 is determined by a solvability condition. The function $\Phi = x^{1/2}\sin(\omega\log x + k\pi)$ is a solution to $\mathcal{L}\Phi = 0$ with $\Phi(1) = 0$ for any integer k, and has the asymptotic behaviour $\Phi = \mathcal{O}(x^{1/2})$ and $\Phi_x = \mathcal{O}(x^{-1/2})$ as $x \to 0$. By applying Lagrange's identity to U_{1a} and Φ over the interval $0 < \sigma < x < 1$, and by using $\Phi(1) = 0$, we obtain

$$0 = \int_\sigma^1 \left(\phi\mathcal{L}U_{1a} - U_{1a}\mathcal{L}\Phi\right) dx = -U_{1a}(1)\Phi_x(1) - \left[\Phi U_{1ax} - U_{1a}\Phi_x\right]_{x=\sigma}\,. \tag{4.1.15}$$

Finally, taking the limit $\sigma \to 0$ in (4.1.15) and using $U_{1a} = o(x^{1/2})$, $U_{1ax} = o(x^{-1/2})$, and $\Phi_x(1) \neq 0$, as $x \to 0$ yields that $U_{1a}(1) = 0$, which determines $\lambda_1 = -3A\lambda_0 \sin\phi_\varepsilon$

from (4.1.14). The preceding calculation is now summarized by the following result:

Principal Result 4.1: *For $\varepsilon \equiv u(0)+1 \to 0^+$ and $\alpha > \alpha_c \equiv -1/2 + (3/2)^{3/2}$ a two-term asymptotic expansion for the bifurcation curve λ versus ε of (4.1.1) is given by*

$$\lambda \sim \lambda_0 + 3A\lambda_0 \varepsilon^q \sin\left(\frac{3\omega}{2+\alpha}\log\varepsilon - \phi\right) + \cdots, \tag{4.1.16a}$$

where q, ω, and λ_0, are defined by

$$q = 1 - \frac{3}{2(\alpha+2)}, \qquad \omega = \frac{1}{2}\sqrt{8\lambda_0 - 1}, \qquad \lambda_0 = \frac{(\alpha-1)(\alpha+2)}{9}. \tag{4.1.16b}$$

The constants A and ϕ, which depend on α, are determined numerically from the solution to (4.1.8a) with far-field behaviour (4.1.9). These constants are given in the first row of Table 3.1 for a few values of α. The asymptotic prediction for the locations of the infinite sequence of fold points, determined by setting $d\lambda/d\varepsilon = 0$, is

$$\begin{gathered} u(0) = -1 + \varepsilon_m, \quad \varepsilon_m = \exp\left[\tfrac{(\alpha+2)}{3\omega}\left(\phi - \tfrac{(2m-1)\pi}{2}\right)\right], \\ \lambda_m = \lambda_0 + 3\lambda_0 A\, \varepsilon_m^q\, (-1)^m, \qquad m = 1, 2, \ldots \end{gathered} \tag{4.1.16c}$$

These fold points are exponentially close to $u(0) = -1$ as $\varepsilon \to 0$.

The analysis leading to Principal Result 4.1 is non-standard as a result of two features. Firstly, the correction term u_1 in the outer expansion for u is not independent of ε, but in fact depends on $\log\varepsilon$. However, although u_1 is weakly oscillatory in ε, it is uniformly bounded as $\varepsilon \to 0$. Secondly, the solvability condition determining λ_1 pertains to a countably infinite sequence of functions $\Phi = x^{1/2}\sin(\omega \log x + k\pi)$ where k is an integer.

4.1.2 Infinite Number Of Fold Points For $N > 1$

Next, a similar analysis is employed to determine the limiting form of the bifurcation diagram for radially symmetric solutions of (1.1.3) in the N-dimensional unit ball. To this end, the solution branches of

$$u_{rr} + \frac{(N-1)}{r}u_r = \frac{\lambda r^\alpha}{(1+u)^2}, \quad 0 < r < 1; \qquad u(1) = 0, \quad u_r(0) = 0, \tag{4.1.17}$$

will be constructed asymptotically in the limit $u(0)+1 = \varepsilon \to 0^+$, where $\alpha \geq 0$ and $N \geq 2$. For $N = 2$, the term r^α represents a variable dielectric permittivity of the membrane (cf. [34], [17]).

In the limit $\varepsilon \to 0$, (4.1.17) is a singular perturbation problem with an outer region where $\mathcal{O}(\gamma) < r < 1$ with $u = \mathcal{O}(1)$, and an inner region with $r = \mathcal{O}(\gamma)$ where

$u = \mathcal{O}(\varepsilon)$. Here $\gamma \ll 1$ is the boundary layer width to be found in terms of ε. The nonlinear eigenvalue parameter λ and the outer solution are expanded as

$$u \sim u_0 + \varepsilon^q u_1 + \cdots, \qquad \lambda \sim \lambda_0 + \varepsilon^q \lambda_1 + \cdots, \tag{4.1.18}$$

for some $q > 0$ to be determined. For the leading-order problem for u_0 and λ_0, a singular solution of (4.1.17) is constructed for which $u_0(0) = -1$. This singular solution is given explicitly by

$$u_0 = -1 + r^p, \qquad \lambda_0 = p^2 + (N-2)p, \qquad p \equiv \frac{(\alpha+2)}{3}. \tag{4.1.19}$$

The substitution of (4.1.18) into (4.1.17), together with using (4.1.19) for u_0, shows that u_1 satisfies

$$\mathcal{L}_N u_1 \equiv u_1'' + \frac{(N-1)}{r} u_1' + \frac{2\lambda_0}{r^2} u_1 = \lambda_1 r^{p-2}, \quad 0 < r < 1; \qquad u_1(1) = 0. \tag{4.1.20}$$

The required singularity behaviour for u_1 as $r \to 0$ will be determined below by matching u_1 to the inner solution.

In the inner region near $r = 0$, local variables v and ρ are introduced and their inner expansion by

$$u = -1 + \varepsilon v, \qquad v = v_0 + \varepsilon^q v_1 + \cdots, \qquad \rho = r/\gamma, \qquad \gamma = \varepsilon^{1/p}. \tag{4.1.21}$$

Substituting (4.1.21) into (4.1.17), reveals that $v_0(\rho)$ and $v_1(\rho)$ satisfy

$$v_0'' + \frac{(N-1)}{\rho} v_0' = \frac{\lambda_0 \rho^\alpha}{v_0^2}, \quad 0 < \rho < \infty; \qquad v_0(0) = 1, \quad v_0'(0) = 0, \tag{4.1.22a}$$

$$v_1'' + \frac{(N-1)}{\rho} v_1' + \frac{2\lambda_0 \rho^\alpha}{v_0^3} v_1 = \frac{\lambda_1 \rho^\alpha}{v_0^2}, \quad 0 < \rho < \infty; \qquad v_1(0) = v_1'(0) = 0. \tag{4.1.22b}$$

The leading-order matching condition is that $v_0 \sim \rho^p$ as $\rho \to \infty$. Linearizing about this far field behaviour by writing $v_0 = \rho^p + w$, where $w \ll \rho^p$ as $\rho \to \infty$, gives that w satisfies

$$w'' + \frac{(N-1)}{\rho} w' + \frac{2\lambda_0}{\rho^2} w = 0. \tag{4.1.23}$$

A solution to this Euler equation is

$$w = \rho^\mu, \qquad \mu = -\frac{(N-2)}{2} \pm \frac{\sqrt{(N-2)^2 - 8\lambda_0}}{2}. \tag{4.1.24}$$

This leads to two different cases, depending on whether $(N-2)^2 > 8\lambda_0$ or $(N-2)^2 < 8\lambda_0$.

	$\alpha = 0$		$\alpha = 1$		$\alpha = 2$		$\alpha = 3$	
N	A	ϕ	A	ϕ	A	ϕ	A	ϕ
1	–	–	–	–	1.1678	3.9932	0.8713	3.7029
2	0.4727	3.2110	0.4728	3.2110	0.4729	3.2110	0.4730	3.2109
3	0.2454	2.5050	0.2864	2.7231	0.3152	2.8351	0.3363	2.9042
4	0.1935	1.8789	0.2193	2.2932	0.2454	2.5048	0.2676	2.6347
5	0.1972	1.2755	0.1935	1.8790	0.2101	2.1886	0.2284	2.3775
6	0.2586	0.7008	0.1909	1.4743	0.1935	1.8790	0.2056	2.1262
7	0.4859	0.1945	0.2095	1.0803	0.1896	1.5746	0.1935	1.8790

Table 4.1: Numerical values of A and ϕ for different exponents α and dimension N computed from the far-field behaviour of the solution to (4.1.22a) with (4.1.25).

Consider first the case $(N-2)^2 < 8\lambda_0$ in which μ takes a complex value. As shown below, this is the case where the bifurcation diagram of λ versus ε has an infinite number of fold points. For this case, the explicit solution for w leads to the following far-field behaviour for the solution v_0 of (4.1.22a):

$$v_0 = \rho^p + A\rho^{1-N/2}\sin\left(\omega_N \log\rho + \phi\right) + o(1)\,, \qquad \rho \to \infty\,; \qquad \omega_N \equiv \frac{1}{2}\sqrt{8\lambda_0 - (N-2)^2}\,. \tag{4.1.25}$$

Here the constants A and ϕ, depending on N and α, must be computed numerically from the solution to (4.1.22a) with far-field behaviour (4.1.25). In Table 4.1 numerical values for these constants are given for different α and N for the parameter range where $(N-2)^2 < 8\lambda_0$. The results for A and ϕ are also plotted in Fig. 4.1(a). In particular, for $N = 2$ and $\alpha = 0$,

$$A = 0.4727\,, \qquad \phi = 3.2110\,. \tag{4.1.26}$$

For $N = 2$ and $\alpha = 0$, in Fig. 4.1(b) the numerically computed far-field behaviour of v_0 is plotted after subtracting off the $\mathcal{O}(\rho^{2/3})$ algebraic growth at infinity. Indeed, this far-field behaviour is oscillatory as predicted by (4.1.25).

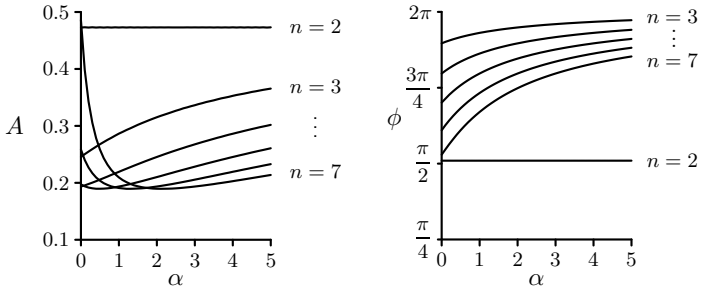

(a) $A(\alpha)$ and $\phi(\alpha)$ for $N = 2, \ldots, 7$.

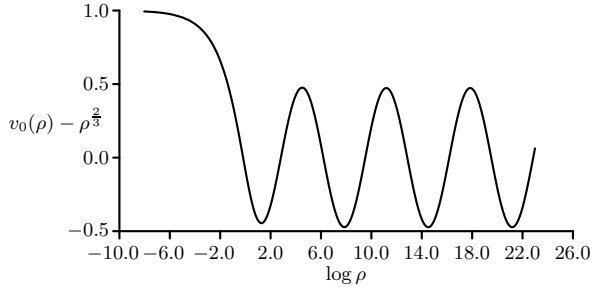

(b) $v_0(\rho)$ for $\rho \gg 1$

Figure 4.1: Left figure: numerical results for the far-field constants A and ϕ in (4.1.25) for different N and α. Right figure: Plot of $v_0 - \rho^{2/3}$ versus $\log \rho$ as computed numerically from (4.1.22a) for $N = 2$ and $\alpha = 0$. The far-field behaviour is oscillatory.

For v_1, the far-field behaviour for (4.1.22b) is determined by its particular solution. Using the far field condition $v_0 \sim \rho^p$ as $\rho \to \infty$ in (4.1.22b) demonstrates that

$$v_1 \sim \frac{\lambda_1}{3\lambda_0}\rho^p\,, \quad \text{as} \quad \rho \to \infty\,. \tag{4.1.27}$$

Therefore, by combining (4.1.25) and (4.1.27), the far-field behaviour of the inner expansion $v \sim v_0 + \varepsilon^q v_1$ is obtained. The matching condition is that this far-field behaviour as $\rho \to \infty$ must agree with the near-field behaviour as $x \to 0$ of the outer expansion in (4.1.18). By using $u = -1 + \varepsilon v$ and $r = \varepsilon^{1/p}\rho$, and by choosing the exponent q in (4.1.18) appropriately, the following singularity behaviour is generated for u_1 (4.1.20) subject to the singular behaviour

$$u_1 \sim A r^{1-N/2} \sin\left(\omega_N \log r + \phi_\varepsilon\right) + \frac{\lambda_1}{3\lambda_0} r^p\,, \quad \text{as} \quad r \to 0\,, \tag{4.1.28}$$

where q and ϕ_ε are defined by

$$q \equiv 1 + \frac{3}{2}\left(\frac{N-2}{\alpha+2}\right)\,, \qquad \phi_\varepsilon = -\frac{3\omega_N}{\alpha+2}\log\varepsilon + \phi\,. \tag{4.1.29}$$

Next, problem (4.1.20) is solve subject to the singular behaviour (4.1.28). The

solution of u_1 is decomposed as

$$u_1 = \frac{\lambda_1}{3\lambda_0} r^p + A r^{1-N/2} \sin\left(\omega_N \log r + \phi_\varepsilon\right) + U_{1a}\,, \tag{4.1.30}$$

to obtain that U_{1a} solves

$$\begin{gathered} \mathcal{L}_N U_{1a} = 0\,, \quad 0 < r < 1\,; \qquad U_{1a}(1) = -\frac{\lambda_1}{3\lambda_0} - A\sin\phi_\varepsilon\,; \\ U_{1a} = o(r^{1-N/2})\,, \quad \text{as} \quad r \to 0\,. \end{gathered} \tag{4.1.31}$$

Since the solution to the homogeneous problem is $\Phi = r^{1-N/2}\sin\left(\omega_N \log r + k\pi\right)$ for any integer $k \geq 0$, then Green's second identity is readily used to obtain a solvability condition for (4.1.31). The application of this identity to U_{1a} and Φ on the interval $\sigma \leq r \leq 1$ yields

$$0 = \int_\sigma^1 r^{N-1}\left(\Phi\mathcal{L}_N U_{1a} - U_{1a}\mathcal{L}_N\Phi\right)\,dr = -r^{N-1}\left(\Phi\partial_r U_{1a} - U_{1a}\partial_r\Phi\right)\Big|_{r=\sigma}^{r=1}. \tag{4.1.32}$$

Since $\Phi(1) = 0$, the passage to the limit $\sigma \to 0$ in (4.1.32) results in

$$U_{1a}\partial_r\Phi|_{r=1} = -\lim_{\sigma\to 0}\sigma^{N-1}\left(\Phi\partial_r U_{1a} - U_{1a}\partial_r\Phi\right)|_{r=\sigma}\,. \tag{4.1.33}$$

Now since $U_{1a} = o(r^{1-N/2})$, $\partial_r U_{1a} = o(r^{-N/2})$, $\Phi = \mathcal{O}(r^{1-N/2})$, and $\partial_r\Phi = \mathcal{O}(r^{-N/2})$ as $r \to 0$, there is no contribution in (4.1.33) from the limit $\sigma \to 0$. Consequently, $U_{1a}(1) = 0$, which determines λ_1 as $\lambda_1 = -3\lambda_0 A\sin\phi_\varepsilon$ from (4.1.31). The asymptotic result is summarized as follows:

Principal Result 4.2: *For $\varepsilon \equiv u(0)+1 \to 0^+$ and when either $N > N_c$, or equivalently $\alpha > \alpha_{cN}$, where*

$$N_c \equiv 2 + \frac{4(\alpha+2)}{3} + \frac{2\sqrt{6}}{3}(\alpha+2)\,, \qquad \alpha_{cN} \equiv -2 + \frac{3(N-2)}{4+2\sqrt{6}}\,, \tag{4.1.34}$$

then a two-term asymptotic expansion for the bifurcation curve λ versus ε for (4.1.17) *is given by*

$$\lambda \sim \lambda_0 + 3\varepsilon^q A\lambda_0 \sin\left(\frac{3\omega_N}{\alpha+2}\log\varepsilon - \phi\right)\,, \tag{4.1.35a}$$

where q is defined in (4.1.29). The constants A and ϕ, depending on N and α, to be computed from the solution to (4.1.22a) with far-field behaviour (4.1.25), are given in Table 3.1 and Fig. 4.1(a). The asymptotic prediction for the locations of the infinite

sequence of fold points, determined by setting $d\lambda/d\varepsilon = 0$*, is*

$$u(0) = -1 + \varepsilon_m, \quad \varepsilon_m = \exp\left[\frac{(\alpha+2)}{3\omega_N}\left(\phi - \frac{(2m-1)\pi}{2}\right)\right], \qquad \lambda_m = \lambda_0 + 3\lambda_0 A\,\varepsilon_m^q\,(-1)^m, \quad m = 1, 2, \ldots \tag{4.1.35b}$$

where ω_N *is defined in* (4.1.25).

The condition on N, or equivalently on α, in (4.1.34) are both necessary and sufficient to guarantee that $8\lambda_0 > (N-2)^2$. For $\alpha = 0$, (4.1.34) yields that the dimension N satisfies $2 \le N \le 7$. For any $N \ge 8$, it follows from (4.1.34) that (4.1.17) has an infinite number of fold points if α is sufficiently large.

Next, the case in which $8\lambda_0 < (N-2)^2$, corresponding to either $N > N_c$, or equivalently to $\alpha < \alpha_{cN}$. For this case, the solution v_0 to (4.1.22a) has the far-field behaviour

$$v_0 \sim \rho^p + \mathcal{A}\rho^{\mu_+}, \quad \text{as} \quad \rho \to \infty; \qquad \mu_+ \equiv 1 - \frac{N}{2} + \frac{\sqrt{(N-2)^2 - 8\lambda_0}}{2}, \tag{4.1.36}$$

for some constant $\mathcal{A}$, which depends on N and α, that must be calculated numerically. A simple calculation shows that $p > \mu_+$. In addition, the far-field behaviour of the solution v_1 to (4.1.22b) has the asymptotic behaviour in (4.1.27).

Then, by using $u = -1 + \varepsilon v$ and $r = \varepsilon^{1/p}\rho$, where $v = v_0 + \varepsilon^q v_1$, and by choosing the exponent q in (4.1.18) appropriately, the following singularity behaviour, to be satisfied by u_1, is established

$$u_1 \sim \mathcal{A} r^{\mu_+} + \frac{\lambda_1}{3\lambda_0} r^p, \quad \text{as } r \to 0, \tag{4.1.37}$$

where $q = 1 - 3\mu_+/(2+\alpha)$. The solution of u_1 admits the decomposition

$$u_1 = \mathcal{A} r^{\mu_+} + \frac{\lambda_1}{3\lambda_0} r^p + U_{1a}, \tag{4.1.38}$$

where from (4.1.20) it is determined that U_{1a} solves

$$\mathcal{L}_N U_{1a} = 0, \quad 0 < r < 1; \qquad U_{1a}(1) = -\frac{\lambda_1}{3\lambda_0} - \mathcal{A}; \qquad U_{1a} = o(r^{\mu_+}), \quad \text{as} \quad r \to 0. \tag{4.1.39}$$

The solvability condition for this problem determines λ_1 as $\lambda_1 = -3\lambda_0\mathcal{A}$. The asymptotic result is summarized as follows:

Principal Result 4.3: *For* $\varepsilon \equiv u(0) + 1 \to 0^+$ *assume that either* $2 < N < N_c$*, or equivalently* $\alpha < \alpha_{cN}$*, where* N_c *and* α_{cN} *are defined in* (4.1.34)*. Then, a two-term*

asymptotic expansion for the bifurcation curve λ *versus* ε *for* (4.1.17) *is given by*

$$u(0) = -1 + \varepsilon\,, \qquad \lambda \sim \lambda_0 - 3\varepsilon^q \mathcal{A}\lambda_0\,, \tag{4.1.40}$$

where $q = 1 - 3\mu_+/(2+\alpha)$ *and* μ_+ *is defined in* (4.1.36)*. The constant* $\mathcal{A}$*, which depends on* α *and* N*, must be computed numerically from the solution to (4.1.22a) with far-field behaviour (4.1.36).*

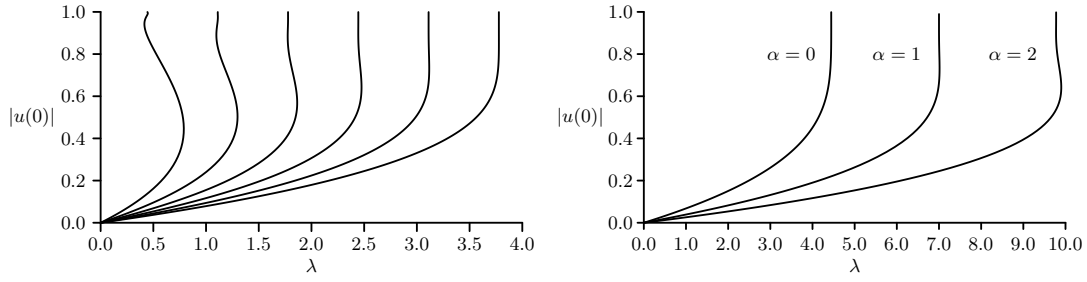

(a) $N = 1, \ldots, 7$ and $\alpha = 0$.

(b) $N = 8$ and $\alpha = 0, 1, 2$.

Figure 4.2: Panel (a): numerical bifurcation curves $|u(0)|$ versus λ for $N = 1, \ldots, 7$ and $\alpha = 0$. Panel (b): numerical bifurcation curves for $N = 8$ and $\alpha = 0, 1, 2$. The results were computed numerically from (4.1.17).

In Fig. 4.2 plots are shown for the bifurcation diagrams of $|u(0)|$ versus λ, as computed numerically from (4.1.17) for $N = 1, \ldots, 7$ and $\alpha = 0$ (see Fig. 4.2(a)) and for $N = 8$ with $\alpha = 0, 1, 2$ (see Fig. 4.2(b)). For representative values of N and α, in Fig. 4.3 it is observed that the asymptotic results for the bifurcation diagram as obtained from either (4.1.35) or (4.1.40) closely approximate the numerically computed bifurcation curves of (4.1.17)

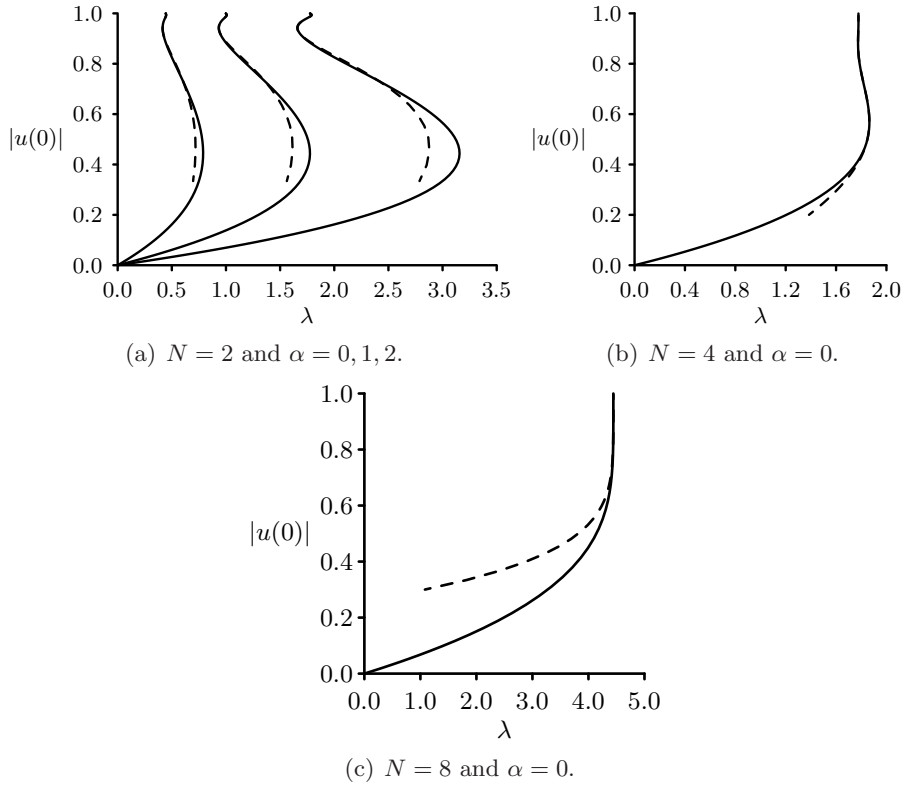

(a) $N = 2$ and $\alpha = 0, 1, 2$.

(b) $N = 4$ and $\alpha = 0$.

(c) $N = 8$ and $\alpha = 0$.

Figure 4.3: Comparison of bifurcation curves for $N = 2$ with $\alpha = 0, 1, 2$ (Panel(a)), $N = 4$ and $\alpha = 0$ (Panel (b)), and $N = 8$ with $\alpha = 0$ (Panel(c)). The solid curves are the full numerical results and the dashed curves are the asymptotic results obtained from either (4.1.35) or (4.1.40).

4.1.3 Fold Points Of The Bratu Problem

In this section, the analysis of § 4.1.2 is extended to study a similar infinite fold points structure present in radially symmetric solutions of the Bratu Problem

$$\Delta u + \lambda e^u = 0, \quad x \in \Omega; \qquad u = 0, \quad x \in \partial\Omega \tag{4.1.41}$$

where Ω is the unit ball in $\mathbb{R}^N$ and $\Delta u \equiv u_{rr} + (N-1)r^{-1}u_r$ for $r = |x|$. The analysis is performed in the limit as $u(0) \to \infty$ by setting $u(0) = -2\log\varepsilon$ and studying the limit $\varepsilon \to 0^+$.

Solutions of (4.1.41) have been investigated thoroughly and have been shown to exhibit many curious features. One such feature, which is of main interest here, is the *Infinite fold points* feature exhibited when $3 \le N \le 9$.

An inner region is introduced in the vicinity of the origin and an outer region else-

where. In the outer region a solution of form

$$u = u_0 + \epsilon^p u_1 + \cdots, \qquad \lambda = \lambda_0 + \epsilon^p \lambda_1 + \cdots \tag{4.1.42}$$

is implemented in equation (4.1.41) where the scaling $p = p(N)$ is to be determined later by matching with the inner problem. Inserting expansion (4.3.3) in equation (4.1.41) and collecting terms of similar order results in the following ODEs satisfied by u_0 and u_1;

$$\frac{d^2u_0}{dr^2} + \frac{N-1}{r}\frac{du_0}{dr} + \lambda_0 e_0^u = 0, \quad 0 < r < 1; \qquad u_0(1) = 0; \tag{4.1.43a}$$

$$\frac{d^2u_1}{dr^2} + \frac{N-1}{r}\frac{du_1}{dr} + \lambda_0 e^{u_0} u_1 = -\lambda_1 e^{u_0}, \quad 0 < r < 1; \qquad u_1(1) = 0. \tag{4.1.43b}$$

In equation (4.1.43a) an anzatz solution of form $u_0(r) = A \log r$ is given and accepted provided $A = -2$ and $\lambda_0 = 2(N-2)$. Inputing u_0 and λ_0 into equation (4.1.43b) reduces the equation satisfied by u_1 to

$$\frac{d^2u_1}{dr^2} + \frac{N-1}{r}\frac{du_1}{dr} + \frac{\lambda_0}{r^2}u_1 = -\frac{\lambda_1}{r^2}, \quad 0 < r < 1; \qquad u_1(1) = 0 \tag{4.1.44}$$

The required singularity behaviour for u_1 as $r \to 0$ will be determined below by matching u_1 to the inner solution. In this inner region, the change of variables

$$y = \gamma x, \qquad u = -2\log\epsilon + v(y) \tag{4.1.45}$$

is implemented to transform (4.1.41) to

$$\frac{1}{\gamma^2}\left(\frac{d^2v}{dy^2} + \frac{N-1}{y}\frac{dv}{dy}\right) + \frac{\lambda}{\epsilon^2}e^v = 0, \quad y > 0; \qquad \begin{matrix} v(0) = 0 \\ v'(0) = 0 \end{matrix}.$$

Balancing all terms with $\gamma = \epsilon$ results in the inner problem

$$\frac{d^2v}{dy^2} + \frac{N-1}{y}\frac{dv}{dy} + \lambda e^v = 0, \quad y > 0; \qquad \begin{matrix} v(0) = 0 \\ v'(0) = 0 \end{matrix}. \tag{4.1.46}$$

Expanding (4.1.46) with

$$v = v_0 + \varepsilon^p v_1 + \cdots \qquad \lambda = \lambda_0 + \varepsilon^p \lambda_1 + \cdots$$

gives the following problems

$$\frac{d^2v_0}{dy^2} + \frac{N-1}{y}\frac{dv_0}{dy} + \lambda_0 e^{v_0} = 0, \quad y > 0; \qquad \begin{matrix} v_0(0) = 0 \\ v_0'(0) = 0 \end{matrix}. \tag{4.1.47a}$$

$$\frac{d^2v_1}{dy^2} + \frac{N-1}{y}\frac{dv_1}{dy} + \lambda_0 e^{v_0} v_1 = -\lambda_1 e^{v_0}, \quad y > 0; \qquad \begin{matrix} v_1(0) = 0 \\ v_1'(0) = 0 \end{matrix}. \tag{4.1.47b}$$

As $y \to \infty$, impose behaviour $v_0(y) \to -2\log y$ and look for a correction term to this leading order behavior by writing

$$v(y) \sim -2\log y + w$$

with $w(y)$ satisfying

$$\frac{d^2w}{dy^2} + \frac{N-1}{y}\frac{dw}{dy} + \frac{\lambda_0}{y^2}w = 0.$$

By writing $w = y^\beta$ it is observed that β satisfies a quadratic equations with roots

$$\frac{(2-N) \pm \sqrt{(N-2)(N-10)}}{2}.$$

These roots are complex only for $3 \leq N \leq 9$ and it is for this range that infinite fold points are present. Thus, the behavior of (4.1.47a) as $y \to \infty$ is summarized by

$$v_0(y) \sim -2\log y + Ay^{1-\frac{N}{2}}\sin(\omega_N \log y + \phi) + \cdots$$

where $A(N)$ and $\phi(N)$ are determined by numerical solution of (4.1.47a) and

$$\omega_N = \frac{\sqrt{(N-2)(10-N)}}{2}. \tag{4.1.48}$$

The far field behaviour of the v_1 equation, formulated in (4.1.47b) is now developed. The equation for v_1 admits the decomposition $v_1 = -\lambda_1/\lambda_0 + v_H$ where

$$\frac{d^2v_H}{dy^2} + \frac{N-1}{y}\frac{dv_H}{dy} + \lambda_0 e^{v_0} v_H = 0 \tag{4.1.49}$$

Using the condition $v_0 \sim -2\log y$ as $y \to \infty$, the far field behaviour of v_H is observed to be $\mathcal{O}(y^{1-\frac{N}{2}})$ as $y \to \infty$. This determines the far field condition of (4.1.46) to be

$$v \sim -2\log y + Ay^{1-\frac{N}{2}}\sin(\omega_N \log y + \phi) + \varepsilon^p\left[-\frac{\lambda_1}{\lambda_0} + \mathcal{O}(y^{1-\frac{N}{2}})\right] + \cdots \tag{4.1.50}$$

Returning to an expression in outer variables via (4.1.45) gives the matching behavior

with which the outer solution must agree. Therefore as $r \to 0$ the matching requires that

$$u \sim -2\log r + A\epsilon^{\frac{N}{2}-1} r^{1-\frac{N}{2}} \sin\left(\omega_N \log r + \phi_\varepsilon\right) + \epsilon^p \left[-\frac{\lambda_1}{\lambda_0} + \mathcal{O}(\varepsilon^{\frac{N}{2}-1})\right] + \cdots \quad (4.1.51)$$

A comparison with equation (4.1.42) as $r \to 0$ reveals that

$$p = \frac{N}{2} - 1, \qquad \phi_\varepsilon(N) = \phi - \omega(N)\log\epsilon. \quad (4.1.52)$$

where again A and ϕ are determined by numerical solution of (4.1.47a). Therefore, singularity condition (4.3.26) gives that

$$u \sim -2\log r + \varepsilon^{1-\frac{N}{2}} \left[-\frac{\lambda_1}{\lambda_0} + A r^{1-\frac{N}{2}} \sin\left(\omega_N \log r + \phi_\varepsilon\right)\right] + \mathcal{O}(\varepsilon^{N-2}) \quad (4.1.53)$$

which in turn furnishes the problem for u_1 (4.1.44) with singularity behavior as $r \to 0$ to give that

$$\frac{d^2u_1}{dr^2} + \frac{N-1}{r}\frac{du_1}{dr} + \lambda_0 e^{u_0} u_1 = -\lambda_1 e^{u_0}, \quad 0 < r < 1; \qquad u_1(1) = 0. \quad (4.1.54a)$$

$$u_1 \sim -\frac{\lambda_1}{\lambda_0} + A r^{1-\frac{N}{2}} \sin\left(\omega_N \log r + \phi_\varepsilon\right) + \cdots \qquad r \to 0 \quad (4.1.54b)$$

Decomposing the solution to (4.1.54) as

$$u_1 = -\frac{\lambda_1}{\lambda_0} + A r^{1-\frac{N}{2}} \sin\left(\omega_N \log r + \phi_\varepsilon\right) + U_{1H} \quad (4.1.55)$$

it is observed that U_{1H} satisfies

$$\frac{d^2U_{1H}}{dr^2} + \frac{N-1}{r}\frac{dU_{1H}}{dr} + \frac{\lambda_0}{r^2}U_{1H} = 0, \quad 0 < r < 1; \qquad U_{1H}(1) = \frac{\lambda_1}{\lambda_0} - A\sin\phi_\varepsilon \quad (4.1.56)$$

and additionally $U_{1H} = o(r^{1-\frac{N}{2}})$ as $r \to 0$. Since the solution to the homogeneous problem is $\Phi = r^{1-N/2}\sin\left(\omega_N \log r + k\pi\right)$ for any integer $k \geq 0$, then Green's second identity is readily used to obtain a solvability condition for (4.1.56). The application of this identity to U_{1H} and Φ on the interval $\sigma \leq r \leq 1$ yields

$$0 = \int_\sigma^1 r^{N-1}\left(\Phi\mathcal{L}_N U_{1H} - U_{1H}\mathcal{L}_N\Phi\right) dr = -r^{N-1}\left(\Phi\partial_r U_{1H} - U_{1H}\partial_r\Phi\right)\Big|_{r=\sigma}^{r=1}. \quad (4.1.57)$$

Since $\Phi(1) = 0$, the passage to the limit $\sigma \to 0$ in (4.1.57) results in

$$U_{1H}\partial_r\Phi|_{r=1} = -\lim_{\sigma\to 0}\sigma^{N-1}\left(\Phi\partial_r U_{1H} - U_{1H}\partial_r\Phi\right)|_{r=\sigma}. \tag{4.1.58}$$

Now since $U_{1H} = o(r^{1-N/2})$, $\partial_r U_{1H} = o(r^{-N/2})$, $\Phi = \mathcal{O}(r^{1-N/2})$, and $\partial_r\Phi = \mathcal{O}(r^{-N/2})$ as $r \to 0$, there is no contribution in (4.1.58) from the limit $\sigma \to 0$. Consequently, $U_{1H}(1) = 0$, which determines λ_1 as $\lambda_1 = \lambda_0 A\sin\phi_{\mathcal{E}}$ from (4.1.56). With λ_1 determined, the asymptotic bifurcation diagram of solutions is given by

$$|u(0)| = -2\log\epsilon \qquad \lambda = \lambda_0 + \lambda_0 A\epsilon^{\frac{N}{2}-1}\sin\phi_{\mathcal{E}} + \mathcal{O}(\varepsilon^{N-2}) \tag{4.1.59}$$

with

$$\lambda_0 = 2(N-2), \qquad \omega_N = \frac{\sqrt{(2-N)(N-10)}}{2}.$$

The fold points of the solution branch may now be located by observing the values of ϵ_m which satisfy

$$\phi_{\mathcal{E}} \equiv \phi - \omega_N\log\epsilon_m = \frac{(2m-1)\pi}{2}$$

for $m = 1, 2, 3, \ldots$. This expression can be rearranged to give

$$\epsilon_m = \exp\left(\frac{\phi}{\omega_N} - \frac{(2m+1)\pi}{2\omega_N}\right).$$

The coordinates of the fold points (α_m, λ_m) can now be given asymptotically as

$$\alpha_m = \frac{(2m+1)\pi}{\omega_N} - \frac{2\phi}{\omega_N}, \qquad \lambda_m = \lambda_0 + \lambda_0 A\epsilon_m^{\frac{N}{2}-1}(-1)^m \tag{4.1.60}$$

The constants $A(N)$ and $\phi(N)$ are determined from the numerical solution of the initial value problem

$$\frac{d^2v}{dy^2} + \frac{N-1}{y}\frac{dv}{dy} + 2(N-2)e^v = 0, \quad y > 0; \qquad \begin{matrix} v(0) = 0 \\ v'(0) = 0 \end{matrix}. \tag{4.1.61}$$

Recall that the behavior of $v(y)$ was earlier in (4.3.25) given as

$$v(y) \sim -2\log y + Ay^{1-\frac{N}{2}}\sin(\omega_N\log y + \phi) + \cdots$$

as $y \to \infty$. The sinusoidal term is isolated by peeling off the leading order behavior, multiplying by $y^{\frac{N}{2}-1}$ and plotting the remainder against $\log y$ at which point the required constants are easily noted. The following table gives approximate values of A and ϕ for relevant values of N:

N	3	4	5	6	7	8	9
A	0.990	0.605	0.493	0.489	0.581	0.850	1.716
ϕ	6.232	5.646	5.071	4.522	3.971	3.501	3.097

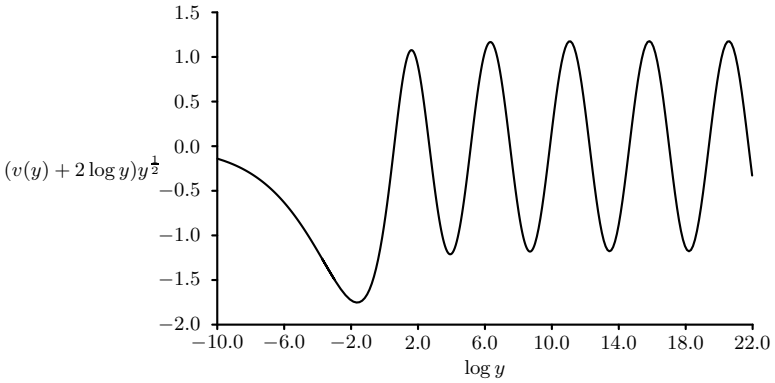

Figure 4.4: Numerical solution of equation (4.1.61) for $N = 3$. The leading order behavior has been peeled off and a logarithmic scale is used on the x-axis to demonstrate the sinusoidal element of the solution.

The following figure provides a comparison between full numerics and asymptotic prediction

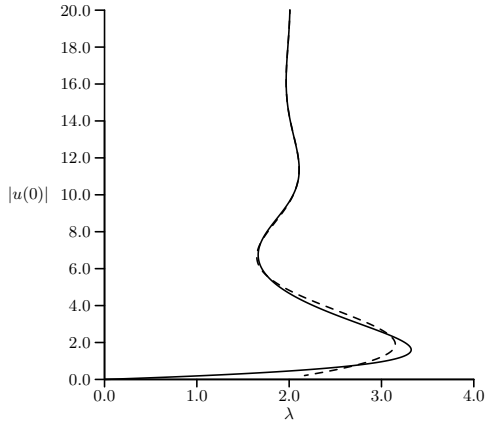

Figure 4.5: Solid line: Numerical solution of equation (4.1.41) for $N = 3$. Dashed line: Asymptotic solution of (4.1.41) for $N = 3$.

The results in Figure.4.5 show that the asymptotic prediction is very good at the first fold point and indistinguishable from the full numerical solution by the second fold point.

4.2 Asymptotics Of The Maximal Solution Branch As $\lambda \to 0$: The Slab Domain

In this section, the limiting asymptotic behaviour of the maximal solution branch for the fringing field problem (1.1.5) as well as the beam problem (1.1.4) in a slab domain is constructed.

4.2.1 The Fringing Field Problem

The method of matched asymptotic expansions to construct the maximal solution branch $(\lambda_\varepsilon, u_\varepsilon)$ of

$$u_{xx} = \frac{\lambda(1+\delta u_x^2)}{(1+u)^2}\,, \quad -1 < x < 1\,; \qquad u(\pm 1) = 0\,, \tag{4.2.1}$$

in the limit where $\varepsilon \equiv u(0) + 1 \to 0^+$. The condition that $\lambda_\varepsilon \to 0$ as $\varepsilon \to 0^+$ is made explicit by assuming that

$$\lambda_\varepsilon \sim \nu(\varepsilon)\lambda_0 + \cdots\,, \tag{4.2.2}$$

where $\nu(\varepsilon) \ll 1$ is to be determined. Since the solution to (4.2.1) is even about $x = 0$, the interval $0 < x < 1$ is considered together with the condition $u_x(0) = 0$. In the outer region, away from $x = 0$, the solution is expanded as

$$u_\varepsilon = u_0 + \nu(\varepsilon)u_1 + \cdots\,, \qquad \lambda_\varepsilon = \nu(\varepsilon)\lambda_0 + \cdots\,. \tag{4.2.3}$$

Substituting this expansion into (4.2.1), and collecting powers of ν, gives the following sequence of problems

$$u_{0xx} = 0, \qquad 0 < x < 1\,; \qquad u_0(1) = 0\,, \tag{4.2.4}$$

$$u_{1xx} = \frac{\lambda_0(1+\delta u_{0x}^2)}{(1+u_0)^2}\,, \qquad 0 < x < 1\,; \qquad u_1(1) = 0\,. \tag{4.2.5}$$

By fixing $u_0(0) = -1$, the solution to (4.2.4) and (4.2.5) is given in terms of an unknown constant a_1 as

$$u_0 = -1 + x\,, \qquad u_1 = -\lambda_0\,(1+\delta)\log x + a_1(x-1)\,. \tag{4.2.6}$$

By introducing the inner variable $y = x/\gamma$, (4.2.6) suggests that to leading order $u \sim -1 + \gamma y + \cdots$ as $x \to 0$. Since $u = -1 + \mathcal{O}(\varepsilon)$ in the inner region, this motivates

the introduction of the local variables y and v defined by

$$y = x/\varepsilon\,, \qquad u = -1 + \varepsilon v(y)\,. \tag{4.2.7}$$

Applying variables (4.2.7) to equations (4.2.1) together with $\lambda_\varepsilon \sim \nu\lambda_0$, gives

$$v'' = \varepsilon^{-1}\nu\frac{[\lambda_0 + \cdots]}{v^2}\left(1 + \delta\left(v'\right)^2\right)\,, \tag{4.2.8}$$

which indicates the correct scaling $\nu = \varepsilon$. With $\nu = \varepsilon$, the two-term outer approximation from (4.2.6) and (4.2.3) in terms of $x = \varepsilon y$ has the local behaviour

$$u \sim -1 + \varepsilon y + (-\varepsilon\log\varepsilon)\left[\lambda_0\left(1+\delta\right)\right] + \varepsilon\left[-\lambda_0(1+\delta)\log y - a_1\right] + \cdots\,.$$

The constant term of order $\mathcal{O}(\varepsilon\log\varepsilon)$ cannot be matched by the inner solution. Therefore, to remove this term, the outer expansion in (4.2.3) must be modified by introducing a switchback term. The modified outer expansion is

$$u_\varepsilon \sim u_0 + (-\varepsilon\log\varepsilon)\,u_{1/2} + \varepsilon u_1 + \cdots\,, \qquad \lambda_\varepsilon \sim \varepsilon\lambda_0 + \left(-\varepsilon^2\log\varepsilon\right)\lambda_1 + \cdots\,. \tag{4.2.9}$$

Upon substituting (4.2.9) into (4.2.1), we obtain that $u_{1/2xx} = 0$ with $u_{1/2}(1) = 0$. This gives $u_{1/2} = a_0(x-1)$. The two-term outer expansion is

$$u_\varepsilon \sim -1 + x + (-\varepsilon\log\varepsilon)\,a_0(x-1) + \varepsilon\left[-\lambda_0(1+\delta)\log x + a_1(x-1)\right] + \cdots\,. \tag{4.2.10}$$

In terms of the inner variable, $y = \varepsilon^{-1}x$, the local behaviour as $x \to 0$ of (4.2.10) is

$$\begin{aligned} u \;&\sim\; -1 + \varepsilon y + (-\varepsilon\log\varepsilon)\left[-a_0 + \lambda_0(1+\delta)\right] \\ &+\; \varepsilon\left[-\lambda_0(1+\delta)\log y - a_1\right] + \left(-\varepsilon^2\log\varepsilon\right)ya_0 + \cdots\,. \end{aligned} \tag{4.2.11}$$

To eliminate the constant term of order $\mathcal{O}(\varepsilon\log\varepsilon)$, the necessary choice for a_0 is

$$a_0 = \lambda_0(1+\delta)\,. \tag{4.2.12}$$

Then, with $u = -1 + \varepsilon v$, (4.2.11) yields the following required far-field behaviour for the inner solution $v(y)$:

$$v \sim y - \lambda_0(1+\delta)\log y - a_1 + (-\varepsilon\log\varepsilon)\left[\lambda_0(1+\delta)y\right] + \cdots\,, \qquad y \to \infty\,. \tag{4.2.13}$$

For the inner problem (4.2.8), the far-field form (4.2.13) suggests the following ex-

pansion for the inner solution

$$v = v_0 + (-\varepsilon \log \varepsilon)\, v_1 + \cdots . \tag{4.2.14}$$

Then, from (4.2.14) and (4.2.13), together with (4.2.9) for λ_ε, we obtain from (4.2.8) that v_0 and v_1 satisfy

$$v_0'' = \frac{\lambda_0}{v_0^2}\left(1 + \delta (v_0')^2\right), \quad y > 0\,; \qquad v_0(0) = 1\,, \quad v_0'(0) = 0\,, \tag{4.2.15a}$$

$$v_0 \sim y - \lambda_0(1+\delta)\log y - a_1\,, \quad \text{as} \quad y \to \infty\,, \tag{4.2.15b}$$

$$\mathcal{L} v_1 \equiv v_1'' + \frac{2\lambda_0}{v_0^3}\, v_1 - \frac{2\lambda_0 \delta v_0'}{v_0}\left(\frac{v_1}{v_0}\right)' = \frac{\lambda_1}{v_0^2}\left(1 + \delta (v_0')^2\right), \quad y > 0\,; \quad v_1(0) = v_1'(0) = 0, \tag{4.2.15c}$$

$$v_1 \sim \lambda_0(1+\delta) y + \cdots, \quad \text{as} \quad y \to \infty\,. \tag{4.2.15d}$$

The solution to these problems determine λ_0, λ_1, and the unknown constant a_1. The two cases $\delta = 0$ and $\delta > 0$ are now considered.

For the case $\delta = 0$, equation (4.2.15a) can be integrated directly after multiplying through by v_0'. Upon using the far-field behaviour $v_0' \to 1$ as $y \to \infty$, the value $\lambda_0 = 1/2$ is obtained and v_0 satisfies

$$v_0' = \sqrt{1 - \frac{1}{v_0}}\,, \quad 0 < y < \infty\,; \qquad v_0(0) = 1\,,$$

which in turn can be integrated to yield

$$\sqrt{v_0}\sqrt{v_0 - 1} + \log\left(\sqrt{v_0} + \sqrt{v_0 - 1}\right) = y\,.$$

For $v_0 \gg 1$, corresponding to $v_0 - 1$, this relation gives that $v_0 + \frac{1}{2}\log v_0 + \log 2 - 1/2 \sim y$, so that

$$v_0 \sim y - \frac{1}{2}\log y + \frac{1}{2} - \log 2\,, \quad \text{as} \quad y \to \infty\,.$$

Upon comparing this expression with (4.2.15b), the valuet $a_1 = \log 2 - 1/2$ is obtained. Next, to determine λ_1 when $\delta = 0$, we first multiply the equation for v_1 in (4.2.15c) by v_0'. Then, by using Green's second identity, together with $\mathcal{L} v_0' = 0$ and the boundary

conditions in (4.2.15) for v_0 and v_1 at $y = 0$ and as $y \to \infty$, we obtain

$$\lim_{R\to\infty} \int_0^R \left(v_0' \mathcal{L} v_1 - v_1 \mathcal{L} v_0' \right) \, dy = \lim_{R\to\infty} \left(v_0' v_1' - v_1 v_0'' \right) \Big|_0^R ,$$

$$\lambda_1 \lim_{R\to\infty} \int_0^R \frac{v_0'}{v_0^2} \, dy = \lim_{R\to\infty} v_0'(R) v_1'(R) ,$$

$$-\lambda_1 \int_0^\infty \frac{d}{dy}\left(\frac{1}{v_0}\right) \, dy = -\lambda_1 \left(\frac{1}{v_0}\right) \Big|_{v_0=0}^\infty = \lambda_0 .$$

Since $v_0(0) = 1$ and $\lambda_0 = 1/2$, the value $\lambda_1 = 1/2$ is obtained.

Next, consider the case $\delta > 0$. For this case, only λ_0 and a_1 are readily determined analytically. To obtain λ_0, let $u_0 = v_0'$, and write (4.2.15a) as a first order separable ODE for $u_0 = u_0(v_0)$ in the form

$$\frac{du_0}{dv_0} = \frac{\lambda_0}{v_0^2}\left(\frac{1+\delta u_0^2}{u_0}\right) , \quad 0 < v_0 < \infty ; \quad u_0(1) = 0 , \quad u_0 \to 1 \quad \text{as} \quad v_0 \to \infty . \tag{4.2.16}$$

Separating variables and integrating over $0 < v_0 < \infty$ yields that $(2\delta)^{-1} \log(1+\delta u_0^2)|_0^1 = (-\lambda_0/v_0)\,|_1^\infty$, which gives $\lambda_0 = (2\delta)^{-1}\log(1+\delta)$. Moreover, $v_0 = v_0(y)$ satisfies the first-order ODE

$$\frac{dv_0}{dy} = \delta^{-1/2}\left[(1+\delta)^{1-1/v_0} - 1\right]^{1/2} , \quad 0 < y < \infty ; \qquad v_0(0) = 1 .$$

An integration of this ODE determines $v_0(y)$ implicitly in terms of a quadrature. By expanding this implicit integral relation as $y \to \infty$, and then comparing the resulting expression with the required far-field behaviour in (4.2.15b), the constant a_1 can be identified as

$$a_1 = \int_1^\infty \left(\left[1 + \frac{(1+\delta)}{\delta}\left((1+\delta)^{-1/x} - 1 \right) \right]^{-1/2} - 1 - \frac{(1+\delta)}{2\delta}\frac{\log(1+\delta)}{x} \right) dx . \tag{4.2.17}$$

The determination of the second-order term λ_1 from (4.2.15c) and (4.2.15d) is tedious, and is omitted.

A summary of the construction of the limiting behaviour of the maximal solution branch of (4.2.1) is as follows:

Principal Result 4.4: *For $\varepsilon \equiv u(0) + 1 \to 0^+$, the maximal solution branch of* (4.2.1) *has the asymptotic behaviour*

$$\lambda_\varepsilon \sim \varepsilon\lambda_0 + \left(-\varepsilon^2 \log\varepsilon\right)\lambda_1 + \cdots , \tag{4.2.18a}$$

where $\lambda_0 = \lambda_1 = 1/2$ *when* $\delta = 0$, *and* $\lambda_0 = (2\delta)^{-1}\log(1+\delta)$ *when* $\delta > 0$. *In the outer region, defined away from* $x = 0$, *a three-term expansion for* u_ε *is*

$$u_\varepsilon \sim -1 + x + (-\varepsilon \log \varepsilon)\,\lambda_0(1+\delta)(x-1) + \varepsilon\left[-\lambda_0(1+\delta)\log x + a_1(x-1)\right]\,, \quad (4.2.18b)$$

where $a_1 = \log 2 - 1/2$ *when* $\delta = 0$, *and* a_1 *is given in* (4.2.17) *when* $\delta > 0$.

A favorable comparison of the full numerical solution of (4.2.1) and the asymptotic prediction λ_ε is given in Fig. 4.6.

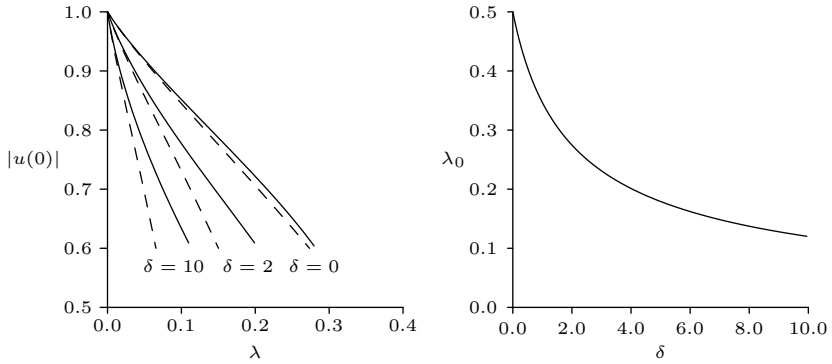

(a) $|u(0)|$ vs. λ for $\delta = 0$, $\delta = 2$, and $\delta = 10$

(b) λ_0 vs. δ

Figure 4.6: Left figure: The full numerical solution of (4.2.1) is favorably compared with the asymptotic predictions of Principal Result 3.1 for the values $\delta = 0, 2, 10$. Good agreement is observed when $\varepsilon \equiv 1 - |u(0)|$ is small. Right figure: Plot of λ_0 vs. δ from $\lambda_0 = (2\delta)^{-1}\log(1+\delta)$.

As a remark, the asymptotics in (4.2.18a) for the case $\delta = 0$ can be verified by calculating the exact solution to (4.2.1). Defining $u(0) = \alpha$, we multiply the equation for u in (4.2.1) by u_x and integrate the resulting expression. By using $u_x(0) = 0$, the following the integral relation is obtained

$$\lambda = \frac{(1+\alpha)}{2}\left[J(\alpha)\right]^2\,, \qquad J(\alpha) \equiv \int_\alpha^0 \sqrt{\frac{1+u}{u-\alpha}}\,du\,. \quad (4.2.19)$$

Changing variables and defining $\alpha = -1 + \varepsilon$, the integral J can be re-written and calculated as

$$J = 2\int_{\sqrt{\varepsilon}}^1 \frac{x^2}{\sqrt{x^2-\varepsilon}}\,dx = \sqrt{1-\varepsilon} + \varepsilon\left[\log\left(1+\sqrt{1-\varepsilon}\right) - \log(\sqrt{\varepsilon})\right]\,. \quad (4.2.20)$$

Substituting (4.2.20) into (4.2.19), and expanding as $\varepsilon \to 0$, it is readily established that $\lambda \sim \varepsilon/2 - \varepsilon^2\log(\varepsilon)/2 + \cdots$, in agreement with (4.2.18a) for the case $\delta = 0$.

4.2.2 The Beam Problem

In this subsection, the method of matched asymptotic expansions is used to construct the maximal solution branch $(\lambda_\varepsilon, u_\varepsilon)$, of the pure biharmonic nonlinear eigenvalue problem

$$-u_{xxxx} = \frac{\lambda}{(1+u)^2}\,, \quad -1 < x < 1\,; \qquad u(\pm 1) = u_x(\pm 1) = 0\,, \tag{4.2.21}$$

in the limit where $\varepsilon \equiv u(0) + 1 \to 0^+$. The assumption that $\lambda_\varepsilon \to 0$ as $\varepsilon \to 0^+$ is made, so that

$$\lambda_\varepsilon \sim \nu(\varepsilon)\lambda_0 + \cdots\,, \tag{4.2.22}$$

where $\nu(\varepsilon) \ll 1$ is a gauge function to be determined. Since u_ε is even in x, the treatment of equation (4.2.21) may be restricted the interval $0 < x < 1$ in conjunction with the symmetry conditions $u_x(0) = u_{xxx}(0) = 0$.

In the outer region for $0 < x < 1$, the solution is initially expanded as

$$u_\varepsilon \sim u_0 + \nu(\varepsilon)u_1 + \cdots\,. \tag{4.2.23}$$

where u_0 and u_1 satisfy the following equations on $0 < x < 1$:

$$u_{0xxxx} = 0\,, \quad 0 < x < 1\,; \qquad u_0(1) = u_{0x}(1) = 0\,, \tag{4.2.24a}$$

$$u_{1xxxx} = -\frac{\lambda_0}{(1+u_0)^2}\,, \quad 0 < x < 1\,; \qquad u_1(1) = u_{1x}(1) = 0\,. \tag{4.2.24b}$$

For (4.2.24a), the point constraints $u_0(0) = -1$ and $u_{0x}(0) = 0$ are imposed in order match to a local solution in the vicinity of $x = 0$. This determines $u_0(x)$ as

$$u_0(x) = -1 + 3x^2 - 2x^3\,. \tag{4.2.25}$$

Since $u_{0xxx}(0) \neq 0$, this leading-order outer solution does not satisfy the symmetry condition $u_{xxx}(0) = 0$ indicating that an inner layer near $x = 0$ is required.

To determine behaviour of the $\mathcal{O}(\nu)$ term, equation (4.2.25) is inserted to (4.2.24b), to yield for $x \ll 1$ that

$$u_{1xxxx} = -\frac{\lambda_0}{(3x^2 - 2x^3)^2} = -\frac{\lambda_0}{9x^4}\left(1 - \frac{2x}{3}\right)^{-2} \sim -\frac{\lambda_0}{9x^4}\left(1 + \frac{4x}{3} + \frac{12x^2}{9} + \cdots\right).$$

By integrating this limiting relation, the local behaviour

$$u_1 \sim \frac{\lambda_0}{54}\log x - \frac{2\lambda_0}{27}x\log x + c_1 + b_1 x + \mathcal{O}(x^2\log x)\,, \quad \text{as} \quad x \to 0\,, \tag{4.2.26}$$

is established in terms of arbitrary constants c_1 and b_1 which pertain to a solution of the homogeneous problem and will be specified later to determine u_1 uniquely. From (4.2.23), (4.2.25), and (4.2.26), the following asymptotic behaviour for u_ε as $x \to 0$ is deduced:

$$u_\varepsilon \sim -1 + 3x^2 - 2x^3 + \nu\left(\frac{\lambda_0}{54}\log x - \frac{2\lambda_0}{27}x\log x + c_1 + b_1 x + \mathcal{O}(x^2\log x)\right) + \cdots . \tag{4.2.27}$$

By rescaling the vicinity of the origin with variable $y = x/\gamma$, the leading order behaviour from (4.2.27) is $u \sim -1 + 3\gamma^2 y^2 + \cdots$ as $x \to 0$. Since $u = -1 + \mathcal{O}(\varepsilon)$ in the inner region, this motivates the scaling of the solution in the vicinity of the origin by using local variables y and v defined by

$$y = x/\varepsilon^{1/2}\,, \qquad u = -1 + \varepsilon v(y)\,. \tag{4.2.28}$$

Balancing the cubic term $-2x^3$ in (4.2.27) with the $\mathcal{O}(\nu)$ term in (4.2.27) gives the scaling $\nu = \varepsilon^{3/2}$. Substituting (4.2.28) and $\lambda_\varepsilon \sim \varepsilon^{3/2}\lambda_0$ into (4.2.21), the problem for $v(y)$ satisfies

$$-v'''' = \varepsilon^{1/2}\frac{[\lambda_0 + \cdots]}{v^2}\,, \quad 0 < y < \infty\,; \qquad v(0) = 1\,, \quad v'(0) = v'''(0) = 0\,. \tag{4.2.29}$$

The correct expansions for the inner and outer solutions are now determined by expressing the local behaviour of the outer expansion in (4.2.27) in terms of the inner variable $x = \varepsilon^{1/2}y$ with $\nu = \varepsilon^{3/2}$, to get

$$u_\varepsilon = -1 + 3\varepsilon y^2 + \left(\varepsilon^{3/2}\log\varepsilon\right)\frac{\lambda_0}{108} + \varepsilon^{3/2}\left(-2y^3 + \frac{\lambda_0}{54}\log y + c_1\right) + \left(-\varepsilon^2\log\varepsilon\right)\frac{\lambda_0}{27}y + \varepsilon^2\left[-\frac{2\lambda_0}{27}y\log y + b_1 y\right] + \mathcal{O}(\varepsilon^{5/2}\log\varepsilon)\,. \tag{4.2.30}$$

The terms of order $\mathcal{O}(\varepsilon^{3/2}\log\varepsilon)$ and order $\mathcal{O}(\varepsilon^2\log\varepsilon)$ cannot be matched to by the inner solution and so they must be removed by the addition of switchback terms to the outer expansion. Additionally, the $\mathcal{O}(\varepsilon)$ term in (4.2.30) and equation (4.2.29) indicate that $v \sim v_0 + o(1)$, where v_0 satisfies

$$v_0'''' = 0\,, \quad 0 < y < \infty\,; \qquad v_0(0) = 1\,, \quad v_0' = v_0'''(0) = 0\,; \quad v_0 \sim 3y^2 \quad \text{as} \quad y \to \infty\,, \tag{4.2.31a}$$

and so admits the exact solution

$$v_0 = 3y^2 + 1\,. \tag{4.2.31b}$$

The constant term in (4.2.31b) then generates the unmatched term ε in the outer region, which can only be removed by introducing a second switchback term into the outer expansion.

This suggests that λ_ε, and the outer expansion for u_ε, must have the form

$$u_\varepsilon = u_0 + \varepsilon u_{1/2} + \left(\varepsilon^{3/2}\log\varepsilon\right) u_{3/2} + \varepsilon^{3/2} u_1 + \cdots, \qquad \lambda_\varepsilon = \varepsilon^{3/2}\lambda_0 + \varepsilon^2\lambda_1 + \cdots. \tag{4.2.32}$$

Upon substituting (4.2.32) into (4.2.21), and collecting similar terms in ε, $u_{1/2}$ is observed to satisfy

$$u_{1/2xxxx} = 0\,, \quad 0 < x < 1\,; \qquad u_{1/2}(0) = 1\,,\ u_{1/2x}(0) = b_{1/2}\,,\ u_{1/2}(1) = u_{1/2x}(1) = 0\,, \tag{4.2.33a}$$

where $b_{1/2}$ is a constant to be found. The condition $u_{1/2}(0) = 1$ accounts for the constant term in v_0. The solution is

$$u_{1/2}(x) = 1 + b_{1/2}x + \left(-3 - 2b_{1/2}\right)x^2 + \left(b_{1/2} + 2\right)x^3\,. \tag{4.2.33b}$$

Similarly, $u_{3/2}(x)$ satisfies $u_{3/2xxxx} = 0$. To eliminate the $\mathcal{O}(\varepsilon^{3/2}\log\varepsilon)$ and $\mathcal{O}(\varepsilon^2\log\varepsilon)$ terms in (4.2.30), $u_{3/2}$ should satisfy $u_{3/2xxxx} = 0$ together with the conditions

$$u_{3/2}(0) = -\frac{\lambda_0}{108}\,, \quad u_{3/2x}(0) = \frac{\lambda_0}{27}\,, \quad u_{3/2}(1) = u_{3/2x}(1) = 0\,. \tag{4.2.34a}$$

The solution for $u_{3/2}$ is

$$u_{3/2} = \lambda_0\left(-\frac{1}{108} + \frac{x}{27} - \frac{5x^2}{108} + \frac{x^3}{54}\right). \tag{4.2.34b}$$

Substituting (4.2.25), (4.2.26), (4.2.33b), (4.2.34b), for u_0, u_1, $u_{1/2}$, and $u_{3/2}$ respectively, into the outer expansion (4.2.32), and writing the resulting expression in terms of the inner variable $x = \varepsilon^{1/2}y$ generates the following behaviour for u_ε as $x \to 0$:

$$\begin{aligned} u \sim -1 + \varepsilon\left(3y^2 + 1\right) + \varepsilon^{3/2}\left(-2y^3 + \frac{\lambda_0}{54}\log y + b_{1/2}y + c_1\right) \\ + \varepsilon^2\left(-(3 + 2b_{1/2})y^2 - \frac{2\lambda_0}{27}y\log y + b_1 y + \cdots\right). \end{aligned} \tag{4.2.35}$$

The local behaviour (4.2.35) suggests that the correct expansion of the inner solution is

$$v = v_0 + \varepsilon^{1/2}v_1 + \varepsilon v_2 + \cdots. \tag{4.2.36}$$

Substituting (4.2.36) and (4.2.32) for λ_ε into (4.2.29), shows that v_0 satisfies (4.2.31),

v_1 satisfies

$$v_1'''' = -\frac{\lambda_0}{v_0^2}\,, \quad 0 < y < \infty\,; \qquad v_1(0) = v_1'(0) = v_1'''(0) = 0\,, \tag{4.2.37a}$$

$$v_1 \sim -2y^3 + \frac{\lambda_0}{54}\log y + b_{1/2}y + c_1\,, \quad \text{as} \quad y \to \infty\,, \tag{4.2.37b}$$

while v_2 satisfies

$$v_2'''' = \frac{2\lambda_0}{v_0^3}v_1 - \frac{\lambda_1}{v_0^2}\,, \quad 0 < y < \infty\,; \qquad v_2(0) = v_2'(0) = v_2'''(0) = 0\,, \tag{4.2.38a}$$

$$v_2 \sim -\left(3 + 2b_{1/2}\right)y^2 - \frac{2\lambda_0}{27}\,y\log y + b_1 y + \cdots\,, \quad \text{as} \quad y \to \infty\,. \tag{4.2.38b}$$

The solution to these problems fix the values of λ_0, λ_1, $b_{1/2}$, c_1 and b_1, as is demonstrated below.

To calculate λ_0, (4.2.37a) is integrated from $0 < y < R$ using $v_0 = (3y^2+1)$ to get

$$\lim_{R\to\infty} v_1'''\Big|_0^R = -\lambda_0\int_0^\infty \frac{1}{(3y^2+1)^2}\,dy = -\frac{\lambda_0}{9}\int_0^\infty \frac{1}{(y^2+1/3)^2}\,dy = -\frac{\lambda_0}{9}\left(\frac{3\sqrt{3}\pi}{4}\right).$$

Using the limiting behaviour $v_1 \sim -2y^3$ as $y \to \infty$ determines that $\lambda_0 = 48\sqrt{3}/\pi$.

To value of $b_{1/2}$ is determined by the following application of Green's second identity,

$$\lim_{R\to\infty}\int_0^R \left(v_0 v_1'''' - v_1 v_0''''\right)\,dy = \lim_{R\to\infty}\left(v_0 v_1''' - v_0' v_1'' + v_0'' v_1' - v_0''' v_1\right)\Big|_0^R.$$

Using $v_0(y) = 3y^2+1$ together with the problem for v_1, (4.2.37), we obtain that

$$\lim_{R\to\infty}\int_0^R v_0 v_1''''\,dy = \lim_{R\to\infty}\left[\left(3R^2+1\right)(-12) - 6R(-12R) + 6\left(-6R^2 + b_{1/2}\right) + \cdots\right],$$

$$-\lambda_0\lim_{R\to\infty}\int_0^R \frac{1}{v_0}\,dy = -\lambda_0\int_0^\infty \frac{1}{3y^2+1}\,dy = -12 + 6b_{1/2}\,. \tag{4.2.39}$$

Evaluating the integral and using $\lambda_0 = 48\sqrt{3}/\pi$ results in $b_{1/2} = -2$.

To determine c_1 in (4.2.37), the value of $v_1''(0)$ is calculated so that (4.2.37) may be posed as an initial value problem for v_1. To determine $v_1''(0)$, multiply (4.2.37) by v_0',

and integrate over $0 < y < R$, to get

$$\lim_{R\to\infty}\int_0^R v_0' v_1'''' \, dy = \lim_{R\to\infty}\left(v_0' v_1''' - v_0'' v_1''\right)\Big|_0^R + \lim_{R\to\infty}\int_0^R v_1'' v_0''' \, dy\,,$$

$$-\lambda_0 \lim_{R\to\infty}\int_0^R \frac{v_0'}{v_0^2}\, dy = v_0''(0)v_1''(0) + \lim_{R\to\infty}\left[6R(-12) - 6(-12R) + \cdots\right]\,,$$

$$\lambda_0 \lim_{R\to\infty}\left(\frac{1}{v_0}\right)\Big|_{v_0=1}^{\infty} = 6v_1''(0)\,. \tag{4.2.40}$$

Since $v_0(0) = 1$, this yields that $v_1''(0) = -\lambda_0/6$. Then, with the initial values $v_1(0) = v_1'(0) = v_1'''(0) = 0$, and $v_1''(0) = -\lambda_0/6$, (4.2.37) can be integrated explicitly for v_1 to obtain

$$v_1 = -\frac{\lambda_0}{12\sqrt{3}}\, y^3 \tan^{-1}(\sqrt{3}y) - \frac{\lambda_0}{36}y^2 + \frac{\lambda_0}{108}\log(1+3y^2) - \frac{\lambda_0}{12\sqrt{3}}\, y \tan^{-1}(\sqrt{3}y)\,. \tag{4.2.41}$$

Using the large argument expansion $\tan^{-1}(z) \sim \pi/2 - z^{-1} + (3z^3)^{-1}$ for $z \to \infty$ in (4.2.41), shows that

$$v_1 \sim -\frac{\lambda_0\pi}{24\sqrt{3}}y^3 + \frac{\lambda_0}{54}\log y - \frac{\lambda_0\pi}{24\sqrt{3}}y + \frac{2\lambda_0}{81} + \frac{\lambda_0 \log 3}{108}\,, \quad \text{as} \quad y \to \infty\,. \tag{4.2.42}$$

Since $\lambda_0 = 48\sqrt{3}/\pi$, a comparison of (4.2.42) with the required far-field behaviour for v_1 in (4.2.37b), determines c_1 as

$$c_1 = \lambda_0\left(\frac{2}{81} + \frac{\log 3}{108}\right)\,, \qquad \lambda_0 = \frac{48\sqrt{3}}{\pi}\,. \tag{4.2.43}$$

Next, λ_1 is calculated from (4.2.38) by integrating (4.2.38a) over $0 < y < \infty$, and applying the condition $v_2''' \to 0$ as $y \to \infty$, to obtain that

$$\lambda_1 \int_0^\infty \frac{1}{v_0^2}\, dy = 2\lambda_0 \int_0^\infty \frac{v_1}{v_0^3}\, dy\,.$$

Then, since $v_0 = 3y^2 + 1$, the above expression simplifies to

$$\lambda_1 = \frac{8\sqrt{3}\lambda_0}{\pi}\int_0^\infty \frac{v_1}{(3y^2+1)^3}\, dy\,. \tag{4.2.44}$$

This integral can be directly evaluated using the known form of v_1, given in equation (4.2.41). In this way, we have that

$$\lambda_1 \equiv \frac{8\sqrt{3}\lambda_0}{\pi}\left[-\frac{\lambda_0}{12\sqrt{3}}I_1 - \frac{\lambda_0}{36}I_2 + \frac{\lambda_0}{108}I_3 - \frac{\lambda_0}{12\sqrt{3}}I_4\right] \tag{4.2.45}$$

where

$$
\begin{aligned}
I_1 &= \int_0^\infty \frac{y^3 \tan^{-1}(\sqrt{3}y)}{(1+3y^2)^3}\,dy = \frac{-1}{12}\int_0^\infty \left[\frac{1}{(1+3y^2)^2}\right]_y y^2 \tan^{-1}(\sqrt{3}y)\,dy \\
&= \frac{1}{12}\int_0^\infty \left[\frac{2y\tan^{-1}(\sqrt{3}y)}{(1+3y^2)^2} + \frac{\sqrt{3}y^2}{(1+3y^2)^3}\right] dy \\
&= -\frac{1}{36}\int_0^\infty \left[\frac{1}{1+3y^2}\right]_y \tan^{-1}(\sqrt{3}y)\,dy + \frac{1}{4\sqrt{3}}\int_0^\infty \frac{y^2}{(1+3y^2)^3}\,dy \\
&= \frac{1}{12\sqrt{3}}\int_0^\infty \frac{dy}{(1+3y^2)^2} + \frac{1}{4\sqrt{3}}\int_0^\infty \frac{y^2\,dy}{(1+3y^2)^3} \\
&= \frac{1}{12\sqrt{3}}\left(\frac{\pi}{4\sqrt{3}}\right) + \frac{1}{4\sqrt{3}}\left(\frac{\pi}{48\sqrt{3}}\right) = \frac{5\pi}{576}.
\end{aligned}
$$

$$
I_2 = \int_0^\infty \frac{y^2\,dy}{(1+3y^2)^3} = \frac{\pi}{48\sqrt{3}}. \qquad I_3 = \int_0^\infty \frac{\log(1+3y^2)}{(1+3y^2)^3}\,dy = \frac{\pi(12\log 2 - 7)}{32\sqrt{3}}.
$$

$$
\begin{aligned}
I_4 &= \int_0^\infty \frac{y\tan^{-1}(\sqrt{3}y)}{(1+3y^2)^3}\,dy = \frac{-1}{12}\int_0^\infty \left[\frac{1}{(1+3y^2)^2}\right]_y \tan^{-1}(\sqrt{3}y)\,dy \\
&= \frac{1}{12}\int_0^\infty \frac{dy}{(1+3y^2)^3} = \frac{\pi}{64}.
\end{aligned}
$$

After some simplification, the following compact expression for λ_1 is obtained:

$$
\lambda_1 = \frac{\lambda_0^2}{108}\,(3\log 2 - 4) \approx -12.454. \tag{4.2.46}
$$

Finally, b_1 is calculated from (4.2.38) by first multiplying (4.2.38a) by v_0 followed by integration of the resulting expression over $0 < y < R$ to get

$$
\int_0^R v_0 v_2''''\,dy = 2\lambda_0 \int_0^R \frac{v_1}{v_0^2}\,dy - \lambda_1 \int_0^R \frac{1}{v_0}\,dy\,. \tag{4.2.47}
$$

Since $v_1 \sim -2y^3$ and $v_0 \sim 3y^2$ as $y \to \infty$, then $v_1/v_0^2 \sim -2/(9y)$ as $y \to \infty$ and therefore the first integral on the right-hand side of (4.2.47) diverges as $R \to \infty$. Equation (4.2.47) must therefore be rewritten as

$$
\begin{aligned}
\left[v_0 v_2'''\Big|_0^R - v_0' v_2''\Big|_0^R + \int_0^R v_0'' v_2''\,dy\right] &= 2\lambda_0 \int_0^R \left(\frac{v_1}{v_0^2} + \frac{2}{9(y+1)}\right) dy \\
&\quad - \frac{4\lambda_0}{9}\log(R+1) - \lambda_1 \int_0^R \frac{1}{v_0}\,dy\,.
\end{aligned} \tag{4.2.48}
$$

Then, by using $v_0 = 3y^2 + 1$ and the asymptotic behaviour of v_2 as $y \to \infty$ in (4.2.38b), the limit $R \to \infty$ may now be taken to get

$$b_1 = -\frac{\lambda_0}{27} + \frac{\lambda_0}{3}\int_0^\infty \left(\frac{v_1}{v_0^2} + \frac{2}{9(y+1)}\right) dy - \frac{2\lambda_0}{3}\int_0^\infty \frac{v_1}{v_0^3}\, dy\,. \tag{4.2.49}$$

In the preceding calculation, the result $\int_0^\infty v_0^{-1}\, dy = \pi/(2\sqrt{3})$ has been used.

The following is a summary of the asymptotic result:

Principal Result 4.5: *For $\varepsilon \equiv u(0)+1 \to 0^+$, the maximal solution branch of* (4.2.21) *has asymptotic behaviour*

$$\lambda_\varepsilon \sim \frac{48\sqrt{3}}{\pi}\left(\varepsilon^{3/2} + \frac{4\varepsilon^2}{3\sqrt{3}\pi}\big(3\log 2 - 4\big) + \cdots\right), \tag{4.2.50a}$$

In the outer region, defined away from $x = 0$, a four-term expansion for u_ε is

$$u_\varepsilon = -1 + 3x^2 - 2x^3 + \varepsilon\left(1 - 2x + x^2\right) + \left(\varepsilon^{3/2}\log\varepsilon\right) u_{3/2} + \varepsilon^{3/2}u_1 + \cdots\,. \tag{4.2.50b}$$

Here $u_{3/2}$ is given in terms of $\lambda_0 = 48\sqrt{3}/\pi$ by (4.2.34b)*, and u_1 is defined uniquely in terms of c_1 and b_1 of* (4.2.43) *and* (4.2.49)*, respectively, by the boundary value problem* (4.2.24b) *with singular behaviour* (4.2.26)*.*

A very favorable comparison of numerical and asymptotic results for $|u(0)|$ versus λ is given in Fig. 4.7. The two-term approximation for λ in (4.2.50a) is shown to be rather accurate even for λ not too small.

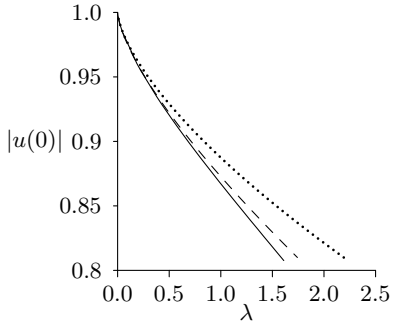

Figure 4.7: The full numerical result (solid line) for $|u(0)| = 1 - \varepsilon$ versus λ for the biharmonic MEMS problem (4.2.21) is compared with the one-term (dotted curve) and the two-term (dashed curve) asymptotic result given in (4.2.50a).

A similar analysis can be done for the more general mixed biharmonic MEMS problem, written as

$$-u_{xxxx} + \beta u_{xx} = \frac{\tilde{\lambda}}{(1+u)^2}\,, \quad |x| < 1\,; \quad u(\pm 1) = u_x(\pm 1) = 0\,, \tag{4.2.51a}$$

where β and $\tilde{\lambda}$ have the following definition $\delta = \mathcal{O}(1)$ by

$$\beta = \delta^{-1}\,, \qquad \lambda = \delta\tilde{\lambda}\,. \tag{4.2.51b}$$

For a fixed $\delta = \mathcal{O}(1)$, the limiting behaviour of the maximal solution branch $(\tilde{\lambda}_\varepsilon, u_\varepsilon)$ is constructed in the limit $u_\varepsilon(0) + 1 = \varepsilon \to 0^+$. Equation (4.2.51a) may be considered on the interval $0 \le x < 1$ with symmetry conditions $u_x(0) = u_{xxx}(0) = 0$.

As for the pure biharmonic problem (4.2.21), the expansion for $\tilde{\lambda}_\varepsilon$ and the outer expansion for u_ε is (see (4.2.32)),

$$u_\varepsilon \sim u_0 + \varepsilon u_{1/2} + \varepsilon^{3/2}\log\varepsilon\; u_{3/2} + \varepsilon^{3/2}u_1 + \cdots\,, \qquad \tilde{\lambda}_\varepsilon \sim \varepsilon^{3/2}\tilde{\lambda}_0 + \varepsilon^2\tilde{\lambda}_1 + \cdots\,. \tag{4.2.52}$$

Upon substituting (4.2.52) into (4.2.51), and imposing the point constraints $u_0(0) = -1$ and $u_{0x}(0) = 0$, we obtain that u_0 and u_1 satisfy

$$-u_{0xxxx} + \beta u_{0xx} = 0\,, \quad 0 < x < 1\,; \qquad \begin{array}{c} u_0(0) = -1\,, \quad u_{0x}(0) = 0 \\ u_0(1) = u_{0x}(1) = 0\,, \end{array} \tag{4.2.53a}$$

$$-u_{1xxxx} + \beta u_{1xx} = \frac{\tilde{\lambda}_0}{(1+u_0)^2}\,, \quad 0 < x < 1\,; \quad u_1(1) = 0\,,\;\; u_{1x}(1) = 0\,. \tag{4.2.53b}$$

Moreover, the two switchback terms $u_{1/2}$ and $u_{3/2}$ are taken to satisfy

$$-u_{1/2xxxx} + \beta u_{1/2xx} = 0\,, \quad 0 < x < 1\,; \qquad \begin{array}{c} u_{1/2}(0) = 1\,, \quad u_{1/2x}(0) = b_{1/2}\,, \\ u_{1/2}(1) = u_{1/2x}(1) = 0 \end{array} \tag{4.2.54a}$$

$$-u_{3/2xxxx} + \beta u_{3/2xx} = 0 \quad 0 < x < 1\,; \qquad \begin{array}{c} u_{3/2}(0) = c_{3/2}\,, \quad u_{3/2x}(0) = b_{3/2} \\ u_{3/2}(1) = u_{3/2x}(1) = 0 \end{array} \tag{4.2.54b}$$

for some constants $c_{3/2}$, $b_{3/2}$, and $b_{1/2}$, to be found.

The solution to (4.2.53a) for u_0 is given by

$$u_0(x) = -1 + C\left[\cosh(\sqrt{\beta}x) - 1\right] + D\left[\sqrt{\beta}x - \sinh\left(\sqrt{\beta}x\right)\right]\,, \tag{4.2.55a}$$

where C and D are constants given in terms of β by

$$C = \left[\sqrt{\beta}\coth\left(\frac{\sqrt{\beta}}{2}\right) - 2\right]^{-1}\,, \qquad D = \left[\sqrt{\beta} - 2\tanh\left(\frac{\sqrt{\beta}}{2}\right)\right]^{-1}\,. \tag{4.2.55b}$$

From (4.2.55), the local behaviour of u_0 is determined to be

$$u_0 \sim -1 + \alpha x^2 + \gamma x^3 + \frac{\alpha\beta}{12} x^4 + \cdots, \quad \text{as} \quad x \to 0\,, \tag{4.2.56a}$$

where α and γ are given by

$$\begin{aligned} \alpha &\equiv \frac{1}{2}\, u_{0xx}(0) = \left(\frac{\beta}{2}\right)\left[\sqrt{\beta}\coth\left(\frac{\sqrt{\beta}}{2}\right) - 2\right]^{-1}, \\ \gamma &\equiv \frac{1}{6}\, u_{0xxx}(0) = -\left(\frac{\beta^{3/2}}{6}\right)\left[\sqrt{\beta} - 2\tanh\left(\frac{\sqrt{\beta}}{2}\right)\right]^{-1}. \end{aligned} \tag{4.2.56b}$$

As $\delta \to \infty$, corresponding to $\beta \to 0$, $(\alpha, \gamma) \to (3, -2)$, which agrees with the result for u_0 given in (4.2.25) for the pure biharmonic case. As required for the analysis below, it is readily established from (4.2.56b) that $\alpha > 0$ and $\gamma < 0$ for all $\delta \geq 0$.

Next, from the problem (4.2.53b) for u_1, the local behaviour as $x \to 0$ for u_1 is

$$u_1 \sim \frac{\tilde{\lambda}_0}{6\alpha^2} \log x + \frac{\gamma\tilde{\lambda}_0}{\alpha^3} x \log x + c_1 + b_1 x\,, \quad \text{as} \quad x \to 0\,. \tag{4.2.57}$$

where c_1 and b_1, representing unknown coefficients associated with the homogeneous solution for u_1, are to be determined. Next, the local behaviours (4.2.56a) and (4.2.57) for u_0 and u_1, respectively, are used together with the local behaviour for $u_{1/2}$ and $u_{3/2}$ from (4.2.54), to obtain the following near-field behaviour as $x \to 0$ of the outer expansion in (4.2.52):

$$\begin{aligned} u \sim\ & -1 + \alpha x^2 + \gamma x^3 + \frac{\alpha\beta}{12} x^4 + \cdots \varepsilon \left(1 + b_{1/2} x + u_{1/2xx}(0)\frac{x^2}{2} + \cdots\right) \\ & + \varepsilon^{3/2} \log\varepsilon \left(c_{3/2} + b_{3/2} x + \cdots\right) + \varepsilon^{3/2} \left(\frac{\tilde{\lambda}_0}{6\alpha^2} \log x + \frac{\gamma\tilde{\lambda}_0}{\alpha^3} x \log x + c_1 + b_1 x + \cdots\right). \end{aligned} \tag{4.2.58}$$

In terms in the inner variable y, defined by $x = \varepsilon^{1/2} y$, (4.2.58) becomes

$$\begin{aligned} u \sim\ & -1 + \varepsilon\left(\alpha y^2 + 1\right) + \left(\varepsilon^{3/2}\log\varepsilon\right)\left(c_{3/2} + \frac{\tilde{\lambda}_0}{12\alpha^2}\right) \\ & + \varepsilon^{3/2}\left(\gamma y^3 + b_{1/2} y + \frac{\tilde{\lambda}_0}{6\alpha^2}\log y + c_1\right) + \left(\varepsilon^2 \log\varepsilon\right)\left(b_{3/2} y + \frac{\gamma\tilde{\lambda}_0}{2\alpha^3} y\right) \\ & + \varepsilon^2\left(u_{1/2xx}(0)\frac{y^2}{2} + \frac{\gamma\tilde{\lambda}_0}{\alpha^3} y \log y + \frac{\alpha\beta}{12} y^4 + b_1 y\right) + \cdots. \end{aligned} \tag{4.2.59}$$

To eliminate the $\mathcal{O}(\varepsilon^{3/2}\log\varepsilon)$ and $\mathcal{O}(\varepsilon^2\log\varepsilon)$ terms, which cannot be matched by the inner solution, the following values must be chosen for $b_{3/2}$ and $c_{3/2}$:

$$c_{3/2} = -\frac{\tilde{\lambda}_0}{12\alpha^2}\,, \qquad b_{3/2} = -\frac{\gamma\tilde{\lambda}_0}{2\alpha^3}\,. \tag{4.2.60}$$

With $c_{3/2}$ and $b_{3/2}$ given by (4.2.60), the solution $u_{3/2}$ to (4.2.54b) is determined explicitly.

In the vicinity of the origin, local variables $y = x/\varepsilon^{1/2}$ and $\varepsilon v(y) = 1 + u(\varepsilon^{1/2}y)$ are introduced, with $v(y)$ taking on expansion $v = v_0 + \varepsilon^{1/2}v_1 + \varepsilon v_2 + \cdots$. Then, from (4.2.51) and (4.2.52) for $\tilde{\lambda}_\varepsilon$, the leading-order inner solution is $v_0 = \alpha y^2 + 1$, and v_1 satisfies

$$v_1'''' = -\frac{\tilde{\lambda}_0}{v_0^2}\,, \quad 0 < y < \infty\,; \qquad v_1(0) = v_1'(0) = v_1'''(0) = 0\,, \tag{4.2.61a}$$

$$v_1 \sim \gamma y^3 + b_{1/2}y + \frac{\tilde{\lambda}_0}{6\alpha^2}\log y + c_1\,, \quad \text{as} \quad y \to \infty\,, \tag{4.2.61b}$$

while v_2 is the solution of

$$v_2'''' = \frac{2\tilde{\lambda}_0}{v_0^3}v_1 - \frac{\tilde{\lambda}_1}{v_0^2} + \beta v_0''\,, \quad 0 < y < \infty\,; \qquad v_2(0) = v_2'(0) = v_2'''(0) = 0\,, \tag{4.2.62a}$$

$$v_2 \sim \frac{\alpha\beta}{12}y^4 + u_{1/2xx}(0)\frac{y^2}{2} + \frac{\gamma\tilde{\lambda}_0}{\alpha^3}y\log y + b_1 y + \cdots\,, \quad \text{as} \quad y \to \infty\,. \tag{4.2.62b}$$

By repeating the analysis of the pure biharmonic case in (4.2.39)–(4.2.49), the values of $\tilde{\lambda}_0$, $\tilde{\lambda}_1$, $b_{1/2}$, c_1, and b_1, can be determined from (4.2.61) and (4.2.62). In fixing $\tilde{\lambda}_1$ and b_1 from (4.2.62), the decomposition $v_2 = \tilde{v}_2 + \alpha\beta y^4/12$ must be made to obtain a problem for $\tilde{v}_2$ without the $v_0'' = 2\alpha$ term in (4.2.62a). From the problem (4.2.61) for v_1, it is calculated that

$$\tilde{\lambda}_0 = -\frac{24\gamma\sqrt{\alpha}}{\pi}\,, \qquad b_{1/2} = \frac{3\gamma}{\alpha} = -\sqrt{\beta}\coth\left(\frac{\sqrt{\beta}}{2}\right)\,, \qquad c_1 = \frac{\tilde{\lambda}_0}{\alpha^2}\left(\frac{2}{9} + \frac{\log\alpha}{12}\right)\,. \tag{4.2.63}$$

By using a simple scaling relation to transform (4.2.61) to (4.2.37), with solution (4.2.41), the solution to (4.2.61) for v_1 is

$$v_1 = -\frac{\tilde{\lambda}_0}{12\sqrt{\alpha}}\,y^3\tan^{-1}(\sqrt{\alpha}y) - \frac{\tilde{\lambda}_0}{12\alpha}y^2 + \frac{\tilde{\lambda}_0}{12\alpha^2}\log(1+\alpha y^2) - \frac{\tilde{\lambda}_0}{4\alpha^{3/2}}\,y\tan^{-1}(\sqrt{\alpha}y)\,. \tag{4.2.64}$$

In terms of the solution v_1, the following values are determined from the problem (4.2.62)

for v_2:

$$\tilde{\lambda}_1 = \frac{8\tilde{\lambda}_0\sqrt{\alpha}}{\pi}\int_0^\infty \frac{v_1}{v_0^3}\,dy\,, \quad b_1 = \frac{\tilde{\lambda}_0\gamma}{2\alpha^3} + \frac{\tilde{\lambda}_0}{\alpha}\int_0^\infty \left(\frac{v_1}{v_0^2} - \frac{\gamma}{\alpha^2(y+1)}\right) dy - \frac{2\tilde{\lambda}_0}{\alpha}\int_0^\infty \frac{v_1}{v_0^3}\,dy\,, \tag{4.2.65}$$

Here $v_0 = \alpha y^2 + 1$. The integral term in the formulation of λ_1 can be evaluated explicitly as was done for the pure biharmonic case (c.f. (4.2.45)-(4.2.46)) to give the following compact expression

$$\tilde{\lambda}_1 = \frac{\lambda_0^2}{12\alpha^2}\big(3\log 2 - 4\big) \tag{4.2.66}$$

The following summarizes the asymptotic result for (4.2.51):

Principal Result 4.6: *For $\varepsilon \equiv u(0)+1 \to 0^+$, the maximal solution branch of* (4.2.51) *has the asymptotic behaviour*

$$\tilde{\lambda}_\varepsilon \sim -\frac{24\gamma\sqrt{\alpha}}{\pi}\left(\varepsilon^{3/2} - \frac{2\gamma\varepsilon^2}{\alpha^{3/2}\pi}\big(3\log 2 - 4\big) + \cdots\right), \tag{4.2.67a}$$

where α and γ are defined in terms of $\beta = \delta^{-1}$ by (4.2.56b)*. In the outer region, defined away from $x = 0$, a four-term expansion for u_ε is*

$$u_\varepsilon \sim u_0 + \varepsilon u_{1/2} + \varepsilon^{3/2}\log\varepsilon\; u_{3/2} + \varepsilon^{3/2}u_1 + \cdots\,. \tag{4.2.67b}$$

Here u_0 is given explicitly in (4.2.55)*, while $u_{1/2}$ and $u_{3/2}$ are the solutions of* (4.2.54) *in terms of the coefficients $c_{3/2}$ and $b_{3/2}$, defined in* (4.2.60)*, and $b_{1/2}$ given in* (4.2.63)*. Finally, u_1 satisfies* (4.2.53b)*, subject to the local behaviour* (4.2.57)*, where c_1 and b_1 are defined in* (4.2.63) *and* (4.2.65)*, respectively.*

We conclude this section with a few remarks. First, note that since $\alpha > 0$ and $\gamma < 0$ for all $\delta > 0$, the limiting behaviour in (4.2.67a) satisfies $\tilde{\lambda}_\varepsilon > 0$, and is defined for all $\delta > 0$. For $\delta \to \infty$, for which $\alpha \to 3$ and $\gamma \to -2$, (4.2.67a) agrees with the pure biharmonic case result in (4.2.50a). Alternatively, for $0 < \delta \ll 1$, a direct calculation of (4.2.56b) shows that $\alpha \sim \left[2\sqrt{\delta}\right]^{-1}$ and $\gamma \sim -\left[6\delta\right]^{-1}$, so that $\lambda_\varepsilon \equiv \delta\tilde{\lambda}_\varepsilon$ has the small δ behaviour $\lambda_\varepsilon \sim \varepsilon^{3/2}\delta^{-1/4}2\sqrt{2}/\pi$, which is not uniformly valid when $\varepsilon^{3/2}\delta^{-1/4} = \mathcal{O}(1)$. Finally, we remark that the two switchback terms can be written explicitly in the form $u_{1/2}(x) = w(x;1,b_{1/2})$ and $u_{3/2}(x) = w(x;c_{3/2},b_{3/2})$, where $w(x;w_0.w_1)$ is the solution to $-w_{xxxx} + \beta w_{xx} = 0$ with $w(0) = w_0$, $w_x(0) = w_1$, $w(1) = w_x(1) = 0$, given explicitly by

$$w(x) = w_0 + w_1 x + \mathcal{C}\left[\cosh\left(\sqrt{\beta}x\right) - 1\right] + \mathcal{D}\left[\sqrt{\beta}x - \sinh\left(\sqrt{\beta}x\right)\right], \tag{4.2.68a}$$

where $\mathcal{C}$ and $\mathcal{D}$ is the unique solution to the 2×2 linear algebraic system

$$\mathcal{C}\left[\cosh\left(\sqrt{\beta}\right) - 1\right] + \mathcal{D}\left[\sqrt{\beta} - \sinh\left(\sqrt{\beta}\right)\right] = -(w_0 + w_1)\,, \tag{4.2.68b}$$

$$\mathcal{C}\sqrt{\beta}\sinh\left(\sqrt{\beta}\right) + \mathcal{D}\sqrt{\beta}\left[1 - \cosh\left(\sqrt{\beta}\right)\right] = -w_1\,. \tag{4.2.68c}$$

In Fig. 4.8 shows a favorable comparison between the two-term asymptotic result (4.2.67a) and the full numerical result for $\lambda_\varepsilon = \delta\tilde{\lambda}_\varepsilon$ when $\delta = 0.1$ and $\delta = 1.0$.

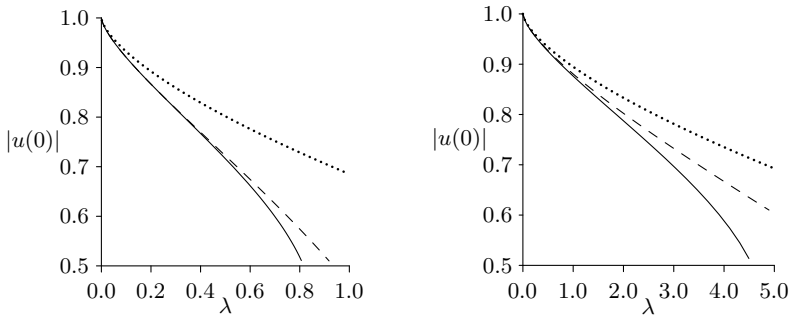

(a) $\delta = 0.1$ (b) $\delta = 1.0$

Figure 4.8: The full numerical result (solid line) for $|u(0)| = 1 - \varepsilon$ versus λ for the mixed biharmonic MEMS problem (4.2.51) is compared with the one-term (dotted curve) and the two-term (dashed curve) asymptotic result given in (4.2.67a) for $\delta = 0.1$ and $\delta = 1.0$.

4.3 Asymptotics Of Maximal Solution Branch As $\lambda \to 0$: Unit Disk

4.3.1 The Beam Problem

For the unit disk in $\mathbb{R}^2$, the limiting behaviour of the maximal solution branch of the pure biharmonic nonlinear eigenvalue problem

$$\Delta^2 u = -\frac{\lambda}{(1+u)^2}\,, \quad 0 < r < 1\,; \qquad u(1) = u_r(1) = 0\,, \tag{4.3.1}$$

and the mixed biharmonic problem

$$\delta\Delta^2 u - \Delta u = -\frac{\lambda}{(1+u)^2}\,, \quad 0 < r < 1\,; \qquad u(1) = u_r(1) = 0\,, \tag{4.3.2}$$

are constructed. Here $\Delta u \equiv u_{rr} + r^{-1}u_r$ and $\delta > 0$. In each case, as with those considered in previous sections, the definition $u(0) + 1 = \varepsilon$ is made and a solution $(\lambda_\varepsilon, u_\varepsilon)$ is constructed such that $\lambda_\varepsilon \sim \nu(\varepsilon)\,\lambda_0$ as $\varepsilon \to 0^+$, where $\nu(\varepsilon)$ is a gauge function

to be determined and satisfies $\nu(\varepsilon) \to 0$ as $\varepsilon \to 0^+$. Since the asymptotic analyses for (4.3.1) and (4.3.2) are very similar, a full analysis is demonstrated for the pure biharmonic case, while the main results for the mixed problem are merely stated.

The main challenge in constructing the asymptotic solution of (4.3.1) as $u(0) \to -1^+$ is determining the gauge function $\nu(\varepsilon)$ and also the correct expansion of u_ε. This is achieved by matching an inner solution valid in a small neighbourhood of the origin to an outer expansion valid elsewhere.

The initial naive expansions for λ and the outer solution are of the form

$$u_\varepsilon = u_0 + \nu(\varepsilon)\, u_1 + \cdots, \qquad \lambda_\varepsilon = \nu(\varepsilon)\, \lambda_0 + \cdots. \tag{4.3.3}$$

Substituting (4.3.3) into (4.3.1), gives the following equations on $0 < r < 1$ satisfied u_0 and u_1

$$\Delta^2 u_0 = 0\,, \qquad u_0(1) = u_{0r}(1) = 0\,; \qquad \Delta^2 u_1 = -\frac{\lambda_0}{(1+u_0)^2}\,, \qquad u_1(1) = u_{1r}(1) = 0\,. \tag{4.3.4}$$

By imposing the point constraints $u_0(0) = -1$ and $u_{0r}(0) = 0$, the solution to (4.3.4) for u_0 is

$$u_0 = -1 + r^2 - 2r^2 \log r\,, \tag{4.3.5}$$

while u_1 satisfies

$$\Delta^2 u_1 = -\frac{\lambda_0}{r^4(1 - 2\log r)^2}\,, \quad 0 < r < 1\,; \qquad u_1(1) = u_1'(1) = 0\,. \tag{4.3.6}$$

Note that $u_{0r}(0) = 0$, while $u_{0rr}(r)$ diverges as $r \to 0$. This indicates that a boundary layer in the vicinity of $r = 0$ is required in order to satisfy the required symmetry condition $u_{rrr}(0) = 0$.

To determine the behaviour of u_1 as $r \to 0$, new variables $\eta = -\log r$ and $w(\eta) = u\,(e^{-\eta})$ are introduced so that $\eta \to \infty$ as $r \to 0$. Using these new co-ordinates, (4.3.6), becomes

$$w'''' + 4w''' + 4w'' = -\frac{\lambda_0}{(1+2\eta)^2} = -\frac{\lambda_0}{4\eta^2}\left(1 + \frac{1}{2\eta}\right)^{-2}. \tag{4.3.7}$$

By using $(1+h)^{-2} \sim 1 - 2h + 3h^2 + \cdots$, for $h \ll 1$, (4.3.7) is solved asymptotically to get

$$w \sim \frac{\lambda_0}{16}\log\eta - \frac{\lambda_0}{32\eta} - \frac{3\lambda_0}{128\eta^2} - \frac{11\lambda_0}{384\eta^3} + \cdots, \quad \text{as} \quad \eta \to \infty\,.$$

Returning to the co-ordinates of the original problem with $\eta = -\log r$, the local be-

haviour for u_1

$$u_1 \sim \frac{\lambda_0}{16}\log(-\log r)+\frac{\lambda_0}{32\log r}-\frac{3\lambda_0}{128\log^2 r}+\frac{11\lambda_0}{384\log^3 r}+a_1+a_2\log r+\cdots\,, \quad \text{as} \quad r\to 0\,, \tag{4.3.8}$$

is established where a_1 and a_2 are constants related to the solution of the homogeneous problem. By determining these constants below, and then by satisfying the two boundary conditions $u_1(1) = u_{1r}(1) = 0$, the solution u_1 to (4.3.6) can be found uniquely. For $r \to 0$, the two-term outer expansion for u, given by (4.3.3), has the limiting behaviour

$$\begin{aligned} u \sim\ & -1 + r^2 - 2r^2\log r \\ & + \nu\left(\frac{\lambda_0}{16}\log(-\log r) + \frac{\lambda_0}{32\log r} - \frac{3\lambda_0}{128\log^2 r} + \frac{11\lambda_0}{384\log^3 r} + a_1 + a_2\log r\right) + \cdots\,. \end{aligned} \tag{4.3.9}$$

In the vicinity of the origin, local variables v and ρ are introduced for (4.3.1) with the usual definition

$$u = -1 + \varepsilon\, v(\rho)\,, \qquad \rho = r/\gamma\,, \tag{4.3.10}$$

where $\gamma \ll 1$ is the boundary layer width to be found. Upon setting $r = \gamma\,\rho$ in (4.3.9), the leading order behaviour

$$u = -1 + \gamma^2\,\rho^2 - 2\gamma^2\,\rho^2(\log\gamma + \log\rho) + \mathcal{O}\left[\nu\log(-\log\gamma)\right]\,, \tag{4.3.11}$$

is established for $\gamma \ll 1$. The largest term of (4.3.11) must be $\mathcal{O}(\varepsilon)$ if the outer and inner expansions are to be successfully matched. In addition, since $u_{0rr}(0)$ is infinite, we expect that $u_{rr}(0) = (\varepsilon/\gamma^2)v''(0)$ is not finite as $\varepsilon \to 0^+$. These considerations show that the boundary layer width is determined implicitly in terms of ε by

$$-\gamma^2\log\gamma = \varepsilon\,, \quad \text{and} \quad \sigma = -\frac{1}{\log\gamma}\,, \tag{4.3.12}$$

Using this scaling, the local behaviour (4.3.9) is written in terms of the inner variable ρ, as

$$\begin{aligned} u \sim\ & -1 + 2\rho^2\varepsilon + \sigma\varepsilon(-2\rho^2\log\rho + \rho^2) + \nu\left(-\frac{\lambda_0}{16}\log\sigma + \frac{\lambda_0}{16}\log(1-\sigma\log\rho)\right. \\ & \left. -\frac{\lambda_0}{32}\frac{\sigma}{(1-\sigma\log\rho)} - \frac{3\lambda_0\sigma^2}{128(1-\sigma\log\rho)^2} - \frac{11\lambda_0\sigma^3}{384(1-\sigma\log\rho)^3} + a_1 - \frac{a_2}{\sigma} + a_2\log\rho\right) + \cdots\,. \end{aligned} \tag{4.3.13}$$

Expanding terms in (4.3.13) for $\sigma \ll 1$, and collecting terms at each order, results in

$$\begin{aligned} u \sim -1 + \varepsilon \big[& 2\rho^2 + \sigma(-2\rho^2 \log\rho + \rho^2) \\ & + \frac{\nu}{\varepsilon}\left[-\frac{\lambda_0}{16}\log\sigma + a_1 - \frac{a_2}{\sigma} + a_2 \log\rho + \sigma\left(-\frac{\lambda_0}{16}\log\rho - \frac{\lambda_0}{32}\right)\right. \\ & + \sigma^2\left(-\frac{\lambda_0}{32}\log^2\rho - \frac{\lambda_0}{32}\log\rho - \frac{3\lambda_0}{128}\right) \\ & \left. + \ \sigma^3\left(-\frac{\lambda_0}{48}\log^3\rho - \frac{\lambda_0}{32}\log^2\rho - \frac{3\lambda_0}{64}\log\rho - \frac{11\lambda_0}{384}\right) + \cdots \right] \Big] \, . \end{aligned} \tag{4.3.14}$$

To determine the scaling of ν, first substitute the local variables (4.3.10) into (4.3.1) to obtain the inner problem

$$\Delta_\rho^2 v = -\frac{\sigma^2\nu}{\varepsilon}\frac{[\lambda_0 + \cdots]}{v^2}\,, \quad 0 < \rho < \infty\,; \qquad v(0) = 1\,, \quad v'(0) = v'''(0) = 0\,, \tag{4.3.15}$$

where Δ_ρ^2 is the Biharmonic operator in terms of ρ. The largest term in (4.3.14) is $\mathcal{O}(\varepsilon)$, which suggests the expansion of v as $v = v_0 + \sigma v_1 + \mathcal{O}(\sigma^2)$. Therefore, the only feasible scalings for ν are $\nu = \varepsilon\sigma^{-2}$ or $\nu = \varepsilon\sigma^{-1}$. If $\nu = \varepsilon\sigma^{-2}$, then to leading order v_0 satisfies $\Delta_\rho^2 v_0 = -\lambda_0/v_0^2$ with $v_0 \sim 2\rho^2$ as $\rho \to \infty$, which has no solution. Therefore, set

$$\nu = \frac{\varepsilon}{\sigma} = -\gamma^2 \log\gamma \left(\frac{-1}{\log\gamma}\right)^{-1} = \gamma^2 (\log\gamma)^2 \, . \tag{4.3.16}$$

Substituting (4.3.16) for ν into (4.3.14), and recalling that $u = -1 + \varepsilon v$, gives the far-field behaviour that the inner solution v must satisfy as $\rho \to \infty$:

$$\begin{aligned} v \sim & -\frac{1}{\sigma^2}a_2 - \frac{\log\sigma}{\sigma}\frac{\lambda_0}{16} + \frac{1}{\sigma}(a_1 + a_2\log\rho) + \left(2\rho^2 - \frac{\lambda_0}{16}\log\rho - \frac{\lambda_0}{32}\right) \\ & + \sigma\left(-2\rho^2\log\rho + \rho^2 - \frac{\lambda_0}{32}\log^2\rho - \frac{\lambda_0}{32}\log\rho - \frac{3\lambda_0}{128}\right) \\ & + \sigma^2\left(-\frac{\lambda_0}{48}\log^3\rho - \frac{\lambda_0}{32}\log^2\rho - \frac{3\lambda_0}{64}\log\rho - \frac{11\lambda_0}{384}\right) + \cdots \, . \end{aligned} \tag{4.3.17}$$

The expansion of (4.3.15) with $v = v_0 + \sigma v_1 + \mathcal{O}(\sigma^2)$, indicates that the $\mathcal{O}(\sigma^{-2})$, $\mathcal{O}(\sigma^{-1})$, and $\mathcal{O}\left(\sigma^{-1}\log\sigma\right)$, terms in (4.3.17) are too large and must be removed. This is achieved by adjusting the outer expansion by introducing switchback terms. The modified outer and nonlinear eigenvalue expansions, in place of the naive original expansions (4.3.3), are

$$u = u_0 + \frac{\varepsilon \log \sigma}{\sigma} u_{1/2} + \frac{\varepsilon}{\sigma} u_1 + \varepsilon \log \sigma \, u_{3/2} + \varepsilon \, u_2 + \varepsilon\sigma \log \sigma \, u_{5/2} + \varepsilon\sigma \, u_3 + \varepsilon\sigma^2 \log \sigma \, u_{7/2} + \varepsilon\sigma^2 \, u_4 + \cdots , \tag{4.3.18a}$$

$$\lambda = \frac{\varepsilon}{\sigma} \left[\lambda_0 + \sigma\lambda_1 + \sigma^2\lambda_2 + \sigma^3\lambda_3 + \cdots \right] . \tag{4.3.18b}$$

Such a lengthy expansion is required in order to completely specify the inner solution $v(\rho)$ up to terms of order $\mathcal{O}(\sigma)$. Upon substituting (4.3.18) into (4.3.1), the following problems are obtained on $0 < r < 1$ for the switchback terms where $j = 1, \ldots, 4$.

$$\Delta^2 u_{(2j-1)/2} = 0 ; \qquad \begin{gathered} u_{(2j-1)/2}(0) = f_{(2j-1)/2} , \quad \partial_r u_{(2j-1)/2}(0) = 0 , \\ u_{(2j-1)/2}(1) = \partial_r u_{(2j-1)/2}(1) = 0 , \end{gathered} \tag{4.3.19}$$

These problems admit solutions

$$u_{(2j-1)/2}(r) = f_{(2j-1)/2} \left(1 - r^2 + 2r^2 \log r \right) , \qquad j = 1, \ldots, 4 , \tag{4.3.20}$$

where $f_{(2j-1)/2}$ for $j = 1, \ldots, 4$ are constants to be determined. Moreover, for $j = 2, 3, 4$, $u_j(r)$ satisfies

$$\Delta^2 u_j = -\frac{\lambda_{j-1}}{(1+u_0)^2} , \quad 0 < r < 1 ; \qquad u_j(1) = \partial_r u_j(1) = 0 , \qquad j = 2, 3, 4 . \tag{4.3.21}$$

The asymptotic behaviour of the solution for u_j as $r \to 0$ for $j = 2, 3, 4$ is (see equation (4.3.8)),

$$\begin{pmatrix} u_2 \\ u_3 \\ u_4 \end{pmatrix} \sim \begin{pmatrix} \lambda_1 \\ \lambda_2 \\ \lambda_3 \end{pmatrix} \left(\frac{\log(-\log r)}{16} + \frac{1}{32 \log r} - \frac{3}{128 \log^2 r} + \frac{11}{384 \log^3 r} \right) + \begin{pmatrix} b_1 \\ c_1 \\ d_1 \end{pmatrix} + \begin{pmatrix} b_2 \\ c_2 \\ d_2 \end{pmatrix} \log r + \cdots . \tag{4.3.22}$$

Here b_1, b_2, c_1, c_2, d_1, and d_2, are constants pertaining to the homogeneous solution. These constants are fixed in the matching process below, which then determines u_j for $j = 2, 3, 4$ uniquely. From (4.3.18), (4.3.20), and (4.3.22), together with $u = -1 + \varepsilon v$, the matching condition between the outer and inner solutions leads to the following

far-field behaviour for the inner solution v as $\rho \to \infty$.

$$\begin{aligned} v &\sim -\frac{1}{\sigma^2}a_2 + \frac{\log\sigma}{\sigma}\left(f_{1/2} - \frac{\lambda_0}{16}\right) + \log\sigma\left(f_{3/2} - \frac{\lambda_1}{16}\right) + \sigma\log\sigma\left(f_{5/2} - \frac{\lambda_2}{16}\right) \\ &+ \sigma^2\log\sigma\left(f_{7/2} - \frac{\lambda_3}{16}\right) + \frac{1}{\sigma}\left(a_1 - b_2 + a_2\log\rho\right) \\ &+ \left(b_1 - \frac{\lambda_0}{32} + c_2 + 2\rho^2 + \left(b_2 - \frac{\lambda_0}{16}\right)\log\rho\right) \\ &+ \sigma\left(-2\rho^2\log\rho + \rho^2 - \frac{\lambda_0}{32}\log^2\rho + \left(c_2 - \frac{\lambda_0}{32} - \frac{\lambda_1}{16}\right)\log\rho + c_1 - d_2 - \frac{\lambda_1}{32} - \frac{3\lambda_0}{128}\right) \\ &+ \sigma^2\left(-\frac{\lambda_0}{48}\log^3\rho - \left(\frac{\lambda_1}{32} + \frac{\lambda_0}{32}\right)\log^2\rho + \left(d_2 - \frac{\lambda_2}{16} - \frac{\lambda_1}{32} - \frac{3\lambda_0}{64}\right)\log\rho\right. \\ &+ \left. d_1 - e_2 - \frac{\lambda_2}{32} - \frac{3\lambda_1}{128} - \frac{11\lambda_0}{384}\right) + \mathcal{O}(\sigma^3) \end{aligned} \tag{4.3.23}$$

The constant e_2 in the order $\mathcal{O}(\sigma^2)$ term above arises from the homogeneous component to the solution u_5 of the $\varepsilon\sigma^3 u_5$ term in the outer expansion, not explicitly written in (4.3.18a).

Since the expansion of the inner solution $v(\rho)$ is

$$v = v_0 + \sigma v_1 + \sigma^2 v_2 + \cdots, \tag{4.3.24}$$

the constant terms in (4.3.23), which are larger than $\mathcal{O}(1)$, and the $\mathcal{O}(\sigma^p\log\sigma)$ terms in (4.3.23), must all be eliminated. This lead us to choose values

$$a_1 = b_2\,, \quad a_2 = 0\,; \qquad f_{(2j-1)/2} = \frac{\lambda_{j-1}}{16}\,, \quad j = 1,\ldots,4\,, \tag{4.3.25}$$

so that (4.3.23) becomes

$$\begin{aligned} v &\sim \left[b_1 - \frac{\lambda_0}{32} + c_2 + 2\rho^2 + \left(b_2 - \frac{\lambda_0}{16}\right)\log\rho\right] \\ &+ \sigma\left[-2\rho^2\log\rho + \rho^2 - \frac{\lambda_0}{32}\log^2\rho + \left(c_2 - \frac{\lambda_0}{32} - \frac{\lambda_1}{16}\right)\log\rho + c_1 - d_2 - \frac{\lambda_1}{32} - \frac{3\lambda_0}{128}\right] \\ &+ \sigma^2\left[-\frac{\lambda_0}{48}\log^3\rho - \left(\frac{\lambda_1}{32} + \frac{\lambda_0}{32}\right)\log^2\rho + \left(d_2 - \frac{\lambda_2}{16} - \frac{\lambda_1}{32} - \frac{3\lambda_0}{64}\right)\log\rho\right. \\ &+ \left. d_1 - e_2 - \frac{\lambda_2}{32} - \frac{3\lambda_1}{128} - \frac{11\lambda_0}{384}\right] + \mathcal{O}(\sigma^3) \end{aligned} \tag{4.3.26}$$

From (4.3.24), (4.3.15), and (4.3.26), the leading order solution v_0 satisfies

$$\Delta_\rho^2 v_0 = 0\,, \quad \rho > 0\,; \qquad v_0(0) = 1\,, \quad v_0'(0) = v_0'''(0) = 0\,; \quad v_0 \sim 2\rho^2\,, \quad \text{as} \quad \rho \to \infty\,. \tag{4.3.27}$$

The solution is $v_0 = 2\rho^2 + 1$. The matching condition from the first line in (4.3.26) determines the constants b_1 and b_2 to be

$$b_2 = \frac{\lambda_0}{16}\,, \qquad b_1 = 1 + \frac{\lambda_0}{32} + c_2\,. \tag{4.3.28}$$

From the $\mathcal{O}(\sigma)$ terms in (4.3.15), (4.3.24), and (4.3.26), the problem for v_1 satisfies

$$\Delta_\rho^2 v_1 = -\frac{\lambda_0}{v_0^2}\,, \quad \rho > 0\,; \qquad v_1(0) = v_1'(0) = v_1'''(0) = 0\,, \tag{4.3.29a}$$

with the far-field behaviour

$$v_1 \sim -2\rho^2 \log\rho + \rho^2 - \frac{\lambda_0}{32}\log^2\rho + \chi_1 \log\rho + \chi_2\,, \quad \text{as} \quad \rho \to \infty\,. \tag{4.3.29b}$$

Here the constants χ_1 and χ_2 are defined by

$$\chi_1 \equiv c_2 - \frac{\lambda_0}{32} - \frac{\lambda_1}{16}, \qquad \chi_2 \equiv c_1 - d_2 - \frac{\lambda_1}{32} - \frac{3\lambda_0}{128}. \tag{4.3.29c}$$

From the $\mathcal{O}(\sigma^2)$ terms in (4.3.15), (4.3.24), and (4.3.26), the problem for v_2 satisfies

$$\Delta_\rho^2 v_2 = -\frac{\lambda_1}{v_0^2} + \frac{2\lambda_0}{v_0^3} v_1\,, \quad \rho > 0\,; \qquad v_2(0) = v_2'(0) = v_2'''(0) = 0\,, \tag{4.3.30a}$$

with the following far-field behaviour as $\rho \to \infty$:

$$\begin{aligned} v_2 \sim\; & -\frac{\lambda_0}{48}\log^3\rho - \left(\frac{\lambda_1}{32} + \frac{\lambda_0}{32}\right)\log^2\rho + \left(d_2 - \frac{\lambda_2}{16} - \frac{\lambda_1}{32} - \frac{3\lambda_0}{64}\right)\log\rho \\ & + d_1 - e_2 - \frac{\lambda_2}{32} - \frac{3\lambda_1}{128} - \frac{11\lambda_0}{384} + \cdots\,. \end{aligned} \tag{4.3.30b}$$

The problem (4.3.29) determines the constants λ_0, χ_1, and χ_2. Thus, (4.3.29c) fixes c_2 in terms of λ_0 and λ_1, and (4.3.28) determines b_1. However, (4.3.29c) only provides one of the two required equations to determine c_1. As shown below, the additional equation is provided by the problem (4.3.30) for v_2. To determine λ_0, the divergence theorem is applied to (4.3.29a) to get

$$\lim_{R\to\infty}\left[\int_0^R \left(\Delta_\rho^2 v_1 + \frac{\lambda_0}{(1+2\rho^2)^2}\right)\rho\,d\rho\right] = \lim_{R\to\infty}\left[\rho\frac{d}{d\rho}\left(\Delta_\rho v_1\right)\big|_{\rho=R} + \frac{\lambda_0}{4}\right] = 0\,. \tag{4.3.31}$$

The leading-order term in the far-field behaviour (4.3.29b) yields that $\Delta_\rho\, v_1 \sim -8\log\rho$ as $\rho \to \infty$ and so (4.3.31) determines that $\lambda_0 = 32$ and consequently $a_1 = 2$, $b_1 = b_2 = 2$, from (4.3.25) and (4.3.28), respectively. Note that λ_0 is determined solely by the leading-

order behaviour $v_1 \sim -2\rho^2 \log \rho$, while the correction term ρ^2 in (4.3.29b) specifies v_1 uniquely, and allows for the determination of χ_1 and χ_2 in (4.3.29b) as demonstrated below

To determine χ_1 and χ_2, equation (4.3.29a) is directly integrated to obtain

$$\Delta_\rho v_1 = -4 \log(1 + 2\rho^2) + C \,, \tag{4.3.32}$$

with the value $C = 4(\log 2 - 1)$ obtained by using the far-field behaviour (4.3.29b) in (4.3.32). Integrating (4.3.32) again with $v_1'(0) = 0$, the following initial value problem for $v_1(y)$ is determined

$$v_{1\rho} = -2\rho \log(\rho^2 + 1/2) - \rho^{-1} \log(1 + 2\rho^2) \,, \qquad v_1(0) = 0 \,. \tag{4.3.33}$$

A further integration of (4.3.33) yields

$$v_1 = \rho^2 - \frac{1}{2} \log 2 - \left(\rho^2 + \frac{1}{2}\right) \log \left(\rho^2 + \frac{1}{2}\right) - \int_0^\rho \frac{\log(1 + 2y^2)}{y} \, dy \,. \tag{4.3.34}$$

In order to identify the constants χ_1 and χ_2 in (4.3.29b), the asymptotic expansion of (4.3.34) as $\rho \to \infty$ must be calculated. To do so, the divergent integral in (4.3.34) must first be manipulated by re-writing it as

$$\begin{aligned}
I &\equiv \int_0^\rho \frac{\log(1 + 2y^2)}{y} \, dy = \frac{1}{2} \int_0^{2\rho^2} \frac{\log(1 + x)}{x} \, dx \\
&= \frac{1}{2} \left[\int_0^1 \frac{\log(1 + x)}{x} \, dx + \int_1^{2\rho^2} \frac{\log(1 + x)}{x} \, dx \right] = \frac{\pi^2}{24} + \frac{1}{2} \int_1^{2\rho^2} \frac{\log(1 + x)}{x} \, dx \\
&= \frac{\pi^2}{24} + \frac{1}{2} \left[\int_1^{2\rho^2} \left(\frac{\log(1 + x)}{x} - \frac{\log x}{x} \right) dx + \int_1^{2\rho^2} \frac{\log x}{x} \, dx \right] , \\
&= \frac{\pi^2}{24} + \frac{1}{4} \left[\log \left(2\rho^2 \right) \right]^2 + \frac{1}{2} \int_1^{2\rho^2} \frac{\log(1 + 1/x)}{x} \, dx \,,
\end{aligned}$$

where the identity $\int_0^1 x^{-1} \log(1 + x) \, dx = \pi^2/12$ has been used. Therefore, (4.3.34) becomes

$$\begin{aligned}
v_1 = &-(\rho^2 + 1/2) \log(\rho^2 + 1/2) + \rho^2 - \frac{1}{2} \log 2 - \frac{\pi^2}{24} - \log^2 \rho \\
&- \log 2 \log \rho - \frac{1}{4} \log^2 2 - \frac{1}{2} \int_1^{2\rho^2} \frac{\log(1 + 1/x)}{x} \, dx \,,
\end{aligned} \tag{4.3.35}$$

where the integral term is finite as $\rho \to \infty$. Now taking the limit as $\rho \to \infty$,

$$v_1 \sim -2\rho^2 \log \rho + \rho^2 - \log^2 \rho - (1 + \log 2) \log \rho \\ - \left(\frac{1}{2} + \frac{1}{2} \log 2 + \frac{1}{4} \log^2 2 + \frac{\pi^2}{24} + \frac{1}{2} \int_1^\infty \frac{\log(1 + 1/x)}{x} \, dx \right) + o(1) \,,$$

where $\int_1^\infty x^{-1} \log(1 + x^{-1}) \, dx = \int_0^1 u^{-1} \log(1 + u) \, du = \pi^2/12$. Upon comparing this asymptotic result with (4.3.29b), the constants χ_1 and χ_2 are identified as

$$\chi_1 = -1 - \log 2 \,, \qquad \chi_2 = -\frac{1}{2} - \frac{1}{2} \log 2 - \frac{\pi^2}{12} - \frac{1}{4} \log^2 2 \,. \tag{4.3.36}$$

Therefore, from (4.3.29c) and (4.3.28), the constants b_1 and c_2 have values

$$c_2 = \frac{\lambda_0}{32} + \frac{\lambda_1}{16} - 1 - \log 2 \,, \qquad b_1 = \frac{1}{16} (\lambda_0 + \lambda_1) - \log 2 \,. \tag{4.3.37}$$

The value of λ_1 is determined by the next order problem (4.3.30) for v_2 as well as additional relations for the unknown constants d_1, d_2, and e_2. The value of λ_1 is obtained by multiplying (4.3.30a) by ρ, integrating the resulting expression over $0 < \rho < R$, and then using the divergence theorem. In passing to the limit $R \to \infty$, note that since $v_2 = o(\rho^2 \log \rho)$ as $\rho \to \infty$ from (4.3.30b), there is no contribution from the flux of $\Delta_\rho v_2$ across the big circle $\rho = R$. In this way, λ_1 is represented by the integral

$$\lambda_1 = 8\lambda_0 \int_0^\infty \frac{v_1}{v_0^3} \rho \, d\rho \,, \tag{4.3.38}$$

where $v_0 = 2\rho^2 + 1$ and v_1 is given in (4.3.35). This expression can be evaluated explicitly with integration by parts and application of equation (4.3.33). The calculation proceeds as follows:

$$\lambda_1 = 8\lambda_0 \int_0^\infty \frac{\rho}{(1 + 2\rho^2)^3} \, v_1 \, d\rho = -\lambda_0 \int_0^\infty \left[\frac{1}{(1 + 2\rho^2)^2} \right]_\rho v_1 \, d\rho \\ = \lambda_0 \int_0^\infty \left[\frac{1}{(1 + 2\rho^2)^2} \right] v_{1\rho} \, d\rho = 2\lambda_0 \log 2 \int_0^\infty \frac{\rho}{(1 + 2\rho^2)^2} \, d\rho - \lambda_0 \int_0^\infty \frac{\log(1 + 2\rho^2)}{\rho(1 + 2\rho^2)} \, d\rho \\ = \frac{\lambda_0}{2} \log 2 - \frac{\lambda_0}{2} \int_0^\infty \frac{\log(1 + u)}{u(1 + u)} \, du = \frac{\lambda_0}{2} \left(\log 2 - \frac{\pi^2}{6} \right) \approx -15.229$$

In the final step, the result $\int_0^\infty \log(1 + u)/(u + u^2) du = \pi^2/6$ has been used.

In terms of the known values of χ_1, λ_0, and λ_1, the constant c_2 is fixed by (4.3.29c). However, the expression for χ_2 in (4.3.29c) gives only one equation for the two further unknowns c_1 and d_2. The solution v_2 of (4.3.30) is uniquely defined, and so provides

the far-field behaviour

$$v_2 = -\frac{\lambda_0}{48}\log^3\rho - \left(\frac{\lambda_1}{32}+\frac{\lambda_0}{32}\right)\log^2\rho + \chi_3\log\rho + \chi_4 + o(1)\,, \quad \text{as} \quad \rho\to\infty\,,$$

for some constants χ_3 and χ_4 determined in terms of the solution. A comparison of this behaviour with (4.3.30b) provides two equations

$$\chi_3 = d_2 - \frac{\lambda_2}{16} - \frac{\lambda_1}{32} - \frac{3\lambda_0}{64}, \qquad \chi_4 = d_1 - e_2 - \frac{\lambda_2}{32} - \frac{3\lambda_1}{128} - \frac{11\lambda_0}{384}\,.$$

Therefore, d_2 is fixed in terms of λ_2, which then determines c_1 from (4.3.29c) for χ_2. The equation for χ_4 gives one equation for d_1 and e_2 in terms of λ_2. This process continues to higher order to determine a further equation for d_1 and e_2.

The preceding calculation is summarized as follows:

Principal Result 4.7: *In the limit $\varepsilon \equiv u(0)+1 \to 0^+$, the limiting asymptotic behaviour of the maximal radially symmetric solution branch of* (4.3.1)*, away from a boundary layer region near $r=0$, is given by*

$$u = u_0 + \frac{\varepsilon}{\sigma}\log\sigma\, u_{1/2} + \frac{\varepsilon}{\sigma}u_1 + \varepsilon\log\sigma\, u_{3/2} + \varepsilon u_2 + \mathcal{O}(\varepsilon\sigma\log\sigma), \qquad \lambda = \frac{\varepsilon}{\sigma}\lambda_0 + \varepsilon\lambda_1 + \mathcal{O}(\varepsilon\sigma)\,, \tag{4.3.39a}$$

where $\sigma = -1/\log\gamma$ and the boundary layer width γ is determined in terms of ε by $-\gamma^2\log\gamma = \varepsilon$. In (4.3.39a),

$$u_0 = -1 + r^2 - 2r^2\log r\,, \quad u_{1/2} = -\frac{\lambda_0}{16}u_0\,, \quad u_{3/2} = -\frac{\lambda_1}{16}u_0\,, \tag{4.3.39b}$$

while u_1 and u_2 are the unique solutions of

$$\Delta^2 u_1 = -\frac{\lambda_0}{(1+u_0)^2}\,, \quad 0<r<1\,; \qquad u_1(1) = u_{1r}(1) = 0\,, \tag{4.3.39c}$$

$$u_1 = \frac{\lambda_0}{16}\log(-\log r) + \frac{\lambda_0}{16} + \mathcal{O}(\log^{-1} r)\,, \quad r\to 0\,, \tag{4.3.39d}$$

$$\Delta^2 u_2 = -\frac{\lambda_1}{(1+u_0)^2}\,, \quad 0<r<1\,; \qquad u_2(1) = u_{2r}(1) = 0\,, \tag{4.3.39e}$$

$$u_2 = \frac{\lambda_1}{16}\log(-\log r) + \frac{1}{16}(\lambda_0+\lambda_1) - \log 2 + \frac{\lambda_0}{16}\log r + \mathcal{O}(\log^{-1} r)\,, \quad r\to 0\,. \tag{4.3.39f}$$

Finally, λ_0 and λ_1 are given by

$$\lambda_0 = 32\,, \qquad \lambda_1 = \frac{\lambda_0}{2}\left(\log 2 - \frac{\pi^2}{6}\right) \tag{4.3.39g}$$

A very similar asymptotic analysis can be performed to determine the limiting behaviour

of the maximal solution branch for the mixed biharmonic problem (4.3.2). The analysis follows very closely that of § 4.4 and so only the key results are highlighted.

The main difference, as compared to the pure biharmonic case, is that now the leading-order outer solution u_0 satisfies

$$\Delta^2 u_0 - \frac{1}{\delta}\Delta u_0 = 0\,, \quad 0 < r < 1\,; \qquad u_0(1) = u_{0r}(1) = 0\,, \tag{4.3.40a}$$

subject to the local behavior

$$u_0 = -1 + \alpha r^2 \log r + \varphi r^2 + o(r^2)\,, \quad \text{as} \quad r \to 0\,, \tag{4.3.40b}$$

for some α and φ, which are functions of δ. The general solution of (4.3.40a) is

$$u_0 = \mathcal{A} + \mathcal{B}\log\, r + \mathcal{C}K_0(\eta r) + \mathcal{D}I_0(\eta r)\,, \qquad \eta \equiv 1/\sqrt{\delta}\,, \tag{4.3.41}$$

where $K_0(z)$ and $I_0(z)$ are the usual modified Bessel functions. By satisfying the boundary conditions in (4.3.40a), together with imposing the local behaviour (4.3.40b) via the point constraints $u_0(0) = -1$ and $u_{0r}(0) = 0$, the arbitrary constants are

$$\begin{aligned} \mathcal{A} &= \left[I_0(\eta)\left(1 + \eta K_0'(\eta)\right) - \eta I_0'(\eta) K_0(\eta)\right]\mathcal{G}(\eta)\,, \\ \mathcal{B} = \mathcal{C} &= \eta I_0'(\eta)\mathcal{G}(\eta)\,, \qquad \mathcal{D} = -\left[1 + \eta K_0'(\eta)\right]\mathcal{G}(\eta)\,, \end{aligned} \tag{4.3.42a}$$

where $\mathcal{G}(\eta)$ is defined by

$$\mathcal{G}(\eta) \equiv \left[\eta I_0'(\eta)\left(K_0(\eta) + \log\left(\eta/2\right) + \gamma_e\right) + \left(1 + \eta K_0'(\eta)\right)\left(1 - I_0(\eta)\right)\right]^{-1}\,. \tag{4.3.42b}$$

Here $\gamma_e \sim 0.5772$ is Euler's constant. Equations (4.3.40b) and (4.3.42), allow an explicit calculation of the functions $\alpha(\eta)$ and $\varphi(\eta)$ in (4.3.40b);

$$\alpha = -\left(\frac{\eta^3}{4}\right) I_0'(\eta)\mathcal{G}(\eta)\,, \qquad \varphi = -\frac{\eta^2}{4}\left[\eta I_0'(\eta)\left(\log\left(\eta/2\right) + \gamma_e - 1\right) + 1 + \eta K_0'(\eta)\right]\mathcal{G}(\eta)\,. \tag{4.3.43}$$

In deriving (4.3.43) and (4.3.42), the well-known small argument expansions for $K_0(z)$ and $I_0(z)$,

$$K_0(z) \sim -\left[\log\left(z/2\right) + \gamma_e\right] I_0(z) + z^2/4\,, \qquad I_0(z) \sim 1 + z^2/4\,, \quad \text{as} \quad z \to 0\,. \tag{4.3.44}$$

have been used.

This explicit solution for α and φ has two key properties. Firstly, the limit $\delta \to \infty$, or equivalently $\eta \to 0$, corresponds to the pure biharmonic case, *i.e.* $(\alpha, \varphi) \to (-2, 1)$ as $\eta \to 0$, in agreement with the pure biharmonic case result (4.3.5). Our second remark

pertains to the sign of $\alpha(\eta)$. The asymptotic analysis leading to Principal Result 4.3 below requires that $\alpha < 0$ for all $\eta > 0$. This is readily verified numerically from the explicit formula for $\alpha(\eta)$ given in (4.3.43) (see Fig. 4.9(b) below).

The solution is expanded, as in the pure biharmonic case, with

$$\begin{aligned} u &= u_0 + \frac{\varepsilon}{\sigma}\log\sigma\, u_{1/2} + \frac{\varepsilon}{\sigma}u_1 + \varepsilon\log\sigma\, u_{3/2} + \varepsilon u_2 + \mathcal{O}(\varepsilon\sigma\log\sigma), \\ \lambda &= \delta\left[\frac{\varepsilon}{\sigma}\lambda_0 + \varepsilon\lambda_1 + \mathcal{O}(\varepsilon\sigma)\right], \end{aligned} \tag{4.3.45}$$

where as before the fractional terms $u_{1/2}, u_{3/2}, \ldots$ satisfy the homogeneous problem with point constraint at $r = 0$ chosen to eliminate terms of order $\mathcal{O}(\varepsilon\sigma^k \log\sigma)$, $k = -1, 0, 1, 2, \ldots$. The terms $u_1, u_2, \ldots$ satisfy $\Delta^2 u_j - \eta^2 \Delta u_j = -\lambda_{j-1}/(1+u_0)^2$ for $j = 1, 2, 3, \ldots$ and exhibit a singularity behaviour which can be deduced by the methods leading to (4.3.22). After some algebra, it is established that (see § 4.4 for more detail)

$$\begin{aligned} &u_j \sim \frac{\lambda_{j-1}}{4\alpha^2}\left[\log(-\log r) - \frac{\Gamma_1}{\log r} + \frac{\Gamma_2}{\log^2 r} - \frac{\Gamma_3}{\log^3 r}\right] + b_j \log r + c_j + \cdots \quad r \to 0 \\ &\Gamma_1 = -\left(1 + \frac{\varphi}{\alpha}\right), \qquad \Gamma_2 = -\left[\frac{3}{4} + \frac{\varphi}{\alpha} + \frac{\varphi^2}{2\alpha^2}\right], \qquad \Gamma_3 = -\left[1 + \frac{3\varphi}{2\alpha} + \frac{\varphi^2}{\alpha^2} + \frac{\varphi^3}{3\alpha^3}\right] \end{aligned} \tag{4.3.46}$$

where the terms $b_j \log r$ and c_j are arbitrary solutions of the homogeneous problem. In a region of width $\mathcal{O}(\gamma)$, where $-\gamma^2 \log\gamma = \varepsilon$ in the vicinity of the origin, local coordinates

$$u = -1 + \varepsilon v(\rho), \quad r = \gamma\rho$$

are used to establish the following problem for $v(\rho)$:

$$\delta\Delta^2 v - \varepsilon\sigma\Delta v = -\frac{\sigma^2\lambda}{\varepsilon v^2}, \quad \rho > 0; \qquad v(0) = 1, \quad v_\rho(0) = v_{\rho\rho\rho}(0) = 0 \tag{4.3.47a}$$

$$\begin{aligned} v \sim\ & -\alpha\rho^2 + \left(b_2 - \frac{\lambda_0}{4\alpha^2}\right)\log\rho + c_2 - b_3 + \frac{\lambda_0\Gamma_1}{4\alpha^2} + \sigma\left[\alpha\rho^2\log\rho + \varphi\rho^2\right. \\ & -\frac{\lambda_0}{8\alpha^2}\log^2\rho + \left(b_3 + \frac{\lambda_0\Gamma_1}{4\alpha^2} - \frac{\lambda_1}{4\alpha^2}\right)\log\rho + c_3 - b_4 + \frac{\lambda_0\Gamma_2}{4\alpha^2} + \frac{\lambda_1\Gamma_1}{4\alpha^2}\Big] \\ & + \sigma^2\left[-\frac{\lambda_0}{12\alpha^2}\log^3\rho + \left(\frac{\lambda_0\Gamma_1}{4\alpha^2} - \frac{\lambda_1}{8\alpha^2}\right)\log^2\rho + \left(b_4 + \frac{\lambda_0\Gamma_2}{2\alpha^2} + \frac{\lambda_1\Gamma_1}{4\alpha^2} - \frac{\lambda_2}{4\alpha^2}\right)\log\rho\right. \\ & \left. + c_4 - b_5 - \frac{\lambda_0\Gamma_3}{4\alpha^2} + \frac{\lambda_1\Gamma_2}{4\alpha^2} + \frac{\lambda_2\Gamma_1}{4\alpha^2}\right] + \mathcal{O}(\sigma^3) \end{aligned} \tag{4.3.47b}$$

The form of far field behavior (4.3.47b) suggests the expansion

$$v = v_0 + \sigma v_1 + \sigma^2 v_2 + \mathcal{O}(\sigma^3), \qquad \lambda = \delta\left[\frac{\varepsilon}{\sigma}\lambda_0 + \varepsilon\lambda_1 + \mathcal{O}(\varepsilon\sigma)\right]. \tag{4.3.48}$$

which at leading order yields the solution $v_0 = 1 - \alpha\rho^2$ and additionally

$$b_2 = \frac{\lambda_0}{4\alpha^2}, \qquad c_2 - b_3 + \frac{\lambda_0\Gamma_1}{4\alpha^2} = 1 \tag{4.3.49}$$

The higher order problems which fix the corrections λ_0 and λ_1 are

$$\Delta^2 v_1 = -\frac{\lambda_0}{v_0^2}, \quad x \in \Omega; \qquad v_1(0) = v_{1\rho}(0) = v_{1\rho\rho\rho}(0) = 0 \tag{4.3.50a}$$

$$\begin{aligned} v_1 \sim{}& \alpha\rho^2\log\rho + \varphi\rho^2 - \frac{\lambda_0}{8\alpha^2}\log^2\rho + \left(b_3 + \frac{\lambda_0\Gamma_1}{4\alpha^2} - \frac{\lambda_1}{4\alpha^2}\right)\log\rho \\ &+ c_3 - b_4 + \frac{\lambda_0\Gamma_2}{4\alpha^2} + \frac{\lambda_1\Gamma_1}{4\alpha^2} + \cdots \qquad \rho \to \infty \end{aligned} \tag{4.3.50b}$$

and

$$\Delta^2 v_2 = -\frac{\lambda_1}{v_0^2} + \frac{2\lambda_0}{v_0^3}v_1, \quad \rho > 0; \qquad v_2(0) = v_{2\rho}(0) = v_{2\rho\rho\rho}(0) = 0 \tag{4.3.51a}$$

$$\begin{aligned} v_2 \sim{}& -\frac{\lambda_0}{12\alpha^2}\log^3\rho + \left(\frac{\lambda_0\Gamma_1}{4\alpha^2} - \frac{\lambda_1}{8\alpha^2}\right)\log^2\rho + \left(b_4 + \frac{\lambda_0\Gamma_2}{2\alpha^2} + \frac{\lambda_1\Gamma_1}{4\alpha^2} - \frac{\lambda_2}{4\alpha^2}\right)\log\rho \\ &+ c_4 - b_5 - \frac{\lambda_0\Gamma_3}{4\alpha^2} + \frac{\lambda_1\Gamma_2}{4\alpha^2} + \frac{\lambda_2\Gamma_1}{4\alpha^2} + \cdots \qquad \rho \to \infty \end{aligned} \tag{4.3.51b}$$

Equations (4.3.51) can be directly integrated to obtain that $\lambda_0 = 8\alpha^2$ and that

$$v_{1\rho} = \alpha\rho\log(\rho^2 - 1/\alpha) - \frac{\log(1-\alpha\rho^2)}{\rho} + \rho(\alpha + 2\varphi), \quad \rho > 0; \qquad v_1(0) = 0 \tag{4.3.52}$$

The final step in the construction of the two term asymptotic solution is a lengthy but straightforward calculation of λ_1. Integrating (4.3.51a) by parts and applying (4.3.52) reveals that

$$\lambda_1 = -\frac{\lambda_0}{2}\left[\frac{\pi^2}{6} - \log(-\alpha) + \left(1 + \frac{2\varphi}{\alpha}\right)\right]. \tag{4.3.53}$$

Again, more detail on the preceding calculation is provided in § 4.4 which outlines the construction of the maximal solution branch on a general 2D domain. The main result characterizing the limiting form for the bifurcation diagram of (4.3.2) is as follows. **Principal Result 4.8**: *In the limit $\varepsilon \equiv u(0)+1 \to 0^+$, the limiting asymptotic behavior of the maximal radially symmetric solution branch of* (4.3.2)*, away from a boundary*

layer region near $r = 0$, is given by

$$\begin{aligned} u &= u_0 + \frac{\varepsilon}{\sigma}\log\sigma\, u_{1/2} + \frac{\varepsilon}{\sigma}u_1 + \varepsilon\log\sigma\, u_{3/2} + \varepsilon u_2 + \mathcal{O}(\varepsilon\sigma\log\sigma), \\ \lambda &= \delta\left[\frac{\varepsilon}{\sigma}\lambda_0 + \varepsilon\lambda_1 + \mathcal{O}(\varepsilon\sigma)\right], \end{aligned} \tag{4.3.54a}$$

where $\sigma = -1/\log\gamma$ and the boundary layer width γ is determined in terms of ε by $-\gamma^2\log\gamma = \varepsilon$. In (4.3.54a),

$$u_0 = \mathcal{A} + \mathcal{B}\log r + \mathcal{C}K_0(\eta r) + \mathcal{D}I_0(\eta r), \qquad u_{1/2} = -\frac{\lambda_0}{4\alpha^2}u_0, \qquad u_{3/2} = -\frac{\lambda_1}{4\alpha^2}u_0, \tag{4.3.54b}$$

where $\mathcal{A}$, $\mathcal{B}$, $\mathcal{C}$, and $\mathcal{D}$ are defined in (4.3.42). Moreover, u_1 and u_2 are the unique solutions of

$$\Delta^2 u_1 - \eta^2\Delta u_1 = -\frac{\lambda_0}{(1+u_0)^2}, \quad 0 < r < 1; \qquad u_1(1) = u_{1r}(1) = 0, \tag{4.3.54c}$$

$$u_1 \sim \frac{\lambda_0}{4\alpha^2}\log(-\log r) + \frac{\lambda_0}{4\alpha^2} + \mathcal{O}(\log^{-1} r), \quad \text{as} \quad r \to 0, \tag{4.3.54d}$$

$$\Delta^2 u_2 - \eta^2\Delta u_2 = -\frac{\lambda_1}{(1+u_0)^2}, \quad 0 < r < 1; \qquad u_2(1) = u_{2r}(1) = 0, \tag{4.3.54e}$$

$$u_2 \sim \frac{\lambda_1}{4\alpha^2}\log(-\log r) + \frac{\lambda_0}{4\alpha^2}\log r + \frac{\lambda_0}{2\alpha^2}\left(1 + \frac{\varphi}{\alpha}\right) + \frac{\lambda_1}{4\alpha^2} - \log(-\alpha) + \mathcal{O}(\log^{-1} r), \tag{4.3.54f}$$

where $\eta \equiv \delta^{-1/2}$. Finally, λ_0 and λ_1 are given by

$$\lambda_0 = 8\alpha^2, \qquad \lambda_1 = -\frac{\lambda_0}{2}\left[\frac{\pi^2}{6} - \log(-\alpha) + \left(1 + \frac{2\varphi}{\alpha}\right)\right]. \tag{4.3.54g}$$

Since $\alpha < 0$ for all $\eta > 0$, the formulae in Principal Result 4.3 are well-defined. In Fig. 4.9, a favourable comparison of asymptotic predictions and numerical results for the limiting behaviour of the maximal solution branch is displayed.

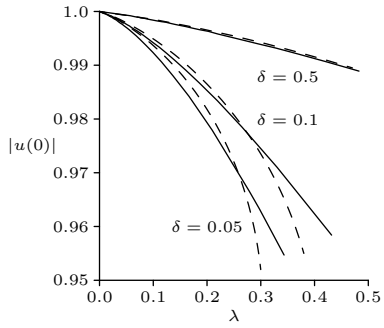

(a) Asymptotic predictions (dashed) and full numerical (solid) bifurcation curves for several δ.

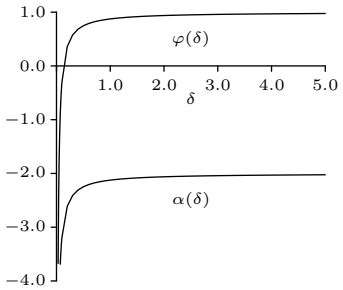

(b) $\alpha(\delta)$ and $\varphi(\delta)$

Figure 4.9: In panel (a), the predictions of Principal Result 4.4 (dashed) are compared with full numerical solutions (solid) for several values of δ and good agreement is observed when $|u(0)|$ is close to 1. In panel (b), $\alpha(\delta)$ and $\varphi(\delta)$ from (4.3.43) are graphed over a range of δ. In agreement with the pure bi-harmonic case, it is observed that $(\alpha, \varphi) \to (-2, 1)$ as $\delta \to \infty$.

4.3.2 The Annulus Problem

In this subsection, the limiting behaviour of the maximal solution branch is constructed for the annulus problem

$$\Delta u = \frac{\lambda}{(1+u)^2}\,, \quad \delta \le r \le 1\,; \qquad u(\delta) = u(1) = 0\,, \tag{4.3.55}$$

with $0 < \delta < 1$ and $\delta = \mathcal{O}(1)$. A solution of (4.3.55) for which $\lambda \to 0$ as $u(r_\varepsilon)+1 \equiv \varepsilon \to 0$ is sought, where r_ε is a free-boundary point to be determined. This problem, which is analyzed by formal asymptotic methods, is related to the problem studied rigorously in [65].

In the outer region, defined away from r_ε, we try an expansion for the outer solution u and for λ in the form

$$u = u_0 + \nu u_1 + \cdots\,, \qquad \lambda = \nu\,(\lambda_0 + \mu\lambda_1 + \cdots)\,, \tag{4.3.56}$$

where $\nu \ll 1$ and $\mu \ll 1$ are gauge functions to be determined. As shown below, this expansion must be adjusted by inserting a certain switchback term in the outer expansion. From (4.3.56) and (4.3.55), we obtain that u_0 and u_1 satisfy

$$\Delta u_0 = 0\,, \quad \delta < r < r_\varepsilon\,, \quad r_\varepsilon < r < 1\,; \qquad u_0(\delta) = u_0(1) = 0\,, \tag{4.3.57a}$$

$$\Delta u_1 = \frac{\lambda_0}{(1+u_0)^2}\,, \quad \delta < r < r_\varepsilon\,, \quad r_\varepsilon < r < 1\,; \qquad u_1(\delta) = u_1(1) = 0\,. \tag{4.3.57b}$$

Upon imposing the point constraint that $u_0(r_\varepsilon) = -1$, the solution of (4.3.57a) gives leading order behaviour

$$u_0 = \begin{cases} -\log(r/\delta)/\log(r_\varepsilon/\delta)\,, & \delta < r < r_\varepsilon \\ \\ -\log r/\log r_\varepsilon\,, & r_\varepsilon < r < 1\,, \end{cases} \tag{4.3.58}$$

which is not differentiable at r_ε. Then, since $u_0 \sim -1 + u_{0r}\left(r_\varepsilon^\pm\right)(r - r_\varepsilon)$ as $r \to r_\varepsilon^\pm$, (4.3.57b) yields $\Delta u_1 = \lambda_0 (r - r_\varepsilon)^{-2}/\left[u_{0r}\left(r_\varepsilon^\pm\right)\right]^2$ as $r \to r_\varepsilon$. Therefore, u_1 must have the following local behaviour as $r \to r_\varepsilon^\pm$:

$$u_1 \sim -\frac{\lambda_0}{\left[u_{0r}\left(r_\varepsilon^\pm\right)\right]^2}\log|r - r_\varepsilon| + a_1 + o(1)\,, \quad \text{as} \quad r \to r_\varepsilon^\pm\,, \tag{4.3.59}$$

where a_1 is a constant associated with the homogeneous solution to (4.3.57b). From (4.3.56), (4.3.58), and (4.3.59), the following limiting behaviour is obtained from the outer expansion

$$\begin{aligned} u \sim\; & -1 + u_{0r}(r_\varepsilon^\pm)(r - r_\varepsilon) + \frac{u_{0rr}(r_\varepsilon^\pm)}{2}(r - r_\varepsilon)^2 \\ & + \nu\left[-\frac{\lambda_0}{\left[u_{0r}\left(r_\varepsilon^\pm\right)\right]^2}\log|r - r_\varepsilon| + a_1 + o(1)\right] + \cdots\,, \end{aligned} \quad \text{as} \quad r \to r_\varepsilon^\pm\,. \tag{4.3.60}$$

In the vicinity of r_ε, an inner solution is introduced with local variables v and ρ by

$$u = -1 + \varepsilon v(\rho)\,, \qquad \rho = (r - r_\varepsilon)/\gamma\,,$$

where $\gamma \ll 1$ is the internal layer width to be determined. The leading-order term in the local behaviour (4.3.60) of the outer expansion gives $u \sim -1 + \gamma u_{0r}(r_\varepsilon^\pm)\rho$, which must match with the inner expansion $u = -1 + \varepsilon v$. The boundary layer width $\gamma = \varepsilon$ is chosen so to leading order the inner solution must have far field behaviour $v \sim u_{0r}(r_\varepsilon^\pm)\rho$ as $\rho \to \pm\infty$. With $\lambda \sim \nu\left[\lambda_0 + \mu\lambda_1 + \cdots\right]$ and $\gamma = \varepsilon$, the following inner problem for $v(\rho)$ is obtained from (4.3.55);

$$v'' + \frac{\varepsilon v'}{r_\varepsilon + \varepsilon\rho} = \frac{\nu}{\varepsilon}\frac{\left[\lambda_0 + \mu\lambda_1 + \cdots\right]}{v^2}\,, \tag{4.3.61}$$

which suggests the scaling $\nu = \varepsilon$. The scale of μ relative to ε is at this stage unknown. Therefore, to leading order, set $r_\varepsilon \sim r_0 + o(1)$ and $v \sim v_0$ to obtain that

$$v_0'' = \frac{\lambda_0}{v_0^2}\,, \quad -\infty < \rho < \infty\,; \qquad \begin{aligned} & v_0(0) = 1\,, \quad v_0'(0) = 0\,; \\ & v_0 \sim u_{0r}(r_0^\pm)\rho\,, \quad \text{as} \quad \rho \to \pm\infty\,. \end{aligned} \tag{4.3.62}$$

The condition $v_0(0) = 1$ and $v_0'(0) = 0$, with $v_0''(0) > 0$, is a necessary and sufficient condition for u to have its minimum value of $-1+\varepsilon$ at $r_\varepsilon = r_0 + o(1)$. From (4.3.62), we conclude that v_0 is even in ρ, and consequently r_0 satisfies $u_{0r}(r_0^+) = -u_{0r}(r_0^-)$. From (4.3.58), this equation for r_0 reduces to $\log r_0 = -\log(r_0/\delta)$, which yields $r_0 = \sqrt{\delta}$. To determine λ_0, multiply equation (4.3.62) for v_0 by v_0', and then integrate from $0 < \rho < \infty$ to get

$$\frac{1}{2}\left[v_0'(\infty)\right]^2 = \lambda_0 \int_0^\infty \frac{v_0'}{v_0^2}\, dy = \lambda_0 \int_1^\infty \frac{dv_0}{v_0^2} = \lambda_0 \left(-\frac{1}{v_0}\right)\Big|_1^\infty = \lambda_0\,. \tag{4.3.63}$$

Then, by using $v_0'(\infty) = u_{0r}(r_0^+) = [r_0 \log r_0]^{-2}$ and $r_0 = \sqrt{\delta}$, we conclude from (4.3.63) that $\lambda_0 = 2\left[\delta(\log\delta)^2\right]^{-1}$.

To construct a higher-order expansion for λ, the free boundary location r_ε, and the inner and outer expansions for (4.3.55), further terms in the far-field behaviour of v_0 as $\rho \to \pm\infty$ must first be calculated. To do so, equation (4.3.62) is integrated to obtain an implicitly-defined exact solution for v_0, given by

$$\sqrt{v_0(v_0-1)} + \log\left(\sqrt{v_0} + \sqrt{v_0-1}\right) = \sqrt{2\lambda_0}\rho\,, \quad \text{for} \quad \rho \geq 0\,. \tag{4.3.64}$$

Since $\sqrt{2\lambda_0} = u_{0r}(r_0^+) = -u_{0r}(r_0^-)$, and $v_0(\rho) = v_0(-\rho)$, the far-field far-field behaviour for v_0 as $\rho \to \pm\infty$, obtained from (4.3.64), is

$$v_0 \sim \pm u_0(r_0^+)\rho - \frac{\lambda_0}{\left[u_{0r}(r_0^+)\right]^2}\log\rho + \chi\,, \quad \text{as} \quad \rho \to \pm\infty\,; \qquad \chi \equiv \frac{1}{2} - \log 2 - \frac{1}{4}\log(2\lambda_0)\,. \tag{4.3.65}$$

By substituting $r - r_\varepsilon = \varepsilon\rho$ into the local behaviour of the outer expansion (4.3.60), the condition

$$\begin{aligned} u \sim -1 - \varepsilon\log\varepsilon\frac{\lambda_0}{\left[u_{0r}\left(r_\varepsilon^\pm\right)\right]^2} + \varepsilon\left[u_{0r}(r_\varepsilon^\pm)\rho - \frac{\lambda_0}{\left[u_{0r}\left(r_\varepsilon^\pm\right)\right]^2}\log\rho + a_1\right] \\ + \frac{\varepsilon^2}{2}u_{0rr}(r_\varepsilon^\pm)\rho^2 + \cdots\,. \quad \text{as} \quad r \to r_\varepsilon^\pm\,. \end{aligned} \tag{4.3.66}$$

is established. The constant $\mathcal{O}(\varepsilon\log\varepsilon)$ term in (4.3.66) cannot be accounted for by the inner expansion and so the outer expansion for u_0 in (4.3.56) must be modified by inserting a switchback term. The modified outer expansion, in place of (4.3.56), is

$$u = u_0 + (-\varepsilon\log\varepsilon)\,u_{1/2} + \varepsilon u_1 + \cdots\,; \qquad \lambda = \varepsilon\left(\lambda_0 + \mu\lambda_1 + \cdots\right)\,. \tag{4.3.67}$$

Upon substituting (4.3.67) into (4.3.55), the equation for $u_{1/2}(r)$ satisfies

$$\Delta u_{1/2} = 0\,, \quad \delta < r < r_\varepsilon\,, \quad r_\varepsilon < r < 1\,; \quad u_{1/2}(\delta) = u_{1/2}(1) = 0\,. \tag{4.3.68}$$

By enforcing the point constraint $u_{1/2}(r_\varepsilon) = -\lambda_0/\left[u_{0r}(r_\varepsilon^\pm)\right]^2$, the constant term of order $\mathcal{O}(\varepsilon\log\varepsilon)$ is eliminated in (4.3.66). In this way, the solution to (4.3.68) can be written in terms of u_0 as

$$u_{1/2}(r) = \frac{\lambda_0}{\left[u_{0r}(r_\varepsilon^\pm)\right]^2} u_0(r)\,. \tag{4.3.69}$$

In addition, a higher-order expansion for the free-boundary point is

$$r_\varepsilon = r_0 + \sigma r_1 + \cdots\,, \tag{4.3.70}$$

where $r_0 = \sqrt{\delta}$ and the gauge function $\sigma \ll 1$ is to be found.

To determine the matching condition between the inner expansion $u = -1 + \varepsilon(v_0 + \mu v_1 + \cdots)$ and the modified outer expansion (4.3.67), we add the local behaviour of $(-\varepsilon\log\varepsilon)\,u_{1/2}$ as $r \to r_\varepsilon$ to (4.3.66) and use (4.3.70) for r_ε and use the far-field behaviour (4.3.65) for v_0. The matching condition, written in terms of the inner variable ρ, is

$$\begin{aligned} &-1 + \varepsilon\left[u_{0r}(r_0^\pm)\rho - \frac{\lambda_0}{\left[u_{0r}(r_0^\pm)\right]^2}\log\rho + a_1\right] + \varepsilon\sigma r_1 u_{0rr}(r_0^\pm)\rho + \left(-\varepsilon^2\log\varepsilon\right)u_{1/2r}(r_0^\pm)\rho \\ &\sim -1 + \varepsilon\left[u_{0r}(r_0^\pm)\rho - \frac{\lambda_0}{\left[u_{0r}(r_0^\pm)\right]^2}\log\rho + \chi\right] + \varepsilon\mu v_1 + \cdots\,. \end{aligned} \tag{4.3.71}$$

This matching condition yields that

$$\mu = -\varepsilon\log\varepsilon\,, \qquad \sigma = -\varepsilon\log\varepsilon\,, \qquad a_1 = \chi\,, \tag{4.3.72}$$

where χ is defined in (4.3.65).

Since $\mu = -\varepsilon\log\varepsilon \gg \mathcal{O}(\varepsilon)$, we conclude from (4.3.61) and (4.3.71) that the inner correction v_1 satisfies

$$\mathcal{L}v_1 \equiv v_1'' + \frac{2\lambda_0}{v_0^3}v_1 = \frac{\lambda_1}{v_0^2}\,, \quad -\infty < \rho < \infty\,, \tag{4.3.73a}$$

$$v_1(0) = 0\,; \qquad v_1 \sim \left[u_{0rr}(r_0^\pm)r_1 + u_{1/2r}(r_0^\pm)\right]\rho\,, \quad \text{as} \quad \rho \to \pm\infty\,. \tag{4.3.73b}$$

Since $u_{0rr}(r_0^\pm) = \mp u_{0r}(r_0^+)/r_0$ from (4.3.57a), and $u_{1/2r}(r_0^\pm) = \pm\lambda_0/\left[u_{0r}(r_0^+)\right]$, as ob-

tained from the explicit solution (4.3.69), the far-field condition (4.3.73b) becomes

$$v_1 \sim \pm A\rho\,, \quad \text{as} \quad \rho \pm \infty\,; \qquad A \equiv -\frac{r_1}{r_0}u_{0r}(r_0^+) + \frac{\lambda_0}{u_{0r}(r_0^+)}\,. \tag{4.3.73c}$$

Since v_0 is an even function, the general solution to (4.3.73a) must be the sum of an even and odd function. The condition $v_1(0) = 0$ enforces that v_1 is odd, and consequently $A = 0$ from (4.3.73c). Since $\lambda_0 = \left[u_{0r}(r_0^+)\right]^2/2$, the condition that $A = 0$ determines r_1 as $r_1 = r_0/2$. Finally, the value of λ_1 is determined from a solvability condition. Multiplying (4.3.73a) by v_0', integrating, and using $\mathcal{L}v_0' = 0$, gives

$$\int_0^\infty v_0'\mathcal{L}v_1\,d\rho = \lambda_1\int_0^\infty \frac{v_0'}{v_0^2}\,d\rho = Av_0'(\infty)\,.$$

However, since $A = 0$, it is clear that $\lambda_1 = 0$. In summary,

Principal Result 4.9: *In the limit $\varepsilon \equiv u(r_\varepsilon) + 1 \to 0^+$ for some free-boundary point r_ε, the limiting asymptotic behaviour of the maximal radially symmetric solution branch of* (4.3.55)*, away from the internal layer region near $r = r_\varepsilon$, is*

$$u \sim u_0(r) + (-\varepsilon\log\varepsilon)\frac{\lambda_0}{\left[u_{0r}(r_0)\right]^2}u_0(r) + \varepsilon u_1(r) + \cdots\,. \tag{4.3.74a}$$

Here, u_0 is given in (4.3.58) and u_1 satisfies (4.3.57b) subject to

$$u_1 \sim -\frac{\lambda_0}{\left[u_{0r}\,(r_0)\right]^2}\log|r - r_0| + \chi + o(1)\,, \quad \text{as} \quad r \to r_0\,, \tag{4.3.74b}$$

where χ is defined in (4.3.65). Finally, λ and the free-boundary point r_ε are given for $\varepsilon \to 0$ by

$$\lambda \sim \frac{2\varepsilon}{\delta\left[\log\delta\right]^2} + o(\varepsilon^2\log\varepsilon)\,, \qquad r_\varepsilon \sim \sqrt{\delta}\left[1 + \frac{(-\varepsilon\log\varepsilon)}{2} + \cdots\right]\,. \tag{4.3.74c}$$

In Fig. 4.10, a comparison of the asymptotic prediction for λ given in (4.3.74c) with the corresponding full numerical result computed from (4.3.55) is provided. Notice that, owing to the small error term in (4.3.74c) for λ, the asymptotic result for λ accurately predicts the full numerical result for λ even when ε is not too small.

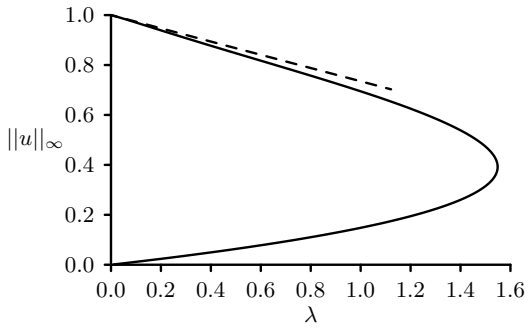

Figure 4.10: Comparison of numerical solution for $||u||_\infty$ versus λ (heavy solid curve) computed from the annulus problem (1.1.6) in $\delta < r < 1$ for $\delta = 0.1$ with the limiting asymptotic approximation (4.3.74c) (dashed curve) valid for $\lambda \to 0$.

4.4 Concentration Phenomena General Domains

In this section, the analysis of (4.3.1) is extended to analyze MEMS concentration for a general 2D domain. In the case of the unit disc, the symmetry of the domain led us to the assumption that the largest deflection should occur at the origin, however, for more general geometries $\Omega \subset \mathbb{R}^2$, it is not clear how to predict at which point the maximum deflection of the device is obtained. To investigate this problem, solutions to

$$\Delta^2 u = -\frac{\lambda}{(1+u)^2}, \quad x \in \Omega; \qquad x \in \partial\Omega; \qquad ||u||_\infty = 1 - \varepsilon \tag{4.4.1}$$

are constructed in the limit as $\varepsilon \to 0$. An important tool in the analysis, is the Biharmonic Neumann's Green Function $G(x, \xi)$ and its Regular Part $R(x; \xi)$, with definition

$$\Delta^2 G = \delta(x - \xi), \quad x \in \Omega; \qquad G = \partial_n G = 0, \quad x \in \partial\Omega \tag{4.4.2a}$$

$$G(x, \xi) = \frac{1}{8\pi}|x - \xi|^2 \log|x - \xi| + R(x; \xi) \tag{4.4.2b}$$

for $\xi \in \Omega$. We suppose that the solution of (4.4.1) concentrates at a single point $x_0 \in \Omega$ in the sense that $u(x_0) = -1 + \varepsilon$. Additionally, it is supposed that the solution is radially symmetric in the vicinity of this concentration points. To this end, motivated by the expansion of (4.3.18), equation (4.4.1) is expanded with

$$u = u_0 + \frac{\varepsilon}{\sigma}\sum_{j=1}^{\infty} \sigma^{j-1}[u_j + (-\log\sigma)u_{(2j-1)/2}] + \mathcal{O}(\varepsilon\mu) \quad \lambda = \frac{\varepsilon}{\sigma}\sum_{i=0}^{\infty} \sigma^j \lambda_j + \mathcal{O}(\varepsilon\mu) \tag{4.4.3}$$

where $\mu \ll \sigma^k$ for any $k \in \mathbb{N}$. To leading order, we have the problem

$$\Delta^2 u_0 = 0, \quad x \in \Omega; \qquad u_0 = \partial_n u_0 = 0 \quad x \in \partial\Omega; \tag{4.4.4a}$$

$$u_0(x_0) = -1, \qquad \nabla_x u_0(x_0) = 0; \tag{4.4.4b}$$

In terms of the Neumann's Green Function (4.4.2), the solution of (4.4.4) may be represented as

$$u_0(x; x_0) = -\frac{G(x; x_0)}{R(x_0; x_0)} \tag{4.4.5}$$

The condition that $\nabla_x u_0(x_0) = 0$ requires $\nabla_x R(x_0; x_0) = 0$ and the condition that $u(x) \geq -1$ requires $R(x_0; x_0) > 0$. These two conditions may be viewed as necessary conditions for solutions of (4.4.2) to concentrate at x_0.

Definition: Single Concentration Point. *If the maximal solution branch of* (4.4.1) *concentrates at some unique* $x_0 \in \Omega$*, then*

$$R(x_0; x_0) > 0, \qquad \nabla_x R(x_0; x_0) = 0, \tag{4.4.6}$$

where $R(x; x_0)$ *is the Regular Part of the Green's Function defined in* (4.4.2).

By expanding (4.4.5) as $x \to x_0$, the following singularity behaviour is established

$$\Delta^2 u_0 = 0, \quad x \in \Omega; \qquad u_0 = \partial_n u_0 = 0 \quad x \in \partial\Omega; \tag{4.4.7a}$$

$$u \sim -1 + \alpha r^2 \log r + r^2[\beta + a_c \cos 2\theta + a_s \sin 2\theta] + \mathcal{O}(r^3), \qquad r = |x - x_0| \to 0 \tag{4.4.7b}$$

where $x - x_0 = r(\cos\theta, \sin\theta)$ and

$$\begin{aligned} \alpha &= \frac{-1}{8\pi R(x_0; x_0)}, \qquad \beta = \frac{-1}{4R(x_0; x_0)} \left[\frac{\partial^2 R}{\partial x_1^2} + \frac{\partial^2 R}{\partial x_2^2}\right]_{x=x_0} \\ a_s &= \frac{-1}{2R(x_0; x_0)} \left[\frac{\partial^2 R}{\partial x_1 \partial x_2}\right]_{x=x_0}, \qquad a_c = \frac{-1}{4R(x_0; x_0)} \left[\frac{\partial^2 R}{\partial x_1^2} - \frac{\partial^2 R}{\partial x_2^2}\right]_{x=x_0} \end{aligned} \tag{4.4.7c}$$

This complete the specification of the leading order solution. The key qualitative features of this solution are its $r^2 \log r$ singularity as $r \to 0$ which permits the point constraint $u(x_0) = -1$ and the constraint $\alpha < 0$. Proceeding to the correction terms from (4.4.3), we have that

$$\Delta^2 u_j = \frac{-\lambda_{j-1}}{(1 + u_0)^2}, \quad x \in \Omega; \qquad u_j = \partial_n u_j = 0, \quad x \in \partial\Omega \tag{4.4.8}$$

for $j = 1, 2, 3, \ldots$ and with behaviour at the origin as $x \to x_0$ to be determined in the following calculation. As $r = |x - x_0| \to 0$ in (4.4.8), local behaviour (4.4.7b) is applied

so that

$$\Delta^2 u_j \sim \frac{-\lambda_{j-1}}{\alpha^2 r^4 \log^2 r}\left[1+\frac{\bar{\beta}}{\alpha \log r}\right]^{-2}, \qquad \bar{\beta}=\beta+a_s\sin 2\theta+a_c\cos 2\theta. \tag{4.4.9}$$

To establish an asymptotic solution to (4.4.9) as $r \to 0$, it is convenient to utilize the variable $\eta = -\log r$ and seek a solution to $v(\eta,\theta) = u(e^{-\eta},\theta)$ as $\eta \to \infty$. This transformation reduces (4.4.9) to

$$\begin{aligned} v_{\eta\eta\eta\eta}+4v_{\eta\eta\eta}+4v_{\eta\eta}+4v_{\theta\theta}+4v_{\theta\theta\eta}+2v_{\theta\theta\eta\eta}+v_{\theta\theta\theta\theta} \\ = \frac{-\lambda_{j-1}}{\alpha^2\eta^2}\left[1+\frac{2\bar{\beta}}{\alpha\eta}+\frac{3\bar{\beta}^2}{\alpha^2\eta^2}+\frac{4\bar{\beta}^3}{\alpha^3\eta^3}+\cdots\right] \end{aligned} \tag{4.4.10}$$

A solution to (4.4.10) is developed which is accurate to $\mathcal{O}(\eta^{-3})$. By noting that

$$\begin{aligned} \bar{\beta}^2 &= \beta^2+\frac{a_c^2+a_s^2}{2}+2\beta(a_c\cos 2\theta+a_s\sin 2\theta)+a_ca_s\sin 4\theta+\frac{a_c^2-a_s^2}{2}\cos 4\theta \\ \bar{\beta}^3 &= \left[\beta^3+\frac{3\beta}{2}(a_c^2+a_s^2)\right]+\sum_{n=1}^{3}(\bar{a}_n\cos n\theta+\bar{b}_n\sin n\theta.) \end{aligned} \tag{4.4.11}$$

the following asymptotic solution is developed as $\eta \to \infty$,

$$\begin{aligned} v(\eta,\theta) \sim \frac{\lambda_{j-1}}{4\alpha^2}\Bigg[\log\eta+\frac{\Gamma_1}{\eta}+\frac{\Gamma_2}{\eta^2}+\frac{\Gamma_3}{\eta^3}-\left[\frac{a_c}{4\alpha}\cos 2\theta+\frac{a_s}{4\alpha}\sin 2\theta\right]\frac{1}{\eta^2}+ \\ +\frac{1}{2\alpha}\frac{1}{\eta^3}\left[\frac{\beta}{\alpha}+\frac{1}{4}\right](a_c\cos 2\theta+a_s\sin 2\theta)+\mathcal{O}(\eta^{-4})\Bigg] \end{aligned} \tag{4.4.12}$$

where the constants Γ_1, Γ_2 and Γ_3 have values

$$\begin{aligned} \Gamma_1 &= -\left(1+\frac{\beta}{\alpha}\right) \\ \Gamma_2 &= -\left[\frac{3}{4}+\frac{\beta}{\alpha}+\frac{\beta^2}{2\alpha^2}+\frac{a_c^2+a_s^2}{4\alpha^2}\right] \\ \Gamma_3 &= -\left[1+\frac{3\beta}{2\alpha}+\frac{\beta^2}{\alpha^2}+\frac{\beta^3}{3\alpha^3}+\left(1+\frac{\beta}{\alpha}\right)\frac{a_c^2+a_s^2}{2\alpha^2}\right] \end{aligned} \tag{4.4.13}$$

Lengthy expressions for the constants $\bar{a}_n, \bar{b}_n$ for $n = 1, 2, 3$ can be obtained but these terms do not play a role in capturing behaviour to $\mathcal{O}(\eta^{-3})$ and so they are omitted. By returning to the variable $r = e^{-\eta}$, singularity behavior (4.4.12) furnishes problems

(4.4.8) for $j = 1, 2, 3, \ldots$ to give;

$$\Delta^2 u_j = \frac{-\lambda_{j-1}}{(1+u_0)^2}, \quad x \in \Omega; \qquad u_j = \partial_n u_j = 0, \quad x \in \partial\Omega \tag{4.4.14a}$$

$$\begin{aligned} u_j \sim \frac{\lambda_{j-1}}{4\alpha^2}\Bigg[\log(-\log r) - \frac{\Gamma_1}{\log r} + \frac{\Gamma_2}{\log^2 r} - \frac{\Gamma_3}{\log^3 r} - \Big[\frac{a_c}{4\alpha}\cos 2\theta + \frac{a_s}{4\alpha}\sin 2\theta\Big]\frac{1}{\log^2 r} \\ -\frac{1}{2\alpha}\frac{1}{\log^3 r}\left[\frac{\beta}{\alpha} + \frac{1}{4}\right](a_c\cos 2\theta + a_s \sin 2\theta) + \mathcal{O}(\log^{-4} r)\Bigg] \\ + b_j \log r + c_j + d_j \cos 2\theta + e_j \sin 2\theta + \cdots \qquad j = 1, 2, 3. \end{aligned} \tag{4.4.14b}$$

Note that the terms $b_j \log r$, c_j, $d_j \sin 2\theta$, $e_j \cos 2\theta$ relate to an arbitrary solution of the homogeneous problem. The logarithmic switchback terms, $u_{(2j-1)/2}$ for $j = 1, 2, 3, \ldots$ are defined as follows

$$\Delta^2 u_{(2j-1)/2} = 0, \quad x \in \Omega; \qquad u_{(2j-1)/2} = \partial_n u_{(2j-1)/2} = 0, \quad x \in \partial\Omega \tag{4.4.15a}$$

$$u_{(2j-1)/2}(x_0) = f_{(2j-1)/2}, \qquad \nabla_x u_{(2j-1)/2}(x_0) = 0; \tag{4.4.15b}$$

$$u_{(2j-1)/2} = -f_{(2j-1)/2}\, u_0; \qquad u_{(2j-1)/2} \sim f_{(2j-1)/2} + \mathcal{O}(r^2 \log r), \quad r \to 0 \tag{4.4.15c}$$

Here, the $f_{(2j-1)/2}$ for $j = 1, 2, 3, \ldots$ are constants whose value will be chosen to remove troublesome large terms in the inner expansion. By employing arguments similar to those used in § 4.3.1, the boundary layer width in the vicinity of the concentration point is found to be of scale $\mathcal{O}(\gamma)$ where

$$\gamma^2 = \varepsilon\sigma, \qquad \sigma = \frac{-1}{\log\gamma} \tag{4.4.16a}$$

Using this information, and local co-ordinates

$$u = -1 + \varepsilon v, \qquad x - x_0 = \varepsilon\rho(\cos\theta, \sin\theta) \tag{4.4.16b}$$

the nature of the expansion (4.4.3) in the vicinity of the concentration point x_0 is explored. After some algebra, and retaining only terms up to $\mathcal{O}(\sigma^2)$, the outer expansion

(4.4.3) is expressed in terms of variables (4.4.16a) to yield that

$$
\begin{aligned}
u \sim -1 + \varepsilon \Big[& -\alpha\rho^2 + \sigma\rho^2(\beta + a_c\cos 2\theta + a_s \sin 2\theta) \\
& + \frac{1}{4\alpha^2}\left[\frac{\lambda_0}{\sigma} + \lambda_1 + \lambda_2\sigma + \cdots\right]\left[\log(1-\sigma\log\rho) + \frac{\sigma\Gamma_1}{1-\sigma\log\rho} + \frac{\sigma^2\Gamma_2}{(1-\sigma\log\rho)^2}\right. \\
& - \frac{\sigma^3\Gamma_3}{(1-\sigma\log\rho)^3} - \frac{1}{4\alpha}\frac{\sigma^2}{(1-\sigma\log\rho)^2}\left(a_c\cos 2\theta + a_s\sin 2\theta\right) \\
& \left. + \frac{1}{2\alpha}\left(\frac{\beta}{\alpha} + \frac{1}{4}\right)\frac{\sigma^3}{(1-\sigma\log\rho)^3}\left(a_c\cos 2\theta + a_s\sin 2\theta\right)\right] \\
& + \sigma^{-2}b_1 + \sum_{j=0}^{3}\sigma^{j-1}[b_j\log\rho + c_j - b_{j+1} + d_j\cos 2\theta + e_j\sin 2\theta] \\
& \left. - \log\sigma\sum_{j=0}^{3}\sigma^{j-1}\left[\frac{\lambda_j}{4\alpha^2} + f_{(2j-1)/2}\right]\right]
\end{aligned}
$$

Expanding for small σ and retaining terms up to $\mathcal{O}(\sigma^2)$ the following expansion for $v(\rho,\theta)$ is obtained

$$
\begin{aligned}
v \sim\ & \sigma^{-2}b_1 + \sigma^{-1}(c_1 - b_2 + b_1\log\rho + d_1\cos 2\theta + e_1\sin 2\theta) + \left(b_2 - \frac{\lambda_0}{4\alpha^2}\right)\log\rho \\
& - \alpha\rho^2 + c_2 - b_3 + \frac{\lambda_0\Gamma_1}{4\alpha^2} + d_2\cos 2\theta + e_2\sin 2\theta - \log\sigma\sum_{j=0}^{3}\sigma^{j-1}\left[\frac{\lambda_j}{4\alpha^2} + f_{(2j-1)/2}\right] \\
& + \sigma\left[\alpha\rho^2\log\rho + \rho^2(\beta + a_c\cos 2\theta + a_s\sin 2\theta) - \frac{\lambda_0}{8\alpha^2}\log^2\rho + \left(b_3 + \frac{\lambda_0\Gamma_1}{4\alpha^2} - \frac{\lambda_1}{4\alpha^2}\right)\log\rho\right. \\
& \left. + \left(d_3 - \frac{\lambda_0 a_c}{16\alpha^3}\right)\cos 2\theta + \left(e_3 - \frac{\lambda_0 a_s}{16\alpha^3}\right)\sin 2\theta + c_3 - b_4 + \frac{\lambda_0\Gamma_2}{4\alpha^2} + \frac{\lambda_1\Gamma_1}{4\alpha^2}\right] \\
& + \sigma^2\left[-\frac{\lambda_0}{12\alpha^2}\log^3\rho + \left(\frac{\lambda_0\Gamma_1}{4\alpha^2} - \frac{\lambda_1}{8\alpha^2}\right)\log^2\rho + \left(b_4 + \frac{\lambda_0\Gamma_2}{2\alpha^2} + \frac{\lambda_1\Gamma_1}{4\alpha^2} - \frac{\lambda_2}{4\alpha^2}\right)\log\rho\right. \\
& - \frac{\lambda_0}{8\alpha^2}(a_c\cos 2\theta + a_s\sin 2\theta)\log\rho + \left(d_4 - \frac{\lambda_1 a_c}{16\alpha^3} + \frac{\lambda_0 a_c}{8\alpha^3}\left(\frac{\beta}{\alpha} + \frac{1}{4}\right)\right)\cos 2\theta \\
& \left. + \left(e_4 - \frac{\lambda_1 a_s}{16\alpha^3} + \frac{\lambda_0 a_s}{8\alpha^3}\left(\frac{\beta}{\alpha} + \frac{1}{4}\right)\right)\sin 2\theta\right] + \mathcal{O}(\sigma^3)
\end{aligned}
\tag{4.4.17}
$$

The condition $v(0,\theta) = 1$ suggests the largest term in expansion (4.4.17) should be $\mathcal{O}(1)$

which asserts the following values on certain constants

$$b_1 = e_1 = e_2 = d_1 = d_2 = 0; \qquad c_1 = b_2; \qquad f_{(2j-1)/2} = -\frac{\lambda_j}{4\alpha^2} \quad j = 1, 2, 3. \quad (4.4.18)$$

Now, applying the transformation (4.4.16) to the main equation (4.4.1), the following equation is obtained for $v(\rho, \theta)$,

$$\Delta^2 v = -\frac{\sigma^2 \lambda}{\varepsilon v^2}, \quad \rho > 0; \qquad \begin{matrix} v(0) = 1 \\ v_\rho(0) = v_{\rho\rho\rho}(0) = 0 \end{matrix} \quad (4.4.19a)$$

which is furnished with far field behavior

$$\begin{aligned} v \sim & -\alpha\rho^2 + \left(b_2 - \frac{\lambda_0}{4\alpha^2}\right)\log\rho + c_2 - b_3 + \frac{\lambda_0\Gamma_1}{4\alpha^2} \\ & + \sigma\left[\alpha\rho^2\log\rho + \rho^2(\beta + a_c\cos 2\theta + a_s\sin 2\theta) - \frac{\lambda_0}{8\alpha^2}\log^2\rho + \left(b_3 + \frac{\lambda_0\Gamma_1}{4\alpha^2} - \frac{\lambda_1}{4\alpha^2}\right)\log\rho\right. \\ & \left. + \left(d_3 - \frac{\lambda_0 a_c}{16\alpha^3}\right)\cos 2\theta + \left(e_3 - \frac{\lambda_0 a_s}{16\alpha^3}\right)\sin 2\theta + c_3 - b_4 + \frac{\lambda_0\Gamma_2}{4\alpha^2} + \frac{\lambda_1\Gamma_1}{4\alpha^2}\right] \\ & + \sigma^2\left[-\frac{\lambda_0}{12\alpha^2}\log^3\rho + \left(\frac{\lambda_0\Gamma_1}{4\alpha^2} - \frac{\lambda_1}{8\alpha^2}\right)\log^2\rho + \left(b_4 + \frac{\lambda_0\Gamma_2}{2\alpha^2} + \frac{\lambda_1\Gamma_1}{4\alpha^2} - \frac{\lambda_2}{4\alpha^2}\right)\log\rho\right. \\ & - \frac{\lambda_0}{8\alpha^2}(a_c\cos 2\theta + a_s\sin 2\theta)\log\rho + \left(d_4 - \frac{\lambda_1 a_c}{16\alpha^3} + \frac{\lambda_0 a_c}{8\alpha^3}\left(\frac{\beta}{\alpha} + \frac{1}{4}\right)\right)\cos 2\theta \\ & \left. + \left(e_4 - \frac{\lambda_1 a_s}{16\alpha^3} + \frac{\lambda_0 a_s}{8\alpha^3}\left(\frac{\beta}{\alpha} + \frac{1}{4}\right)\right)\sin 2\theta + c_4 - b_5 - \frac{\lambda_0\Gamma_3}{4\alpha^2} + \frac{\lambda_1\Gamma_2}{4\alpha^2} + \frac{\lambda_2\Gamma_1}{4\alpha^2}\right] \\ & + \mathcal{O}(\sigma^3) \end{aligned} \quad (4.4.19b)$$

The form of the far field condition (4.4.19b) suggests that the solution of (4.4.19a) should admit the expansion

$$v = v_0 + \sigma v_1 + \sigma^2 v_2 + \mathcal{O}(\sigma^3), \qquad \lambda = \frac{\varepsilon}{\sigma}\left[\lambda_0 + \sigma\lambda_1 + \sigma^2\lambda_2 + \mathcal{O}(\sigma^3)\right]$$

At leading order $v_0 = v_0(\rho)$ satisfies

$$\Delta^2 v_0 = 0, \quad \rho > 0; \qquad \begin{matrix} v_0(0) = 1 \\ v_{0\rho}(0) = v_{0\rho\rho\rho}(0) = 0 \end{matrix} \quad (4.4.20a)$$

$$v_0 \sim -\alpha\rho^2 + \left(b_2 - \frac{\lambda_0}{4\alpha^2}\right)\log\rho + c_2 - b_3 + \frac{\lambda_0\Gamma_1}{4\alpha^2} \quad (4.4.20b)$$

and admits the solution $v_0(\rho) = 1 - \alpha\rho^2$ which in turn specifies

$$b_2 = \frac{\lambda_0}{4\alpha^2}, \qquad c_2 = 1 + b_3 - \frac{\lambda_0\Gamma_1}{4\alpha^2} \tag{4.4.21}$$

Equating terms at $\mathcal{O}(\sigma)$ gives that $v_1(\rho,\theta)$ satisfies

$$\Delta^2 v_1 = -\frac{\lambda_0}{v_0^2}, \quad x \in \Omega; \qquad v_1(0,\theta) = v_{1\rho}(0,\theta) = v_{1\rho\rho\rho}(0,\theta) = 0 \tag{4.4.22a}$$

with far field behavior

$$v_1 \sim \alpha\rho^2\log\rho + \rho^2(\beta + a_c\cos 2\theta + a_s\sin 2\theta) - \frac{\lambda_0}{8\alpha^2}\log^2\rho + \left(b_3 + \frac{\lambda_0\Gamma_1}{4\alpha^2} - \frac{\lambda_1}{4\alpha^2}\right)\log\rho$$
$$+ \left(d_3 - \frac{\lambda_0 a_c}{16\alpha^3}\right)\cos 2\theta + \left(e_3 - \frac{\lambda_0 a_s}{16\alpha^3}\right)\sin 2\theta + c_3 - b_4 + \frac{\lambda_0\Gamma_2}{4\alpha^2} + \frac{\lambda_1\Gamma_1}{4\alpha^2} \tag{4.4.22b}$$

as $\rho \to \infty$. Consider the decomposition $v_1(\rho,\theta) = \mathcal{V}(\rho,\theta) + \bar{v}(\rho)$ where

$$\Delta^2\mathcal{V} = 0, \quad \rho > 0; \qquad \mathcal{V}(0,\theta) = \mathcal{V}_\rho(0,\theta) = \mathcal{V}_{\rho\rho\rho}(0,\theta) = 0 \tag{4.4.23a}$$

with far field behavior

$$\mathcal{V} \sim \rho^2(a_c\cos 2\theta + a_s\sin 2\theta) + \left(d_3 - \frac{\lambda_0 a_c}{16\alpha^3}\right)\cos 2\theta + \left(e_3 - \frac{\lambda_0 a_s}{16\alpha^3}\right)\sin 2\theta \tag{4.4.23b}$$

as $\rho \to \infty$. The solution to problem (4.4.23) is $\mathcal{V} = \rho^2(a_c\cos 2\theta + a_s\sin 2\theta)$ which in turn gives that

$$d_3 = \frac{\lambda_0 a_c}{16\alpha^3}, \qquad e_3 = \frac{\lambda_0 a_s}{16\alpha^3} \tag{4.4.24}$$

The problem for $\bar{v}(\rho)$ is now

$$\Delta^2\bar{v} = -\frac{\lambda_0}{v_0^2}, \quad \rho > 0; \qquad \bar{v}(0,\theta) = \bar{v}_\rho(0,\theta) = \bar{v}_{\rho\rho\rho}(0,\theta) = 0 \tag{4.4.25a}$$

with far field behavior

$$\bar{v} \sim \alpha\rho^2\log\rho + \beta\rho^2 - \frac{\lambda_0}{8\alpha^2}\log^2\rho + \left(b_3 + \frac{\lambda_0\Gamma_1}{4\alpha^2} - \frac{\lambda_1}{4\alpha^2}\right)\log\rho + c_3 - b_4 + \frac{\lambda_0\Gamma_2}{4\alpha^2} + \frac{\lambda_1\Gamma_1}{4\alpha^2} \tag{4.4.25b}$$

as $\rho \to \infty$. By recalling that $v_0 = 1 - \alpha\rho^2$, equation (4.4.25a) is directly integrated to show that

$$\lambda_0 = 8\alpha^2 \tag{4.4.26}$$

More information on the solution of (4.4.25) can be extracted by direct integration. Indeed, some simple algebraic manipulations show that

$$\Delta\bar{v} = 2\alpha\log(1-\alpha\rho^2) + C \tag{4.4.27}$$

where the constant C can be seen from (4.4.25b) to take the value $C = 4(\alpha+\beta) - 2\alpha\log(-\alpha)$. Integrating once more yields that

$$\bar{v}_\rho = \alpha\rho\log(\rho^2 - 1/\alpha) - \frac{\log(1-\alpha\rho^2)}{\rho} + \rho(\alpha+2\beta), \quad \rho > 0; \qquad \bar{v}(0) = 0 \tag{4.4.28}$$

and one final additional integration gives

$$\bar{v} = \frac{\alpha}{2}\left(\rho^2 - \frac{1}{\alpha}\right)\log(\rho^2 - 1/\alpha) + \beta\rho^2 - \frac{1}{2}\log(-\alpha) - \int_0^\rho \frac{\log(1-\alpha x^2)}{x}\,dx \tag{4.4.29}$$

Using manipulations very similar to those leading to (4.3.35), we have that

$$\int_0^\rho \frac{\log(1-\alpha x^2)}{x}\,dx = \frac{\pi^2}{24} + \frac{1}{4}\log^2(-\alpha\rho^2) + \frac{1}{2}\int_1^{-\alpha\rho^2} \frac{\log(1+1/x)}{x}\,dx \tag{4.4.30}$$

and so the final specification of $\bar{v}(\rho)$ is

$$\begin{aligned}\bar{v}(\rho) = {} & \frac{\alpha}{2}\left(\rho^2 - \frac{1}{\alpha}\right)\log(\rho^2 - 1/\alpha) + \beta\rho^2 - \log^2\rho - \log(-\alpha)\log\rho \\ & - \left[\frac{\pi^2}{24} + \frac{1}{4}\log^2(-\alpha) + \frac{1}{2}\int_1^{-\alpha\rho^2} \frac{\log(1+1/x)}{x}\,dx\right]\end{aligned} \tag{4.4.31}$$

where the integral term on the right hand side of (4.4.31) is finite as $\rho \to \infty$. In fact, (4.4.31) has far field behavior

$$\bar{v} \sim \alpha\rho^2\log\rho + \beta\rho^2 - \log^2\rho - (1+\log(-\alpha))\log\rho - \frac{1}{2}\left[\frac{\pi^2}{6} + \frac{1}{2}\log^2(-\alpha) + \log(-\alpha) + 1\right] \tag{4.4.32}$$

as $\rho \to \infty$ where the identity $\int_1^\infty x^{-1}\log(1+1/x)\,dx = \pi^2/12$ has been used. A comparison of (4.4.32) with far field behaviour (4.4.25b) indicates that

$$\begin{aligned} b_3 &= \frac{\lambda_1}{4\alpha^2} - \frac{\lambda_0\Gamma_1}{4\alpha^2} - 1 - \log(-\alpha), \\ c_3 &= b_4 - \frac{\lambda_0\Gamma_2}{4\alpha^2} - \frac{\lambda_1\Gamma_1}{4\alpha^2} - \frac{1}{2}\left[\frac{\pi^2}{6} + \frac{1}{2}\log^2(-\alpha) + \log(-\alpha) + 1\right]. \end{aligned} \tag{4.4.33}$$

This concludes the analysis of terms at $\mathcal{O}(\sigma)$. At $\mathcal{O}(\sigma^2)$, the relevant equations are

$$\Delta^2 v_2 = -\frac{\lambda_1}{v_0^2} + \frac{2\lambda_0}{v_0^3} v_1, \quad \rho > 0; \qquad v_2(0) = v_{2\rho}(0) = v_{2\rho\rho\rho}(0) = 0 \tag{4.4.34a}$$

furnished with the far field condition

$$\begin{aligned} v_2 \sim & -\frac{\lambda_0}{12\alpha^2}\log^3\rho + \left(\frac{\lambda_0\Gamma_1}{4\alpha^2} - \frac{\lambda_1}{8\alpha^2}\right)\log^2\rho + \left(b_4 + \frac{\lambda_0\Gamma_2}{2\alpha^2} + \frac{\lambda_1\Gamma_1}{4\alpha^2} - \frac{\lambda_2}{4\alpha^2}\right)\log\rho \\ & - \frac{\lambda_0}{8\alpha^2}(a_c\cos 2\theta + a_s\sin 2\theta)\log\rho + \left(d_4 - \frac{\lambda_1 a_c}{16\alpha^3} + \frac{\lambda_0 a_c}{8\alpha^3}\left(\frac{\beta}{\alpha} + \frac{1}{4}\right)\right)\cos 2\theta \\ & + \left(e_4 - \frac{\lambda_1 a_s}{16\alpha^3} + \frac{\lambda_0 a_s}{8\alpha^3}\left(\frac{\beta}{\alpha} + \frac{1}{4}\right)\right)\sin 2\theta + c_4 - b_5 - \frac{\lambda_0\Gamma_3}{4\alpha^2} + \frac{\lambda_1\Gamma_2}{4\alpha^2} + \frac{\lambda_2\Gamma_1}{4\alpha^2} + \cdots \end{aligned} \tag{4.4.34b}$$

as $\rho \to \infty$. To fix λ_1, (4.4.34a) is integrated directly over $0 < \rho < \infty$. The far field behaviour gives no contribution to the flux of Δv_2, therefore

$$\lambda_1 \int_0^{2\pi}\int_0^\infty \frac{1}{v_0^2}\,\rho d\rho d\theta = \lambda_0 \int_0^{2\pi}\int_0^\infty \frac{2v_1}{v_0^3}\,\rho d\rho d\theta$$

Integration over the angular component makes no contribution to the integrals and so we have that

$$\lambda_1 = -4\alpha\lambda_0 \int_0^\infty \frac{\bar{v}}{v_0^3}\,\rho d\rho \tag{4.4.35}$$

where $\bar{v}(\rho)$ is the radially symmetric component of $v_1(\rho,\theta)$, defined in (4.4.29). Recalling that $v_0 = 1 - \alpha\rho^2$ and integrating (4.4.35) by parts yields that

$$\begin{aligned} \lambda_1 &= -\lambda_0 \int_0^\infty \bar{v}\left[\frac{1}{(1-\alpha\rho^2)^2}\right]_\rho d\rho = \lambda_0 \int_0^\infty \bar{v}_\rho \left[\frac{1}{(1-\alpha\rho^2)^2}\right] d\rho \\ &= \lambda_0 \int_0^\infty \left[\alpha\rho\log(\rho^2 - 1/\alpha) - \frac{\log(1-\alpha\rho^2)}{\rho} + \rho(\alpha+2\beta)\right]\left(\frac{1}{1-\alpha\rho^2}\right)^2 d\rho \\ &= \lambda_0[\alpha + 2\beta - \alpha\log(-\alpha)]\int_0^\infty \frac{\rho d\rho}{(1-\alpha\rho^2)^2} - \lambda_0\int_0^\infty \frac{\log(1-\alpha\rho^2)}{\rho(1-\alpha\rho^2)}\,d\rho \\ &= -\frac{\lambda_0}{2}\left[1 + \frac{2\beta}{\alpha} + \log(-\alpha)\right] - \frac{\lambda_0}{2}\int_0^\infty \frac{\log(1+x)}{x(1+x)}\,dx \\ &= -\frac{\lambda_0}{2}\left[\frac{\pi^2}{6} - \log(-\alpha) + \left(1 + \frac{2\beta}{\alpha}\right)\right]. \end{aligned}$$

In the preceding calculation, the identity $\int_0^\infty \log(1+x)/(x+x^2)dx = \pi^2/6$ has been used. This completes a two-term asymptotic construction of the maximal solution to

(4.4.1) and a general geometry in two dimensions. The following is a summary:
Principal Result 4.10: *In the limit as* $\varepsilon \equiv u(x_0) + 1 \to 0^+$, *the limiting behaviour of the maximal solution branch of* (4.4.1) *has asymptotic formulation*

$$\begin{aligned} u &= u_0 - \frac{\varepsilon \log \sigma}{\sigma} u_{1/2} + \frac{\varepsilon}{\sigma} u_1 - \varepsilon \log \sigma u_{3/2} + \varepsilon u_2 + \mathcal{O}(\varepsilon \sigma \log \sigma) \\ \lambda &= \frac{\varepsilon}{\sigma} \lambda_0 + \varepsilon \lambda_1 + \mathcal{O}(\varepsilon \sigma) \end{aligned} \tag{4.4.36a}$$

where $\sigma = -1/\log \gamma$ *and the boundary layer width* γ *is determined in terms of* ε *by* $-\gamma^2 \log \gamma = \varepsilon$. *The point* $x_0 \in \Omega$ *is assumed to be the unique point satisfying*

$$\nabla R(x_0; x_0) = 0, \qquad R(x_0; x_0) > 0 \tag{4.4.36b}$$

where $R(x; x_0)$ *is the Regular part of the Green's function, defined in* (4.4.2). *In terms of this Green's function,*

$$u_0 = -\frac{G(x; x_0)}{R(x_0; x_0)}, \qquad u_{1/2} = \frac{\lambda_0}{4\alpha^2} u_0, \qquad u_{1/2} = \frac{\lambda_1}{4\alpha^2} u_0 \tag{4.4.36c}$$

where

$$u_0 \sim -1 + \alpha r^2 \log r + r^2(\beta + a_c \cos 2\theta + a_s \sin 2\theta) + \cdots, \tag{4.4.36d}$$

as $x - x_0 = r(\cos\theta, \sin\theta) \to 0$ *and* $(\alpha, \beta, a_c, a_s)$ *are given in* (4.4.7c) *in terms of* $R(x; x_0)$. *Additionally,* u_1 *and* u_2 *satisfy*

$$\begin{aligned} \Delta u_1 &= -\frac{\lambda_0}{(1+u_0)^2}, \quad x \in \Omega; \qquad u_1 = \partial_n u_1 = 0, \quad x \in \partial\Omega \\ u_1 &\sim \frac{\lambda_0}{4\alpha^2} \log(-\log r) + \frac{\lambda_0}{4\alpha^2} + \mathcal{O}(\log^{-1} r), \quad r \to 0 \end{aligned} \tag{4.4.36e}$$

$$\begin{aligned} \Delta u_2 &= -\frac{\lambda_1}{(1+u_0)^2}, \quad x \in \Omega; \qquad u_2 = \partial_n u_2 = 0, \quad x \in \partial\Omega \\ u_2 &\sim \frac{\lambda_1}{4\alpha^2} \log(-\log r) + \frac{\lambda_0}{4\alpha^2} \log r + \frac{\lambda_0}{2\alpha^2}\left(1 + \frac{\beta}{\alpha}\right) + \frac{\lambda_1}{4\alpha^2} - \log(-\alpha) + \mathcal{O}(\log^{-1} r) \end{aligned} \tag{4.4.36f}$$

Finally, λ_0 *and* λ_1 *are given by*

$$\lambda_0 = 8\alpha^2, \qquad \lambda_1 = -\frac{\lambda_0}{2}\left[\frac{\pi^2}{6} - \log(-\alpha) + \left(1 + \frac{2\beta}{\alpha}\right)\right] \tag{4.4.36g}$$

By assumption $\alpha < 0$ *and so all formulae in Principal Result 4.10 are well defined.*

In this calculation of the maximal solution branch, it has been assumed that the

limiting solution concentrates at a unique $x_0 \in \Omega$ satisfying condition (4.4.6). While this assumption seems reasonable for a large class of two dimensional geometries, we speculate that for certain domains, for example dumbbell shaped domains, the limiting singular solution may concentrate at multiple points. The multiplicity of such concentration points satisfying (4.4.6) can be determined for particular domains by a numerical investigation of the Green's function (4.4.2).

4.5 Conclusions

In this Chapter the analysis of several MEMS models has been conducted in the singular limit $||u||_\infty \to 1$. In each case, the definition $||u||_\infty = 1 - \varepsilon$ has been made and matched asymptotic expansions have been used to resolve the $\lambda/(1+u)^2$ nonlinearity near the point of maximum deflection in the lim $\varepsilon \to 0^+$. In each of the models considered, the singular solution can be constructed and an asymptotic form of the limiting branch determined.

In § 4.1, the infinite fold point structure of the membrane problem (1.1.3), originally observed by [34], is analyzed. Conditions are established on N and α under which the bifurcation diagram of (1.1.3) undergoes an infinite number of folds and an asymptotic representation of this curve is obtained. The explicit nature of our method allows for the location of each fold point to be accurately determined in terms of $\varepsilon = 1 + u(0)$. It is observed that fold points are located exponentially close to $u = -1$.

In the case of equations (1.1.4)-(1.1.6), it is observed numerically that the infinite fold point structure is destroyed and what remains is a maximal solution branch with limiting behaviour $\lambda \to 0$ as $||u||_\infty \to 1$. This limiting solution is constructed for (1.1.4) on the slab in § 4.2 , on the unit disk in § 4.3 and on a general two dimensional geometry in § 4.4. In each case a two term asymptotic expansion is obtained and careful use of logarithmic switchback terms is required. Good agreement with numerical calculations is observed.

A interesting observation is that the perturbation $-\delta\Delta^2 u$ changes the singularity behaviour of the limiting solution from $u \sim -1 + r^{2/3}$ in the membrane case (1.1.2) to $u \sim -1 + \alpha r^2 \log r$ in the biharmonic case (1.1.4). We conjecture that a necessary condition for a perturbation of (1.1.2) to destroy the infinite fold point structure is that it must alter the singularity of the limiting solution.

The analysis of § 4.3.2 deals with the construction of the radially symmetric maximal solution branch for the annulus problem (1.1.6). An added complication in this problem is that the point of maximum deflection, or the concentration point, is not known a priori. This point is determined along with the construction of the singular solution as part of a free boundary problem.

Finally in § 4.4, the problem of constructing the maximal solution branch for the pure biharmonic MEMS problem (4.4.1) is considered. Knowledge of a Neumann Green's function, defined in (4.4.2), is key to the analysis. Under the assupmtion that the singular solution concentrates at some $x_0 \in \Omega$ as $u(x_0) \to -1$, the maximal branch is constructed in terms of the Regular Part of the Green's function (4.4.2) and conditions on the point x_0 are established.

This Chapter forms the basis of the paper [30] titled *Asymptotics of some nonlinear eigenvalue problems for a MEMS capacitor: Part II: Fold point Multiple Solutions and Singular Asymptotics* under consideration for The European Journal of Applied Mathematics.

Chapter 5

Persistence in Patchy Domains

In this chapter the indefinite weight eigenvalue problem

$$\Delta\phi + \lambda m(x)\phi = 0\,, \quad x \in \Omega\,; \qquad \partial_n\phi = 0\,, \quad x \in \partial\Omega\,; \quad \int_\Omega \phi^2\,dx = 1\,. \tag{5.0.1}$$

is studied. Equation (5.0.1) has been studied in the context of mathematical ecology by many authors (c.f. [45], [46], [59], [60]). The function $m(x)$ appearing in (5.0.1) represents the local per capita growth rate of a species evolving in Ω and is tailored to represent the variable quality of the habitat Ω. The principal eigenvalue λ of (5.0.1), corresponding to a positive eigenfunction, is known as the persistence threshold. For a species with density $u(x,t)$ evolving according to the Logistic equation

$$u_t = D\Delta u + u\left[m(x) - u\right]\,, \quad x \in \Omega\,; \qquad \partial_n u = 0\,, \quad x \in \partial\Omega\,; \tag{5.0.2a}$$

$$u(x,0) = u_0(x) \geq 0\,, \qquad x \in \Omega, \tag{5.0.2b}$$

it was shown in [59] that if $1/D > \lambda$, then $u(x,t) \to u^*$ as $t \to \infty$ where u^* is a non-negative equilibrium of (5.0.2). When $1/D < \lambda$, $u(x,t) \to 0$ as $t \to \infty$ indicating that the species has become extinct. Therefore, when λ is as small as possible, the species whose density is represented by $u(x,t)$, persists for the largest range of diffusivities D.

An interesting question to ask is, among all $m(x)$ for which $\int_\Omega m(x)$ is fixed, which $m(x)$ generates the smallest positive λ where λ is the principal eigenvalue of (5.0.1)?

This question has been addressed by many authors over the last 20 years and while a large quantity of information is now known about the optimal functions $m(x)$, the problem remains largely open. Two key established results are the following. The first of which, due to Senn and Hess [68], states that the principal eigenvalue λ of (5.0.1) is positive if and only if $\int_\Omega m < 0$ and $m(x)$ is positive on some subset of Ω with positive measure. The second key result of [59] states that, the optimal $m(x)$ must be of bang-bang type, *i.e.* a piecewise constant.

In this chapter, the principal eigenvalue of (5.0.1) is constructed and optimized for

a particular class of *patchy* $m(x)$ given by

$$m_\varepsilon(x) = \begin{cases} m_j/\varepsilon^2\,, & x \in \Omega_{\varepsilon_j}\,, \quad j = 1, \ldots, n\,, \\ \\ -m_b\,, & x \in \Omega \backslash \bigcup_{j=1}^n \Omega_{\varepsilon_j}\,. \end{cases} \tag{5.0.3}$$

Here $\Omega_{\varepsilon_j} \equiv \{x \,|\, |x - x_j| \leq \varepsilon\rho_j \cap \Omega\}$, so that the patches Ω_{ε_j} are the portions of the circular disks of radius $\varepsilon\rho_j$ that are strictly inside Ω. The constant m_j is the local growth rate of the j^{th} patch, with $m_j > 0$ for a favourable habitat and $m_j < 0$ for a non-favourable habitat. The constant $m_b > 0$ is the background bulk decay rate for the unfavourable habitat. In terms of this patch arrangement, the condition $\int_\Omega m\,dx < 0$ is asymptotically equivalent for $\varepsilon \to 0$ to

$$\int_\Omega m\,dx = -m_b|\Omega| + \frac{\pi}{2}\sum_{j=1}^n \alpha_j m_j \rho_j^2 + \mathcal{O}(\varepsilon^2) < 0\,. \tag{5.0.4}$$

To enforce the condition that $m(x)$ is positive on some subdomain of Ω with positive measure, at least one $m_j > 0$ for some j. The parameters of the problem must always be chosen so that these conditions hold.

Based on this specific but relatively general class of $m(x)$, the eigenvalue problem (5.0.1) is solved with the method of matched asymptotic expansion in the limit $\varepsilon \to 0$. In § 5.1, λ is calculated for $m(x)$ corresponding to a single positive patch which is located either completely interior to Ω, or centred on a boundary point of Ω. It is observed that a patch centred on the boundary point of Ω always generates a smaller persistence threshold λ than that of a patch centred on an interior point of Ω.

In § 5.2, the persistence threshold is calculated asymptotically for a configuration of n patches corresponding to $m(x)$ given in (5.0.3). The two term asymptotic expansion

$$\lambda_\varepsilon = \nu\mu_0 + \nu^2\mu_1(x_1, \ldots, x_n) + \cdots \qquad \nu = \frac{-1}{\log\varepsilon} \tag{5.0.5}$$

is obtained for the persistence threshold λ. The second order term μ_1, which has an explicit dependence on the centres of the patches, is determined in terms the Neumann Green's function (5.1.19).

In § 5.3, the persistence threshold is optimized with respect to patch fragmentation and location. Interestingly, a large amount of information concerning the optimal arrangement of patches is contained in the leading order term of the expansion of λ.

In § 5.3.2, several qualitative results are established. It is observed that a favourable patch centred on the boundary of Ω always produces a lower persistence threshold than a patch centred at an interior point of Ω. If the boundary of the domain has corners (

e.g. squares, triangles), the corner of smallest angle is the most preferred location for a favourable patch.

It is also shown that when one favourable interior patch is split into two favourable interior patches, the persistence threshold λ is always increased. This indicates that fragmentation of resources is generally not advantageous to the species. It is observed that splitting a favourable interior patch into a favourable interior and a favourable boundary patch is only advantageous if the boundary patch is sufficiently strong.

Finally in § 5.3.3, the degenerate case where the leading order term in λ is optimized for multiple configurations is considered. In this scenario, optimization of the second order term, μ_1 is investigated and some instructive examples are constructed.

5.1 Determination Of The Persistence Threshold For One Patch

In this section, the method of matched asymptotic expansions is used to derive a two-term asymptotic expansion for the positive principal eigenvalue λ of (1.2.3) for the case of one localized favourable habitat centered at either a point interior to Ω or a point on $\partial\Omega$.

5.1.1 A Single Interior Patch

First, the case where one interior circular patch centered at $x_0 \in \Omega$, with $\mathrm{dist}(x_0, \partial\Omega) \gg \mathcal{O}(\varepsilon)$ is calculated. The positive principal eigenvalue $\lambda > 0$ and the corresponding eigenfunction $\phi > 0$ of

$$\Delta\phi + \lambda\, m_\varepsilon(x)\phi = 0\,, \quad x \in \Omega; \qquad \partial_n\phi = 0\,, \quad x \in \partial\Omega\,; \qquad \int_\Omega \phi^2\, dx = 1\,, \tag{5.1.1a}$$

are calculated asymptotically in the small patch radius limit $\varepsilon \to 0$, where the growth rate function $m_\varepsilon(x)$ is defined as

$$m_\varepsilon(x) = \begin{cases} m_+/\varepsilon^2\,, & x \in \Omega_{\varepsilon_0}\,, \\ -m_b, & x \in \Omega\backslash\Omega_{\varepsilon_0}\,. \end{cases} \tag{5.1.1b}$$

Here the patch Ω_{ε_0} is the circular disk $\Omega_{\varepsilon_0} \equiv \{x \,|\, |x - x_0| \le \varepsilon\,\}$. In (5.1.1b), $m_+ > 0$ is the local growth rate of the favourable habitat, while $m_b > 0$ gives the background bulk decay rate for the unfavourable habitat.

The condition $\int_\Omega m\, dx < 0$ for the existence of a positive principal eigenvalue is

asymptotically equivalent to

$$\int_\Omega m\,dx = -m_b|\Omega| + \pi m_+ + \mathcal{O}(\varepsilon^2) < 0\,, \tag{5.1.2}$$

in the limit $\varepsilon \to 0$. It is assumed that the constants m_b and m_+ are chosen so that this condition holds.

The positive principal eigenvalue λ of (5.1.1) is expanded as

$$\lambda \sim \mu_0\nu + \mu_1\nu^2 + \cdots\,, \qquad \nu = -1/\log\varepsilon\,, \tag{5.1.3}$$

for some coefficients μ_0 and μ_1 to be found. In the outer region, defined away from an $\mathcal{O}(\varepsilon)$ neighbourhood of x_0, we expand the corresponding eigenfunction as

$$\phi \sim \phi_0 + \nu\phi_1 + \nu^2\phi_2 + \cdots\,. \tag{5.1.4}$$

Upon substituting (5.1.3) and (5.1.4) into (5.1.1), ϕ_0 is observed to be a constant with the normalization condition $\int_\Omega \phi_0^2\,dx = 1$ yielding $\phi_0 = |\Omega|^{-1/2}$, where $|\Omega|$ is the area of Ω. In addition, ϕ_1 and ϕ_2 are found to satisfy

$$\begin{gathered}\Delta\phi_1 = \mu_0 m_b\phi_0\,, \quad x\in\Omega\backslash\{x_0\}\,; \qquad \partial_n\phi_1 = 0\,, \quad x\in\partial\Omega\,;\\ \int_\Omega \phi_1\,dx = 0\,,\end{gathered} \tag{5.1.5a}$$

$$\begin{gathered}\Delta\phi_2 = \mu_1 m_b\phi_0 + \mu_0 m_b\phi_1\,, \quad x\in\Omega\backslash\{x_0\}\,; \qquad \partial_n\phi_2 = 0\,, \quad x\in\partial\Omega\,;\\ \int_\Omega \left(\phi_1^2 + 2\phi_0\phi_2\right)\,dx = 0\,.\end{gathered} \tag{5.1.5b}$$

The matching of ϕ_1 and ϕ_2 to an inner solution defined in an $\mathcal{O}(\varepsilon)$ neighborhood of the patch at x_0, as done below, will yield singularity conditions for ϕ_1 and ϕ_2 as $x \to x_0$.

In the inner region near the patch centered at x_0 the local variables y and ψ are introduced by

$$y = \varepsilon^{-1}(x - x_0)\,, \qquad \psi(y) = \phi(x_0 + \varepsilon y)\,. \tag{5.1.6}$$

With these new variables, (5.1.1) becomes

$$\Delta\psi = \begin{cases} -\lambda m_+\psi\,, & |y| < 1\,,\\ \\ \mathcal{O}(\varepsilon^2)\,, & |y| > 1\,. \end{cases} \tag{5.1.7}$$

The inner approximation to the eigenfunction is expanded as

$$\psi \sim \psi_0 + \nu\psi_1 + \nu^2\psi_2 + \cdots\,, \qquad \nu = -1/\log\varepsilon\,. \tag{5.1.8}$$

where to leading order ψ_0 is observed to be an unknown constant while ψ_1 and ψ_2 satisfy

$$\Delta\psi_k = \begin{cases} \mathcal{F}_k\,, & |y| \le 1\,, \\ 0\,, & |y| \ge 1\,. \end{cases} \tag{5.1.9a}$$

Here $\mathcal{F}_k$ for $k = 1, 2$ is defined by

$$\mathcal{F}_1 = -\mu_0 m_+ \psi_0\,, \qquad \mathcal{F}_2 = -\mu_0 m_+ \psi_1 - \mu_1 m_+ \psi_0\,. \tag{5.1.9b}$$

The solution ψ_1 to (5.1.9) is calculated to be

$$\psi_1 = \begin{cases} A_1\rho^2/2 + \bar{\psi}_1\,, & \rho \le 1\,, \\ A_1 \log\rho + \dfrac{A_1}{2} + \bar{\psi}_1\,, & \rho \ge 1\,, \end{cases} \tag{5.1.10a}$$

where $\rho = |y|$. Here $\bar{\psi}_1$ is an unknown constant and A_1 is given by

$$A_1 = \frac{\mathcal{F}_1}{2} = -\frac{1}{2}\mu_0 m_+ \psi_0\,. \tag{5.1.10b}$$

Additionally, the solution ψ_2 is observed to have far-field behaviour

$$\psi_2 \sim A_2 \log\rho + \mathcal{O}(1)\,, \quad \text{as} \quad \rho \to \infty\,, \qquad A_2 \equiv \int_0^1 \mathcal{F}_2\,\rho\,d\rho\,. \tag{5.1.11a}$$

The value of A_2 is determined by using (5.1.10) and (5.1.9b) for $\mathcal{F}_2$ to obtain

$$A_2 = -\mu_0 m_+ \int_0^1 \left(A_1\frac{\rho^2}{2} + \bar{\psi}_1\right)\rho\,d\rho - \frac{1}{2}\mu_1 m_+ \psi_0 = \frac{A_1}{\psi_0}\left(\frac{A_1}{4} + \bar{\psi}_1 + \frac{\mu_1}{\mu_0}\psi_0\right)\,. \tag{5.1.11b}$$

The matching condition is that the near-field behaviour as $x \to x_0$ of the outer representation of the eigenfunction must agree asymptotically with the far-field behaviour of the inner eigenfunction as $|y| = \varepsilon^{-1}|x - x_0| \to \infty$, so that

$$\phi_0 + \nu\phi_1 + \nu^2\phi_2 + \cdots \sim \psi_0 + \nu\psi_1 + \nu^2\psi_2 + \cdots\,. \tag{5.1.12}$$

Upon using the far-field behaviour of ψ_1 and ψ_2, as given in (5.1.10) and (5.1.11) respectively, (5.1.12) becomes

$$\begin{aligned} \phi_0 + \nu\phi_1 + \nu^2\phi_2 + \cdots \sim \psi_0 + A_1 + \nu\left(A_1\log|x - x_0| + \frac{A_1}{2} + \bar{\psi}_1 + A_2\right) \\ + \nu^2\left(A_2\log|x - x_0| + \mathcal{O}(1)\right)\,. \end{aligned} \tag{5.1.13}$$

Matching at leading order gives the following condition on the constants ϕ_0 and ψ_0

$$\phi_0 = \psi_0 + A_1 \,. \tag{5.1.14}$$

The $\mathcal{O}(\nu)$ term in the matching condition (5.1.13), provides the singularity condition

$$\phi_1 \sim A_1 \log|x - x_0| + \frac{A_1}{2} + \bar{\psi}_1 + A_2 \,, \quad \text{as} \quad x \to x_0 \,. \tag{5.1.15}$$

which, together with (5.1.5a), completes the specification of ϕ_1.

Note that the singularity behaviour in (5.1.15) specifies both the regular and singular part of a Coulomb singularity. Consequently, this singularity structure provides one constraint relating A_1, A_2, and $\bar{\psi}_1$.

The problem for ϕ_1 can be written in terms of the Dirac distribution as

$$\Delta\phi_1 = \mu_0 m_b \phi_0 + 2\pi A_1 \delta(x - x_0) \,, \quad x \in \Omega \,; \qquad \partial_n \phi_1 = 0 \,, \quad x \in \partial\Omega \,. \tag{5.1.16}$$

An application of the divergence theorem then yields

$$A_1 = -\frac{1}{2\pi} \left(\mu_0 m_b |\Omega| \phi_0\right) \,. \tag{5.1.17}$$

Next, the solution to (5.1.16) is written in terms of the Neumann Green's function $G(x; x_0)$ as

$$\phi_1 = -2\pi A_1 G(x; x_0) = \mu_0 m_b |\Omega| \phi_0 G(x; x_0) \,. \tag{5.1.18}$$

Here $G(x; x_0)$ is the unique solution to

$$\Delta G = \frac{1}{|\Omega|} - \delta(x - x_0) \,, \quad x \in \Omega \,; \qquad \partial_n G = 0 \,, \quad x \in \partial\Omega \,; \qquad \int_\Omega G \, dx = 0 \,, \tag{5.1.19a}$$

$$G(x; x_0) \sim -\frac{1}{2\pi} \log|x - x_0| + R(x_0; x_0) \,, \quad \text{as} \quad x \to x_0 \,, \tag{5.1.19b}$$

where $R(x_0; x_0)$ is the regular part of $G(x; x_0)$ at $x = x_0$. By expanding ϕ_1 in (5.1.18) as $x \to x_0$ and equating the non-singular part of the resulting expression with that of (5.1.15), the following condition is obtained

$$-2\pi A_1 R(x_0; x_0) = \frac{A_1}{2} + \bar{\psi}_1 + A_2 \,. \tag{5.1.20}$$

From the $\mathcal{O}(\nu^2)$ terms in matching condition (5.1.13) the singularity behaviour $\phi_2 \sim A_2 \log|x - x_0|$ as $x \to x_0$ is obtained where ϕ_2 is the solution to (5.1.5b). In terms of

the Dirac mass, this problem for ϕ_2 can be written as

$$\Delta\phi_2 = \mu_1 m_b\phi_0 + \mu_0 m_b\phi_1 + 2\pi A_2\delta(x-x_0)\,, \quad x\in\Omega\,; \qquad \partial_n\phi_2 = 0\,, \quad x\in\partial\Omega\,, \tag{5.1.21}$$

with normalization condition $\int_\Omega \left(\phi_1^2 + 2\phi_0\phi_2\right)\,dx = 0$. The divergence theorem, together with $\int_\Omega \phi_1\,dx = 0$, then yields that

$$2\pi A_2 = -\mu_1 m_b|\Omega|\phi_0\,. \tag{5.1.22}$$

The leading-order eigenvalue correction μ_0 is obtained by combining (5.1.14) and (5.1.17), together with using $A_1 = -\mu_0 m_+\psi_0/2$ from (5.1.10b) to see that

$$\phi_0 = \frac{\pi m_+}{|\Omega|m_b}\psi_0\,, \qquad \phi_0 = \left(1 - \frac{\mu_0 m_+}{2}\right)\psi_0\,. \tag{5.1.23}$$

Now rearranging for μ_0,

$$\mu_0 = \frac{2}{m_+}\left[1 - \frac{\pi m_+}{|\Omega|m_b}\right]\,, \qquad \psi_0 = \frac{|\Omega|m_b}{\pi m_+}\phi_0\,, \qquad \phi_0 = |\Omega|^{-1/2}\,. \tag{5.1.24}$$

Since $\int_\Omega m\,dx < 0$, then $m_+\pi/(|\Omega|m_b) < 1$ from (5.1.2). Consequently, it follows from (5.1.24) that $\mu_0 > 0$. Combining (5.1.17) and (5.1.22) reveals that the ratio A_2/A_1 has value $A_2/A_1 = \mu_1/\mu_0$ which in turn allows $\bar\psi_1$ and the eigenvalue correction μ_1 to be determined from (5.1.20) and (5.1.11b)

$$\bar\psi_1 = -\frac{A_1}{4}\,, \qquad \mu_1 = -\left(\frac{1}{4} + 2\pi R(x_0;x_0)\right)\mu_0\,. \tag{5.1.25}$$

Finally, a two-term expansion for the eigenfunction in the outer region is obtained from (5.1.4) by using (5.1.18) for ϕ_1. The corresponding two-term inner approximation to the eigenfunction is given by (5.1.8), where ψ_1 is given in (5.1.10) with $\bar\psi_1 = -A_1/4$. In Summary,

Principal Result 5.1: *In the limit of small patch radius, $\varepsilon\to 0$, the positive principal eigenvalue λ of (5.1.1) has the following two-term asymptotic expansion in terms of the logarithmic gauge function $\nu = -1/\log\varepsilon$:*

$$\lambda = \mu_0\nu - \mu_0\nu^2\left[\frac{1}{4} + 2\pi R(x_0;x_0)\right] + \mathcal{O}(\nu^3)\,; \qquad \mu_0 \equiv \frac{2}{m_+}\left[1 - \frac{\pi m_+}{|\Omega|m_b}\right]\,. \tag{5.1.26a}$$

A two-term asymptotic expansion for the corresponding eigenfunction in the outer region $|x-x_0| \gg \mathcal{O}(\varepsilon)$ is

$$\phi \sim \phi_0\left(1 + \nu\mu_0 m_b|\Omega|G(x;x_0)\right)\,. \tag{5.1.26b}$$

Here $G(x;x_0)$ is the Neumann Green's function of (5.1.19) with regular part $R(x_0;x_0)$. The corresponding inner approximation to the eigenfunction, with $y=\varepsilon^{-1}(x-x_0)$ and $\rho=|y|=\mathcal{O}(1)$, is

$$\psi \sim \frac{m_b|\Omega|}{m_+\pi}\phi_0\left(1-\frac{\mu_0 m_+}{2}\nu\tilde{\psi}_1(\rho)\right), \tag{5.1.26c}$$

where $\phi_0=|\Omega|^{-1/2}$, and $\tilde{\psi}_1(\rho)$ is defined by

$$\tilde{\psi}_1(\rho)\equiv\begin{cases}\rho^2/2-1/4\,, & \rho\le 1\,,\\ \log\rho+1/4\,, & \rho\ge 1\,.\end{cases} \tag{5.1.26d}$$

The eigenvalue problem (5.1.1) is explicitly solvable only for the special case where Ω is the unit disk with a circular patch of radius ε centered at the origin. For this special case, the solution to (5.1.1), which is continuous across the patch boundary $r=\varepsilon$, is

$$\phi=\begin{cases} C\left[I_0\left(\sqrt{\lambda m_b}r\right)-\dfrac{I_0'\left(\sqrt{\lambda m_b}\right)}{K_0'\left(\sqrt{\lambda m_b}\right)}K_0\left(\sqrt{\lambda m_b}r\right)\right], & \varepsilon\le r\le 1,\\ C\left[I_0\left(\sqrt{\lambda m_b}\varepsilon\right)-\dfrac{I_0'\left(\sqrt{\lambda m_b}\right)}{K_0'\left(\sqrt{\lambda m_b}\right)}K_0\left(\sqrt{\lambda m_b}\varepsilon\right)\right]\dfrac{J_0\left(\sqrt{\lambda m_+}r/\varepsilon\right)}{J_0\left(\sqrt{\lambda m_+}\right)}, & 0\le r\le\varepsilon.\end{cases} \tag{5.1.27}$$

Here $I_0(z)$ and $K_0(z)$ are the modified Bessel functions of the first and second kind of order zero. By imposing that ϕ is smooth across $r=\varepsilon$, and recalling that $J_0'(z)=-J_1(z)$, $I_0'(z)=I_1(z)$ and $K_0'(z)=-K_1(z)$, the following transcendental equation for λ is obtained:

$$\varepsilon\sqrt{\frac{m_b}{m_+}}\frac{J_0\left(\sqrt{\lambda m_+}\right)}{J_1\left(\sqrt{\lambda m_+}\right)}=\frac{K_0\left(\sqrt{\lambda m_b}\varepsilon\right)I_1\left(\sqrt{\lambda m_b}\right)+K_1\left(\sqrt{\lambda m_b}\right)I_0\left(\sqrt{\lambda m_b}\varepsilon\right)}{K_1\left(\sqrt{\lambda m_b}\varepsilon\right)I_1\left(\sqrt{\lambda m_b}\right)-K_1\left(\sqrt{\lambda m_b}\right)I_1\left(\sqrt{\lambda m_b}\varepsilon\right)}\,. \tag{5.1.28}$$

The first positive root of (5.1.28) is the positive principle eigenvalue of (5.1.1). For $\varepsilon\to 0$, we expand this root as

$$\lambda=\mu_0\nu+\mu_1\nu^2+\cdots\,,\qquad \nu\equiv -1/\log\varepsilon\,. \tag{5.1.29a}$$

By using well-known asymptotic formulae for the Bessel and Modified Bessel functions of small argument, we substitute (5.1.29a) into (5.1.28), and equate coefficients in powers of ν to obtain that

$$\mu_0=\frac{2}{m_+}\left[1-\frac{m_+}{m_b}\right],\qquad \mu_1=\frac{\mu_0}{2}\,. \tag{5.1.29b}$$

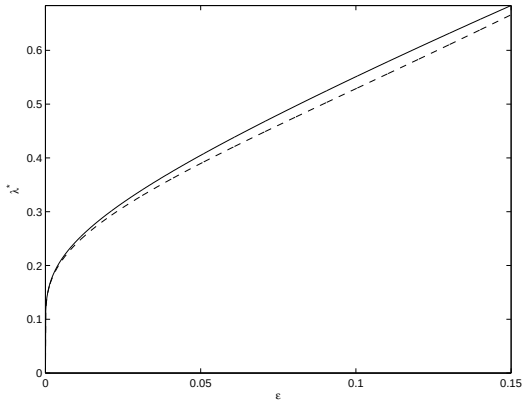

Figure 5.1: Plot of the two-term asymptotic expansion (dashed curve) (5.1.29) for λ versus ε when Ω is the unit disk with a concentric circular patch of radius ε centered at the origin. The solid curve is the eigenvalue λ as obtained from the exact transcendental relation (5.1.28). The parameter values are $m_b = 2$ and $m_+ = 1$.

For the special case where Ω is the unit disk containing a circular patch of radius ε, we need only substitute $|\Omega| = \pi$ and $R(0;0) = -3/(8\pi)$, obtained from Appendix B of [31], into (5.1.26a). The resulting two-term expansion for λ agrees with (5.1.29). In Fig. 5.1 a very favourable comparison is displayed between the two-term expansion (5.1.29) for λ and the corresponding exact result obtained by finding the first positive root of (5.1.28) numerically.

5.1.2 A Single Boundary Patch

Next, the case where the center x_0 of the circular patch is on the boundary of the domain $\partial\Omega$ where $\partial\Omega$ is piecewise differentiable, but may have corners with nonzero angle. The boundary patch $\Omega_{\varepsilon_0} \equiv \{x \,|\, |x - x_0| \le \varepsilon\rho_0 \cap \Omega\}$ with $x_0 \in \partial\Omega$ is the portion of a circular disk of radius $\varepsilon\rho_0$ that is strictly contained within Ω. In the limit $\varepsilon \to 0$, and for $x - x_0 = \mathcal{O}(\varepsilon)$, define $\pi\alpha_0$ to be the angular fraction of the circular patch that is contained within Ω. More specifically, $\alpha_0 = 1$ whenever x_0 is at a smooth point of $\partial\Omega$, and $\alpha_0 = 1/2$ when x_0 is at a $\pi/2$ corner of $\partial\Omega$. The eigenvalue problem associated with this boundary patch is

$$\Delta\phi + \lambda\, m_\varepsilon(x)\phi = 0\,, \quad x \in \Omega; \qquad \partial_n\phi = 0\,, \quad x \in \partial\Omega\,; \qquad \int_\Omega \phi^2\, dx = 1\,, \quad (5.1.30a)$$

where $m_\varepsilon(x)$ is defined as

$$m_\varepsilon(x) = \begin{cases} m_+/\varepsilon^2\,, & x \in \Omega_{\varepsilon_0}\,, \\ \\ -m_b\,, & x \in \Omega\backslash\Omega_{\varepsilon_0}\,. \end{cases} \tag{5.1.30b}$$

The condition $\int_\Omega m\,dx < 0$ is asymptotically equivalent when $\varepsilon \to 0$ to

$$\int_\Omega m\,dx = -m_b|\Omega| + \frac{\alpha_0\pi}{2}\left(m_+\rho_0^2\right) + \mathcal{O}(\varepsilon^2) < 0\,. \tag{5.1.31}$$

The parameters of the problem are assumed to be chosen such that this condition on $\int_\Omega m\,dx$ holds. Since the asymptotic calculation of λ for a boundary patch is similar to that for the interior patch case, we mainly highlight the new features that are required in the analysis.

First, λ is expanded in terms of $\nu = -1/\log\varepsilon$ as in (5.1.3). In the outer region, defined for $|x - x_0| \gg \mathcal{O}(\varepsilon)$, the expansion of the outer solution, as in (5.1.4), is used to obtain that ϕ_0 is a constant, and that ϕ_1 and ϕ_2 satisfy (5.1.5a) and (5.1.5b) in Ω, respectively, with $\partial_n\phi_k = 0$ for $x \in \partial\Omega\backslash\{x_0\}$ for $k = 1, 2$.

Since the expansion of the inner solution is again in powers of $\nu = -1/\log\varepsilon$ as in (5.1.8), the effect of the curvature of the domain boundary near $x = x_0$ can be neglected to any power of ν, provided that this curvature is finite. Consequently, when x_0 is at a smooth point of $\partial\Omega$, the inner region near $x = x_0$ can be approximated by the tangent line to $\partial\Omega$ through $x = x_0$. Alternatively, when x_0 is at corner point of $\partial\Omega$, the inner region is the angular wedge of angle $\pi\alpha_0$ bounded by the intersection of the one-sided tangent lines to $\partial\Omega$ at $x = x_0$. The local variable $y = \varepsilon^{-1}(x - x_0)$ is used so that the inner region is the angular wedge $\beta_0 < \arg y \le \alpha_0\pi + \beta_0$ for some β_0. The favourable habitat is the circular patch $|y| \le \rho_0$ that lies within this wedge. Since the no-flux boundary conditions $\partial_n\psi = 0$ holds on the two sides of the wedge, a local radially symmetric inner solution is established within the angular wedge.

Therefore, in the inner region, the solution is expanded as in (5.1.8) to obtain that ψ_0 is a constant, and that ψ_k for $k = 1, 2$ satisfies

$$\Delta\psi_k = \begin{cases} \mathcal{F}_k\,, & |y| \le \rho_0\,, \quad \beta_0 \le \arg y \le \pi\alpha_0 + \beta_0\,, \\ \\ 0\,, & |y| \ge \rho_0\,, \quad \beta_0 \le \arg y \le \pi\alpha_0 + \beta_0\,. \end{cases} \tag{5.1.32}$$

Here $\mathcal{F}_k$ for $k = 1, 2$ are defined in (5.1.9b). The solution for ψ_1, with $\rho = |y|$, is

$$\psi_1 = \begin{cases} A_1\left(\dfrac{\rho^2}{2\rho_0^2}\right) + \bar{\psi}_1\,, & 0 \le \rho \le \rho_0\,, \quad \beta_0 \le \arg y \le \pi\alpha_0 + \beta_0\,, \\ A_1 \log\left(\dfrac{\rho}{\rho_0}\right) + \dfrac{A_1}{2} + \bar{\psi}_1\,, & \rho \ge \rho_0\,, \quad \beta_0 \le \arg y \le \pi\alpha_0 + \beta_0\,, \end{cases} \tag{5.1.33}$$

where $\bar{\psi}_1$ is an unknown constant and $A_1 = \mathcal{F}_1\rho_0^2/2$. For ψ_2, we obtain that $\psi_2 \sim A_2 \log\rho$ as $\rho \to \infty$. The calculation of A_2 proceeds exactly as in (5.1.11b) to obtain that

$$A_1 = -\frac{\mu_0}{2} m_+ \rho_0^2 \psi_0\,, \qquad A_2 = \frac{A_1}{\psi_0}\left(\frac{A_1}{4} + \bar{\psi}_1 + \frac{\mu_1}{\mu_0}\psi_0\right). \tag{5.1.34}$$

The matching condition between the outer solution as $x \to x_0$ and the inner solution for $|y| = \varepsilon^{-1}|x - x_0| \to \infty$ is given by (5.1.12). Upon using (5.1.33) for ψ_1 when $\rho \gg 1$, together with $\psi_2 \sim A_2 \log\rho$ for $\rho \gg 1$, the condition

$$\begin{aligned} \phi_0 + \nu\phi_1 + \nu^2\phi_2 + \cdots \sim \psi_0 + A_1 + \nu\left(A_1 \log|x - x_0| - A_1 \log\rho_0 + \frac{A_1}{2} + \bar{\psi}_1 + A_2\right) \\ + \nu^2\left(A_2 \log|x - x_0| + \mathcal{O}(1)\right). \end{aligned} \tag{5.1.35}$$

is established. The leading order matching condition from (5.1.35) is that

$$\phi_0 = \psi_0 + A_1\,. \tag{5.1.36}$$

Appending the singularity condition established from the $\mathcal{O}(\nu)$ terms of (5.1.35) to problem (5.1.5a), gives the following complete specification of ϕ_1

$$\Delta\phi_1 = \mu_0 m_b \phi_0\,, \quad x \in \Omega\,; \qquad \partial_n\phi_1 = 0\,, \quad x \in \partial\Omega\backslash\{x_0\}\,; \qquad \int_\Omega \phi_1\,dx = 0\,, \tag{5.1.37a}$$

$$\phi_1 \sim A_1 \log|x - x_0| - A_1 \log\rho_0 + \frac{A_1}{2} + \bar{\psi}_1 + A_2\,, \quad \text{as} \quad x \to x_0\,. \tag{5.1.37b}$$

The singularity condition from the $\mathcal{O}(\nu^2)$ terms in (5.1.35) are appended to the problem for ϕ_2 (5.1.5b) to give

$$\Delta\phi_2 = \mu_1 m_b \phi_0 + \mu_0 m_b \phi_1\,, \quad x \in \Omega\,; \qquad \partial_n\phi_2 = 0\,, \quad x \in \partial\Omega\backslash\{x_0\}\,; \tag{5.1.38a}$$

$$\int_\Omega \left(\phi_1^2 + 2\phi_0\phi_2\right) dx = 0; \qquad \phi_2 \sim A_2 \log|x - x_0| + \mathcal{O}(1)\,, \quad \text{as} \quad x \to x_0\,. \tag{5.1.38b}$$

The divergence theorem is now applied to (5.1.37) over $\Omega\backslash\Omega_\sigma$, where Ω_σ is a wedge of angle $\pi\alpha_0$ and small radius $\sigma \ll 1$ centered at $x_0 \in \partial\Omega$. Imposing the singularity

condition (5.1.37b) on $|x - x_0| = \sigma$ and taking the limit $\sigma \to 0$, the relationship

$$\mu_0 m_b |\Omega| \phi_0 = -\alpha_0 \pi A_1 \,. \tag{5.1.39}$$

is established. In a similar way, applying the divergence theorem to (5.1.38), noting that $\int_\Omega \phi_1 \, dx = 0$, gives the following equality involving A_2

$$\mu_1 m_b |\Omega| \phi_0 = -\alpha_0 \pi A_2 \,. \tag{5.1.40}$$

Combining (5.1.39) and (5.1.40) gives that $A_2/A_1 = \mu_1/\mu_0$, which yields $\bar{\psi}_1 = -A_1/4$ from the equation for A_2 in (5.1.34). Then, by combining (5.1.36), (5.1.34) for A_1, and (5.1.39), the leading order correction terms

$$\psi_0 = \frac{2m_b|\Omega|}{\alpha_0 \pi m_+ \rho_0^2} \phi_0 \,, \qquad \mu_0 = \frac{2}{m_+ \rho_0^2} \left[1 - \frac{\alpha_0 \pi m_+ \rho_0^2}{2 m_b |\Omega|} \right] \,. \tag{5.1.41}$$

are established. Since $\int_\Omega m \, dx < 0$ from (5.1.31), it follows that $\mu_0 > 0$ in (5.1.41).

Equation (5.1.37) admits the compact representation

$$\phi_1 = -\alpha_0 \pi A_1 G_s(x; x_0) \,. \tag{5.1.42}$$

in terms of the surface Neumann Green's function $G_s(x; x_0)$, defined as the unique solution of

$$\Delta G_s = \frac{1}{|\Omega|} \,, \quad x \in \Omega \,; \qquad \partial_n G_s = 0 \,, \qquad x \in \partial\Omega \backslash \{x_0\} \,; \qquad \int_\Omega G_s \, dx = 0 \,, \tag{5.1.43a}$$

$$G_s(x; x_0) \sim -\frac{1}{\alpha_0 \pi} \log|x - x_0| + R_s(x_0; x_0) \,, \quad \text{as } \; x \to x_0 \in \partial\Omega \,. \tag{5.1.43b}$$

Here $|\Omega|$ is the area of Ω, and $R_s(x_0; x_0)$ is the regular part of the surface Neumann Green's function at $x = x_0$.

By expanding ϕ_1 as $x \to x_0$ using (5.1.43b), the $\log|x - x_0|$ term matches automatically whereas matching the nonsingular part of ϕ_1 as $x \to x_0$ gives the condition (5.1.37b) to obtain

$$-\alpha_0 \pi A_1 R_s(x_0; x_0) = -A_1 \log \rho_0 + \frac{A_1}{2} + \bar{\psi}_1 + A_2 \,. \tag{5.1.44}$$

Using $\bar{\psi}_1 = -A_1/4$ and $A_2/A_1 = \mu_1/\mu_0$ in (5.1.44), and solving for μ_1 gives

$$\mu_1 = \mu_0 \left[\log \rho_0 - \frac{1}{4} - \alpha_0 \pi R_s(x_0; x_0) \right] \,. \tag{5.1.45}$$

In summary:

Principal Result 5.2: *In the limit of small boundary patch radius, $\varepsilon \to 0$, a two-term asymptotic expansion for the positive principal eigenvalue λ of (5.1.30) in terms of $\nu = -1/\log\varepsilon$ is*

$$\lambda = \mu_0\nu - \mu_0\nu^2\left[\frac{1}{4} + \alpha_0\pi R_s(x_0;x_0) - \log\rho_0\right] + \mathcal{O}(\nu^3)\,; \qquad \mu_0 \equiv \frac{2}{m_+\rho_0^2}\left[1 - \frac{\alpha_0\pi m_+\rho_0^2}{2|\Omega|m_b}\right]. \tag{5.1.46a}$$

A two-term asymptotic expansion for the corresponding eigenfunction in the outer region $|x - x_0| \gg \mathcal{O}(\varepsilon)$ is

$$\phi \sim \phi_0\left(1 + \nu\mu_0 m_b|\Omega|G_s(x;x_0)\right). \tag{5.1.46b}$$

Here $G_s(x;x_0)$ is the surface Neumann Green's function of (5.1.43) with regular part $R_s(x_0;x_0)$.

The implication of Principal Results 5.1 and 5.2 for the determination of the persistence threshold is discussed in § 5.3.1.

5.2 The Persistence Threshold For Multiple Patches

In this section the analysis of § 5.1 is generalized to treat the case of an arbitrary but fixed number n of circular patches, each of which is centered either inside Ω or on $\partial\Omega$. To this end, the positive principal eigenvalue of

$$\Delta\phi + \lambda\, m_\varepsilon(x)\phi = 0\,, \quad x \in \Omega; \qquad \partial_n\phi = 0\,, \quad x \in \partial\Omega\,; \qquad \int_\Omega \phi^2\,dx = 1\,, \tag{5.2.1a}$$

is calculated asymptotically where the growth rate function $m_\varepsilon(x)$ is defined by

$$m_\varepsilon(x) = \begin{cases} m_j/\varepsilon^2\,, & x \in \Omega_{\varepsilon_j}\,, \quad j = 1,\ldots,n\,, \\ -m_b\,, & x \in \Omega\backslash\bigcup_{j=1}^n \Omega_{\varepsilon_j}\,. \end{cases} \tag{5.2.1b}$$

Here $\Omega_{\varepsilon_j} \equiv \{x\,|\,|x - x_j| \le \varepsilon\rho_j \cap \Omega\}$, so that the patches Ω_{ε_j} are the portions of the circular disks of radius $\varepsilon\rho_j$ that are strictly inside Ω. The constant m_j is the local growth rate of the j^{th} patch, with $m_j > 0$ for a favourable habitat and $m_j < 0$ for a non-favourable habitat. The constant $m_b > 0$ is the background bulk decay rate for the unfavourable habitat. In terms of this patch arrangement, the condition $\int_\Omega m\,dx < 0$ is

asymptotically equivalent for $\varepsilon \to 0$ to

$$\int_\Omega m\,dx = -m_b|\Omega| + \frac{\pi}{2}\sum_{j=1}^{n}\alpha_j m_j \rho_j^2 + \mathcal{O}(\varepsilon^2) < 0\,. \tag{5.2.2}$$

The parameters of the problem must always be chosen so that this condition holds. The patches are assumed to be well-separated in the sense mentioned in § 1.2. The parameters in the growth rate are the centers $x_1,\ldots,x_n$ of the circular patches, their radii $\varepsilon\rho_1,\ldots,\varepsilon\rho_n$, the local growth rates $m_1,\ldots,m_n$, the angular fractions $\pi\alpha_1,\ldots,\pi\alpha_n$ of the circular patches that are contained in Ω, and the constant bulk growth rate m_b. Recall that $\alpha_j = 2$ whenever $x_j \in \Omega$, $\alpha_j = 1$ when $x_j \in \partial\Omega$ and x_j is a point where $\partial\Omega$ is smooth, and $\alpha_j = 1/2$ when $x_j \in \partial\Omega$ is at a $\pi/2$ corner of $\partial\Omega$, etc.

To asymptotically analyze (5.2.1), both the Neumann Green's function and the surface Neumann Green's function are used. As such, the following definition for a generalized modified Green's function $G_m(x;x_j)$ is useful,

$$G_m(x;x_j) \equiv \begin{cases} G(x;x_j)\,, & x_j \in \Omega\,, \\ \\ G_s(x;x_j)\,, & x_j \in \partial\Omega\,. \end{cases} \tag{5.2.3a}$$

Here $G(x;x_j)$ is the Neumann Green's function of (5.1.19), and $G_s(x;x_j)$ is the surface Neumann Green's function of (5.1.43). Therefore, the local behaviour of $G_m(x;x_j)$ is

$$\begin{aligned} G_m(x;x_j) &\sim -\frac{1}{\alpha_j\pi}\log|x-x_j| + R_m(x_j;x_j)\,, \quad \text{as} \quad x \to x_j; \\ R_m(x_j;x_j) &\equiv \begin{cases} R(x_j;x_j)\,, & x_j \in \Omega\,, \\ \\ R_s(x_j;x_j)\,, & x_j \in \partial\Omega\,. \end{cases} \end{aligned} \tag{5.2.3b}$$

Here $R(x_j;x_j)$ and $R_s(x_j;x_j)$ are the regular part of the Neumann Green's function (5.1.19) and the surface Neumann Green's function (5.1.43), respectively.

To derive a two-term expansion for the positive principal eigenvalue of (5.2.1), λ is expanded as in (5.1.3), and ϕ as in (5.1.4). Upon substituting (5.1.3) and (5.1.4) into (5.2.1), $\phi_0 = |\Omega|^{-1/2}$ is observed to be a constant, and that ϕ_1 and ϕ_2 satisfy

$$\begin{gathered} \Delta\phi_1 = \mu_0 m_b\phi_0\,, \quad x \in \Omega\backslash\Omega^I\,; \qquad \partial_n\phi_1 = 0\,, \quad x \in \partial\Omega\backslash\Omega^B\,; \\ \int_\Omega \phi_1\,dx = 0\,, \end{gathered} \tag{5.2.4a}$$

$$\begin{gathered} \Delta\phi_2 = \mu_1 m_b\phi_0 + \mu_0 m_b\phi_1\,, \quad x \in \Omega\backslash\Omega^I\,; \qquad \partial_n\phi_2 = 0\,, \quad x \in \partial\Omega\backslash\Omega^B\,; \\ \int_\Omega \left(\phi_1^2 + 2\phi_0\phi_2\right)\,dx = 0\,. \end{gathered} \tag{5.2.4b}$$

In the inner region, near the j^{th} patch, local variables $y = \varepsilon^{-1}(x - x_j)$ and $\psi(y) = \phi(x_j + \varepsilon y)$ are introduced. In this region, ψ is expanded for $y = \mathcal{O}(1)$ with

$$\psi \sim \psi_{0j} + \nu\psi_{1j} + \nu^2\psi_{2j} + \cdots , \tag{5.2.5}$$

where ψ_{0j} is a constant to be determined. For an interior patch with $x_j \in \Omega^I$, ψ_{kj} for $k = 1, 2$ satisfy

$$\Delta\psi_{kj} = \begin{cases} \mathcal{F}_{kj} , & |y| \le \rho_j , \\ \\ 0 , & |y| \ge \rho_j , \end{cases} \tag{5.2.6}$$

where $\mathcal{F}_{1j} = -\mu_0 m_j \psi_{0j}$ and $\mathcal{F}_{2j} = -\mu_0 m_j \psi_{1j} - \mu_1 m_j \psi_{0j}$. The solution for ψ_{1j}, with $\rho = |y|$, is

$$\psi_{1j} = \begin{cases} A_{1j}\left(\dfrac{\rho^2}{2\rho_j^2}\right) + \bar{\psi}_{1j} , & 0 \le \rho \le \rho_j , \\ \\ A_{1j}\log\left(\dfrac{\rho}{\rho_j}\right) + \dfrac{A_{1j}}{2} + \bar{\psi}_{1j} , & \rho \ge \rho_j , \end{cases} \tag{5.2.7}$$

where $\bar{\psi}_{1j}$ is an unknown constant. In addition, $\psi_{2j} \sim A_{2j}\log\rho$ as $\rho \to \infty$. The divergence theorem is used to calculate A_{1j} and A_{2j} from (5.2.6) to obtain

$$A_{1j} = -\frac{\mu_0}{2} m_j \rho_j^2 \psi_{0j} , \qquad A_{2j} = \frac{A_{1j}}{\psi_{0j}}\left(\frac{A_{1j}}{4} + \bar{\psi}_{1j} + \frac{\mu_1}{\mu_0}\psi_{0j}\right) . \tag{5.2.8}$$

For a boundary patch, for which $x_j \in \Omega^B$, then (5.2.6) holds in the wedge $\beta_j < \arg(y) < \beta_j + \pi\alpha_j$, for some β_j and $0 < \alpha_j < 2$. For this boundary case, the constants A_{1j} and A_{2j} are also given by (5.2.8).

The matching condition between the outer solution as $x \to x_j$ and the inner solution as $|y| = \varepsilon^{-1}|x - x_j| \to \infty$ is

$$\begin{aligned} \phi_0 + \nu\phi_1 + \nu^2\phi_2 + \cdots \sim\ & \psi_{0j} + A_{1j} \\ & + \nu\left(A_{1j}\log|x - x_j| - A_{1j}\log\rho_j + \frac{A_{1j}}{2} + \bar{\psi}_{1j} + A_{2j}\right) \\ & + \nu^2\left(A_{2j}\log|x - x_j| + \mathcal{O}(1)\right) . \end{aligned} \tag{5.2.9}$$

The leading-order matching condition from (5.2.9) yields

$$\phi_0 = \psi_{0j} + A_{1j} , \quad j = 1, \ldots, n . \tag{5.2.10}$$

From the $\mathcal{O}(\nu)$ terms in (5.2.9), the following singularity behaviour is obtained for ϕ_1

as $x \to x_j$

$$\phi_1 \sim A_{1j} \log|x - x_j| - A_{1j} \log \rho_j + \frac{A_{1j}}{2} + \bar{\psi}_{1j} + A_{2j}\,, \quad \text{as} \quad x \to x_j\,. \tag{5.2.11}$$

In addition, from the $\mathcal{O}(\nu^2)$ terms in (5.2.9), we conclude that

$$\phi_2 \sim A_{2j} \log|x - x_j| + \mathcal{O}(1)\,, \quad \text{as} \quad x \to x_j\,. \tag{5.2.12}$$

Next, by using the divergence theorem on the solution ϕ_1 to (5.2.4a) with singular behaviour (5.2.11), the following equality is established

$$\mu_0 m_b |\Omega| \phi_0 = -\pi \sum_{j=1}^{n} \alpha_j A_{1j}\,. \tag{5.2.13}$$

Similarly, the divergence theorem applied to (5.2.4b) with singular behaviour (5.2.12), and noting $\int_\Omega \phi_1\, dx = 0$, yields

$$\mu_1 m_b |\Omega| \phi_0 = -\pi \sum_{j=1}^{n} \alpha_j A_{2j}\,. \tag{5.2.14}$$

Combining (5.2.10) and (5.2.8) allows the values of A_{1j} and ψ_{0j} to be isolated as

$$\psi_{0j} = \frac{2\phi_0}{2 - m_j \rho_j^2 \mu_0}\,, \qquad A_{1j} = -\frac{m_j \rho_j^2 \mu_0 \phi_0}{2 - m_j \rho_j^2 \mu_0}\,, \qquad j = 1, \ldots, n\,. \tag{5.2.15}$$

From (5.2.13), together with (5.2.15) for A_{1j}, the leading-order eigenvalue correction μ_0 is observed to satisfy the following algebriac equation

$$\frac{m_b |\Omega|}{\pi} = \sum_{j=1}^{n} \frac{\alpha_j m_j \rho_j^2}{2 - m_j \rho_j^2 \mu_0}\,. \tag{5.2.16}$$

The properties of this equation are studied below in § 5.3 and will be shown to provide a large amount of information on the optimal configuration of $m(x)$.

The value of the next correction, μ_1 is now determined in terms of the Neumann Green's Function $G(x; x_0)$ and its regular part $R(x; x_0)$, defined in (5.1.19). Firstly, the solution ϕ_1 to (5.2.4a), with singular behaviour (5.2.11), is written in terms of the modified Green's function $G_m(x; x_j)$ of (5.2.3) as

$$\phi_1 = -\pi \sum_{i=1}^{n} \alpha_i A_{1i} G_m(x; x_i)\,. \tag{5.2.17}$$

Then, by expanding ϕ_1 as $x \to x_j$ and by using (5.2.3b) for the local behaviour of $G_m(x;x_j)$, the condition

$$\phi_1 \sim A_{1j}\log|x-x_j| - \pi\alpha_j A_{1j}R_{mjj} + B_j, \quad x \to x_j\,; \qquad B_j \equiv -\pi\sum_{\substack{i=1\\ i\neq j}}^{n}\alpha_i A_{1i}G_{mji}\,, \tag{5.2.18}$$

is obtained where $G_{mji} \equiv G_m(x_j;x_i)$. The requirement that the nonsingular terms in (5.2.11) and (5.2.18) agree yields the constraints

$$-\pi\alpha_j A_{1j}R_{mjj} + B_j = -A_{1j}\log\rho_j + \frac{A_{1j}}{2} + \bar{\psi}_{1j} + A_{2j}\,, \qquad j = 1,\ldots,n\,, \tag{5.2.19}$$

where $R_{mjj} \equiv R_m(x_j;x_j)$ is the regular part of the generalized modified Green's function as defined in (5.2.3b).

Expressions (5.2.8), (5.2.15), and (5.2.19) can be combined to isolate A_{2j}, then μ_1 is determined from (5.2.14) after first solving (5.2.19) for $\bar{\psi}_{1j}$. Upon substituting the resulting expression for $\bar{\psi}_{1j}$, together with $A_{1j}/\psi_{0j} = -m_j\rho_j^2\mu_0/2$ from (5.2.8), into (5.2.8) for A_{2j}, the following is obtained for each $j = 1,\ldots,n$ that

$$A_{2j} = -\frac{m_j\rho_j^2\mu_0}{2}\left(-\frac{A_{1j}}{4} - \pi\alpha_j A_{1j}R_{mjj} + B_j + A_{1j}\log\rho_j - A_{2j}\right) + \frac{\mu_1}{\mu_0}A_{1j}\,. \tag{5.2.20}$$

Upon solving this equation for A_{2j}, and using (5.2.18) for B_j, the product $\alpha_j A_{2j}$ is found to be

$$\begin{aligned}\alpha_j A_{2j} = -\frac{m_j\rho_j^2\mu_0}{\left(2-m_j\rho_j^2\mu_0\right)}\Big[&-\pi\alpha_j^2 A_{1j}R_{mjj} + \alpha_j A_{1j}\log\rho_j \\ &-\frac{\alpha_j A_{1j}}{4} - \pi\sum_{\substack{i=1\\ i\neq j}}^{n}\alpha_i\alpha_j A_{1i}G_{mji}\Big] + \frac{\mu_1}{\mu_0}\left(\frac{2A_{1j}\alpha_j}{2-m_j\rho_j^2\mu_0}\right).\end{aligned} \tag{5.2.21}$$

Next, it is convenient to introduce a new variable κ_j and to rewrite A_{1j} of (5.2.15) in terms of this variable as

$$\kappa_j \equiv \frac{\sqrt{\alpha_j}m_j\rho_j^2}{2-m_j\rho_j^2\mu_0}\,, \qquad A_{1j} = -\frac{\mu_0\kappa_j}{\sqrt{\alpha_j}}\phi_0\,, \qquad j = 1,\ldots,n\,. \tag{5.2.22}$$

It is also convenient to introduce the symmetric $n \times n$ Green's matrix $\mathcal{G}_m$, and the

diagonal matrix $\mathcal{P}$, with matrix entries $\mathcal{G}_{mij}$ and $\mathcal{P}_{ij}$ defined by

$$\begin{aligned} \mathcal{G}_{mij} &= \sqrt{\alpha_i \alpha_j} G_{mij}\,, \quad i \neq j\,; \qquad \mathcal{G}_{mjj} = \alpha_j R_{mjj}\,; \\ \mathcal{P}_{ij} &= 0\,, \quad i \neq j\,; \qquad \mathcal{P}_{jj} = \log \rho_j\,. \end{aligned} \tag{5.2.23}$$

In terms of κ_j, $\mathcal{G}_m$, $\mathcal{P}$, and the vector $\kappa = (\kappa_1, \ldots, \kappa_n)^t$, (5.2.21) readily reduces to

$$\alpha_j A_{2j} = -\mu_0^2 \phi_0 \kappa_j \left[\pi \left(\mathcal{G}_m \kappa \right)_j - \left(\mathcal{P} \kappa \right)_j + \frac{\kappa_j}{4} \right] - \frac{2\mu_1 \kappa_j^2}{m_j \rho_j^2} \phi_0\,, \tag{5.2.24}$$

where $\left(\mathcal{P}\kappa\right)_j$ and $\left(\mathcal{G}_m\kappa\right)_j$ denote the j^{th} component of the vectors $\mathcal{P}\kappa$ and $\mathcal{G}_m\kappa$, respectively.

Finally, by substituting (5.2.24) into (5.2.14), and solving the following expression for μ_1 is obtained

$$\mu_1 \left[\frac{m_b |\Omega|}{\pi} - \sum_{j=1}^{n} \frac{2\kappa_j^2}{m_j \rho_j^2} \right] = \mu_0^2 \left[\kappa^t \left(\pi \mathcal{G}_m - \mathcal{P} \right) \kappa + \frac{1}{4} \kappa^t \kappa \right]\,. \tag{5.2.25}$$

The left-hand side of (5.2.25) is simplified by using the equation (5.2.16) for μ_0 to obtain

$$\begin{aligned} \frac{m_b |\Omega|}{\pi} - \sum_{j=1}^{n} \frac{2\kappa_j^2}{m_j \rho_j^2} &= \sum_{j=1}^{n} \frac{\alpha_j}{\left(2 - m_j \rho_j^2 \mu_0\right)} \left[m_j \rho_j^2 - \frac{2 m_j \rho_j^2}{\left(2 - m_j \rho_j^2 \mu_0\right)} \right]\,, \\ &= -\sum_{j=1}^{n} \frac{\alpha_j}{\left(2 - m_j \rho_j^2 \mu_0\right)} \left[\frac{\mu_0 m_j^2 \rho_j^4}{\left(2 - m_j \rho_j^2 \mu_0\right)} \right] = -\mu_0 \kappa^t \kappa\,. \end{aligned} \tag{5.2.26}$$

This determines μ_1 from (5.2.25) in terms of a Rayleigh-type quotient. In summary:

Principal Result 5.3: *In the limit of small patch radius, $\varepsilon \to 0$, the positive principal eigenvalue λ of (5.2.1) has the following two-term asymptotic expansion in terms of the logarithmic gauge function $\nu = -1/\log \varepsilon$:*

$$\lambda = \mu_0 \nu - \mu_0 \nu^2 \left(\frac{\kappa^t \left(\pi \mathcal{G}_m - \mathcal{P} \right) \kappa}{\kappa^t \kappa} + \frac{1}{4} \right) + \mathcal{O}(\nu^3)\,. \tag{5.2.27}$$

Here $\mu_0 > 0$ is the first positive root of $\mathcal{B}(\mu_0) = 0$, where $\mathcal{B}(\mu)$ is defined by

$$\mathcal{B}(\mu) \equiv -m_b |\Omega| + \pi \sum_{j=1}^{n} \frac{\alpha_j m_j \rho_j^2}{2 - m_j \rho_j^2 \mu}\,. \tag{5.2.28}$$

In (5.2.27), $\kappa = (\kappa_1, \ldots, \kappa_n)^t$, where κ_j is defined in (5.2.22), while $\mathcal{G}_m$ and $\mathcal{P}$ are the

$n \times n$ matrices as defined in (5.2.23). In addition, a two-term expansion for the outer solution is given by

$$\phi \sim \phi_0 \left(1 + \nu\pi\mu_0 \sum_{j=1}^{n} \sqrt{\alpha_j}\kappa_j G_m(x; x_j) \right) . \tag{5.2.29}$$

Next, equation (5.2.28) is shown to admit a positive root $\mu_0 > 0$. Since $\int_\Omega m\, dx < 0$ from (5.2.2), it follows that $\mathcal{B}(0) < 0$ from (5.2.28). In addition, $\mathcal{B}(\mu) \to +\infty$ as $\mu \to 2/(m_J\rho_J^2)$ from below, where $m_J\rho_J^2$ is defined by

$$m_J\rho_J^2 = \max_{m_j>0}\{ m_j\rho_j^2 \,|\, j = 1, \ldots, n \} . \tag{5.2.30}$$

There must be at least one j for which $m_j > 0$, so that (5.2.30) is attained at some $j = J$. Moreover, (5.2.28) readily yields that $\mathcal{B}'(\mu) > 0$ on $0 < \mu < 2/(m_J\rho_J^2)$. Therefore, there exists a unique root $\mu = \mu_0$ on $0 < \mu < 2/(m_J\rho_J^2)$ satisfying $\mathcal{B}(\mu_0) = 0$. The corresponding leading-order eigenfunction in the inner region, ψ_{0j}, satisfies $\psi_{0j} > 0$ from (5.2.15). Therefore, μ_0 is the leading-order term in the asymptotic expansion of the positive principal eigenvalue of (5.2.1).

Although the required root to (5.2.28) must in general be computed numerically, there are two special cases where it can be found analytically. In the symmetric case where $m_j = m_c$ and $\rho_j = \rho_c$ for $j = 1, \ldots, n$, then, the root of (5.2.28) is simply

$$\mu_0 = \frac{2}{m_c\rho_c^2}\left[1 - \frac{\pi\alpha_s m_c\rho_c^2}{2m_b|\Omega|} \right] , \qquad \alpha_s \equiv \sum_{j=1}^{n} \alpha_j . \tag{5.2.31}$$

In addition, if there are only two types of patches, such as $m_j\rho_j^2 = m_c\rho_c^2$ for $j = 1, \ldots, n-1$ and $m_n\rho_n^2$, then (5.2.28) reduces to a quadratic equation for μ_0, which can be solved explicitly.

Note that the asymptotic analysis leading to Principal Result 5.3 has two limitations. Firstly, it is valid only when all interior or boundary patches are well-separated in the sense that $|x_i - x_j| \gg \mathcal{O}(\varepsilon)$ for $i \neq j$. Secondly, all interior patches required to be not too close to the boundary, in the sense that $|x - x_j| \gg \mathcal{O}(\varepsilon)$ for $x_j \in \Omega^I$ and $x \in \partial\Omega$. The easement of either of these two restrictions leads to more complicated inner patch problems that do not appear to be tractable analytically.

5.3 The Effect Of Habitat Fragmentation And Location On Species Persistence

In this section, the formulae derived in § 5.1 and § 5.2 for the persistence threshold, $\lambda(\varepsilon)$, are used to determine the optimal strategy for distributing a fixed quantity of resources in some domain where favourable and unfavourable patches may already be present. The constraint that the resources being distributed are fixed is expressed mathematically by

$$-m_b|\Omega| + \frac{\pi}{2}\sum_{j=1}^{n}\alpha_j m_j \rho_j^2 + \mathcal{O}(\varepsilon^2) = \int_\Omega m\,dx = -K\,, \tag{5.3.1}$$

where $K > 0$ is kept constant as m_b, or α_j, m_j, and ρ_j, for $j = 1, \ldots, n$ are varied.

5.3.1 The Persistence Threshold for One Patch

Consider first the case of one favourable habitat. For an interior patch of area $\pi\varepsilon^2$, recall that λ is given in (5.1.26a) of Principal Result 5.1. For a boundary patch of the same area, we must set $\pi\alpha_0\varepsilon^2\rho_0^2/2 = \pi\varepsilon^2$ in (5.1.46a) of Principal Result 5.2. Thus, $\rho_0 = \sqrt{2/\alpha_0}$, so that (5.1.46a) becomes

$$\begin{gathered}\lambda = \mu_0\nu - \mu_0\nu^2\left[\frac{1}{4} + \alpha_0\pi R_s(x_0;x_0) - \frac{1}{2}\log\left(\frac{2}{\alpha_0}\right)\right] + \mathcal{O}(\nu^3)\,;\\ \mu_0 \equiv \frac{\alpha_0}{m_+}\left[1 - \frac{\pi m_+}{|\Omega| m_b}\right]\,.\end{gathered} \tag{5.3.2}$$

By comparing the leading-order $\mathcal{O}(\nu)$ terms in (5.3.2) and (5.1.26a), and noting that $\alpha_0 < 2$ for a boundary patch, the following result is established:

Principal Result 5.4: *For a favourable habitat of area $\pi\varepsilon^2$, the positive principal eigenvalue λ is always smaller for a boundary patch than for an interior patch. For a domain boundary with corners, λ is minimized when the boundary patch is centered at the corner with the smallest corner angle $\pi\alpha_0$. For a domain with smooth boundary, for which $\alpha_0 = 1$ for any $x_0 \in \partial\Omega$, then λ in (5.3.2) is minimized when the center x_0 of the boundary patch is located at the global maximum of the regular part $R_s(x_0;x_0)$ of the surface Neumann Green's function of (5.1.43) on $\partial\Omega$.*

Principal Result 5.4 shows that for a square, the best choice for the favourable habitat is to concentrate resources near one of the four corners of the square. However, for a domain Ω with a smooth boundary $\partial\Omega$, it is not clear whether the maximization of $R_s(x_0;x_0)$, as required to minimize λ, has an obvious geometrical interpretation. When Ω is a smooth perturbation of the unit disk, the question of whether the global maximum

of $R_s(x_0;x_0)$ must necessarily coincide with the global maximum of the curvature of the boundary is addressed. The following result of [62] allows the determination of the critical points of $R_s(x_0;x_0)$ for domains that are smooth perturbations of the unit disk:
Principal Result 5.5: [From [62]]: *Let Ω be a smooth perturbation of the unit disk with boundary given in terms of polar coordinates by*

$$r = r(\theta) = 1 + \delta\sigma(\theta)\,, \qquad \sigma(\theta) = \sum_{n=1}^{\infty} \left(a_n \cos(n\theta) + b_n \sin(n\theta)\right)\,, \qquad \delta \ll 1\,. \quad (5.3.3)$$

Let $x_0 = x_0(\theta_0) = (r_0\cos\theta_0, r_0\sin\theta_0)$ be a point on the boundary where $r_0 = 1+\delta\sigma(\theta_0)$. For $x \in \partial\Omega$ we define

$$\rho(\theta) \equiv R_s(x;x_0) \qquad \text{and} \qquad \rho(\theta_0) \equiv R_s(x_0;x_0)\,, \quad (5.3.4)$$

where $R_s(x;x_0)$ is the regular part of the Green's function defined by

$$R_s(x;x_0) = G_s(x;x_0) + \frac{1}{\pi}\log|x-x_0|\,, \quad x \in \Omega\,. \quad (5.3.5)$$

Then, for $\delta \ll 1$, $\rho'(\theta_0)$ satisfies

$$\rho'(\theta_0) = \frac{\delta}{\pi}\sum_{n=1}^{\infty}\left(n^2+n-2\right)\left(b_n\cos n\theta_0 - a_n \sin n\theta_0\right) + \mathcal{O}(\delta^2)\,. \quad (5.3.6)$$

The proof of this result was given in [62].

The following two examples use Principal Result 5.5 to investigate the relationship between the curvature of the boundary and the critical points of the regular part of the surface Green's function $R_s(x;x_0)$.

For the first example, take the domain boundary to be $r = 1+\delta\,\sin(2\theta)$, so that $\rho'(\theta_0) = 4\delta\pi^{-1}\cos(2\theta_0)$ from (5.3.6). For $\delta \ll 1$, the curvature of the domain boundary is calculated to be

$$\kappa(\theta) = \frac{r^2 + 2r_\theta^2 - r r_{\theta\theta}}{\left(r^2+r_\theta^2\right)^{3/2}} \sim 1 - \delta\left(\sigma + \sigma_{\theta\theta}\right) + \mathcal{O}(\delta^2)\,. \quad (5.3.7)$$

so that for the case $r = 1+\delta\,\sin(2\theta)$,

$$\rho(\theta) = \frac{2\delta}{\pi}\sin(2\theta) + C\,, \qquad \kappa(\theta) = 1 + 3\delta\sin(2\theta)\,, \quad (5.3.8)$$

where C is some constant. For this example the global maxima of ρ and κ over $0 \le \theta < 2\pi$ do coincide, and are attained at $\theta = \pi/4$ and $\theta = 5\pi/4$.

The following examples uses Principal Result 5.5 to establish the following result:

Principal Result 5.6: *The global maximum of $R_s(x_0, x_0)$ for $x_0 \in \partial\Omega$ does not necessarily coincide with the global maximum of the curvature $\kappa(\theta)$ of the boundary of a smooth perturbation of the unit disk. Consequently, for $\varepsilon \to 0$, the persistence threshold $\lambda(\varepsilon)$ from Principal Result 5.2 is not necessarily minimized when the center of the circular patch is located at the global maximum of the curvature of the smooth boundary $\partial\Omega$.*

To prove this result, a counterexample is constructed. Take $a_2 = 1$, $b_3 = b$, with $a_n = 0$ for $n \neq 2$ and $b_n = 0$ for $n \neq 3$ in (5.3.3), so that

$$\sigma(\theta) = \cos(2\theta) + b\sin(3\theta)\,. \tag{5.3.9}$$

For $\delta \ll 1$, the curvature κ of $\partial\Omega$ is calculated from (5.3.7) to be

$$\begin{gathered}\kappa = 1 + \delta\left[3\cos(2\theta) + 8b\sin(3\theta)\right]\,, \qquad \kappa'(\theta) = -6\delta\left[\sin(2\theta) - 4b\cos(3\theta)\right]\,, \\ \kappa''(\theta) = -12\delta\left[\cos(2\theta) + 6b\sin(3\theta)\right]\,.\end{gathered} \tag{5.3.10}$$

From (5.3.6) $\rho'(\theta)$ and its derivative are calculated to be

$$\rho'(\theta) = -\frac{4\delta}{\pi}\left[\sin(2\theta) - \frac{5b}{2}\cos(3\theta)\right]\,, \qquad \rho''(\theta) = -\frac{8\delta}{\pi}\left[\cos(2\theta) + \frac{15b}{4}\sin(3\theta)\right]\,.$$

Therefore, in terms of an unknown constant C, we obtain that

$$\rho(\theta) = \frac{\delta}{\pi}\left[2\cos(2\theta) + \frac{10b}{3}\sin(3\theta)\right] + C\,. \tag{5.3.11}$$

We observe that $\theta = \pi/2$ and $\theta = 3\pi/2$ are the only two critical points shared by κ and ρ. The nature of these local extrema depend on the values of

$$\begin{aligned}\kappa''(\pi/2) &= 12\delta(1+6b)\,, \quad \rho''(\pi/2) = \frac{8\delta}{\pi}\left(1 + \frac{15b}{4}\right)\,, \\ \kappa''(3\pi/2) &= 12\delta(1-6b)\,, \quad \rho''(3\pi/2) = \frac{8\delta}{\pi}\left(1 - \frac{15b}{4}\right)\,.\end{aligned}$$

Therefore, when b is chosen to satisfy $-4/15 < b < -1/6$, then κ has a local maximum while ρ has a local minimum at $\theta = \pi/2$. Similarly, for this range of b, κ has a local minimum while ρ has a local minimum at $\theta = 3\pi/2$.

Since the only critical points shared by κ and ρ are local minima of ρ, it is concluded that the absolute maximum value of ρ occurs at a point where $\kappa'(\theta) \neq 0$. Therefore, in general, the point(s) where the absolute maximum value of ρ is attained do not coincide precisely with the maximum curvature of the boundary of the domain. Fig. 5.2(a)

shows a plot of the domain boundary when $\delta = 0.1$ and $b = -1/5$ while Fig. 5.2(b) plots $\rho(\theta) - C$ and $\kappa(\theta) - 1$ from (5.3.11) and (5.3.10), respectively, for $\delta = 0.1$ and $b = -1/5$ and demonstrates that the global maxima of ρ and $\kappa - 1$ occur at different, but nearby, locations.

In §3.3 of [62] a boundary element method (BEM) was formulated and implemented to numerically compute the regular part of the surface Neumann Green's function for an arbitrary bounded two-dimensional domain with smooth boundary. In Fig. 5.3 a very favourable comparison between full numerical results for $\rho(\theta)$ and the perturbation formula (5.3.11) is demonstrated for $\delta = 0.1$ and $b = -1/5$. The constant C in (5.3.11) was fitted to the full numerical results at $\theta = 0$. This figure provides a numerical validation of the perturbation result (5.3.11).

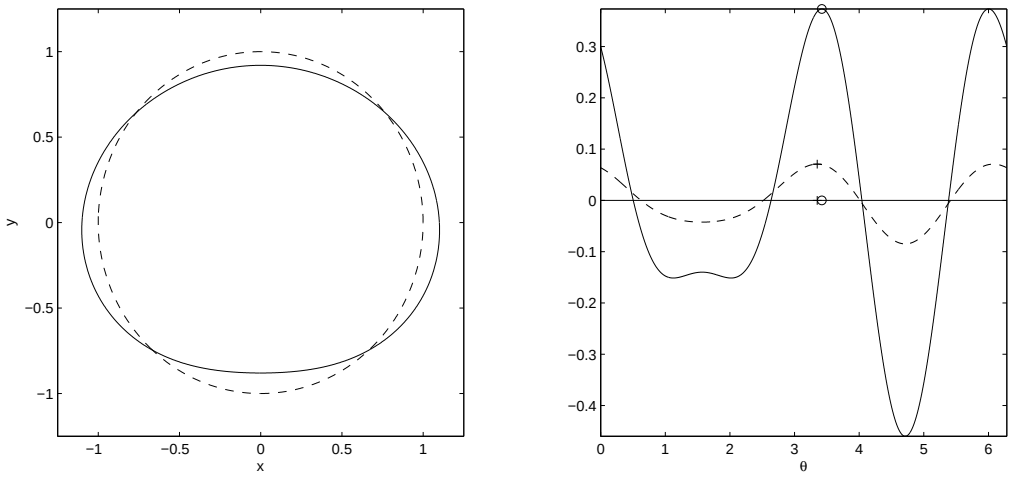

(a) perturbation of the unit disk

(b) $\kappa(\theta) - 1$ and $\rho(\theta)$ versus θ

Figure 5.2: Left figure: plot of the unit disk (dashed curve) and the perturbed unit disk (solid curve) with boundary $r = 1 + \delta\,(\cos(2\theta) + b\sin(3\theta))$, where $\delta = 0.1$ and $b = -1/5$. Right figure: plot of the curvature perturbation $\kappa(\theta) - 1$ (solid curve) and the regular part $\rho(\theta)$ of the surface Neumann Green's function defined in (5.3.11) (dashed curve) with $C = 0$. The absolute maximum of $\kappa - 1$ and ρ are observed to occur at distinct, but nearby points, as indicated in the figure.

It is conjectured that the relationship between the maximum of the boundary curvature and the location of the favourable habit that yields the minimum value of λ for a fixed $\int_\Omega m\,dx < 0$ is qualitatively similar to that for steady-state bubble-type transition-layer solutions for the Cahn-Hilliard model studied in [50]. In this latter context, it was shown from variational considerations in [50] that the minimal-energy bubble solution attaches orthogonally to the domain boundary at two points, with the global maximum

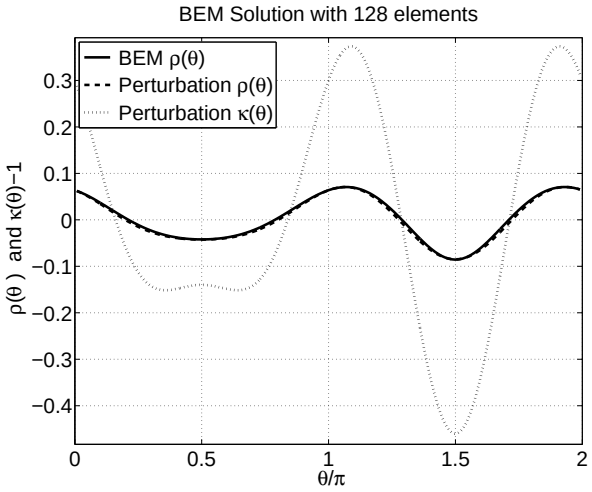

Figure 5.3: Plot of $\rho(\theta) \equiv R(x_0(\theta), x_0(\theta))$ computed by the BEM method (heavy solid curve) and the perturbation formula (5.3.11) (dashed curve) versus θ/π for a domain with boundary $r = 1 + \delta\,[\cos(2\theta) + b\sin(3\theta)]$ with $\delta = 0.1$ and $b = -1/5$. The curvature perturbation $\kappa(\theta) - 1$ is given by the dotted curve. Plot reproduced from [72].

of the boundary curvature located somewhere between these two points. The transition layer associated with this bubble solution is the arc of a circle connecting these two attached boundary points. Similarly, for our boundary patch problem, we expect that for ε small but fixed, the maximum boundary curvature is located somewhere along the curved boundary segment that connects the points where the circular patch intersects the boundary, but is not necessarily at the midpoint of this segment.

5.3.2 Multiple Patches And The Effect Of Fragmentation

In this section the effect of both the location and the fragmentation of resources on the leading-order term, μ_0, in the asymptotic expansion of λ is considered under the assumption of a fixed value for the constraint in (5.3.1). The analysis below leads to three specific qualitative results. The following simple lemma is central to the derivation of these results:

Lemma 5.7: *Consider two smooth functions $C_{old}(\zeta)$ and $C_{new}(\zeta)$ defined on $0 \le \zeta < \mu_m^{old}$ and $0 \le \zeta < \mu_m^{new}$, respectively, with $C_{old}(0) = C_{new}(0) < 0$, and $C_{old}(\zeta) \to +\infty$ as $\zeta \to \mu_m^{old}$ from below, and $C_{new}(\zeta) \to +\infty$ as $\zeta \to \mu_m^{new}$ from below. Suppose further that there exist unique roots $\zeta = \mu_0^{old}$ and $\zeta = \mu_0^{new}$ to $C_{old}(\zeta) = 0$ and $C_{new}(\zeta) = 0$ on the intervals $0 < \zeta < \mu_m^{old}$ and $0 < \zeta < \mu_m^{new}$, respectively. Then,*

- *Case I:* *If $\mu_m^{new} \le \mu_m^{old}$ and $C_{new}(\zeta) > C_{old}(\zeta)$ on $0 < \zeta < \mu_m^{new}$, then*

$\mu_0^{new} < \mu_0^{old}$.

- *Case II:* *If* $\mu_m^{new} \geq \mu_m^{old}$ *and* $C_{new}(\zeta) < C_{old}(\zeta)$ *on* $0 < \zeta < \mu_m^{old}$, *then* $\mu_0^{new} > \mu_0^{old}$.

The proof of this lemma is a routine exercise in calculus and is omitted. This simple lemma is used to obtain three main qualitative results.

First, suppose that the center of the j^{th} patch of radius $\varepsilon\rho_j$ with associated angle $\pi\alpha_j$ is moved to an unoccupied location, with the new patch having radius $\varepsilon\rho_k$ and associated angle $\pi\alpha_k$. To satisfy the constraint (5.3.1), the equality $\alpha_j m_j \rho_j^2 = \alpha_k m_k \rho_k^2$ must hold. The change in $\mathcal{B}(\zeta)$, with $\mathcal{B}(\zeta)$ as defined in (5.2.28), induced by this action is

$$\begin{aligned} \mathcal{B}_{\text{new}}(\zeta) - \mathcal{B}_{\text{old}}(\zeta) &= \frac{\pi\alpha_k m_k \rho_k^2}{2 - \zeta m_k \rho_k^2} - \frac{\pi\alpha_j m_j \rho_j^2}{2 - \zeta m_j \rho_j^2} \\ &= \pi \left(\frac{\alpha_j}{\alpha_k}\right) \frac{m_j^2 \rho_j^4 \zeta}{(2 - \zeta m_j \rho_j^2)(2 - \zeta m_k \rho_k^2)} \left(\alpha_j - \alpha_k\right) . \end{aligned} \tag{5.3.12}$$

Recall from § 5.2 that $\mathcal{B}_{\text{old}}(\zeta) = 0$ has a positive root $\zeta = \mu_0^{\text{old}}$ on $0 < \zeta < \mu_{\text{m}}^{\text{old}} \equiv 2/(m_J \rho_J^2)$, where $m_J \rho_J^2$ was defined in (5.2.30).

Assume that $\alpha_j > \alpha_k$, *e.g.* that the center of an interior patch, for which $\alpha_j = 2$, is moved to a smooth point on the domain boundary, for which $\alpha_k = 1$. First, suppose that the patches are favourable so that $m_j > 0$ and $m_k > 0$. When $\alpha_j > \alpha_k$, it follows from the constraint $\alpha_j m_j \rho_j^2 = \alpha_k m_k \rho_k^2$ that $m_k \rho_k^2 > m_j \rho_j^2$, and so the first vertical asymptote for $\mathcal{B}_{\text{new}}(\zeta)$ cannot be larger than that of $\mathcal{B}_{\text{old}}(\zeta)$. Consequently, we define $m_K \rho_K^2 \equiv \max\{m_J \rho_J^2, m_k \rho_k^2\}$, and from § 5.2 conclude that there is a unique root $\zeta = \mu_0^{\text{new}}$ to $\mathcal{B}_{\text{new}}(\zeta) = 0$ on $0 < \zeta < \mu_{\text{m}}^{\text{new}} \equiv 2/(m_K \rho_K^2)$. Since $\mu_{\text{m}}^{\text{new}} \leq \mu_{\text{m}}^{\text{old}}$, and (5.3.12) shows that $\mathcal{B}_{\text{new}}(\zeta) > \mathcal{B}_{\text{old}}(\zeta)$ for $0 < \zeta < \mu_{\text{m}}^{\text{new}}$, then Case I of Lemma 5.7 proves that $\mu_0^{\text{new}} < \mu_0^{\text{old}}$. Alternatively, for the situation where habitats are unfavourable, so that $m_j < 0$ and $m_k < 0$, then the first vertical asymptotes of $\mathcal{B}_{\text{old}}(\zeta)$ and $\mathcal{B}_{\text{new}}(\zeta)$ must be the same, since these asymptotes are defined only in terms of the favourable patches. For this case, (5.3.12) again shows that $\mathcal{B}_{\text{new}}(\zeta) > \mathcal{B}_{\text{old}}(\zeta)$ for $0 < \zeta < 2/(m_J \rho_J^2)$. Case I of Lemma 5.7 then establishes that $\mu_0^{\text{new}} < \mu_0^{\text{old}}$.

Therefore, it is concluded that moving the center of an interior patch to a point on the domain boundary will decrease the leading-order term μ_0 in the asymptotic expansion of the principal eigenvalue λ in (5.2.27) of Principal Result 5.3. Moreover, for a convex domain with piecewise smooth boundary, Qualitative Result I together with Principal Result 5.4 shows that μ_0 will be reduced the most by the movement of an interior patch to a non-smooth boundary point with the smallest corner contact angle.

Since this patch was chosen arbitrarily, it is clear that μ_0 is minimized by the placement of all interior patches to the boundary of the domain. This feature is encapsulated in the following qualitative result:

Qualitative Result I: *The movement of either a single favourable or unfavourable habitat to the boundary of the domain is advantageous for the persistence of the species.*

Next, the effect of fragmentation on species persistence is considered. More specifically, the effect of splitting the i^{th} patch, of radius $\varepsilon\rho_i$ and growth rate m_i, into two distinct patches, one with radius $\varepsilon\rho_j$ and growth rate m_j, and the other with radius $\varepsilon\rho_k$ and growth rate m_k. The condition $m_i\rho_i^2 = m_j\rho_j^2 + m_k\rho_k^2$ is imposed to satisfy the constraint (5.3.1). To isolate the role of fragmentation, the assumption $\alpha_i = \alpha_j = \alpha_k$ is made so that either an interior patch is split into two interior patches, or a boundary patch into two boundary patches, with each boundary patch centered at either a smooth point of $\partial\Omega$ or at a corner point of $\partial\Omega$ with the same contact angle. This action leads to the following qualitative result:

Qualitative Result II: *The fragmentation of one favourable interior habitat into two separate favourable interior habitats is not advantageous for species persistence. Similarly, the fragmentation of a favourable boundary habitat into two favourable boundary habitats with each either centered at either a smooth point of $\partial\Omega$, or at a corner point of $\partial\Omega$ with the same contact angle, is not advantageous. Finally, the fragmentation of an unfavourable habitat into two separate unfavourable habitats increases the persistence threshold λ.*

First, consider the case where one favourable habitat is broken into two smaller favourable habitats. Then, $m_i > 0$, $m_j > 0$, and $m_k > 0$. For the original patch distribution, it follows from § 5.2 that $\mathcal{B}_{\rm old}(\zeta) = 0$ has a positive root $\zeta = \mu_0^{\rm old}$ on $0 < \zeta < \mu_{\rm m}^{\rm old} \equiv 2/(m_J\rho_J^2)$, where $m_J\rho_J^2$ was defined in (5.2.30). Clearly the first vertical asymptote for $\mathcal{B}_{\rm new}(\zeta)$ cannot be smaller than that of $\mathcal{B}_{\rm old}(\zeta)$ under this fragmentation, therefore it follows from § 5.2 that $\mathcal{B}_{\rm new}(\zeta) = 0$ has a positive root $\zeta = \mu_0^{\rm new}$ on $0 < \zeta < \mu_{\rm m}^{\rm new}$ with $\mu_{\rm m}^{\rm new} \geq \mu_{\rm m}^{\rm old}$. From (5.2.28), the change in $\mathcal{B}(\zeta)$ induced by this fragmentation action is calculated under the constraint $m_i\rho_i^2 = m_j\rho_j^2 + m_k\rho_k^2$:

$$\begin{aligned}\mathcal{B}_{\rm new}(\zeta) - \mathcal{B}_{\rm old}(\zeta) &= \frac{\pi\alpha_i m_j\rho_j^2}{(2-\zeta m_j\rho_j^2)} + \frac{\pi\alpha_i m_k\rho_k^2}{(2-\zeta m_k\rho_k^2)} - \frac{\pi\alpha_i m_i\rho_i^2}{(2-\zeta m_i\rho_i^2)} \\ &= \frac{-\pi\alpha_i\zeta(m_j\rho_j^2 m_k\rho_k^2)\left[(2-\zeta m_j\rho_j^2)+(2-\zeta m_k\rho_k^2)\right]}{(2-\zeta m_i\rho_i^2)(2-\zeta m_j\rho_j^2)(2-\zeta m_k\rho_k^2)}.\end{aligned} \tag{5.3.13}$$

Hence, from (5.3.13), it is clear that $\mathcal{B}_{\rm new}(\zeta) < \mathcal{B}_{\rm old}(\zeta)$ on $0 < \zeta < \mu_{\rm m}^{\rm old} \equiv 2/(m_J\rho_J^2)$. Since, in addition $\mu_{\rm m}^{\rm new} \geq \mu_{\rm m}^{\rm old}$, it follows from Case II of Lemma 4.4 that $\mu_0^{\rm new} > \mu_0^{\rm old}$.

This proves the first two statements of Qualitative Result II.

To prove the final statement of this result, suppose that an unfavourable habitat is broken into two smaller unfavourable habitats, so that $m_i < 0$, $m_j < 0$, and $m_k < 0$. For this situation, the first vertical asymptotes of $\mathcal{B}_{\rm old}(\zeta)$ and $\mathcal{B}_{\rm new}(\zeta)$ are the same, and (5.3.13) again shows that $\mathcal{B}_{\rm new}(\zeta) < \mathcal{B}_{\rm old}(\zeta)$ on $0 < \zeta < \mu_{\rm m}^{\rm old} \equiv 2/m_J\rho_J^2$. By Case II of Lemma 4.4, we conclude that $\mu_0^{\rm new} > \mu_0^{\rm old}$, which proves the last statement of Qualitative Result II.

The combination of Qualitative Results I and II show that, given some fixed amount of favourable resources to distribute, the optimal strategy is to clump them all together at a point on the boundary of the domain, and more specifically at the corner point of the boundary (if any are present) with the smallest contact angle less than π degrees. This strategy will ensure that the value of μ_0, and consequently the leading-order term for λ, is as small as possible, thereby maximizing the range of diffusivities D in (1.2.1) for the persistence of the species.

Our final qualitative result addresses whether it is advantageous to fragment a single interior favourable habitat into a smaller interior favourable habit together with a favourable boundary habitat. To study this situation, consider the constraint

$$m_i\rho_i^2 = m_j\rho_j^2 + \frac{\alpha_k}{2}m_k\rho_k^2\,, \tag{5.3.14}$$

with $\alpha_i = \alpha_j = 2$, and $\alpha_k < 2$. The subscript i represents the original interior habitat, whereas j and k represent the new smaller interior habitat and new boundary habitat, respectively. It is not clear apriori whether this action is advantageous, given that fragmentation of a favourable interior habitat into two favourable interior habitats increases the persistence threshold λ, but the relocation of a favourable interior habitat to the boundary decreases λ. A sufficient condition to treat this case, together with two additional related results, are summarized as follows:

Qualitative Result III: *The fragmentation of one favourable interior habitat into a new smaller interior favourable habitat together with a favourable boundary habitat, is advantageous for species persistence when the boundary habitat is sufficiently strong in the sense that*

$$m_k\rho_k^2 > \frac{4}{2-\alpha_k}m_j\rho_j^2 > 0\,. \tag{5.3.15}$$

Such a fragmentation of a favourable interior habitat is not advantageous when the new boundary habitat is too weak in the sense that

$$0 < m_k\rho_k^2 < m_j\rho_j^2\,. \tag{5.3.16}$$

Finally, the clumping of a favourable boundary habitat and an unfavourable interior

habitat into one single interior habitat is not advantageous for species persistence when the resulting interior habitat is still unfavourable.

To prove this result, first impose the constraint (5.3.14), and then calculate from (5.2.28) that

$$\mathcal{B}_{\rm new}(\zeta) - \mathcal{B}_{\rm old}(\zeta) = \frac{2\pi m_j \rho_j^2}{(2-\zeta m_j \rho_j^2)} + \frac{\pi \alpha_k m_k \rho_k^2}{(2-\zeta m_k \rho_k^2)} - \frac{2\pi m_i \rho_i^2}{(2-\zeta m_i \rho_i^2)}\,,$$

$$= \frac{\pi \alpha_k \zeta \beta_k}{(2-\zeta\beta_i)(2-\zeta\beta_j)(2-\zeta\beta_k)} \left[\begin{array}{c} (2-\alpha_k)\beta_k - 4\beta_j \\ +\zeta\beta_j \left(\beta_j + \dfrac{\alpha_k}{2}\beta_k\right) \end{array} \right], \quad (5.3.17a)$$

$$= \frac{\pi \alpha_k \zeta \beta_k}{(2-\zeta\beta_i)(2-\zeta\beta_j)(2-\zeta\beta_k)} \left[\begin{array}{c} 2(\beta_k - \beta_j) - \beta_j(2-\zeta\beta_j) \\ -\dfrac{\alpha_k\beta_k}{2}(2-\zeta\beta_j) \end{array} \right], \quad (5.3.17b)$$

where $\beta_i \equiv m_i\rho_i^2$, $\beta_j \equiv m_j\rho_j^2$, and $\beta_k \equiv m_k\rho_k^2$. There are three parameter ranges of interest, corresponding to the three statements in Qualitative Result III.

First suppose that $\beta_i > 0$ and $\beta_k > \frac{4}{2-\alpha_k}\beta_j > 0$. Then, from (5.3.14), it follows that $\beta_i > \beta_j$, and

$$\beta_i < \frac{(2-\alpha_k)}{4}\beta_k + \frac{\alpha_k}{2}\beta_k = \beta_k - \frac{1}{2}\left(1 - \frac{\alpha_k}{2}\right)\beta_k\,,$$

so that $\beta_i < \beta_k$ since $0 < \alpha_k < 2$. It then readily follows that the first vertical asymptote $\mu_{\rm m}^{\rm new}$ and $\mu_{\rm m}^{\rm old}$ for $\mathcal{B}_{\rm new}(\zeta)$ and $\mathcal{B}_{\rm old}(\zeta)$, respectively, must satisfy $\mu_{\rm m}^{\rm new} \le \mu_{\rm m}^{\rm old}$. Furthermore, it follows from (5.3.17a) that $\mathcal{B}_{\rm new}(\zeta) > \mathcal{B}_{\rm old}(\zeta)$ on $0 < \zeta < \mu_{\rm m}^{\rm new}$. Consequently, Case I of Lemma 5.7 ensures that $\mu_0^{\rm new} < \mu_0^{\rm old}$. This establishes the first statement of Qualitative Result III.

Secondly, suppose that $\beta_i > 0$ and $\beta_j > \beta_k > 0$. Then, from (5.3.14), it follows that $\beta_i > \beta_j$, and $\beta_i > \beta_k + \alpha_k\beta_k/2 > \beta_k$ since $0 < \alpha_k < 2$. The condition that $\beta_i > \beta_j$ and $\beta_i > \beta_k$ ensures that the first vertical asymptotes of $\mathcal{B}_{\rm new}(\zeta)$ and $\mathcal{B}_{\rm old}(\zeta)$ must satisfy $\mu_{\rm m}^{\rm new} \ge \mu_{\rm m}^{\rm old}$. Furthermore, it follows from (5.3.17b) that $\mathcal{B}_{\rm new}(\zeta) < \mathcal{B}_{\rm old}(\zeta)$ on $0 < \zeta < \mu_{\rm m}^{\rm old}$. Consequently, Case II of Lemma 5.7 yields that $\mu_0^{\rm old} < \mu_0^{\rm new}$. This establishes the second statement of Qualitative Result III.

Finally, suppose that $\beta_j < 0$, $\beta_k > 0$, and $\beta_i = \beta_j + \alpha_k\beta_k/2 < 0$. Then, since $\beta_i < 0$, it follows that the first vertical asymptote $\mu_{\rm m}^{\rm old}$ for $\mathcal{B}_{\rm old}(\zeta)$ cannot occur from the $i^{\rm th}$ patch. The condition $\beta_k > 0$ then ensures that $\mu_{\rm m}^{\rm new} \le \mu_{\rm m}^{\rm old}$, where $\mu_{\rm m}^{\rm new}$ is the vertical asymptote of $\mathcal{B}_{\rm new}(\zeta)$. Furthermore, it follows from (5.3.17a) that $\mathcal{B}_{\rm new}(\zeta) > \mathcal{B}_{\rm old}(\zeta)$ on $0 < \zeta < \mu_{\rm m}^{\rm new}$. Consequently, Case I of Lemma 5.7 establishes that $\mu_0^{\rm old} < \mu_0^{\rm new}$, which proves the final statement of Qualitative Result III.

As a remark, an interpretation of the first statement of Qualitative Result III is

provided in terms of the areas of the patches for the special case where $m_j = m_k = 1$. Then, from (5.3.15) it follows that the fragmentation of a favourable interior habitat is advantageous when the area $\varepsilon^2 A_k \equiv \pi\varepsilon^2\rho_k^2/2$ of a new favourable habitat centered at a smooth point of the boundary is at least twice as large as the area $\varepsilon^2 A_j \equiv \pi\varepsilon^2\rho_j^2$ of the new smaller favourable interior habitat. If the new boundary habitat is located at a $\pi/2$ corner of the domain, for which $\alpha_k = 1/2$, then a sufficient condition for this fragmentation to be advantageous is when the area ratio satisfies $A_k/A_j = \rho_k^2/(4\rho_j^2) > 2/3$.

The following examples are provided to illustrate Qualitative Results I–III.

Example I: (The Unit Disk): Let Ω be the unit disk, a domain for which the Neumann Green's function and its regular part are known explicitly (c.f. Appendix B of [31]) to be

$$G(x;x_0) = \frac{-1}{2\pi}\log|x-x_0| + R(x;x_0)\,, \tag{5.3.18a}$$

$$R(x;x_0) = \frac{-1}{2\pi}\Big(\log\Big|x|x_0| - \frac{x_0}{|x_0|}\Big| - \frac{1}{2}(|x|^2+|x_0|^2) + \frac{3}{4}\Big)\,, \tag{5.3.18b}$$

We will compare the two-term asymptotic formula for λ in (5.2.27) of Principal Result 5.3 for three different arrangements of favourable resources inside Ω with $m_b = 2$ and $m_j = 1$ for $j = 1,\ldots,n$. For each of the three arrangements below, the constraint (5.3.1) has fixed value $\int_\Omega m\,dx = -\pi$. In the first example, favourable resources are clumped into one interior patch centered at the origin of radius ε. Substituting $m_+ = 1$, $m_b = 2$, $|\Omega| = \pi$, and $R(0;0) = -3/(8\pi)$ from (5.3.18b), into (5.1.26a) yields that

$$\lambda \sim \nu + \nu^2/2\,, \qquad \text{(interior patch)}\,, \tag{5.3.19}$$

where $\nu = -1/\log\varepsilon$. Next, consider the optimal case where the favourable resources are all concentrated at a patch of radius $\sqrt{2}\varepsilon$ that is centered on the boundary of the unit disk. Since Ω is a disk, any such boundary point x_0 yields the minimum value of λ. Substituting $m_+ = 1$, $m_b = 2$, $|\Omega| = \pi$, $\alpha_0 = 1$, $\rho_0 = \sqrt{2}$, and $R_s(x_0;x_0) = 1/(8\pi)$ from (5.3.18b), into (5.1.46a) gives that

$$\lambda \sim \frac{\nu}{2} - \frac{\nu^2}{2}\left(\frac{3}{8} - \log\sqrt{2}\right)\,, \qquad \text{(boundary patch)}\,. \tag{5.3.20}$$

The next example supposes that n favourable patches of a common smaller radius $\varepsilon/\sqrt{n}$ have centers at the equally spaced points $x_j = re^{2\pi ij/n}$ on a ring of radius $r < 1$, where $i = \sqrt{-1}$. In this case, set $m_b = 2$, $|\Omega| = \pi$, $m_j = 1$, $\rho_j = 1/\sqrt{n}$, and $\alpha_j = 2$ for

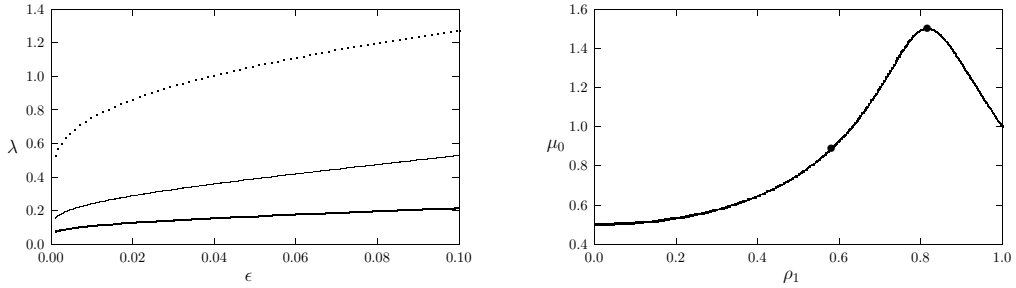

(a) λ versus ε (b) μ_0 versus ρ_1

Figure 5.4: Example 1: Choose $m_b = 2$, and $m_j = 1$ for $j = 1, \ldots, n$, in the unit disk with $\int_\Omega m\, dx = -\pi$. Left figure: λ versus ε for three different cases: a single boundary patch (5.3.20) (heavy solid curve); a single interior patch centered at the origin (5.3.19) (solid curve); four small patches equally spaced on a ring of radius $r = 0.5$ (5.3.21) (dashed curve). The boundary patch gives the smallest λ, followed by the non-fragmented interior patch solution. Right figure: the leading order coefficient μ_0 versus ρ_1 from (5.3.22b) for the partial fragmentation of an interior patch of radius ε into a smaller interior patch of radius $\varepsilon\rho_1$ together with a boundary patch of radius $\varepsilon\rho_0$, while maintaining $\int_\Omega m\, dx = -\pi$. The bullets indicate the bounds from (5.3.15) and (5.3.16) of Qualitative Result III. Fragmentation is advantageous only when $\rho_1 < \sqrt{2/5}$.

$j = 1, \ldots, n$, in (5.2.31) for μ_0 and (5.2.27) for λ. In this way, $\mu_0 = n$, and the two-term expansion of λ (5.2.27) reduces to

$$\lambda \sim n\nu - n\nu^2 \left(q_n(r) + \frac{1}{2}\log n + \frac{1}{4} \right), \qquad q_n(r) \equiv \frac{2\pi}{n^2} p_n(r), \tag{5.3.21a}$$

where $p_n(r) \equiv n e^T \mathcal{G}^{(N)} e$. Here $e = (1, \ldots, 1)^T$, and $\mathcal{G}^{(N)}$ is the $n \times n$ Neumann Green matrix with matrix elements $\left(\mathcal{G}^{(N)}\right)_{ij} = G(x_i; x_j)$ for $i \neq j$ and $\left(\mathcal{G}^{(N)}\right)_{jj} = R(x_j; x_j)$, where $G(x_i; x_j)$ and $R(x_j; x_j)$ are the Neumann Green's function of (5.1.19), given explicitly for the unit disk in (5.3.18). For n equally spaced patch centers on a ring of radius $r < 1$, $p_n(r)$ can be calculated explicitly, and is given in Proposition 4.3 of [57]. In this way, a direct calculation of $q_n(r)$ in (5.3.21a) gives

$$q_n(r) = r^2 - \frac{3}{4} - \frac{1}{n}\log\left(n r^{n-1}\right) - \frac{1}{n}\log\left(1 - r^{2n}\right). \tag{5.3.21b}$$

In Fig. 5.4(a), the three different two-term expansions for λ versus ε, given in (5.3.19), (5.3.20), and (5.3.21) with $n = 4$ and ring radius $r = 1/2$, representing the three different spatial arrangements of favourable resources. In agreement with predictions made in Qualitative Results I and II, the best choice is to concentrate resources on the boundary of the domain, while clumping resources at the center of the domain provides a better

alternative than fragmenting the favourable resources into four separate patches on a ring.

The next example is an illustration of Qualitative Result III. Consider fragmenting a single interior patch solution of radius ε centered at the origin into a boundary patch of radius $\varepsilon\rho_0$ and a smaller interior patch of radius $\varepsilon\rho_1$, while maintaining $\int_\Omega m\,dx = -\pi$. Thus, ρ_0 and ρ_1, with $0 < \rho_1 < 1$, must satisfy the constraint

$$1 = \rho_1^2 + \frac{1}{2}\rho_0^2\,. \tag{5.3.22a}$$

As remarked following (5.2.31), for a two-patch problem (5.2.28) reduces to a quadratic equation. In this case, that quadratic equation in μ_0 is

$$\mu_0^2\rho_1^2\left(1-\rho_1^2\right) + \mu_0\left(-2 + \frac{5}{2}\rho_1^2 - \frac{3}{2}\rho_1^4\right) + 1 = 0\,. \tag{5.3.22b}$$

Notice that $\mu_0 = 1$ when $\rho_1 = 1$, and $\mu_0 = 1/2$ when $\rho_1 = 0$, as expected. A plot of the smallest root to (5.3.22b) versus ρ_1 is shown in Fig. 5.4(b). The bound (5.3.16) in Qualitative Result III states that the partial fragmentation of the interior patch into a boundary patch is undesirable when $\rho_1 > \rho_0$, which yields $\rho_1 > \sqrt{2/3}$ from (5.3.22a). Alternatively, (5.3.15) together with (5.3.22a) shows that such a fragmentation is advantageous when $\rho_1 < 1/\sqrt{3}$. These two bounds are shown by the bullets in Fig. 5.4(b). For this simple two-patch case, we can readily show from the exact result (5.3.22b) that $\mu_0 = 1$ when $\rho_1 = \sqrt{2/5}$, or equivalently $\rho_0 = \sqrt{6/5}$. Thus, fragmentation is advantageous when $\rho_1 < \sqrt{2/5}$, or equivalently $\rho_0 > \sqrt{6/5}$.

The final example illustrates Qualitative Result III for the case where the unit disk has one pre-existing favourable interior patch of radius ε and growth rate $m_+ = 1$, together with one pre-existing unfavourable interior patch of radius ε and growth rate $m_- = -1$. An additional favourable resource of area $\varepsilon^2 A_0$, if separated from the other two patches, is introduced with local growth rate $m_0 = 1$. The bulk decay rate is chosen to be $m_b = 3$. Three different possible options for using this additional favourable resource are now explored, subject to the constraint that $\int_\Omega m\,dx = -3\pi + A_0$ remains fixed. If the additional favourable resources are concentrated at a smooth point on the boundary, then from (5.2.28) μ_0 satisfies

$$-3 + 2\left(\frac{1}{2-\mu_0} - \frac{1}{2+\mu_0}\right) + \frac{A_0/\pi}{1-\mu_0 A_0/\pi} = 0\,. \tag{5.3.23a}$$

Alternatively, if the additional favourable resource is used to strengthen the pre-existing

favourable interior patch, then from (5.2.28) μ_0 satisfies

$$-3+\frac{2\rho_+^2}{2-\rho_+^2\mu_0}-\frac{2}{2+\mu_0}=0\,,\qquad \rho_+^2=1+A_0/\pi\,. \tag{5.3.23b}$$

Finally, if the additional favourable resource is used to diminish the strength of the unfavourable pre-existing interior patch, then μ_0 satisfies

$$-3+\frac{2}{2-\mu_0}+\frac{m_-}{2-m_-\mu_0}=0\,,\qquad m_-=-1+A_0/\pi\,. \tag{5.3.23c}$$

In Fig. 5.3.2, the three curves for μ_0 obtained from (5.3.23a)–(5.3.23c) are plotted against A_0/π. A zoom of Fig. 5.5(a) for a subrange of A_0/π is shown in Fig. 5.5(b). From the plots we conclude that inserting a favourable boundary patch is preferable only when it has a sufficiently large size, and that if one only has a limited amount of an additional favourable resource, it is preferable to re-enforce the pre-existing favourable habitat. In addition, Fig. 5.5(b) shows that it is not optimal for any range of A_0/π to use the additional favourable resource to mitigate the effect of the unfavourable interior patch.

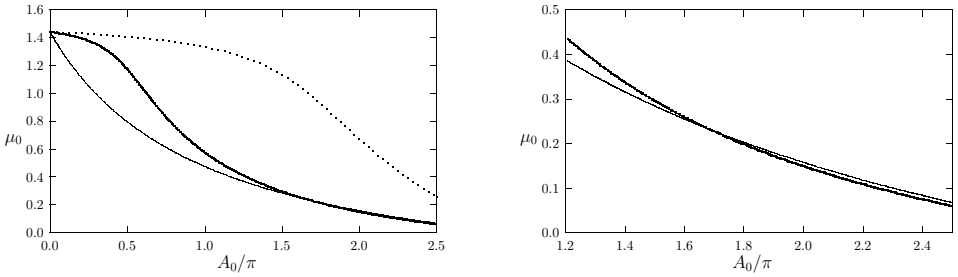

(a) μ_0 versus A_0/π (b) μ_0 versus A_0/π

Figure 5.5: Example 1: Choose $m_b = 3$ and consider a pre-existing patch distribution of one favourable interior patch of local growth rate $m_+ = 1$ and radius ε and an unfavourable interior patch of local growth rate $m_- = -1$ and radius ε. Assume an additional favourable resource of local growth rate $m_0 = 1$ that can occupy an area $\varepsilon^2 A_0$ if it separated from the two pre-existing interior patches. Plotted is μ_0 versus A_0/π when the additional resource is on the domain boundary (5.3.23a) (heavy solid curve), when it is used to re-enforce the existing favourable interior patch (5.3.23b) (solid curve), and when it is used to mitigate the effect of the unfavourable interior patch (5.3.23c) (dotted curve).

5.3.3 Optimization at Second Order

The minimization of λ in (5.2.27) is typically accomplished from the optimization of the coefficient μ_0 of the leading-order $\mathcal{O}(\nu)$ term in its asymptotic expansion. However, in certain degenerate cases, such as if a fixed distribution of interior patches is already present in the domain, the problem of optimizing the persistence threshold λ can require a careful examination of the coefficient μ_1 of the $\mathcal{O}(\nu^2)$ term in the asymptotic expansion of λ in (5.2.27). The coefficient μ_1 has an explicit dependence on the patch locations and accounts for interaction effects between the patches. An optimization problem of this type occurs in choosing the best location to place an additional favourable resource in a square domain. If this resource is sufficiently strong, then to minimize μ_0 it should be centered on the boundary of the square at a $\pi/2$ corner, and should not be used to strengthen a pre-existing favourable interior patch. In the situation where no other interior patches are present, each of the four corners of the square offers an equally good location to concentrate resources. However, if a distribution of fixed patches is already present in the domain, the best choice of corner to place an additional favourable patch is not clear apriori, and will depend on the spatial configuration of the fixed pre-existing patch distribution. In this case, the information required to make the optimal choice is provided by μ_1, which takes into account the interaction between the patches.

To formulate this restricted optimization problem, define x_j for $j = 1, \ldots, n$ to be a fixed pre-existing configuration of n circular patches in the interior of the domain whose local growth rates are m_j for $j = 1, \ldots, n$ respectively, where m_j is either positive (favourable habitat) or negative (unfavourable habit). Now consider the introduction of a single new favourable habitat, and assume that μ_0 is smallest when this additional habitat is located on the boundary of the domain. We then consider the problem of determining the optimal boundary location, x_0, of the center of the additional circular patch whose radius is $\varepsilon\rho_0$, local growth rate $m_0 > 0$ and angle $\pi\alpha_0$. Earlier analysis showed that to optimize μ_0, x_0 should be centered at a boundary point with the smallest contact angle $\pi\alpha_0$. In degenerate situations where this point is not uniquely determined, the coefficient of the $\mathcal{O}(\nu^2)$ term in (5.2.27) must be optimized. To do so, label $x_{n+1} = x_0$ and block the $(n+1) \times (n+1)$ matrices in (5.2.27) into an $n \times n$ block, labeled by $\mathcal{G}_m$ and $\mathcal{P}$, representing the fixed patch distribution, and a term $p(x_0)$ representing the interaction of the fixed patch distribution with the additional favourable resource. This determines μ_1 in (5.2.27) as

$$\mu_1 = \mu_0 \left(-\frac{1}{4} + \frac{\kappa^T \left(\mathcal{P} - \pi\mathcal{G}_m\right)\kappa + \kappa_0^2 \log\rho_0 - \pi p(x_0)}{\kappa^T\kappa + \kappa_0^2} \right) . \tag{5.3.24a}$$

In terms of the fixed distribution of patches, $\kappa = (\kappa_1, \ldots, \kappa_n)^T$, where κ_j for $j = 1, \ldots, n$

is defined in (5.2.22), while $\mathcal{G}_m$ and $\mathcal{P}$ are the $n \times n$ matrices as defined in (5.2.23). The scalar $p(x_0)$ in (5.3.24a), representing the interaction of the additional favourable boundary patch, centered at x_0, with the fixed patch distribution is given by

$$p(x_0) = \alpha_0 \kappa_0^2 R_m(x_0; x_0) + 2 \sum_{j=1}^{n} \sqrt{\alpha_0 \alpha_j} \kappa_0 \kappa_j G_m(x_j; x_0)\,, \qquad \kappa_0 \equiv \frac{\sqrt{\alpha_0} m_0 \rho_0^2}{2 - \mu_0 m_0 \rho_0^2}\,, \tag{5.3.24b}$$

where $\alpha_j = 2$ for $j = 1, \ldots, n$. From (5.2.28), the leading-order coefficient μ_0 in the asymptotic expansion of λ is the smallest positive root of

$$-m_b|\Omega| + \pi\sqrt{\alpha_0}\kappa_0 + \pi \sum_{j=1}^{n} \sqrt{\alpha_j}\kappa_j = 0\,, \qquad \kappa_j \equiv \frac{\sqrt{\alpha_j} m_j \rho_j^2}{2 - \mu_0 m_j \rho_j^2}\,, \quad j = 1, \ldots, n\,. \tag{5.3.25}$$

The minimization of the persistence threshold λ corresponds to determining the location of the maximum of $p(x_0)$ for $x_0 \in \partial\Omega$. The problem of maximizing $p(x_0)$ is now illustrated for two specific examples.

Example 2: Pre-Existing Patch Distribution (Unit Disk): Let Ω be the unit disc and $x_0 \in \partial\Omega$, for which $\alpha_0 = 1$. Since $x_0 \in \partial\Omega$, then $G_m(x_j; x_0) = G_s(x_j; x_0)$ and $R_m(x_0; x_0) = R_s(x_0; x_0)$ are the surface Neumann Green's function and its regular part given explicitly in (5.3.18) after setting $|x_0| = 1$. Now consider placing the centers x_j for $j = 1, \ldots, n$ of the fixed patches on a ring of radius r so that $x_j = r\exp(2\pi i j/n)$ and $\alpha_j = 2$ for $j = 1, \ldots, n$, with $0 < r < 1$. Then, from (5.3.24b) and (5.3.18), and with $\alpha_0 = 1$, we obtain

$$\begin{aligned} p(x_0) &= \frac{\kappa_0^2}{8\pi} + 2\kappa_0 \sum_{j=1}^{n} \sqrt{\alpha_j}\kappa_j \left[\frac{r^2}{4\pi} - \frac{1}{8\pi} - \frac{1}{2\pi}\log|x_j - x_0|^2\right], \\ &= \frac{\kappa_0^2}{8\pi} + \frac{\kappa_0}{2\pi}\left(r^2 - \frac{1}{2}\right)\sum_{j=1}^{n}\sqrt{\alpha_j}\kappa_j - \frac{\sqrt{2}\kappa_0}{\pi}\sum_{j=1}^{n}\kappa_j \log|x_j - x_0|^2\,, \\ &= \frac{\kappa_0^2}{8\pi} + \frac{\kappa_0}{2\pi}\left(r^2 - \frac{1}{2}\right)(m_b - \kappa_0) - \frac{\sqrt{2}\kappa_0}{\pi}\sum_{j=1}^{n}\kappa_j \log|x_j - x_0|^2\,, \end{aligned} \tag{5.3.26}$$

where in the last equality the identity $\sum_{j=1}^{n}\sqrt{\alpha_j}\kappa_j = m_b - \kappa_0$ from (5.3.25) has been used. Finally, writing $x_0 = e^{i\theta_0}$ and calculating the logarithmic interaction term in (5.3.26) yields that $p = p(\theta_0)$, where

$$p(\theta_0) = \frac{\kappa_0^2}{8\pi} + \frac{\kappa_0}{2\pi}\Big(r^2 - \frac{1}{2}\Big)(m_b - \kappa_0) - \frac{\sqrt{2}\kappa_0}{\pi}\sum_{j=1}^{n}\kappa_j \log\Big(r^2 + 1 - 2r\cos\Big(\theta_0 - \frac{2\pi j}{n}\Big)\Big)\,. \tag{5.3.27}$$

The location of the maximum value of $p(\theta_0)$ in (5.3.27) is now determined, which cor-

responds to the optimum location to insert the additional favourable resource on the boundary of the unit disk.

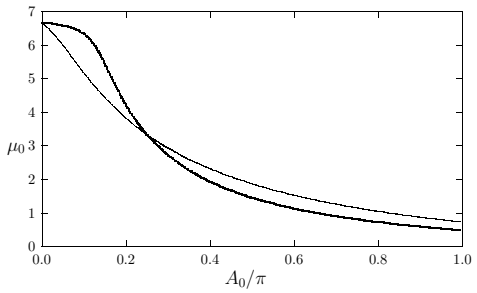

Figure 5.6: Example 2: Choose $m_b = 3$ and center five patches each of radius $\varepsilon/\sqrt{5}$ equidistantly on a ring of radius $r = 1/2$ in the unit disk with $m_j = 1$ for $j = 1, \ldots, 5$. Plot of μ_0, defined as the root of (5.2.28), versus A_0/π for an additional patch of area $\varepsilon^2 A_0$ located on the boundary of the domain (heavy solid curve) or used to re-enforce any one of the interior patches (solid curve). The boundary patch is preferable when $A_0/\pi = 1/2$, which corresponds to the boundary patch radius $\rho_0 = 1$. The bound (5.3.15) states that the boundary patch is favourable when its radius satisfies $\rho_0 > 2/\sqrt{5}$ (or $A_0/\pi > 2/5$), while from (5.3.16) the boundary patch is not favourable when $\rho_0 < 1/\sqrt{5}$ (or $A_0/\pi < 1/10$).

By supposing that $m_j = m_c$ for $j = 1, \ldots, n$, so that $\kappa_j = \kappa_c$ for $j = 1, \ldots, n$, *i.e.* asserting that all patches on the ring have the same strength, (5.3.27) simplifies to

$$\begin{aligned} p(\theta_0) &= \frac{\kappa_0^2}{8\pi} + \frac{\kappa_0}{2\pi}\Big(r^2 - \frac{1}{2}\Big)(m_b - \kappa_0) - \frac{\sqrt{2}\kappa_0\kappa_c}{\pi}\chi(\theta_0)\,, \\ \chi(\theta_0) &\equiv \sum_{j=1}^{n} \log\left[r^2 + 1 - 2r\cos\left(\theta_0 - \frac{2\pi j}{n}\right)\right]. \end{aligned} \tag{5.3.28}$$

The function $\chi(\theta_0)$ is reduced further by the following steps

$$\begin{aligned} \chi(\theta_0) &= \sum_{j=1}^{n} \log\left[\left(r - \cos\left(\theta_0 - \frac{2\pi j}{n}\right)\right)^2 + \sin^2\left(\theta_0 - \frac{2\pi j}{n}\right)\right] = 2\log\Big(\prod_{j=1}^{n}|r - z_j|\Big) \\ &= 2\log|r^n - e^{in\theta_0}| = \log\left[(r^n - \cos(n\theta_0))^2 + \sin^2(n\theta_0)\right], \end{aligned} \tag{5.3.29}$$

where $z_j \equiv e^{i(\theta_0 - 2\pi j/n)}$. In obtaining the second to last equality in (5.3.29), the fact that z_j are the roots of $r^n - e^{in\theta_0} = 0$ has been used. Upon differentiating (5.3.29) with respect to θ_0, it readily follows that the critical points of $\chi(\theta_0)$, and therefore $p(\theta_0)$,

satisfy $\sin(n\theta_0) = 0$, which admits the $2n$ solutions

$$\theta_0 = \frac{2\pi j}{n}, \qquad \theta_0 = \frac{\pi(2j-1)}{n}, \qquad j = 1, \ldots, n\,, \tag{5.3.30}$$

on the interval $0 < \theta_0 \leq 2\pi$. When $\kappa_c > 0$ in (5.3.28), then $\theta_0 = 2\pi j/n$ for $j = 1, \ldots, n$, clearly correspond to maxima of $p(\theta_0)$, while the remaining critical points in (5.3.30) are minima of $p(\theta_0)$. This result shows that when $\kappa_c > 0$, for which the ring is composed of n equally distributed favourable patches, the optimal boundary locations for the one additional favourable patch centered at x_0 is at the shortest distance to any of the n favourable habits on the ring. This result for $p(\theta_0)$ is illustrated by the heavy solid curve of Fig. 5.7(a) for $n = 5$ pre-existing patches for the parameter set $m_b = 3$, $m_0 = 1$, $\rho_0 = 1$, and with $m_j = 1$ and $\rho_j = 1/\sqrt{5}$ for $j = 1, \ldots, 5$. For this parameter set, where the favourable boundary patch is sufficiently strong in the sense of (5.3.15) of Qualitative Result III, μ_0 is indeed minimized when the favourable resource is concentrated on the boundary of the domain, rather than being used to re-enforce an interior favourable habitat. In Fig. 5.6, μ_0 is plotted against A_0/π, where $\varepsilon^2 A_0$ is the area of the additional favourable habitat for the case where the habitat is located on the boundary, and for the case when it is used to re-enforce one of the pre-existing favourable interior habitats. From this plot, we observe that a boundary habitat with $\rho_0 = 1$ and $A_0/\pi = 1/2$ provides $\mu_0 = 1.455$, which is the smaller of the two values for μ_0.

Alternatively, when $\kappa_c < 0$, only the locations $\theta_0 = \pi(2j-1)/n$ for $j = 1, \ldots, n$ correspond to maxima of $p(x_0)$. For this case, where the ring is composed of n equally spaced unfavourable habitats, the optimal boundary locations for the one additional favourable patch centered at x_0 is such that it maximizes the distance to any of the n unfavourable habitats on the ring. This result for $p(\theta_0)$ is illustrated by the solid curve in Fig. 5.7(a) for $n = 5$ pre-existing patches for the parameter set $m_b = 3$, $m_0 = 1$, $\rho_0 = 1$, and with $m_j = -1$ and $\rho_j = 1/\sqrt{5}$ for $j = 1, \ldots, 5$. For this parameter set $\mu_0 = 1.740$.

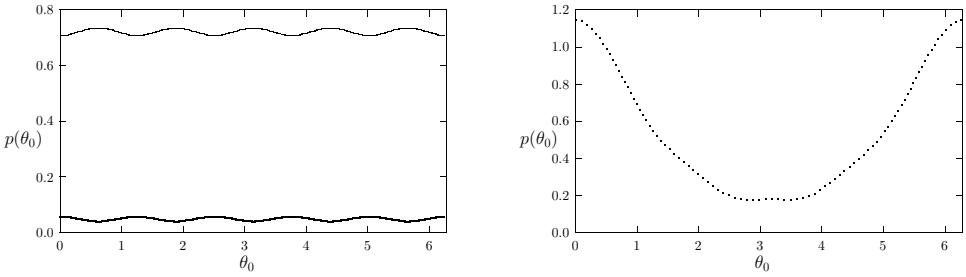

(a) $p(\theta_0)$ versus θ_0 (b) $p(\theta_0)$ versus θ_0

Figure 5.7: Example 2: Choose $m_b = 3$ and center five patches each of radius $\varepsilon/\sqrt{5}$ equidistantly on a ring of radius $r = 1/2$ in the unit disk. Insert a favourable boundary patch of radius $\rho_0 = 1$ and growth rate $m_0 = 1$ at $x_0 = e^{i\theta_0}$ on the boundary of the unit disk. Left figure: $p(\theta_0)$ versus θ_0 from (5.3.27) for favourable interior patches (heavy solid curve) with $m_j = 1$ for $j = 1, \ldots, 5$, and for unfavourable interior patches (solid curve) with $m_j = -1$ for $j = 1, \ldots, 5$. Right figure: $p(\theta_0)$ versus θ_0 for four unfavourable interior patches with $m_j = -1$ for $j = 1, \ldots, 4$ and one favourable interior patch at $x_1 = (r, 0)$ with $m_5 = 1$.

A further example considers the case of n patches with a common radius $\varepsilon\rho_c$ but with $m_j = -m_c$ for $j = 1, \ldots, n-1$, and $m_n > 0$, where $m_c > 0$. Therefore, there are $n-1$ unfavourable habitats on the ring, with the only favourable habitat on the ring being centered at $x_n = (r, 0)$. For this case, $p(\theta_0)$ is given by (5.3.27) provided that we replace κ_j in (5.3.27) with

$$\kappa_j \equiv -\frac{\sqrt{2}m_c\rho_c^2}{2 + \mu_0 m_c \rho_c^2}\,, \quad j = 1, \ldots, n-1\,, \qquad \kappa_n \equiv \frac{m_n\rho_c^2}{2 - \mu_0 m_n \rho_c^2}\,. \tag{5.3.31}$$

A simple calculation from (5.3.27) shows that the maximum of $p(\theta_0)$ occurs at $\theta_0 = 0$. Therefore, the best location for the favourable boundary habitat is to insert it as close as possible to the only favourable interior habitat on the ring, which effectively decreases the effect of fragmentation. This result for $p(\theta_0)$ is illustrated by the dashed curve in Fig. 5.7(b) for $n = 5$ pre-existing patches for the parameter set $m_b = 3$, $m_0 = 1$, $\rho_0 = 1$, $m_j = -1$ and $\rho_j = 1/\sqrt{5}$ for $j = 1, \ldots, 4$, and $m_5 = 1$ with $\rho_5 = 1/\sqrt{5}$. For this parameter set $\mu_0 = 1.709$. The figure shows that $p(\theta_0)$ is minimized when $\theta_0 = \pi$, corresponding to the location on $\partial\Omega$ furthest from the only favourable interior habitat.

Example 3: Pre-Existing Patch Distribution (The Unit Square) The final example considers the problem of optimizing the location of one additional favourable resource in the unit square domain $\Omega = [0, 1] \times [0, 1]$ given a certain distribution of pre-existing patches. This optimization problem is somewhat simpler than the previous example for the unit disk, since if the patch is sufficiently strong, the optimization of

μ_0 requires that the additional resource be located at the corner x_0 of the square that maximizes $p(x_0)$ in (5.3.24b). For the unit square, explicit analytical formulae for the Neumann Green's function and its regular part, required to optimize $p(x_0)$, are obtained in §3.2 of [62]. The calculations leading to these formulae are lengthy and so only the results are stated. The Neumann Green's function with an interior singularity is given by

$$G(x;x_0) = -\frac{1}{2\pi}\log|x-x_0| + R(x;x_0)\,, \tag{5.3.32a}$$

where the regular part $R(x;x_0)$ is given explicitly by

$$\begin{aligned} R(x;x_0) = -\frac{1}{2\pi}\sum_{n=0}^{\infty}\log(&|1-q^n z_{+,+}||1-q^n z_{+,-}||1-q^n z_{-,+}||1-q^n\zeta_{+,+}| \\ &\times|1-q^n\zeta_{+,-}||1-q^n\zeta_{-,+}||1-q^n\zeta_{-,-}|) \\ &-\frac{1}{2\pi}\log\frac{|1-z_{-,-}|}{|r_{-,-}|} + H(x^{(1)},x_0^{(1)}) - \frac{1}{2\pi}\sum_{n=1}^{\infty}\log|1-q^n z_{-,-}|\,. \end{aligned} \tag{5.3.32b}$$

and $x=(x^{(1)},x^{(2)})$ and $x_0=(x_0^{(1)},x_0^{(2)})$. Here the eight complex constants $z_{\pm,\pm}$ and $\zeta_{\pm,\pm}$ are defined in terms of additional complex constants $r_{\pm,\pm}$, $\rho_{\pm,\pm}$ by

$$z_{\pm,\pm} \equiv \mathrm{e}^{\pi r_{\pm,\pm}}\,, \quad \zeta_{\pm,\pm}\equiv \mathrm{e}^{\pi\rho_{\pm,\pm}}\,, \qquad q\equiv \mathrm{e}^{-2\pi}<1\,, \tag{5.3.33a}$$

$$r_{+,\pm} \equiv -|x^{(1)}+x_0^{(1)}| + i(x^{(2)}\pm x_0^{(2)})\,, \qquad r_{-,\pm}\equiv -|x^{(1)}-x_0^{(1)}| + i(x^{(2)}\pm x_0^{(2)})\,, \tag{5.3.33b}$$

$$\rho_{+,\pm} \equiv |x^{(1)}+x_0^{(1)}| - 2 + i(x^{(2)}\pm x_0^{(2)})\,, \qquad \rho_{-,\pm}\equiv |x^{(1)}-x_0^{(1)}| - 2 + i(x^{(2)}\pm x_0^{(2)})\,. \tag{5.3.33c}$$

In (5.3.32) and (5.3.33), $|\omega|$ is the modulus of the complex number ω. In (5.3.32b), $H(x^{(1)},x_0^{(1)})$ is defined by

$$H(x^{(1)},x_0^{(1)}) \equiv \frac{1}{12}\left[h(x^{(1)}-x_0^{(1)}) + h(x_1^{(1)}+x_0^{(1)})\right]\,, \qquad h(\theta)\equiv 2-6|\theta|+3\theta^2\,. \tag{5.3.34}$$

The self-interaction term $R(x_0;x_0)$, required in (5.1.19b) is obtained by setting $x=x_0$ in (5.3.32b).

Let x_0 be the location of a patch of favourable resource with radius ε and local growth rate $m_0=1$ and assume that there is a configuration of four pre-existing patches in Ω centered at $x_1=(1/4,1/4)$, $x_2=(1/4,3/4)$, $x_3=(3/4,1/4)$, and $x_4=(3/4,3/4)$. Let each patch have a common radius $\varepsilon/2$ (i.e. $\rho_j=1/2$ for $j=1,\ldots,4$) with local growth rate $m_1=m_2=m_3=-1$, $m_4=1$, and the background decay rate $m_b=3$. For this parameter set, where the favourable boundary patch is sufficiently strong in the

sense of (5.3.15) of Qualitative Result III, μ_0 is minimized when the favourable resource is concentrated at one of the four corners on the square, rather than being used to re-enforce the only favourable interior habitat. By determining the root μ_0 of (5.2.28) numerically, the value $\mu_0 = 1.605$ is obtained when the additional favourable resource is at a corner of the square, and $\mu_0 = 2.681$ when the additional favourable resource is used to strengthen the favourable resource at x_4. Therefore, μ_0 is smallest when x_0 is at a corner of the square. Then, by varying x_0 over the four corners of the square, the following numerical results for $p(x_0)$ are obtained from (5.3.24b):

$$x_0 = (0,0) \quad p(x_0) = -0.8522\,; \quad x_0 = (1,1) \quad p(x_0) = -0.2100\,.$$
$$x_0 = (1,0) \text{ or } x_0 = (0,1) \quad p(x_0) = -0.7163\,;$$

The largest value for $p(x_0)$ occurs when $x_0 = (1,1)$. Therefore, these results show that the persistence threshold λ is smallest when the additional favourable habitat is positioned at the corner of the square that is closest to the only favourable interior habitat. This action effectively decreases the effect of fragmentation.

In cases where μ_0 is lowest positive value at a discrete set of points, as in the previous example, optimization of the $\mathcal{O}(\nu^2)$ terms in λ can certainly be achieved by calculating μ_1 at each of these discrete points and sorting for the smallest. This method does rely on the availability of values for $R(x; x_0)$, which may in general be calculated numerically as in [62]. In the previous example, the optimal choice was that which minimized the euclidean distance between the one existing favourable resource and the favourable additional resource. Heuristically, this action can be thought of as effectively decreasing the the fragmentation of the resource configuration. For more complex configurations however, it is not clear if a rule of thumb can be established, as consideration of a more complicated fragmentation metric may be required.

5.4 Conclusions

For a specific but fairly general class of functions $m(x)$, a definitive strategy for the optimization of the principal eigenvalue of (5.0.1) has been established. For a class of $m(x)$ consisting of a background decay rate plus localized patches of either highly favourable or unfavourable rates, a two term expansion of the persistence threshold was developed in (5.2.27).

Interestingly, a large quantity of information regarding the optimal configuration of patches is contained in the leading order term even although it has no explicit dependence on the path centers. In certain degenerate cases, the second order term must be considered to find the optimal configuration of resources.

By directly optimizing the persistence threshold λ, Qualitative Results I–III were obtained in § 5.3.2. In particular it was shown that moving a favourable patch from an interior location to a boundary location is always advantageous to species persistence. If the boundary of the domain has corners, then the corner with the smallest angle produces the lowest persistence threshold. It was also shown that splitting one favourable interior patch into two favourable interior patches always increased the persistence threshold and in this sense, fragmentation can be thought of a deleterious to the well-being of a species evolving in Ω. The division of a single interior patch is into a boundary patch and an interior patch is only advantageous provided the boundary patch is sufficiently strong.

The findings reported here agree well with known optimization results for the 1D strip (c.f. [60, 46]) and numerical results in higher dimensions (c.f. [42]).

This work forms the basis of paper [31], titled *An Asymptotic Analysis of the Persistence Threshold for the Diffusive Logistic Model in Spatial Environments with Localized Patches* to appear in Discrete and Continuous Dynamical Systems Series B.

Chapter 6

Discussion

In this section, I will provide an overview of the results of the two problems studied and place these results in context with the published literature on models of MEMS devices and Mathematical Ecology. There are several areas where open problems remain for which further investigation is warranted and in relation to this work, several of these will be discussed.

6.1 Micro-Electro Mechanical Systems

The motivation for our mathematical study of the models of Micro-Electro Mechanical Systems is two fold. The first motivation is the study of the *pull-in* phenomena which manifests itself mathematically as a saddle-node bifurcation in a non-linear eigenvalue problem. The *pull-in* instability is crucial to the effective design of MEMS devices and so characterizing it mathematically is an important and interesting problem. Previous work in the mathematical study of the *pull-in* stability has furnished the area with many important rigorous results, particularly those pertaining to the existence, stability and regularity of an extremal solution at the end of the minimal solution branch for (1.1.3) [16]. While our work lacks a rigorous basing, indeed many of our results can be thought of as predictions, its advantage lies in its explicit characterization of the solution structure. Numerical evidence can be useful to bolster the veracity of our predictions, but a rigorous analysis would certainly complement our findings well.

In Chapter 3, the location of this fold point was determined explicitly by means of matched asymptotic expansions for three particular models, the beam problem (1.1.4), the fringing fields problem (1.1.5) and the annulus problem (1.1.6). A comparison with full numerics shows that the location of the fold point is accurately predicted by asymptotic calculations for a large range of physical parameters. Accurate determination of the fold point located at the end of the minimal branch is crucial in the design of MEMS devices as typically such devices are operated very close to this threshold. The asymptotic formulae derived in result (3.3.19) may therefore be useful to MEMS practitioners who rely on accurate determination of this value. By including more physical effects in the modeling, this may add refinement to the current practice of MEMS design.

The second motivation for the mathematical study of MEMS models concerns the

nature of singular solutions as $||u||_\infty \to 1$ which are dominated by the $\lambda/(1+u)^2$ nonlinearity ubiquitous in equations of MEMS. In this regime, several rigorous results pertaining to solution multiplicity have been established (c.f. [20, 13, 9]), in particular, it has been established that (1.1.2) exhibits an infinite number of solutions. Building on this understanding, the asymptotic techniques developed in this thesis allows for these singular solutions to be constructed *explicitly* for certain domains. This explicit characterization allows for very particular predictions to be made on the nature of the solutions.

One common feature in the analysis of these singular solutions is the definition $||u||_\infty = 1-\varepsilon$, *i.e.* the maximum absolute deflection of the plate is specified to be some small distance from 1. This allows the resolution, by means of asymptotic methods, of the $\lambda/(1+u)^2$ nonlinearity near the point of maximum absolute deflection and so facilitates the construction of singular solutions as $\varepsilon \to 0^+$. It is shown in § 4.1 that solutions to (1.1.2) for the unit disc exhibit an infinite number of fold points centred on a determined value of $\lambda = \lambda^* > 0$ as $||u||_\infty \to 1$. The locations of these fold points are determined explicitly in the analysis and are observed to be exponentially close to $u = -1$. Predictions are shown to agree very well with numerical calculations (see Fig. 4.3).

While the fringing fields, beam and annulus perturbations induce a quantitative change on the location of the *pull-in* instability, these same perturbations are observed to destroy the infinite fold point structure and the bifurcation diagrams of the three problems are left with a finite number of fold points followed by limiting behaviour $\lambda \to 0$ as $||u||_\infty \to 1$. This was initially observed in the numerical study of Pelesko (c.f. [38]). In Chapter 4 of this work I have concentrated on characterizing this final limiting branch of solutions.

In the case of the beam problem and the annulus problem, this limiting behaviour is calculated explicitly by constructing the limiting solution branch as $||u||_\infty \to 1$. In the case of the unit disc, an interesting observation is that the nature of the singularity at the origin has changed from $u \sim -1 + r^{2/3}$ in the membrane problem (1.1.2) to $u \sim -1 - 2r^2 \log r$ in the beam problem (1.1.4). It is conjectured that this change in singularity of the limiting solution is a necessary condition to destroy the infinite fold point structure. For the case of the fringing fields problem, a full characterization of the limiting behaviour as $u \to -1$ remains elusive. I believe this is a tractable problem but, despite its perhaps innocuous appearance, the $\delta|\nabla u|^2$ term induces a solution whose singularity structure is significantly more complex than that of the unperturbed problem.

An explicit characterization of the break-up of the infinite fold points structure remains to be developed. An attempt to do so would require the analysis of equations

(1.1.4)-(1.1.6) in the limit $\lambda = \mathcal{O}(1)$ with $\varepsilon \equiv 1 - ||u||_\infty \to 0^+$ and $\delta \to 0$ where $\delta = \delta_0\mu(\varepsilon)$ for some gauge $\mu(\varepsilon)$ satisfying $\mu \to 0$ as $\varepsilon \to 0$. I believe these problems to be very challenging but ultimately resolvable by skillful use of matched asymptotic expansions.

In § 4.4, the characterization of the maximal solution branch of the pure biharmonic MEMS problem (4.4.1) on a general geometry $\Omega \subset \mathbb{R}^2$ is considered. Under the assumption that the solution concentrates at a unique $x_0 \in \Omega$ as $u(x_0) \to -1$, the maximal branch is constructed and conditions on the point x_0 are established in terms of the regular part of a Green's function whose definition is given in (4.4.2).

These results can be potentially expanded to consider certain domains for which the maximal solution branch may concentrate at multiple points in the domain, *e.g.* dumbbell shaped domains. It would be very interesting to rigorously establish the asymptotic results outlined here and in doing so definitively characterize the limiting behaviour of the biharmonic MEMS problems for general two dimensional geometries.

The techniques implemented here have the potential to characterize concentration phenomena in other nonlinear eigenvalue problems which arise from the consideration of different physical situations. A few of these interesting problems are discussed in the following section.

6.1.1 Concentration Behavior in Other Nonlinear Eigenvalue Problems

Bratu's Problem is a description for the temperature u in a chemical reactor with geometry $\Omega \subset \mathbb{R}^3$. For a spherical reactor of unit radius, the problem is formulated as

$$\frac{d^2u}{dr^2} + \frac{2}{r}\frac{du}{dr} + \lambda e^u = 0, \quad 0 < r < 1; \qquad u(1) = u'(0) = 0. \tag{6.1.1}$$

where the term e^u arises from the Arrhenius rate law. The general properties of (6.1.1) are now well known. For example, it is well known that there exists a $\lambda_c > 0$ such that for $\lambda > \lambda_c$, (6.1.1) has no solutions ([25]). In addition, it is known that (6.1.1) exhibits an infinite fold point structure with limiting behaviour $\lambda \to 2$ as $u(0) \to \infty$ as developed in § 4.1.3 (see also [12]). While some perturbations to this equation destroy this structure when introduced, other perturbations do not and leave the solution with essentially the same qualitative behaviour. For example, the problem

$$\frac{d^2u}{dr^2} + \frac{2}{r}\frac{du}{dr} + \lambda \exp\left[\frac{u}{1+\delta u}\right] = 0, \quad 0 < r < 1; \qquad u(1) = u'(0) = 0. \tag{6.1.2}$$

for $\delta > 0$ has a bifurcation diagram with only a finite number of fold points and positive solutions for all $\lambda > 0$ (c.f. [2]) indicating a significant deviation in character from the

$\delta = 0$ case. Alternatively, the problem

$$\frac{d^2u}{dr^2} + \frac{2}{r}\frac{du}{dr} - \delta u + \lambda e^u = 0, \quad 0 < r < 1; \qquad u(1) = u'(0) = 0. \tag{6.1.3}$$

retains all the qualitative features of (6.1.1) for $\delta > 0$ including the infinite fold points structure and so too does the problem

$$\frac{d^2u}{dr^2} + \frac{2}{r}\frac{du}{dr} + \lambda e^u = 0, \quad 0 < r < 1; \qquad u(1) = \delta u'(1), \qquad u'(0) = 0. \tag{6.1.4}$$

It is conjectured that the regularity of the limiting solution is key to determining the qualitative effects for each perturbation. It would be interesting to characterize more fully the quantitative and qualitative effects of the mentioned perturbed equations on the infinite fold point structure of the unperturbed equation (6.1.2).

6.1.2 Quenching Behavior in Fourth Order Time-Dependent MEMS

A significant area for future work on MEMS devices relates to properties of the time dependent problem for $u(x,t)$ where

$$\frac{\partial u}{\partial t} = -\delta\Delta^2 u + \Delta u - \frac{\lambda}{(1+u)^2}, \quad x \in \Omega; \qquad \begin{matrix} u = \partial_n u = 0 & x \in \partial\Omega \\ u(x,0) = 0 & \end{matrix} \tag{6.1.5}$$

Here Ω is a bounded region of $\mathbb{R}^2$ with smooth boundary $\partial\Omega$. Analysis from § 3.1.1 and [29] indicates that there is a critical value λ^* such that if $\lambda > \lambda^*$, equation (6.1.5) does not have a steady state solution. In this case, it is expected that u will take the value -1 at some set of points in some finite time T. This phenomena is called *touchdown*. In the parlance of PDE theory, behavior of this type is called *quenching* and corresponds to derivatives of the solution becoming unbounded. Recall that a solution *blows up* in a finite time T at a point x if $|u(x,t)| \to \infty$ as $t \to T^-$ which is not the situation here as physical constraints demand that $-1 \le u \le 0$ for all time.

The theory of singularity formation in second order differential equations is relatively well developed and accordingly touchdown in the case $\delta = 0$ is has been analyzed in some depth. In [70], the value of T was estimated and the resulting touchdown profile was characterized by means of a formal asymptotic expansion. These results have been rigorously verified in the work of [14] and [15] for several choices of $f(x)$ and thus touchdown behavior for the second order problem

$$u_t = \Delta u - \frac{\lambda f(x)}{(1+u)^2}, \quad x \in \Omega; \qquad u(x,t) = 0, \quad x \in \partial\Omega; \qquad u(x,0) = 0, \quad x \in \Omega. \tag{6.1.6}$$

is considered to be relatively well understood. Singularity formation in higher order problems is significantly more complicated and so presently the touchdown profile of the fourth order problem (6.1.5) has not been well characterized. One such complication is the observation that higher order problems may exhibit a countably infinite number of blowup profiles with only the observed solution being stable [3]. Numerical identification of such solutions is hampered by the presence of spurious positive eigenvalues generated as a byproduct of the similarity transforms [73], [74].

In the instance where Ω corresponds to the unit square, slab or unit disc, (6.1.5) may be discretized in space by replacing derivatives by differences quotients and in time by applying an explicit method (*e.g.* Adams-Bashforth) to the nonlinear term $\lambda/(1+u)^2$ and an implicit method to the differential term. The solution can be integrated relatively close to touchdown by making the time step sufficiently small, however, accurate determination of the touchdown profile very close to singularity requires special attention and has been considered in [73].

In the cases of the slab domain $(-1,1)$ and the unit disc $\{|x| \leq 1\}$, it has been shown ([14, 15]) that for (6.1.6) touchdown is achieved only at the origin. The following numerical computations suggest that the inclusion of the bi-harmonic term , *i.e.* $\delta > 0$ in (6.1.5), has a pronounced effect on touchdown behavior, in particular touchdown may occur at multiple points for certain choices of Ω and regimes of λ, δ.

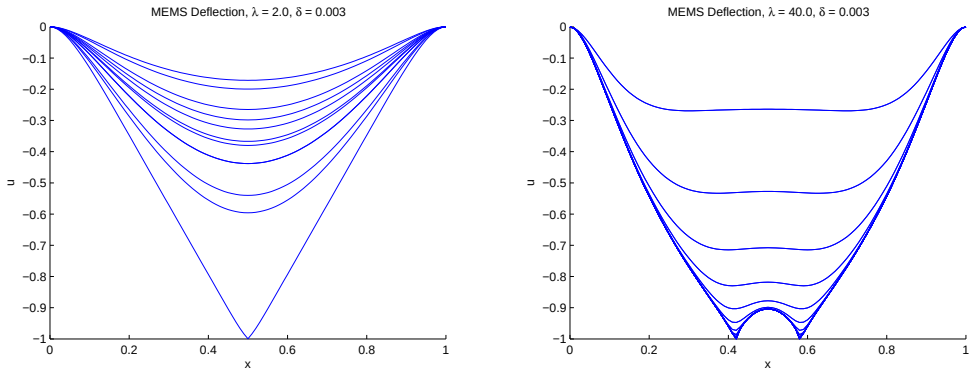

Figure 6.1: The left panel shows the dynamic deflection for $\lambda = 2.0$ and $\delta = 0.003$ and touchdown at one point. Steady state is reached after approximately 0.3950 units of time. The right panel shows the dynamic deflection for $\lambda = 40.0$ and $\delta = 0.003$. Touchdown occurs after 0.1190 units of time.

In Fig. 6.1 we see that in the case of $\Omega = (0,1)$ and $\delta = 0.003$, equation (6.1.5) touches down at a single point for $\lambda = 2$ indicating that $\lambda^* < 2$. In the case where $\lambda = 40$, touchdown occurs in finite time at two distinct points. This suggests the existence of some critical value $\lambda_c(\delta)$ satisfying $\lambda_c(\delta) > \lambda^*(\delta)$ and with the property that if $\lambda > \lambda_c(\delta)$, touchdown is achieved at two points while if $\lambda^*(\delta) < \lambda < \lambda_c(\delta)$, the

beam touches down at a single point only.

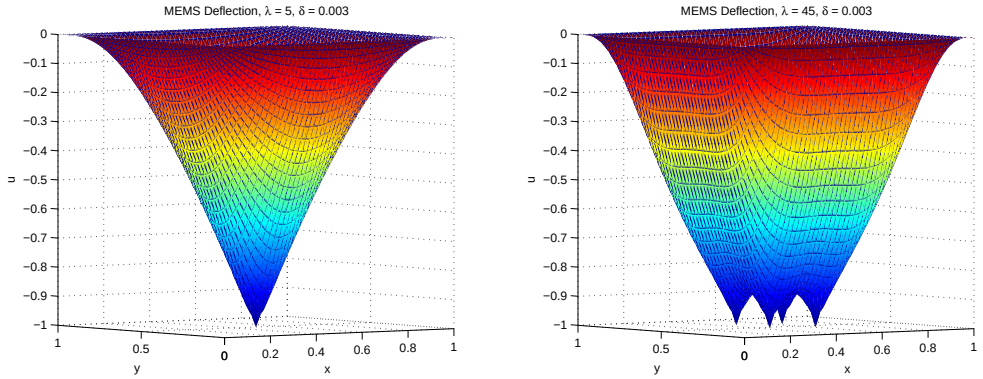

Figure 6.2: The left panel shows the configuration of the deflecting plate close to touchdown when $\delta = 0.003$ and $\lambda = 5$. Touchdown occurs at the center point $(0.5, 0.5)$. The right panel shows the configuration of the deflecting plate close to touchdown when $\delta = 0.003$ and $\lambda = 45$. In this case touchdown occurs at four distinct points.

In Fig. 6.2, we see that in the case $\Omega = (0,1)\times(0,1)$ and $\delta = 0.003$, touchdown occurs at one point only when $\lambda = 5$ and at four distinct point when $\lambda = 45$ again suggesting the existence of some threshold $\lambda_c(\delta)$. The presence of four distinct touchdown points in the unit square domain suggests that this phenomena may be generated by the boundaries of the domain in some way. In the case of the unit disc (not pictured) touchdown is observed to occur on a small inner disc further suggesting that this phenomena is due to some boundary effect.

To explain this multiple touchdown behavior, it is instructive to consider the reduced problem

$$u_t = -\delta u_{xxxx} - \frac{\lambda}{(1+u)^2}, \quad -1 < x < 1; \qquad u(\pm 1, t) = u_x(\pm 1, t) = 0, \qquad u(x,0) = 0 \tag{6.1.7}$$

in which (6.1.5) has been simplified by omitting the effects of tension and fixing $\Omega = (-1,1)$. This problem is the simplest non-tailored ($f(x) = 1$) MEMS deflection equation which has been observed numerically to exhibit touchdown at multiple locations.

Let us consider the situation at the center of the beam for times close to $t = 0$. Assuming t is small enough, the only forces experienced by the center of the beam should be that of the uniform electric field present in the gap between the plates. If that is the case, one might expect the term δu_{xxxx} to be negligible in the center section of the beam and thus it should deflect uniformly according to the equation

$$u_t = -\frac{\lambda}{(1+u)^2}, \qquad u(0) = 0 \tag{6.1.8}$$

which has solution $u(t) = -1+(1-3\lambda t)^{1/3}$. In Fig. 6.3, the numerical solution of (6.1.7) is displayed along with the solution of (6.1.8) at four selected time steps. In the figure very good agreement is observed between these two quantities in the center of the beam

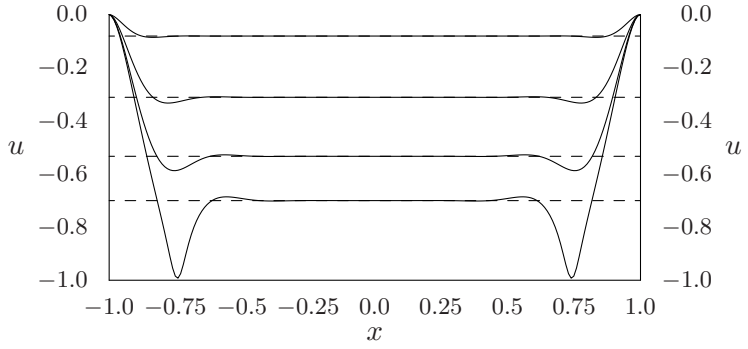

Figure 6.3: Numerical solutions of equation (6.1.7) for $\delta = 0.001$ and $\lambda = 100$ at four time steps $t = 0.000745$, $t = 0.002245$, $t = 0.002995$ and $t = 0.003244$. The curves are arranged in order of increasing time from top to bottom. At each time step, the solution of (6.1.8) is overlaid.

Numerical evidence lend weight to the suggestion that solutions of (6.1.7) for $\delta \ll 1$ are composed of a flat central region with governing equation (6.1.8) coupled to a propagating boundary effect. The case of multiple touchdowns then arises when the center of the beam touches down before the boundary effect has time to propagate to the mid point.

The dynamics of u after touchdown, *i.e.* $t > T$, may be studied in some weak sense where one might expect that u takes the value of -1 on open regions of Ω. This has been studied for blow-up phenomena in [11] in the context of fourth order reaction diffusion equations. In an actual MEMS device this would require some kind of insulating layer be present on the surface of the fixed plate to prevent the capacitor discharging from the contact between the two plates.

6.2 Eigenvalue Optimization Problems In Mathematical Ecology

In Chapter 5, the two-term asymptotic expansion of the persistence threshold λ for the diffuse logistic model (1.2.1) in a highly patchy environment with spatially heterogeneous growth rate (1.2.4) is calculated. The analysis permits for a relatively large class of spatially localized favourable and unfavourable habitats that are either interior to or on the boundary of a two-dimensional domain. The effect of habitat fragmentation on the coefficient of the leading-order term in the asymptotic expansion of λ is studied

and some general principles regarding the effect of fragmentation are established. These principles are summarized in Qualitative Results I–III of § 5.3.2. In certain degenerate cases, the optimization of λ requires the examination of the higher-order coefficient in the asymptotic expansion of λ.

There are several interesting problems that warrant further study. Firstly, it would be interesting to extend the single-species analysis to the case of multi-species interaction, such as predator-prey interactions, for which a partial fragmentation of the prey habitat may become beneficial for the persistence of the prey, rather than clumping the prey into a single habitat. This is based on the field observation that when one species is congregated, its predator has a distinct advantage and so the single species strategy may be sub-optimal.

One possible avenue for investigating this multi-species case leads to the consideration of the diffusive Kermack-McKendrick Model

$$\begin{aligned} u_t &= D_1\Delta u + u(m(x) - u) - \beta uv, \\ v_t &= D_2\Delta v - \sigma v + \mu + \beta uv \end{aligned} \qquad x \in \Omega; \qquad \partial_n u = \partial_n v = 0, \quad x \in \partial\Omega \tag{6.2.1}$$

Here, D_1, D_2, σ, μ and β are positive constants. By investigating the linearized stability of the equilibrium $(u, v) = (0, \sigma/\mu)$, one is led to the following eigenvalue problem

$$\Delta u + \lambda u(m(x) - \chi), \quad x \in \Omega; \qquad \partial_n u = 0, \quad x \in \partial\Omega. \tag{6.2.2}$$

where $\chi = \beta\sigma/\mu$ controls the strength of the predation. An asymptotic analysis of (6.2.1) may reveal that for certain $m(x)$ a threshold χ_c can be established such that whenever $\chi > \chi_c$, fragmentation is optimal.

Another interesting problem to be considered is that involving the so-called Allee effect (c.f. [32]), whereby individuals in a population find it difficult to locate a mate when their population is small. This effect is captured by the term $a > 0$ in

$$u_t = D\Delta u + m(x)u(1 - u)(u + a), \quad x \in \Omega; \qquad \partial_n u = 0, \quad x \in \partial\Omega. \tag{6.2.3}$$

A schematic bifurcation diagram of equilibrium solutions to (6.2.3) is given in Fig. 6.4 where it is observed that the persistence threshold is now determined by new critical value located by a fold point at the end of an unstable branch of solutions.

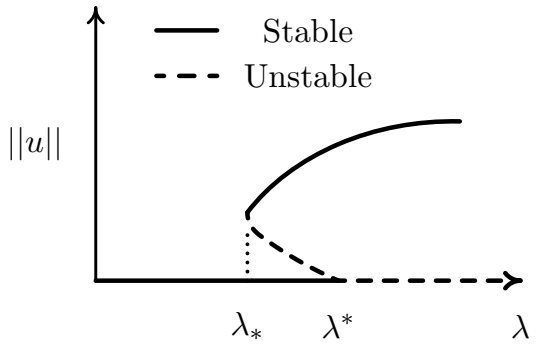

Figure 6.4: The Allee effect. Schematic bifurcation diagram of (6.2.3) for $a > 0$ indicating the new persistence threshold λ_*.

In this case, the optimal strategy is now determined by calculating and minimizing λ_* rather than λ^*, as in the problem treated in Chapter 5.

A third interesting avenue for future investigation involves the inclusion of more sophisticated mechanisms for population transport. For instance, suppose that individuals in a population not only diffuse, but advect along the gradient of the resources available to them. Under this assumption, the following advection diffusion model was proposed in [49],

$$u_t = \nabla \cdot [D\nabla u - \alpha u \nabla m] + u(m-u), \quad x \in \Omega; \qquad \partial_n u - \alpha u \partial_n m = 0, \quad x \in \partial\Omega \quad (6.2.4)$$

In this model, one might expect the geometry of the habitat to have a large effect on a fragmentation strategy as for non convex domains, individuals will not be able to advect directly towards favourable resources when they are located in tight corners.

Problems (6.2.1)-(6.2.4) are but a few of the many interesting ecological problems where the consequences of habitat fragmentation can be effectively analyzed with the techniques of matched asymptotic expansions.

6.3 Conclusion

This thesis has been concerned with the implementation of contemporary singular perturbation methods to two problems arising in the natural sciences and engineering. While asymptotic methods lack formal rigour, they have many other advantages which lend themselves well to the study of challenging mathematical problems. They can systematically reduce difficult problems into a sequence of tractable ones which are readily solvable. For example, in Chapter 3 the location of the principal fold points of (1.1.4)-(1.1.6) were deduced based solely on knowledge of the fold point of the unperturbed problem (1.1.2). This technique avoids the need to solve additional non linear problems

and so offers a significant simplification.

In Chapter 4, asymptotic methods are used to resolve the $\lambda/(1+u)^2$ nonlinearity for $||u||_\infty \to 1$ and provide an explicit solution characterization of the limiting solutions to MEMS problems. These results concern dynamically unstable solutions are therefore somewhat less important to practitioners, however, I hope they can provide the PDE community with avenues for further investigation.

In Chapter 5, matched asymptotic expansions have to used to attack a long standing open problem in Mathematical Ecology. The work contained here does not resolve the question entirely as some particular assumptions have been made on the resource function $m(x)$. However, for the particular $m(x)$ considered, the analysis is powerful enough to answer the question completely. I hope the progress made here on this problem can motivate other researchers in the areas to conclusively resolve this interesting problem.

Bibliography

[1] U. Ascher, R. Christiansen, R. Russell, *Collocation Software for Boundary Value ODE's*, Math. Comp., **33**, (1979), pp. 659–679.

[2] Ed Ash, Brian Eaton and Karl Gustafson, *Counting the number of solutions in combustion and reactive flow problems*, Journal of Applied Mathematics and Physics (ZAMP), Vol. 41, July (1990)

[3] C. J. Budd, V. A. Galaktionov, J. F. Williams, *Self-similar blow-up in higher-order semilinear parabolic equations*, SIAM J. Appl Math Vol.64, No. 5, pp. 1775-1809

[4] H. C. Nathanson, W. E. Newell, R. A. Wickstrom and J. R. Davis, *The Resonant Gate Transistor*, IEEE Trans. on Electron Devices, 14 (1967), pp. 117-133.

[5] D. Cassani, J. Marcos do Ó, N. Ghoussoub, *On a Fourth Order Elliptic Problem with a Singular Nonlinearity*, Journal of Advanced Nonlinear Studies, Vol. 9 (2009) p. 177-197

[6] C. V. Coffman, R. J. Duffin, *On the Fundamental Eigenfunctions of a Clamped Punctured Disk*, Adv. in Appl. Math. **13**, No. 2, (1992), pp. 142–151.

[7] C. V. Coffman, R. J. Duffin, *On the Structure of Biharmonic Functions Satisfying the Clamped Plate Conditions on a Right Angle*, Adv. in Appl. Math., **1**, No. 4, (1980), pp. 373-389.

[8] C. Cowan, P. Esposito, N. Ghoussoub, *The Critical Dimension for a Fourth Order Elliptic Problem with Singular Nonlinearity*, Arch. Ration. Mech. Anal., In press (2009) 19 pp

[9] P. Esposito, N. Ghoussoub, Y. Guo, *Compactness Along the Branch of Semi-Stable and Unstable Solutions for an Elliptic Equation with a Singular Nonlinearity*, Comm. Pure Appl. Math. **60**, No. 12, (2007), pp. 1731–1768.

[10] P. Feng, Z. Zhou, *Multiplicity and Symmetry Breaking for Positive Radial Solutions of Semilinear Elliptic Equations Modeling MEMS on Annular Domains*, Electron. J. Differential Equations, No. 146, (2005), 14 pp. (electronic)

[11] V. A. Galaktionov, *Incomplete self-similar blow-up in a semilinear fourth-order reaction-diffusion equation.* arXivL0902.1090v1

[12] I.M. Gelfand, *Some Problems in the theory of quasilinear equations*, Trans. Amer. Math. Soc., 2 (1963), pp. 295-381

[13] N. Ghoussoub, Y. Guo, *On the Partial Differential Equations of Electrostatic MEMS Devices: Stationary Case*, SIAM J. Math. Anal. **38**, No. 5, (2006/07), pp. 1423–1449.

[14] N. Ghoussoub, Y. J. Guo: Estimates for the quenching time of a parabolic equation modeling electrostatic MEMS, Methods and Applications of Analysis (2007) 16 pp

[15] N. Ghoussoub, Y. J. Guo: On the Partial Differential Equations of Electrostatic MEMS Devices II: Dynamic Case, Nonlinear Differential Equations and Applications, Vol. 15, No. 1-2 (2008) p. 115-145

[16] P. Esposito, N. Ghoussoub, Y. Guo *Mathematical Analysis of Partial Differential Equations Modeling Electrostatic MEMS*, Courant Lecture Notes, In press (2009) 332 pp

[17] Y. Guo, Z. Pan, M. J. Ward, *Touchdown and Pull-In Voltage Behaviour of a MEMS Device with Varying Dielectric Properties*, SIAM J. Appl. Math., **66**, No. 1, (2005), pp. 309–338.

[18] Z. Guo, J. Wei, *Symmetry of Nonnegative Solutions of a Semilinear Elliptic Equation with Singular Nonlinearity*, Proc. Roy. Soc. Edinburgh Sect. A, **137**, No. 5, (2007), pp. 963–994.

[19] Z. Guo, J. Wei, *Infinitely Many Turning Points for an Elliptic Problem with a Singular Nonlinearity*, Journal of London Mathematical Society, 78(2008), no.1, 21-35.

[20] Z. Guo, J. Wei, *Asymptotic Behavior of Touchdown Solutions and Global Bifurcations for an Elliptic Problem with a Singular Nonlinearity*, Comm. Pure Appl. Anal. 7(2008), no.4, 765-786.

[21] Z. Guo, J. Wei, *Entire Solutions and Global Bifurcations for a Biharmonic Equation with Singular Nonlinearity*, accepted, Advances Diff. Equations, 13 (2008), no.7-8, 743-780.

[22] Z. Guo, J. Wei, *On a Fourth Order Nonlinear Elliptic Equation with Negative Exponent*, SIAM J. Math. Anal. 40(2008/09), no.5, 2034-2054.

[23] D. Ye, J. Wei, *On MEMS equation with fringing field*, To appear, Proc. American Math. Soc, (2010).

[24] H. B. Keller, *Lectures on Numerical Methods in Bifurcation Problems*, Tata Institute of Fundamental Research, Bombay, (1987).

[25] H. Keller and D. Cohen, *Some positone problems suggested by nonlinear heat generation*. J. Math. Mech. 16, 1361 1376 (1967).

[26] F. Lin, Y. Yang, *Nonlinear Non-Local Elliptic Equation Modeling Electrostatic Actuation*, Proc. Roy. Soc. A, **463**. (2007), pp. 1323–1337.

[27] P. Lagerstrom, *Matched Asymptotic Expansions: Ideas and Techniques*, Applied Mathematical Sciences, **76**, Springer-Verlag, New York, (1988).

[28] P. Lagerstrom, D. Reinelt, *Note on Logarithmic Switchback Terms in Regular and Singular Perturbation Problems*, SIAM J. Appl. Math., **44**, No. 3, (1984), pp. 451–462.

[29] A. E. Lindsay M.J. Ward, (2008) Asymptotics of some nonlinear eigenvalue problems for a MEMS capacitor: Part I: Fold point asymptotics, Methods and Applications of analysis, Vol. 15, No. 3, 42. pp.297-326.

[30] A. E. Lindsay, M. J. Ward, *Asymptotics of Nonlinear Eigenvalue Problems Modeling a MEMS Capacitor: Part II: Multiple Solutions and Singular Asymptotics*, Submitted European Journal of Applied Mathematics, (2009).

[31] A. E. Lindsay, M. J. Ward, *An Asymptotic Analysis of the Persistence Threshold for the Diffusive Logistic Model in Spatial Environments with Localized Patches*, To Appear, Discrete and Continuous Dynamical Systems Series B, (2010).

[32] V Mendez, D. Campos, *Population extinction and survival in a hostile environment*, Physical Review EE **77**, 022901, (2008).

[33] J. A. Pelesko, D. H. Bernstein, *Modeling MEMS and NEMS*, Chapman Hall and CRC Press, (2002).

[34] J. A. Pelesko, *Mathematical Modeling of Electrostatic MEMS with Tailored Dielectric Properties*, SIAM J. Appl. Math., **62**, No. 3, (2002), pp. 888–908.

[35] J. A. Pelesko, D. Bernstein, J. McCuan, *Symmetry and Symmetry Breaking in Electrostatic MEMS*, Proceedings of MSM 2003, (2003), pp. 304–307.

[36] N. Popovic, P. Szymolyan, *A Geometric Analysis of the Lagerstrom Model Problem*, J. Differential Equations, **199**, No. 2, (2004), pp. 290–325.

[37] N. Popovic, P. Szymolyan, *Rigorous Asymptotic Expansions for Lagerstrom's Model Equation - A Geometric Approach*, Nonlinear Anal., **59**, No. 4, (2004), pp. 531–565.

[38] J. A. Pelesko, T. A. Driscoll, *The Effect of the Small Aspect Ratio Approximation on Canonical Electrostatic MEMS Models*, J. Engrg. Math., **53**, No. 3-4, (2005), pp. 239–252.

[39] G. Sweers, *When is the First Eigenfunction for the Clamped Plate Equation of Fixed Sign?*, Electronic J. Differ. Equ. Conf., **6**, Southwest Texas State Univ., San Marcos, Texas, (2001), pp. 285–296.

[40] E. Van De Velde, M. J. Ward, *Criticality in Reactors Under Domain or External Temperature Perturbation*, Proc. R. Soc. Lond. A, **1991**, No. 1891, (1991), pp. 341–367

[41] M. J. Ward, W. D. Henshaw, J. Keller, *Summing Logarithmic Expansions for Singularly Perturbed Eigenvalue Problems*, SIAM J. Appl. Math, Vol. 53, No. 3, (1993), pp. 799–828.

[42] H. Berestycki, F. Hamel, L. Roques, *Analysis of the Periodically Fragmented Environment Model: I - Species Persistence*, J. Math. Biol., **51**, No. 1, (2005), pp. 75–113.

[43] K. J. Brown, S. S. Lin, *On the Existence of Positive Eigenfunctions for an Eigenvalue Problem with Indefinite Weight Function*, J. Math. Anal. Appl., **75**, No. 1, (1980), pp. 112–120.

[44] A. Burchard, J. Denzler, *On the Geometry of Optimal Windows, with Special Focus on the Square*, SIAM J. Math. Anal., **37**, No. 6, (2006), pp. 1800-1827.

[45] R. S. Cantrell, C. Cosner, *Diffusive Logistic Equations with Indefinite Weights: Population Models in Disrupted Environments*, Proc. Roy. Soc. Edinburgh, **112A**, No. 3-4, (1989), pp. 293–318.

[46] R. S. Cantrell, C. Cosner, *Diffusive Logistic Equations with Indefinite Weights: Population Models in Disrupted Environments II*, SIAM J. Math. Anal., **22**, No. 4, (1991), pp. 1043–1064.

[47] R. S. Cantrell, C. Cosner, *The Effects of Spatial Heterogeneity in Population Dynamics*, J. Math. Biol., **29**, No. 4, (1991), pp. 315–338.

[48] R. S. Cantrell, C. Cosner, *Spatial Ecology via Reaction-Diffusion Systems*, Wiley Series in Mathematical and Computational Biology, John Wiley & Sons, Ltd., Chichester, 2003, xvi+411 pp.

[49] F. Belgacem and C. Cosner, *The effects of dispersal along environmental gradients on the dynamics of populations in heterogeneous environment*, Canadian Appl. Math. Quarterly 3 (1995) 379-397.

[50] X. Chen, M. Kowalczyk, *Existence of Equilibria for the Cahn-Hilliard Equation via Local Minimizers of the Perimeter*, Comm. Partial Differential Equations, **21**, No. 7-8, (1996), pp. 1207-1233.

[51] D. Coombs, R. Straube, M. J. Ward, *Diffusion on a Sphere with Localized Traps: Mean First Passage Time, Eigenvalue Asymptotics, and Fekete Points*, SIAM J. Appl. Math., **70**, No. 1, (2009), pp. 302–332.

[52] A. M. Davis, S. G. Llewellyn Smith, *Perturbation of Eigenvalues due to Gaps in Two-Dimensional Boundaries*, Proc. Roy. Soc. A, **463**, No. 2079, (2007), pp. 759–786.

[53] J. Denzler, *Windows of Given Area with Minimal Heat Diffusion*, Trans. Amer. Math. Soc., **351**, No. 2, (1999), pp. 569-580.

[54] E. M. Harrell II, P. Kröger, K. Kurata, *On the Placement of an Obstacle or a Well so as to Optimize the Fundamental Eigenvalue*, SIAM J. Math. Anal., **33**, No. 1, (2001), pp. 240–259.

[55] P. Hess, *Periodic-Parabolic Boundary Value Problems and Positivity*, Pitman Research Notes in Mathematics, Vol. 247, Longman, Harlow, U.K. (1991).

[56] C. Y. Kao, Y. Lou, E. Yanagida, *Principal Eigenvalue for an Elliptic System with Indefinite Weight on Cylindrical Domains*, Math. Biosc. Eng. **5**, No. 2 (2008), pp. 315–335.

[57] T. Kolokolnikov, M. Titcombe, M. J. Ward, *Optimizing the Fundamental Neumann Eigenvalue for the Laplacian in a Domain with Small Traps*, European J. Appl. Math., **16**, No. 2, (2005), pp. 161–200.

[58] K. Kurata, J. Shi, *Optimal Spatial Harvesting Strategy and Symmetry-Breaking*, Appl. Math. Optim., **58**, No. 1, (2008), pp. 89–110.

[59] Y. Lou, E. Yanagida, *Minimization of the Principal Eigenvalue for an Elliptic Boundary Value Problem with Indefinite Weight and Applications to Population Dynamics*, Japan J. Indust. Appl. Math., **23**, No. 3, (2006), pp. 275–292.

[60] Y. Lou, *Some Challenging Mathematical Problems in Evolution of Dispersal and Population Dynamics*, Tutorials in Mathematical Biosciences. IV, 171–205, Lecture Notes in Math., **1922**, Springer, Berlin, (2008).

[61] S. Ozawa, *Singular Variation of Domains and Eigenvalues of the Laplacian*, Duke Math. J., **48**, No. 4, (1981), pp. 767-778.

[62] S. Pillay, M. J. Ward, A. Peirce, R. Straube, T. Kolokolnikov, *An Asymptotic Analysis of Mean First Passage Time Problems with Narrow Escape*, accepted ,SIAM j. Multiscale Modeling, (2009), (28 pages).

[63] L. Roques, F. Hamel, *Mathematical Analysis of the Optimal Habitat Configurations for Species Persistence*, Math. Biosci., **210**, No. 1, (2007), pp. 34–59.

[64] L. Roques, R. Stoica, *Species Persistence Decreases with Habitat Fragmentation: An Analysis in Periodic Stochastic Environments*, J. Math. Biol., **2007**, No. 2, (2007), pp. 189–205.

[65] M. Grossi, *Asymptotic Behavior of the Kazdan-Warner Solution in the Annulus*, J. Differential Equations, **223**, No. 1, (2006), pp. 96–111.

[66] J. C. Saut, B. Scheurer, *Remarks on a Nonlinear Equation Arising in Population Genetics*, Comm. Part. Diff. Eq., **23**, (1978), pp. 907–931.

[67] N. Shigesada, K. Kawasaki, *Biological Invasions: Theory and Practice*, Oxford Series in Ecology and Evolution, Oxford: Oxford University Press, (1997).

[68] S. Senn, P. Hess, *On Positive Solutions of a Linear Elliptic Boundary Value Problem with Neumann Boundary Conditions*, Math. Ann. **258**, (1982), pp. 459–470.

[69] J. G. Skellam, *Random Dispersal in Theoretical Populations*, Biometrika, **38**, (1951), pp. 196–218.

[70] M. J. Ward, Y. Guo and Z. Pan *Touchdown and Pull-In Voltage Behavior of a MEMS Device with Varying Dielectric Properties* , SIAM J. Applied Math, Vol. 66, No. 1, (2006), pp. 309-338.

[71] M. J. Ward, J. B. Keller, *Strong Localized Perturbations of Eigenvalue Problems*, SIAM J. Appl. Math, Vol. 53, No. 3, (1993), pp. 770–798.

[72] M. J. Ward, S. Pillay, A. Peirce, and T. Kolokolnikov, *An Asymptotic Analysis of the Mean First Passage Time for Narrow Escape Problems: Part I: Two-Dimensional Domains with* , To Appear, SIAM Multiscale Modeling and Simulation, (December 2009), 28 pages.

[73] T. P. Witelski, *Computing finite time singularities in interfacial flows. Modern Methods in Scientic Computing and Applications*, pp. 451487. Kluwer. (2002).

[74] T. P. Witelski, A. J. Bernoff, *Stability and Dynamics of Self-Similarity in Evolution Equations*